NORTH DAKOTA STATE UNIVERSITY
OF AGRICULTURE AND APPLIED SCIENCE
FARGO, NORTH DAKOTA 58105

THE GRADUATE SCHOOL
OFFICE OF THE DEAN
TELEPHONE (701) 231-7033

CONSENT TO PHOTOCOPY
DISQUISITION

I hereby give ✓ / do not give _____ the North Dakota State University Library permission to make up to three photocopies of my disquisition titled: _____

Durability of Concrete Members strengthened with cFRP sheets under Harsh Environmental conditions

10-18-2010
Date

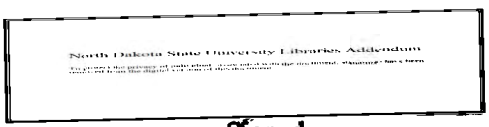

Signed

Copies made:

Date	Signature of Library employee
1.	
2.	
3.	

DURABILITY OF CONCRETE MEMBERS STRENGTHENED WITH CFRP SHEETS UNDER HARSH ENVIRONMENTAL CONDITIONS

A Thesis
Submitted to The Graduate Faculty
of the
North Dakota State University
of Agriculture and Applied Science

By

Md. Mozahid Hossain

In Partial Fulfillment of the Requirements
for the Degree of
MASTER OF SCIENCE

Major Department:
Civil Engineering

June 2010

Fargo, North Dakota

North Dakota State University
Graduate School

Title

DURABILITY OF CONCRETE MEMBERS STRENGTHENED WITH CFRP SHEETS

UNDER HARSH ENVIRONMENTAL CONDITIONS

By

MD. MOZAHID HOSSAIN

The Supervisory Committee certifies that this ***disquisition*** complies with North Dakota State University's regulations and meets the accepted standards for the degree of

MASTER OF SCIENCE

SUPERVISORY COMMITTEE:

ABSTRACT

Hossain, Md. Mozahid, M.S., Department of Civil Engineering, College of Engineering and Architecture, North Dakota State University, June 2010. Durability of Concrete Members Strengthened with CFRP Sheets under Harsh Environmental Conditions. Major Professor: Dr. Jimmy Kim.

The deterioration of concrete structures is a major concern to the infrastructure community. Typical sources of deterioration may include aging, increased service load, and environmental damage. Structural rehabilitation using carbon fiber reinforced polymer (CFRP) sheets has recently attracted attention to the infrastructure community because of the superior strengthening effects in comparison to conventional repair methods. The CFRP sheets may be bonded on the deteriorated concrete structure using bonding agents to enhance load-carrying capacity. The most important consideration in such a strengthening method may be the long term durability under harsh environmental conditions. Furthermore, premature debonding of bonded CFRP sheets may also cause significant losses of the strengthening effects. Although extensive research has been reported on the debonding mechanism of CFRP sheets, there is still lack of understanding on the durability of CFRPs subject to low temperature effects. This thesis presents some major findings of the durability performance of concrete members strengthened with CFRP sheets subjected to harsh environments.

ACKNOWLEDGEMENTS

My time spent as a graduate student at North Dakota State University has afforded me the opportunity to grow as an individual and to get to know many fascinating people, including colleagues, faculty, and staff. I would like to recognize all of those that played a role in the completion of this research. I would like to express my sincere gratitude and appreciation to the members of my committee for their willing participation to accommodate me amidst their busy schedules.

It was a tremendous experience to work under the guidance of Dr. Jimmy Kim, whose valuable advice and encouragement were very important for the completion of this research. I would like to express my sincere gratitude and indebtedness for his endless guidance, patience, and support during the course of this research. My gratitude also extends to all my friends and colleagues for all the discussions, cooperation and for the wonderful time we have shared. I would like to acknowledge and express particular thanks to the organizations that provided financial support for the research project without which none of this work would have been possible.

Finally, I will always have my cordial appreciation and love to my mother, brothers and sisters for their love, understanding and moral support throughout this time. This thesis is dedicated to my father's soul that is a never-ending source of love, pride and inspiration to me; and to everyone who helped and supported me during my hard time as a diminutive way of saying *Thank You.*

TABLE OF CONTENTS

ABSTRACT..... iii

ACKNOWLEDGEMENTS..... iv

LIST OF TABLES..... xi

LIST OF FIGURES..... xiii

NOTATIONS..... xix

CHAPTER 1. INTRODUCTION..... 1

1.1. GENERAL..... 1

1.2. RESEARCH OBJECTIVE..... 3

1.3. SCOPE..... 4

1.4. OUTLINE OF THESIS..... 6

1.5. REFERENCES..... 7

CHAPTER 2. LITERATURE REVIEW..... 9

2.1. GENERAL..... 9

2.2. FRP FOR STRUCTURAL REHABILITATION..... 9

2.2.1. History of FRP Composites..... 10

2.2.2. Fiber Reinforced Polymer (FRP)..... 12

2.3. ENVIRONMENTAL EFFECTS..... 14

2.3.1. Effects of Low Temperature on Concrete..... 14

2.3.2. Effects of Low Temperature on FRP 17

2.3.3. Effects of Moisture 19

2.3.4. Cold Temperature Effects on Bond between FRP and concrete... 20

2.4. CONCLUSION..... 22

2.5. REFERENCES..... 22

CHAPTER 3. MATERIAL PROPERTIES..... 26

3.1. SYNOPSIS..... 26

3.2. INTRODUCTION..... 27

3.3. DURABILITY OF EPOXY ADHESIVE..... 28

3.4. EXPERIMENTAL PROGRAM..... 29

3.4.1. Materials..... 29

3.4.1.1. Steel Strips..... 29

3.4.1.2. Epoxy Adhesive..... 30

3.4.2. Specimen Configuration..... 30

3.4.3. Environmental Effects..... 31

3.4.4. Test Equipment and Loading Information..... 34

3.5. EXPERIMENTAL RESULTS..... 35

3.5.1. Load-carrying Capacity (Task I)..... 35

3.5.2. Load-carrying Capacity (Task II)..... 38

3.5.3. Cold Temperature Effects 42

3.5.4. Failure Mode..... 43

3.6. ANALYTICAL MODEL 47

3.7. MATERIALS PROPERTIES OF CFRP COMPOSITE 53

3.7.1. Carbon Fiber Reinforced Polymer Sheet..... 53

3.7.2. Coupon Preparation..... 53

3.7.3. Environmental Effects 54

3.7.4. Testing and Instrumentation 55

3.7.5. Test Results 55

3.8. DISCUSSION AND CONCLUSION 60

3.9. REFERENCES..... 60

CHAPTER 4. AXIAL CONCRETE MEMBER..... 63

4.1. SYNOPSIS..... 63

4.2. INTRODUCTION..... 63

4.3. RESEARCH SIGNIFICANCE 65

4.4. BACKGROUND 66

4.4.1. Bridges in North Dakota..... 66

4.4.2. Critical Sources of Bridge Deterioration..... 66

4.5. EXPERIMENTAL PROGRAM..... 68

4.5.1. Materials 68

4.5.2. Casting of Concrete Cylinders 68

4.5.3. CFRP Sheet Application 69

4.5.4. Environmental Cycling and Live Load Effects 72

4.5.5. Crack Width Measurement 74

4.5.6. Instrumentation and Testing 76

4.6. EXPERIMENTAL RESULTS 76
4.6.1. Load-carrying Capacity 76
4.6.2. Stress-strain Response 78
4.6.3. Relationship between Hoop and Axial Strains 81
4.6.4. Volumetric Strains 87
4.6.5. Crack Pattern during Load Cycling 88
4.6.6. Failure Modes 91
4.7. ANALYTICAL MODELS 93
4.7.1. Models by ACI440 (2001) and ISIS Canada (2001) 94
4.7.1.1. Model by ACI 440 (2001) 94
4.7.1.2. Model by ISIS Canada (2001) 97
4.7.2. Model by Karbhari and Gao (1997) 98
4.7.3. Comparisons 98
4.8. SUMMARY AND CONCLUSION 101
4.9. REFERENCES 102
CHAPTER 5. CONCRETE BLOCKS 105
5.1. SYNOPSIS 105
5.2. INTRODUCTION 105
5.3. RESEARCH OBJECTIVE 107
5.4. EXPERIMENTAL PROGRAM 108
5.4.1. Materials 108

5.4.1.1. Carbon Fiber Reinforced Polymer (CFRP) Sheets ... 108

5.4.1.2. Epoxy Adhesive 108

5.4.2. Formwork 108

5.4.3. Casting of Concrete Blocks 109

5.4.4. CFRP Sheet Application 110

5.4.5. Environmental Effects 112

5.4.6. Instrumentation and Testing 114

5.4.7. Laser Scanning 115

5.5. EXPERIMENTAL RESULTS 116

5.5.1. Load-carrying Capacity and Interfacial Fracture Energy..... 116

5.5.2. Cold Temperature Effects 123

5.5.3. Strain Distribution 125

5.5.4. Failure Modes..... 129

5.6. ANALYTICAL MODEL 132

5.7. COMPARISON 136

5.8. DISCUSSION AND CONCLUSION 138

5.9. REFERENCES..... 142

CHAPTER 6. SUMMARY AND CONCLUSIONS..... 144

6.1. SUMMARY OF RESEARCH PROGRAM..... 144

6.2. DISCUSSION AND 145

6.3. RECOMMENDATIONS FOR FUTURE WORK 149

APPENDIX A. REPORT CARD FOR AMERICAN'S INFRASTRUCTURE..... 151

APPENDIX B. MATERIALS PROPERTIES OF EPOXY ADHESIVE AND CFRP SHEETS..... 153

APPENDIX C. STRENGTHENING OF AXIAL CONCRETE MEMBER WITH CFRP SHEETS..... 184

APPENDIX D. DURABILITY OF BOND BETWEEN CFRP AND CONCRETE..... 187

LIST OF TABLES

Table		Page
2.1.	Coefficients of thermal expansion of partially dried concrete	17
3.1.	Mechanical properties of Steel strips and epoxy adhesive	30
3.2.	Test results of control specimens	36
3.3.	Test results of wet-dry effects (Task I)	36
3.4.	Test results of freeze-thaw effects (Task I)	38
3.5.	Test results of wet-dry effects (Task II)	42
3.6.	Test results of freeze-wet-dry effects (Task II)	43
3.7.	Test results of constant freezing for 2000 hours (Task II)	47
3.8.	Mechanical properties of CFRP sheet as given by the manufacturer	54
3.9.	Test Result for mechanical properties of CFRP coupon	58
4.1.	Results of unconfined concrete cylinders	79
4.2.	Results of confined concrete cylinders	80
4.3.	Numerical results obtained using ISIS Canada (2001) Model	100
4.4.	Numerical results obtained using ACI 440 (2001) confinement model	100
4.5.	Comparison of confinement models (Control)	100
4.6.	Comparison of confinement models (100 Cycles)	100

Table Page

4.7. Numerical results obtained using Karbhari and Gao (1997) model..... 101

4.8. Comparison of confined concrete strength..... 101

5.1. Mechanical properties of CFRP sheet as given by the manufacturer..... 109

5.2. Material properties of epoxy adhesive..... 109

5.3. Test results of control specimens..... 119

5.4. Test results of wet-dry effects..... 119

5.5. Test results of freezing-wet-dry effects..... 120

5.6. Test results of constant freezing effects for 2,000 hours..... 125

5.7. Numerical results obtained using Wu et al. (2008) Model..... 141

5.8. Comparison of confined concrete response..... 141

LIST OF FIGURES

Figure		Page
2.1.	Typical application of FRPs to structural elements.....	12
2.2.	Example of concrete cracking from freeze-thaw effects.....	15
2.3.	Reinforced concrete cylinders following freeze-thaw cycling.....	16
2.4.	Stresses in bonding line incompatibility of matrix and fibers.....	19
3.1.	Double-lap shear test specimen.....	31
3.2.	Test specimens: (a) Bonding steel strips; (b) Assembled specimen.....	32
3.3.	Environmental cycling: (a) water bath; (b) freezing; (c) temperature variation in the environmental chamber for Task I; (d) environmental cycling for Task II	33
3.4.	Freezing: (a) environmental Chamber; (b) temperature variation in the environmental chamber for Task II	34
3.5.	A specimen clamped in the testing machine before test starts.....	34
3.6.	Load carrying capacity (Task I): (a) effect of wet-dry cycles; (b) failure Load(W-D); (c) effect of freeze-thaw; (d) failure Load(F-T); (e) failure load comparison; (f) comparisons of the effect of wet-dry and freeze-thaw cycles.....	37
3.7.	Average shear stress (Task I): (a) effect of wet-dry cycles; (b) effect of freeze-thaw cycles; (c) comparisons the effects of freeze-wet-dry and wet-dry cycles.....	39
3.8.	Average stiffness (Task I): (a) effect of wet-dry cycles; (b) best-fit (W-D); (c) effect of freeze-thaw cycles; (d) best-fit (F-T); (e) comparisons of the effect of wet-dry and freeze-thaw cycles; (f) stiffness comparison.....	40
3.9.	Load-carrying capacity (Task II): (a) effect of wet-dry cycles; (b) effect of freeze-wet-dry; (c) failure Load(W-D); (d) failure Load(F-W-D); (e) failure load comparisons; (f) comparisons of the effect of wet-dry and freeze-wet-dry cycles.....	44

Figure

Page

3.10. Average shear stress: (a) effect of wet-dry cycles; (b) effect of freeze-wet-dry cycles; (c) comparisons the effects of freeze-wet-dry and wet-dry cycles..... 45

3.11. Average stiffness (Task II): (a) effect of wet-dry cycles; (b) effect of freeze-wet-dry; (c) effect of wet-dry cycles; (d) effect of freeze-wet-dry; (e) comparison the effects of wet-dry and freeze-wet-dry cycles; (d) effects of wet-dry/freeze-wet-dry cycles..... 46

3.12. Summary of test results of 2000 hours constant freezing at different low temperatures: (a) average failure load variation with temperature; (b) average stifneess variation; (c) failure load; (d) stiffness variations; (e) effects of cold temperature..... 48

3.13. Failure mode of test specimens: (a) schematic view of the failed specimen; (b)control; (c) wet-dry; (d) freeze-thaw..... 49

3.14. Pull–push shear test of a single-lap plate-to-concrete bonded joint: (a) elevation; (b) plan (Yuan et al. 2004)..... 51

3.15. Different state of load displacement curve (Yuan et al. 2004)..... 52

3.16. Quarter of Double strap joint, boundary conditions and loads..... 52

3.17. Load-displacement response of double strap joints..... 52

3.18. CFRP sheets uses in the research project..... 53

3.19. Some prepared CFRP coupons before testing..... 54

3.20. Typical CFRP coupons tested in uniaxial tension after exposure to harsh environment..... 55

3.21. Stress-strain response of control specimens..... 58

3.22. Failure of CFRP coupons in tension..... 59

3.23. Test results: (a) ultimate tensile stress; (b) elastic modulus; (c) elastic modulus comparison..... 59

4.1. Critical sources of bridge deterioration in North Dakota (Kim and Yoon 2010): (a) bridge status; (b) relationship between structurally deficient bridges and contributing factors 67

Figure		Page
4.2.	Surface cleaning.....	69
4.3.	Wrapping of cylinder with CFRP sheets: (a) CFRP sheet; (b) apply epoxy to CFRP sheet and cylinder rolling on it; (c) fiber direction; (d) complete confined cylinders.....	71
4.4.	Sealing both ends of cylinders with epoxy adhesive.....	72
4.5.	Sequences of environmental cycling.....	72
4.6.	Environmental sequence: (a) freezing; (b) submerging; (c) drying; (d) live load per cycles.....	73
4.7.	Temperature variation in the environmental chamber.....	74
4.8.	Crack width measurement during the load cycle: (a) crack measuring microscope; (b) cracked cylinder; (c) typical crack width measured with crack microscope	75
4.9.	Instrumentations: (a) testing; (b) strain gage locations; (c) Novotechlink TR100 linear potentiometer; (d) foil strain gage.....	77
4.10.	Relationship between the ultimate strength of cylinders and live load effect: (a) unconfined cylinders; (b) confined cylinders.....	81
4.11.	Stress-strain responses of unconfined cylinders: (a) axial direction; (b) hoop direction.....	82
4.12.	Stress-strain responses of confined cylinders: (a) axial direction; (b) hoop direction	83
4.13.	Relationship between axial and hoop strains of unconfined cylinders: (a) Env+0% (Cylinder G); (b) Env+20% (Cylinder H); (c) Env+40%(Cylinder K) ; (d) Env+60% (Cylinder N).....	85
4.14.	Relationship between axial and hoop strains of confined cylinders: (a) Env+0% (Cylinder 6); (b) Env+20% (Cylinder 9); (c) Env+40% (Cylinder 12); (d) Env+60% (Cylinder 15)	86
4.15.	Variation of volumetric strain of unconfined cylinders: (a) Env+0% (Cylinder G); (b) Env+20% (Cylinder H); (c) Env+40% (Cylinder K); (d) Env+60% (Cylinder N)	87
4.16.	Variation of volumetric strain of confined cylinders: (a) Env+0% (Cylinder 6); (b) Env+20% (Cylinder 9); (c) Env+40% (Cylinder 12); (d) Env+60% (Cylinder 13)	89

Figure		Page
4.17.	Crack patterns during the load cycle: (a) Env + 0% (Cylinder G); (b) Env + 20% (Cylinder I); (c) Env + 40% (Cylinder M); (d) Env + 60% (Cylinder P)	90
4.18.	Crack width variations with the load cycle: (a) Env + 60% (Cylinder P); (b) Env + 60% (Cylinder O); (c) Env + 60% (Cylinder N); (d) Env + 40% (Cylinder L) ; (d) Env + 40% (Cylinder K).....	92
4.19.	Crack width variations with the load cycle: (a) Env + 20% (Cylinder J); (b) Env + 20% (Cylinder I); (c) Env + 20% (Cylinder H).....	93
4.20.	Failed test specimens: (a) Control; (b) Environmental effect + 0% live Load.....	94
4.21.	Failed test specimens: (a) Environmental effect + 20% live load; (b) Environmental effect + 40% live load; (c) Environmental effect + 60% live load	95
4.22.	Failed test specimens: (a) Control; (b) Environmental effect + 0% live load; (c) Environmental effect + 20% live load; (d) Environmental effect + 40% live load; (e) Environmental effect + 60% live load	96
5.1.	Casting of Concrete: (a) plywood formwork; (b) smooth of surface after trowelling.....	110
5.2.	Surface preparation: (a) concrete blocks after removal from formwork; (b) high speed water flow for cleaning the surface.....	111
5.3.	CFRP application; (a) location of CFRP sheets; (b) epoxy applied to the concrete surface; (c) epoxy saturated CFRP sheet; (d) CFRP sheet bonding with concrete block.....	113
5.4.	Environmental cycling: (a) freezing; (b) specimen submerse in water bath; (c) environmental cycling; (d) environmental chamber.....	115
5.5.	Temperature variation in the environmental chamber.....	116
5.6.	Strain gage locations along CFRP sheet.....	116
5.7.	Single lap test: (a) illustration of gripping frame; (b) tension test	117
5.8.	Laser scanning of the failed CFRP sheets.....	118
5.9.	Effect of wet-dry cycles: (a) average ultimate strength with standard deviation; (b) average ultimate strength; (c) interfacial fracture energy with standard deviation; (d) interfacial fracture energy	121

Figure Page

5.10. Effect of freeze-wet-dry cycles: (a) average ultimate strength with standard deviation; (b) average ultimate strength; (c) interfacial fracture energy with standard deviation; (d) interfacial fracture energy 122

5.11. Effects of freeze-wet-dry and wet-dry cycles: (a) average ultimate load; (b) average fracture energy 123

5.12. Average shear stress: (a) freezing (-30°C: 16 hours)-wet (4 hours)-dry (8 hours); (b) wet (16 hours)-dry (8 hours); (c) comparison between freeze-wet-dry and wet-dry cycles 124

5.13. Effect of constant freezing of 2000 hours: (a) average load-carrying capacity; (b) interfacial fracture energy with standard deviation; (c) interfacial fracture energy 126

5.14. Stain distribution along CFRP-concrete of control specimen (R5)..... 127

5.15. Stain distribution along CFRP-Concrete joint of constant freezing for 2000 hours: (a) freeze at 0 ^{0}C (CT-0-1); (b) freeze at -10 ^{0}C (CT-10-2); (c) freeze at -20 ^{0}C (CT-20-1); (d) freeze at -30 ^{0}C (CT-30-4) 128

5.16. Stain distribution along CFRP-to-concrete joint under freeze-wet-dry effects: (a) 25 cycles (FWD4-25); (b) 50 cycles (FWD2-50); (c) 100 cycles (FWD2-100); (d) 150 cycles (FWD4-150)..... 130

5.17. Stain distribution along CFRP-to-concrete joint under wet-dry effects: (a) 25 cycles(WD4-25); (b) 50cycles(WD3-50); (c) 100 cycles(WD2-100); (d) 150 cycles (WD2-150) 131

5.18. Debonded CFRP sheet (CT-30-1/4) 132

5.19. Interface of control specimen: (a) control (R6); (b) control (R7); (c) control (R2)..... 133

5.20. Effect of freeze-wet-dry: (a) 25 cycles (FWD1-25); (b) 25 cycles (FWD3-25); (c) 50 cycles (FWD3-50); (d) 100 cycles (FWD1-100) 134

5.21 Effect of wet-dry-freezing cycles: (a) 100 cycles (FWD4-100); (b) 150 cycles (FWD2-150) 135

Figure Page

5.22. Effect of constant freezing of 2000 hours: (a) 0°C (CT-0-2); (b) 0°C (CT-0-3); (c) – 10°C (CT-10-2); (d) – 20°C (CT-20-4)..... 137

5.23. Effect of constant freezing of 2000 hours: (a) at -20 °C (Specimen CT-20-1); (b) at -30°C (Specimen CT-30-4) 138

5.24. Effect of wet-dry cycles: (a) 25 cycles (WD2-25); (b) 25 cycles (WD3-25); (c) 50 cycles (WD2-50); (d) 50 cycles (WD4-50) 139

5.25. Effect of wet-dry: (a) 100 cycles (WD1-100); (b) 150 cycles (WD1-150); (c) 150 cycles (WD4-150) 140

5.26. Comparison of experimental result with analytical model..... 141

NOTATIONS

α_{pc}	Performance coefficient of circular column
b_c	The width of the concrete member (mm)
b_p	The width of the FRP (mm)
C_E	Environmental reduction factor
E_c	Modulus of elasticity of concrete (MPa)
E_f	Modulus of elasticity of FRP (MPa)
E_p	Modulus of elasticity of external FRP reinforcement (MPa)
f_c'	Compressive strength of concrete (MPa)
f'_{cc}	Confining strength of concrete
f^*_{fu}	Tensile strength of FRP by manufacture
f_{frpu}	Tensile strength of FRP
f_{fe}	Effective stress in FRP
f_{fu}	Design ultimate tensile strength of FRP
f_l	Lateral stress produced by confinement
f_{lfrp}	Confining pressure due to FRP reinforcement
G_F	Interfacial fracture energy (N/mm)
h	Over all depth of concrete section (mm)
h_c	Diameter of circular column
k_a	Efficiency factor of FRP, (based on shape of section)
k_b	Width influence factor

NOTATIONS (Continued)

L	Bonded length (mm)
L_e	Effective bonding length (mm)
n	No of plies
N_b	Number of layers
P_u	Maximum transferable load (bond capacity/bond strength)
ρ_f	Reinforcement ratio
t_f	Nominal thickness of one ply (mm)
t_{frp}	Thickness of FRP (mm)
t_p	Thickness of FRP plate or sheet (mm)
t_p	Thickness of FRP plate or sheet (mm)
τ_f	Local bond strength
ε^*_{fu}	Ultimate rupture strain of FRP
Φ_c	Resistance factor of concrete
Φ_{frp}	Resistance factor of FRP
ϖ_w	Volumetric ratio of FRP strength to concrete strength
Δ	Axial displacement (mm)

CHAPTER 1. INTRODUCTION

1.1. GENERAL

Approximately 25%, one in four, of the nation's 590,750 bridges in the United States are either structurally deficient or functionally obsolete (ASCE 2005). The ASCE Report Card 2005 (ASCE 2005) on America's Infrastructure showed a depressing status of existing infrastructure. The Report Card gives a C (mediocre) grade for the current bridge status and estimates a need for a budget of $9.4 billion per year for the next 20 years to improve the current bridge status in the United States alone. In fact, between 2000 and 2003, the percentage of the nation's 590,750 bridges rated structurally deficient or functionally obsolete decreased slightly from 28.5% to 27.1% (ASCE 2005). Meanwhile the report gives an overall D grade (poor condition) for the infrastructures and announced a budget of $1.6 trillion is required in the United States alone to bring the infrastructures in an acceptable condition.

A number of factors influence the service life of concrete structures, such as the increased traffic loads, aging, corrosion, sulfate attack, alkali-silica reaction, freeze-thaw, and impact damage (Shahrooz et al. 2002; Enright and Frangopol 2000; Kim et al. 2008). Cold weather climates necessitate the extensive use of deicing salts on roads and bridges. These salts cause corrosion of the reinforcing steel and deterioration of concrete. In Canada, more than 40% of bridges built over 30 years ago are in serious need of repair or replacement either because of corrosion of the reinforcing steel or because current loads exceed original design limits (Rizkalla and Labossière 1999). In the province of Ontario, the estimated annual cost of regaining the structural status was CAN$24.5 million (Bickley

et al. 1993). Thus, a severe infrastructure crisis exists and results in costly repairs and safety hazards. To alleviate this huge infrastructure deficiency; a novel, cost effective and environmental friendly strategies must be developed. Rehabilitation can be used as a cost effective alternative to the replacement of these deteriorated structures and is often the only feasible solution.

Over the last two decades, the applications of fiber reinforced polymer (FRP) in civil engineering has emerged and increasingly being applied for the rehabilitation and strengthening of structures to improve load-carrying capacity (i.e., flexural, shear, and axial compressive load). FRPs are composite materials consisting of high strength fibers embedded in a polymer matrix. Fibers carry major portion of the applied loads, while the matrix transfers these loads to the fibers, and also protects them from environmental and mechanical damage. Fibers are typically made of carbon, glass or aramid, while commonly used polymer matrices include epoxy, vinylesters and polyesters (ISIS 2003). Some of the advantages of FRP composites in infrastructure applications include their high strength to weight ratios, resistance to environmental, and ease and rapid in installation. Rapid installation is particularly attractive in repair applications.

Strengthening of deteriorated concrete structures with FRP has gained as a cost effective method. All research to date have indicated that the use of FRP in repair and retrofitting provide deteriorated infrastructure with new life and longevity. FRP, for example CFRP, sheets can be externally bonded to the tensile soffit of deteriorated concrete structures to improve the load-carrying capacity. FRP-wrapped technique can be used for improving the load-carrying capacity of axial concrete members. FRP sheets are generally wrapped around the columns with fibers oriented mainly in the circumferential

direction. The fibers confine the concrete and increase the axial strength by creating a triaxial stress condition. This technique also increases the shear resistance of columns and prevents premature spalling failures when columns are subjected to lateral loadings (i.e., earthquakes).

Despite the crucial advantages of these externally bonded CFRP strengthening techniques in the battle against deteriorated concrete structures, a general lack of confidence in the durability of CFRP in aggressive environments (i.e., freeze-wet-dry, wet-dry, and constant cold temperatures) has barred their widespread use. This type of environments is particularly important in cold regions environments. Although significant amounts of research efforts have been reported on CFRP-strengthening, still there is lack of understanding on the bond behavior of CFRP-concrete interface subject to a freeze-wet, dry and low temperature effects. The main limitation includes the bond characteristics between CFRP-concrete interface which may govern the "premature" debonding failures and may cause a significant loss of the strengthening effect which may make the use of CFRP uneconomical. CFRP composites may also be successfully used for strengthening of axial concrete members. The durability of CFRP-wrapped concrete columns exposed to freeze-wet-dry effects combined with live load effects must be well-understood before their widespread applications.

1.2. RESEARCH OBJECTIVE

Research work presented in this thesis is categorized into three phases. Phase I will be discussed in Chapter 3 that includes the ancillary test to determine the material properties that were used for analytical modeling (will be discussed in Chapter 4 and Chapter 5). The primary objective of Phase I was to examine the constitutive material

characteristics of epoxy adhesives and CFRP sheets under variable cold temperatures, wet-dry, and freeze-wet-dry effects that may be required to bond CFRP-concrete substrates. To achieve the main objective the following was conducted.

- Experimental work was conducted to demonstrate the material characteristics of epoxy adhesives and CFRP sheets subjected to various low temperatures and harsh environmental conditions.

Phase II will be discussed in Chapter 4 that includes environmental effects combined with physical loads, critical factors influencing the durability of CFRP-wrapped concrete members. The primary objective of this research work was:

- To demonstrate the durability of concrete cylinder exposed to harsh environmental conditions (wet-dry-cold temperature) combined with various levels of instantaneous load.

The objective of Phase III (to be discussed in Chapter 5) is to demonstrate the bond behavior of CFRP-concrete interface subjected to aggressive environmental conditions. The broad objectives of all phases will be discussed separately in the corresponding chapters.

1.3. SCOPE

Scope of Phase I consists of examination of material properties of epoxy adhesive and CFRP sheets under harsh environmental conditions, namely freeze-thaw, wet-dry, freeze-wet-dry and different constant low temperatures. Chapter 3 includes experimental work to examine the constituitive material characteristics of adhesives for CFRP sheets subjected to harsh environment conditions, including wet-dry, freeze-thaw, freeze-wet-dry and various constant low temperatures (0 °C, -10 °C, -20 °C and -30 °C), which is

particularly important for cold regions applications. Key parameters varied in this study include: the number of wet-dry, freeze-thaw, and freeze-wet-dry cycles. A total of 100 double-lap shear specimens were tested in monotonic load to examine bond performance and corresponding failure modes. Also, an existing confinement models proposed by Yuan et al. (2004) was compared against test data.

Chapter 3 also includes the examination of materials properties of CFRP sheets subjected up to 100 cycles of freeze-wet-dry and constant freezing at - 30°C for 2,400 hours. A total 20 CFRP coupons were tested to examine the tensile strength and tensile elastic modulus.

Chapter 4 presents an experimental study on the durability of 15 CFRP-confined, and 16 unconfined concrete cylinders (75 x 150 mm) subjected to harsh environmental conditions combined with live load effects. The live load intensives are 20%, 40%, and 60% of the compressive strength of concrete specimens. All the cylinders are applied load to complete failure and ultimate load-carrying capacity and stress-strain responses are recorded. Also, existing confinement models proposed by ACI440 (2002), ISIS Canada (2001), and Karbhari and Gao (1997) are compared against test data.

Scope of Phase III consists of extensive experimental examinations of the durability of epoxy bonded CFRP-concrete interface exposed to freeze-wet-dry, wet-dry, and different constant low temperatures (0 °C, -10 °C, -20 °C, and -30 °C). The specimens were exposed up to 150 freeze-wet-dry cycles consisting of 16 hours of freezing at -30 °C, 4 hours of submerging under water, dry at room temperature for 4 hours, and constant freezing for 2,000 hours. After environmental exposure, the specimens were tested to failure. The development of strains along the bond length and the failure mode are

presented for all types of the specimens. Also, existing three parameters model proposed by Wu et al. (2009) was compared against test data.

1.4. OUTLINE OF THESIS

This thesis includes six chapters organized into stand-alone papers in addition to appendices that present the supplementary data and calculations.

Chapter 1 addresses the motivation and general background, and provides the research significance and objectives of the project, scope of this research.

Chapter 2 provides a thorough review the state-of-the-art knowledge regarding durability issues and strengthening behaviour under elevated low temperature.

Chapter 3 describes the ancillary tests for determining constitutive properties of epoxy adhesive and CFRP sheets. A detailed description of the materials properties, specimen preparation, different environmental effects, different cold temperatures effects, testing program are given, including the test setup and instrumentation. It also includes the test results of the experimental program with detailed discussion of the data obtained.

Chapter 4 describes the experimental program to examine the durability of partially cracked CFRP sheet strengthened axial concrete members subjected to harsh environmental conditions combined with different level of live load effects. It will also include the specimen's preparation, environmental cycling, instrumentation, testing and analysis of test results.

Chapter 5 presents the experimental investigation to investigate the long term durability of epoxy bonded FRP-concrete interface subjected to aggressive environmental conditions. This chapter presents specimens preparation, environmental cycling,

instrumentation and testing. This chapter also gives a brief comparison between test results and analytical models.

Chapter 6 provides precise conclusions from test results and provides short lists of observations, and general remarks on the recommendations for future work.

Appendix A presents ASCE 2005 infrastructure progress report that shows the current infrastructure condition in the United States, budget required to bring the infrastructures condition to an acceptable level. Appendix B shows detailed data base and calculations used for Chapter 3. Appendix C shows the related plots used for Chapter 4 and Appendix D shows plots comparison and related calculation required for Chapter 5.

1.5. REFERENCES

1. ACI Committee 440.2R-02. "Guide for the design and construction of externally bonded FRP systems for strengthening concrete structures", *ACI*, MI, 2002.

2. ASCE. "Report card for America's infrastructure, American Society of Civil Engineers", Reston, VA, 2005.

3. Basheer, L., Kropp, J., and Cleland, D. "Assessment of the durability of concrete from its permeation properties: a review", *Const. and Building materials*, 15, 93-103, 2001.

4. Buyukorturk, O. and Hering, B."Failure behavior of pre-cracked concrete beams retrofitted with FRP," *Journal of Composites for Construction*, 3(2):138-44, 1998.

5. Bickley, J.A., Neale, K.W., and Fabbruzzo, G. "Market potential and identification of suppliers of advanced industrial materials for construction of bridges and other structures", Vols. 1 and 2", John A. Bickley Associate, Toronto, Ont, 1993.

6. Cai, H. and Liu, X. "Freeze-thaw durability of concrete: ice formation process in pores", *Cement and Concrete Research*, 28(9), 1281-1287, 1998.

7. Enright, M.P. and Frangopol, D.M. "Survey and Evaluation of Damaged Concrete Bridges", *Journal of Bridge Engineering*, ASCE, 5(1), 31-38, 2000.

8. Fenner, R.T. "Mechanics of solids", CRC Press, Boca Raton, FL, 1999.

9. ISIS. "ISIS Educational Module No. 2: FRP Composites for Construction", ISIS, Canada, 2003.

10. ISIS Canada. "Strengthening reinforced concrete structures with externally-bonded fiber reinforced polymers," Canadian Network of Centres of Excellence on Intelligent Sensing for Innovative Structures (ISIS), Design Manual No. 4, 2001

11. Kim, Y.J., Green, M.F., and Fallis, G.J. "Repair of bridge girder damaged by impact loads with prestressed CFRP sheets", *Journal of Bridge Eng.*, ASCE, 13(1), 15-23, 2008.

12. Karbhari, V.M., *and* Gao, Y. "Composite jacketed concrete under uniaxial compression verification of simple design equations", *J. Mater. Civil Eng.* ASCE 9(4), 1997, pp. 185–193

13. Rizkalla, S., and Labossière, P. "Structural engineering with FRP in Canada", *ACI Concrete International Journal*, 21(10): 25– 28, 1999.

14. Yuan , H., Teng, J. G., Seracino, R., Wu, Z. S., and Yao, J. "Full-range behavior of FRP-to-concrete bonded joints", *Engineering Structures,* 26(5), April 2004, 553-565.

CHAPTER 2. LITERATURE REVIEW

2.1. GENERAL

This chapter represents a selected literature review. With emerging the uses of FRP composites for strengthening of concrete structures; a growth of exponential investigation on their long term serviceability under different environmental conditions has resulted in an enormous amount of published literature. The objective of this chapter is to provide a state-of-the art review of the current progress of relevant research and information related to the aim of this research work. To provide a better understanding of the objective of this extensive research work, the relevant research and information regarding the performance of FRPs exposed to freeze-thaw, wet-dry and combined of them will be reviewed separately in the relevant chapters.

2.2. FRP FOR STRUCTURAL REHABILITATION

Fiber reinforced polymers (FRPs) have been used regularly over more than three decades as one of the most innovative materials in the broad areas ranging from the aerospace industry to prevalent sport goods and facilities. Now, it is well demonstrated that the FRP composites are more durable; can be successfully and safely used in replacing the conventional materials (Niu, 1993). The most attractive properties of FRP includes durability, excellent corrosive resistant, high tensile strength, ease in application, good adhesion characteristics and can be given complex shape without significantly increasing the manufacturing cost; and ability to be pre-fabricated in the factory (Lau et al. 2002). Furthermore, light weight and simple construction equipments can be used for construction with FRP materials; and thus it may reduce the constructions cost and the risk from fatal

accidents. Although FRP materials carrying lots of benefits but the real picture of the application of FRPs in civil engineering construction or rehabilitation is very much disappointed. The utilization of the FRP composites as reinforcements in civil construction is still limited so far due to the lack of appropriate and sufficient knowledge on design guidelines, lack of internationally recognized design specifications and fabrication cost.

The application of FRP in externally strengthened concrete structures has demonstrated as an innovative alternative for conducting major repairs or even total replacement of the deficient structures. FRP can be easily bonded to the tension soffit to improve load-carrying capacity. This procedure has the potential to significantly increase the lifespan of old deteriorated structures (i.e., bridges). Many researchers have paid much attention to the developments of using the FRP in retrofitting and strengthening of concrete structures in the recent years. The implementations of the researches are mainly grouped into five areas which include (Lau et al. 2002):

- Concrete confinement by FRP wrap and grid systems,
- Beam strengthening in flexure by using an externally bonded FRP patch,
- Seismic damage resistance of a concrete column,
- Investigation on the failure mechanisms, and
- Environmental effects of FRP strengthened structures.

2.2.1. History of FRP Composites

While the concept of composite (i.e., bricks made from mud and straw) has been used in constructions for thousands of years, the incorporation of modern FRP composite technology into the construction industrial has emerged less than a century (ACI-440

2007). The age of plastics emerged just after 1900 and the first known FRP product was a boat hull which was manufactured in the mid of 1930s (ACMA MDA 2006). During the World War II, FRP research was encouraged heavily by the defense industry particularly for use in aerospace and naval applications due to their high strength-to-weight ratio and excellent corrosion resistance. Within a very short period of time, FRP composites applications had been flourished in transportation, aerospace, marine, electrical, and corrosion resistance industries. The benefits of FRP composites, especially its corrosion resistance properties, were communicated to the public sector and they became more motivated to use FRP in construction industry. FRP materials were first experimenting as reinforcement into reinforce concrete structures in the mid of 1950s (ACMA MDA 2006). Then in the 1980s, rebirth in interest arose for uses of FRPs in the construction industries when new developments were launched to apply FRP reinforcing bars in concrete constructions. Composites have evolved since the 1950s, starting with temporary structures and continuing with restoration of historic buildings and structural applications.

The applications of composite reinforcing were demonstrated in Europe and Asia during the late 1970s and early 1980s. The world's first highway bridge, using composite reinforcing tendons, was built in Germany in 1986 (ACI-440 2007); then the first FRP composites strengthening of bridge girder was took place in Switzerland in 1991 (ACMA MDA 2006). The first all-composite pedestrian bridge was installed in Aberfeldy, Scotland in 1992. In the United States, the first FRP-reinforced concrete bridge deck was at McKinleyville, West Virginia, built in 1996 followed by the first all composite vehicular bridge deck in Russell, Kansas. Numerous composite pedestrian bridges have been installed in U.S. state and national parks in remote locations not accessible by heavy

construction equipment, or for spanning over roadways and railways (ACMA MDA 2006). Meanwhile, the application of externally bonded FRP for rehabilitation and strengthening of concrete structures, as shown in Fig. 2.1, has made a significant impact within the civil engineering community.

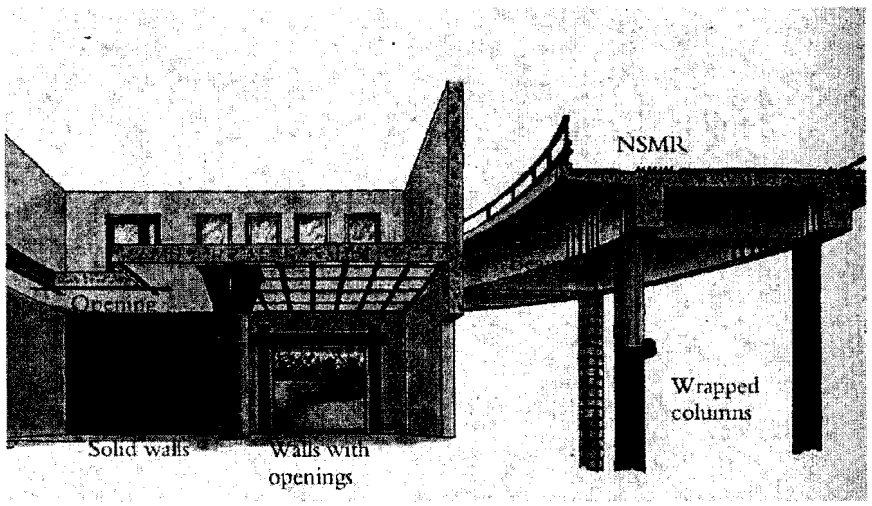

Figure 2.1. Typical application of FRPs to structural elements (McDonnell 2007)

2.2.2. Fiber Reinforced Polymer (FRP)

Fibers Reinforced Polymer (FRP) are composite materials essentially consist of strong fibers set in a resin matrix. The most commonly used fibers in the construction industry are the Carbon, Aramid and Glass fibers, meanwhile the carbon fibers is preferred in most cases due to the excellent environmental properties such as a good resistance against moisture and the excellent mechanical properties like high tensile strength and Young's modulus (Klamer et al. 2008). Whereas, Peter (1999) suggested that Aramid fiber (Kevlar) has many advantages over carbon fiber in reinforcement for concrete structures, which may include (i) low density; (ii) non-catastrophic failure, which can give alerts before failure and thus reduce the risk due to sudden fail; (iii) better impact resistance (it is,

suitable for structures liable to collision damage and seismic disturbances); and (iv) electric insulator (so it can be used close to power lines or communication facilities).

The fibers generally carry the bulk portion of the applied loads in the system. They also provide the strength and stiffness in longitudinal direction. Whereas, the main function of the matrix material is to hold the fibers together and spread the load between the individual fibers, and to protect the fibers against environmental influences (i.e., moisture, corrosion and wear-tears). FRP is one of the recent emerging materials in application for strengthening of reinforced concrete structures. The emergence of FRP composites in the civil engineering industry has been driven by their numerous advantages over steel and concrete, including:

- High strength-to-weight ratio compared to steel
- Higher level of corrosion resistance properties (good for marine environments)
- Light weight & flexibility in shape (ease in installation & reduce construction cost)
- Non electromagnetic properties (glass-FRP and aramid-FRP)
- Low thermal conductivity (glass-FRP and aramid-FRP)
- Can be prefabricated in industries.

Despite their numerous benefits, some disadvantages such as initial cost, brittle failure, and highly susceptibility to temperature are the critical factors that limit the widely acceptance in construction industry. Although, high initial cost may limit the importance or effectiveness to the consumers, but they are often comparable or even cheaper than conventional construction materials in long runs as FRP composites provide longer span of life of a structure. FRP composites are avoided sometimes in construction industry due to their brittle behaviour, experiencing explosive and sudden failure modes which are

undesirable in structures. While this may be the case, the failure strain of FRP is larger than the yielding strain of steel, providing additional warning to those using the structure. Their susceptibility to high temperatures and fire has hindered their use for enclosed structures and the majority of their use to date has occurred in bridges and other outdoor applications. Lastly, many of the design engineers hesitate to use the FRP composites in construction because of the lack of knowledge regarding the long term durability of composite in service state conditions or unfamiliar with the provision of design code for incorporating them into the construction. With large amounts of research having taken place over the past 20 years, and with the results looking promising, it may just be a matter of time before the construction community is compelled to accept these new products.

2.3. ENVIRONMENTAL EFFECTS

2.3.1. Effects of Low Temperature on Concrete

Durability of deteriorated concrete structures under freeze-thaw conditions is a great concern to infrastructure community in cold regions. Many researchers studied the ice formation process in concrete pores which is necessary to evaluate the damages in concrete caused by freezing action. Freeze-thaw durability of concrete has close relationship with its pore structure in concrete. The volume, radius, and size distribution of pores decide the freezing point of pore water and the amount of ice formed in pores (McDonnell 2007). Generally, within a certain temperature interval, water frozen in pore of concrete induces greater internal hydraulic pressure and, consequently, more severe frost damages. The freezing point and the amount of frozen solution (water) in pores reflect the frost durability of concrete. When water in wet concrete freezes, it expands by approximately 9% which creates hydraulic pressures in the pores of the cement paste and aggregate. Once these

pressures exceed the tensile strength of the binding matrix, namely cement, cracks will occur. Typical freeze-thaw damages are shown in Fig. 2.2. Concrete exhibits mild increases in compressive strength, elastic modulus and flexural strength at low temperature (Baumert 1995). Moisture content can have a significant effect on the amount of volume increase, since the strength gain is due primarily to the formation of ice in the pores of the hydrated cement paste (Neville 1997). From experimental result, the increased strength of concrete was recorded due to freezing action; however, it has great concern about the effects of thawing effects (Neville 2002).

Figure 2.2. Example of concrete cracking from freeze-thaw effects (McDonnell 2007)

While the concrete may retain its strength in a frozen state, upon thawing the concrete is left weaker than original condition. The repetition of this process, later referred as freeze-thaw cycling, has the potential to weaken concrete or even destroy it completely without proper air-entertainment, as shown in Fig. 2.3. Current practices employ air entrainment as the main defense against freeze-thaw damage in concrete. When the water in concrete begins to expand during freezing, damage can be avoided if the water can readily escape into adjacent air-filled voids. Air entraining admixtures help to stabilize the

air bubbles produced in a concrete during the mixing process and also introduce small voids into the matrix. The overall result is a greater number and closer spacing of voids in the hardened concrete. The use of air entrainment is the most effective way to increase a hardened concrete's resistance to deterioration from freezing and thawing cycles. The air entrainment also increases the paste volume and acts as a lubricant. This allows for the reduction in the water to cement ratio of the mix while retaining the same workability. The higher paste volume also reduces the unit weight of the concrete and some believe promotes a better surface finish (Day 1995). There may be a decrease in bleeding of the mix and reduction in segregation of the aggregate during pumping and after placement.

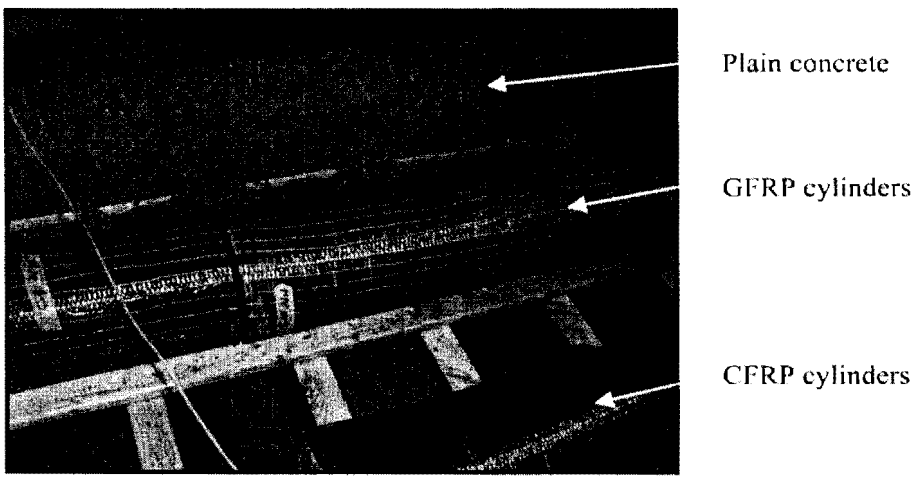

Figure 2.3. Reinforced concrete cylinders following freeze-thaw cycling (Kong 2005)

However, there are some disadvantages to the use of air entrainment. Too much air trapped in the paste serves to weaken it, resulting in lower concrete strength and possible lower durability. Even at recommended doses, the strength of the concrete will be lower than non air-entrained concrete, unless the allowable reduction in water to cement ratio is made. This reduction will often offset any strength loss due to the admixture. It has been found that air entrainment between 5 to 8% provides sufficient protection for normal and

high-strength concrete exposed to freeze-thaw cycling (Neville 1995). Additionally, it is recommended that the concrete should have a water-cement ratio less than 0.45, a minimum cement content of 335 kg/m^3, adequate drainage, a minimum of seven days of moist curing above 10°C, a minimum 30 day drying period after curing, and a minimum compressive strength of 24 MPa at the time of first frost exposure (Neville 1995). If these conditions are met, detrimental effects due to freeze-thaw should be minimal. It has been found that the rate of concrete expansion (Table 2.1) changes with temperature.

Table 2.1. Coefficients of thermal expansion of partially dried concrete

Experiment	Temperature(°C)	Co-efficient of Thermal Expansion(/°C)
Yamane(1978)	20	12×10^{-6}
	–70	10×10^{-6}
Browne & Bamforth(1981)	20	$10 \times 10^{-6} – 12 \times 10^{-6}$
	–165	$5 \times 10^{-6} – 6 \times 10^{-6}$

2.3.2. Effects of Low Temperature on FRP

Very little literature has been reported on the mechanical properties of FRPs when exposed in elevated low temperature, namely cold temperature and freeze-thaw. When FRP materials exposed to cold weather conditions or freeze-thaw environments, two basic effects may occur i) thermal incompatibility between fibers and matrix due the mismatch of thermal expansion, and ii) polymer embrittlement (Green 2007, Täljsten et al. 2007). The first effect is related to the thermal expansions of the constituent materials such as fibers and polymer matrix. Some researchers (Dutta et al. 1995) reported slight negative coefficient of thermal expansion (CTE) for CFRP in the range of -0.5×10^{-6} to -0.1×10^{-6} /°C, and relatively high positive coefficient of thermal expansion for the polymer matrices in the range of 45×10^{-6} to 120×10^{-6} /°C. Whereas, Mufti et al. (1991) reported that CTE

of most of the matrix in FRP, namely epoxy resins, are in the range of 45 to 65 × 10^{-6}/°C; meanwhile, glass fibers have a coefficient of 5 × 10^{-6}/°C, carbon fibers generally have a slightly negative coefficient in the range between –0.2 to 0.6 × 10^{-6}/°C. Due to the considerable differences between the coefficient of thermal expansions of fibers than those of matrices, temperature changes may develop internal stresses (FRP's necessity to undergo in a uniform strain) in the FRP composites at the fiber-matrix interface. The resulting tensile stresses in the matrix render it susceptible to micro-cracking. Dutta et al. (1995) address low temperature effects on fiber composite and concluded that low temperature might produce internal stresses in composites of polymeric materials. The polymeric matrix becomes stiffer, and may suffer from damage-induced stresses resulting from thermal coefficient mismatch of fibers and resins. This concept is shown in Fig. 2.4. While this can also affect the bond between the concrete and FRP in case of flexural strengthening of concrete members, but this is not a critical issue for wrapped cylinders. The introduction of thermal cycling can increase the size of these cracks, allowing them to propagate in the resin matrix and ultimately lead to strength degradation or failure (Dutta 1989). Raiche (1999) investigated the long term durability of FRP (CFRP and GFRP) composites under different environmental effects such as moisture, temperature and deicing salts. Elastic modulus of the FRP composites materials was almost constant before and after environmental exposure. CFRP products showed excellent material properties under harsh environmental to GFRP product, despite higher water absorption. The combined effect of moisture and temperature was more aggressive than the presence of deicing salt for both composites.

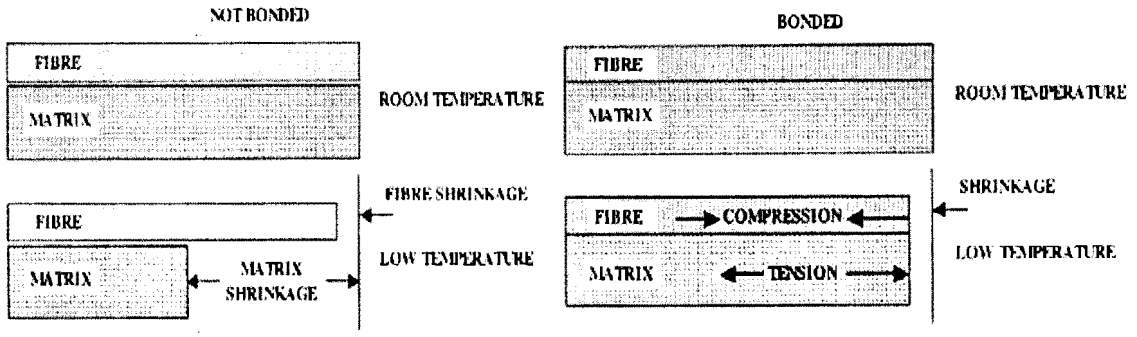

Figure 2.4. Stresses in bonding line incompatibility of matrix and fibers (Dutta 1989)

2.3.3. Effects of Moisture

The effect of humid or water on CFRP retrofitted systems may lead to the degradation of the matrix and the adhesive bonded joint. Carbon fibers are not highly affected by water (Hollaway and Leeming 2003). Most adhesives can absorb moisture by surface absorption and diffusion. Usually the moisture concentration increases initially with time until reaching saturation after several days of exposure to humid atmosphere. Moisture uptake depends on several factors including thickness of material, void content, polymer type, temperature and presence of microcracks (Alfar 2006). The degree of moisture absorption is aggravated when adhesives are exposed to temperatures above glass transition values, i.e., adhesives in the rubbery form tend to absorb more water than in the rigid form. Water may plasticize, induce relaxation and swell the adhesives causing degradation in the mechanical properties (Alfar 2006). The elastic moduli and strengths are significantly reduced by water-induced plasticization (Mays and Hutchinson 1992). Also, water may lead to unwanted chemical reactions in the polymers causing depress their glass transition temperatures (Hollaway and Leeming 2003). Drying can reverse the process but may not result in complete attainment of original mechanical properties. It was concluded

from several research studies that the exposure to aqueous solutions had a significant detrimental effect on the retrofitted systems, with most degradation at the level of the adhesive layer between the composite and the concrete (Karbhari et al. 2003).

2.3.4. Cold Temperature Effects on Bond between FRP and Concrete

Internal stresses between fibers and matrix interface may occur at elevated cold temperature that may cause micro-crack in the matrix or the matrix-fibers interface during freezing as discussed earlier section. These cracks can degrade the mechanical properties (i.e. strength, impact resistance, fatigue life, and stiffness) of FRP composites. Another important factor also should take into account. Thermal co-efficient of resins and concrete are also different as discussed earlier section. So under low temperature strain incompatibility may occur and this can affects the FRP-strengthening process. The differences in the coefficients of thermal expansion between concrete and CFRP sheets could damage the bond of CFRP-concrete interface (Kaiser 1989). He studied a plain concrete beam reinforced with CFRP and freezed up to –60 °C. At this elevated low temperature, the plate did not debond. This test result could not convince researchers enough because he tested only one beam at this temperature. Dutta et al. (1995) tested small-scale beams (1.0 m and 2.0 m spans) strengthened with CFRP sheets at low temperature (–28 °C). It reported a degradation of the strength of the strengthened beams due to short-term, low-temperature exposure. It should be noted here that all the beams failed in a shear-peeling mode; however, the ultimate strength of the CFRP sheets was not tested. Although some tests have been conducted on CFRP at low temperature, the author is not aware of any other studies that have considered bonding properties of CFRP sheets at low temperature. Tommaso et al. (2001) investigated the influence of temperature ranging

from -100°C up to 40°C on the strengthened RC (Reinforced Concrete) beams. A reduced failure load was recorded in both high and low temperatures as compared to the control specimens. Furthermore, different types of failure modes were also found depending on the applied temperature, for example at −100°C temperature bond delamination of CFRP strengthened technique was observed.

As each constituent material (concrete, epoxy and polymers) of an FRP strengthened concrete member have different co-efficient of thermal expansion as discussed earlier, at elevated low temperature, concrete and epoxy may expand whereas the carbon fibers become shorten and hence peeling force may developed in between the interface, and finally, these interactions between the materials may also contribute to the overall performance of the strengthened system. In near surface mounted (NSM) strengthened system the bond deterioration showed more detrimental as compared with externally-bonded FRP-strengthening because a greater thickness of polymer resin is typically required for NSM systems. The coefficient of thermal expansion of concrete is sensitive to moisture content, but is usually assumed to be between 10 and 12 × 10^{-6}/°C over the range of 20°C to −70°C (Baumert 1995). Again, this represents a full order of magnitude difference compared to typical epoxy resins, potentially causing thermal stress and possible bond deterioration between the resin and the concrete. Polymer embrittlement is caused by an increase in the strength and stiffness of epoxies at low temperature (Täljsten et al. 2007). The increased stiffness may also reduce the effectiveness of the polymer resin to transfer stress between the fibers and concrete (Green 2007). It is worth noting that freeze-thaw cycling may also have a significant effect on the behaviour of FRP strengthened members.

2.4. CONCLUSION

After receiving much attention and praise in other industries, research is showing that FRP has an enormous potential as a means of strengthening and rehabilitating concrete structures in cold regions. The application of FRP to the concrete members has the ability to significantly improve strength and performance. Despite, some obstacles, looks to be a large piece of the puzzle in solving our society's sizeable infrastructure crisis.

From the literature review, it could be said that elevated low temperature may cause damage in composites and reduce the capacity of epoxy that may use for bonding FRP to concrete. Low temperature may produce internal stresses in composites of polymeric materials. The polymeric matrix might be stiffer and suffer from damaged induced stresses resulting from thermal coefficient mismatch of fibers and resin.

In order to make the construction industry and engineers more confident with the use of FRP, studies are being conducted to look at their durability in various harsh environmental conditions. A complete discussion on this topic is given in the subsequent chapters.

2.5. REFERENCES

1. ACI440. "Report on fiber-reinforced polymer (FRP) reinforcement for concrete structures." *ACI Committee 440.XR-07, American Concrete Institute*, Farmington Hills, Michigan, USA, 2007, pp.100.

2. ACMA MDA. "*American composites manufacturers association market development Alliance*," Arlington, Virginia, 2006, USA.

3. Alfar, A. "Durability of reinforced concrete members strengthened with CFRP plates and subjected to moisture and salts," M.S. thesis, University of Jordan, Jordan, June, 2006.

4. Al-Salloum, Y. A., Alsayed, S. H., and Almusallam, T. H. "Effect of aggressive environments on strength of RC beams strengthened with composite laminates," *46 th International SAMPE Symposium*, May 2001, pp. 485-496.

5. Apicella, A., Nicolais, L., Astarita, G., and Drioli, E. "Effect of thermal history on water sorption, elastic properties and the glass transition of epoxy resins," *Polymer,* V 20, 1979, pp. 1143–1148.

6. Bao, L.R., Yee, A.F., and Lee, C.Y.C. "Moisture absorption and hygrothermal aging in a bismaleimide resin," *Polymer*, V. 42, No. 17, 2001, pp. 7327-7333.

7. Browne, R.D., and Bamforth, P.B. "The use of concrete for cryogenic storage: A summary of research, past and present." *Proceedings of the 1st International Conference on Cryogenic Concrete*, the Concrete Society, March 1981, London, pp. 135-166.

8. Day, K.W. "Concrete mix design, quality control and specification," 1st ed., Chapman and Hall, London, England, 1995, pp. 1-265.

9. Dutta, P. K. "Fiber composite materials in arctic environments," *Proceedings of the sessions related to structural materials at Structures Congress*, 1989 (ASCE), San Francisco, California, USA, 1989, pp. 216-225.

10. Ekenel, M., and Myers, J. J. "Effect of environmental conditioning & sustained Loading on the fatigue performance of RC beams strengthened with bonded CFRP fabrics," *Submitted to ACI Materials Journal*, September 2004.

11. Grace, N. F. "Concrete repair with CFRP," *Concrete International*, V. 26, No. 5, May 2004, pp. 45-52.

12. Green, M.F. "FRP repair of concrete structures: performance in cold regions," *Int. J. Materials and Product Technology*, Vol. 28, No. 1/2, 2007, pp. 160-177.

13. Green, M. F., Bisby, L. A., Beaudoin, Y., and Labossiere, P. "Effect of freeze-thaw cycles on the bond durability between fibre reinforced polymer plate reinforcement and concrete," *Canadian Journal of Civil Engineering*, V. 27, No. 5, October 2000, pp. 949-959.

14. Hand H.M., Arah C.O., McNamara D.K., and Mecklenburg M.F. "Effects of environmental exposure on adhesively bonded joints," *International Journal of Adhesive and Adhesion*, V. 11, No. 1, 1991, pp. 15-23.

15. Hollaway, L., and Leeming, M., "Strengthening of Reinforced Concrete Structures", Washington DC, CRC Press LLC, 2003.

16. Klamer, E. L., Hordijk, D, A., and Hermes, M.C. "The influence of temperature on RC beams strengthened with externally bonded CFRP reinforcement," *HERON,* V. 53, No. 3, 2008.

17. Karbhari, V.; Chin, J.; Hunston, D.; Benmokrane, B.; Juska, T.; Morgan, R.; Lesko J.; Sorathia U.; Reynaud, D. "Durability Gap Analysis for Fiber-Reinforced Polymer Composites in Civil Engineering", *Journal of Composite Construction*, ASCE, Vo. 7, No. 3, pp.238-247, 2003.

18. Lau, K. T., Zhou, L. M., Cheung, P. T., and YUAN, L. "Applications of composites, optical fibre sensors and smart composites for concrete rehabilitation: an overview," *Applied Composite Materials 9*, 2002, pp. 221–247.

19. Mays, G., and Hutchinson, A., "Adhesives in Civil Engineering", Cambridge University Press, Redwood Press ltd, UK, 1992.

20. McDonnell, T. F. "Effect of mineral admixtures and coarse aggregate size on compressive strength and freeze-thaw resistance of Portland cement concrete," M.S. thesis, University of Akron, Akron, OH, 2007.

21. Miller, B., and Nanni, A. "Bond between CFRP sheets and concrete," *ASCE 5th Materials Congress*, Cincinnati, OH, L.C. Bank, Editor, May 10-12, 1999, pp. 240-247.

22. Mufti, A., Erki, M., and Jaeger, L. "Advanced composite materials with application to bridges," *Canadian Society of Civil Engineering*, Montreal, Quebec, 1991, pp. 21-70.

23. Myers, J.J., and Shen, X. "Effect of Surface Roughness and Putty Thickness on the Bond Performance of FRP Laminates," *Center for Infrastructure Engineering Studies*, Report Number 03-41, October 2002.

24. National Climatic Data Center (NCDC), *Climate watch magazine*, 2010, available online at http://www.ncdc.noaa.gov/oa/ncdc.html.

25. Neville, A. M. "Properties of concrete," John Wiley & Sons Inc., 2002, New York, USA.

26. Neville, A. M. (1995). "Properties of concrete", 4th ed., John Wiley & Sons Inc., New York, New York, USA.

27. Niu, C. M. "Airframe structural design, practical design information and data on aircraft structures," Technical Book Company, California, USA, 1993, pp. 65.

28. Raiche, A. "Durability of Composite Materials used as external reinforcement for RC beams," *Annual Conference of the American Society for Civil Engineering*, Regina, Saskatchewan, Canada, 1999, pp. 155-164.

29. Ren, H., Hu, A., and Zhao, G. "Freeze-Thaw Resistance Behavior of Bonded Joints between FRP and Concrete,' *Journal of Dalian University of Technology*, V. 43, No. 4, July 2003, pp. 495-499.

30. Peter, E. 'Strengthening and Protecting Concrete', *Advanced Composite Bulletin*, September 1999, 8.

31. Sen, R., Shahawy, M., Mullins, G., Spain, J. "Durability of Carbon Fiber-Reinforced Polymer/Epoxy/Concrete Bond in Marine Environment," *ACI Structural Journal*, V. 96, No. 6, November/December 1999. pp. 906-914.

32. Staunton, R. "Environmental Effects on Properties of Composites," Handbook of composites, Van Nostrand Reinhold Co., New York, 1982, p. 514-530.

33. Toutanji, H. A., and Gomez, W. "Durability Characteristics of Concrete Beams Externally Bonded with FRP Composite Sheets," *Cement and Concrete Composites*, V. 19, 1997, pp. 351-358.

34. Yamane, S., Kasami, H., and Okumo, T. "Properties of concrete at Very Low Temperatures." *International Symposium on Concrete and Concrete Structures*, ACI SP-55, 1978, pp. 207-221.

CHAPTER 3. MATERIAL PROPERTIES

3.1. SYNOPSIS

Carbon fiber reinforced polymer (CFRP) composites are a promising alternative to conventional construction materials. CFRP composites, consisting of carbon fibers and an epoxy adhesive, may be bonded on the tensile soffit of deteriorated concrete structures to increase load-carrying capacity. The benefits of such a strengthening method include a favorable strength-to-weight ratio, non-corrosive characteristics, good fatigue and chemical resistance, prompt execution on site, and reduced long-term maintenance expenses. Although significant amounts of research efforts have been reported on CFRP-strengthening applications for concrete structures, very limited information is available in the area of constitutive material responses of bonding agents and materials properties of CFRP sheets subjected to cold regions environments, which may govern the performance of CFRP-strengthening systems. This chapter presents an experimental program to study the constituitive material characteristics of adhesives for CFRP sheets subjected to harsh environment conditions, such as wet-dry, freeze-wet-dry, freeze-thaw, and various constant low temperatures (0 °C, -10 °C, -20 °C, and -30 °C). These environmental conditions are particularly important for cold regions applications of CFRP-strengthening. Key parameters in this study include: duration and number of wet-dry, freeze-wet-dry, freeze-thaw up to 150 cycles that are equivalent to 3,600 hours, and different levels of constant cold temperature effects up to 2,000 hours. A total of 100 double-lap shear specimens are tested in monotonic load to examine the bond response and corresponding failure modes. The presence of moisture provides additional curing to the adhesives during environmental

cycles. The bond strength of the adhesives, however, decreases when the number of wet-dry cycles increases from 50 to 150. The failure mode of the control specimens is governed by cohesion, whereas the failure of the environmentally-cycled specimens is dominated by interfacial debonding.

This chapter also discusses materials properties of CFRP sheets subjected to harsh environmental conditions, including the effect of freeze-wet-dry up to 100 cycles that are equivalent to 400 hours of exposure to water, 1,600 hours freeze at - 30°C, and 400 hours of dry at room temperature. The CFRP specimens are exposed to a constant temperature of - 30°C for 2,400 hours. A total 20 CFRP coupons are tested in monotonic load to examine the tensile strength and tensile modulus. Initially tensile strength shows an increasing trend up to 75 cycles and then decreases when the freeze-wet-dry cycles increases from 75 to 100. The tensile elastic modulus of the CFRP, however decreases when the number of freeze-wet-dry cycle increases.

3.2. INTRODUCTION

Deterioration of infrastructure is a critical issue over the world. Typical sources of deterioration include increased service loads, corrosion damage, and sulphate attack (Kim et al. 2006). The effect of environment is particularly important for civil structures situated in cold regions (Kim and Yoon 2010). Cold weather climates necessitate the extensive use of deicing salts on roads and bridges, resulting in corrosion damage of reinforcing steels and deterioration of concrete. Rehabilitation may be a cost-effective alternative to replacement of deteriorated structures. Carbon fiber reinforced polymer (CFRP) composite for structural strengthening is a state-of the art rehabilitation method. The benefits of CFRP applications include a favorable weight-to-strength ratio, non-corrosive characteristics,

strong chemical and fatigue resistance, and reduced long-term maintenance costs (Bakis et al. 2002; Teng et al. 2003; Kim and Heffernan 2008). Epoxy adhesives are widely used to bond CFRP composites to the tensile soffit of deteriorated structures. The bond characteristics of an adhesive may govern the performance of CFRP-strengthening systems. Although significant amounts of research efforts have been made for concrete structures strengthened with CFRP composites, relatively limited information is available in the area of constitutive material responses of bonding agents themselves and mechanical properties of CFRP sheets subjected to harsh environmental conditions. To ensure the adequate performance of CFRP composites bonded to civil structures, the durability of bonding agents as well as CFRP sheet requires a thorough understanding. This chapter presents a experimental works regarding the behavior of epoxy adhesives and CFRP sheets subjected to different aggressive environments, which is particularly important for cold regions applications of CFRP-strengthening.

3.3. DURABILITY OF EPOXY ADHESIVE

Epoxy adhesives for bonding CFRP composites may be exposed to cold regions environments. The presence of moisture and thermal stresses in epoxy resins can influence the behavior of adhesives, including the degradation of bond strength. Cold temperature may cause matrix hardening, micro-cracking, and bond degradation of adhesives (Crasto and Kim 1996; Green 2007). According to test results (Ashcroft et al. 2001), mechanical behavior of epoxy adhesives was sensitive to temperature variations. For example, the modulus of elasticity, yield strength, and load-carrying capacity of adhesives decreased when temperature increased. Moisture causes plasticization and swelling of adhesives (Minford 1993; Bao et al. 2001), which may decrease the bond strength (Hand et al. 1991).

The effect of moisture may generate irreversible damage along the interfacial bond line (Bowditch 1996). Moisture diffusion can create micro-cavities inside an adhesive that may induce permanent damage of the adhesive (Apicella et al. 1979). Failure modes of epoxy adhesives may be dependent upon the amount of moisture (Al-Harthi et al. 2004; Comrie et al. 2006; Loh at al. 2002). In addition, thermal coefficients of epoxy and CFRP are also different as discussed in Chapter 2. So under elevated low temperatures strain incompatibility may occur and this can affect the performance of CFRPs.

3.4. EXPERIMENTAL PROGRAM

3.4.1. Materials

As this investigation aims at studying the long-term behavior of CFRP-strengthened structures under severe environments, it is important to understand the properties of the materials that have been used in this investigation. This is especially true for the adhesives. There are many different types of structural adhesives that are used as bonding agents, which may react differently under different environments. The FRP composites and adhesive materials selected for this research work were mostly representative of typical materials used in previous concrete repair research programs. Furthermore, adhesive was selected from good reputation materials available at the market place, on the basis of their well defined properties for providing a balance of suitable performance under severe environmental conditions (Apicella1979). Structural epoxy adhesives and steel strips used for this investigation are briefly described.

3.4.1.1. Steel Strips

To evaluate the constitutive characteristics of epoxy adhesives subjected to harsh environmental conditions, a simple double-lab shear test consisting of steel strips (100 mm

long × 38 mm wide × 6.4 mm thick) bonded with an epoxy adhesive was conducted. Table 3.1 shows mechanical properties of the steel strip (ASTM A36) used for the present study.

3.4.1.2. Epoxy Adhesive

The epoxy encapsulation resin used was a two-part system, including saturant resin (Part A) and hardener (Part B) (MBrace 2007). The saturant resin was premixed for 3 minutes. The hardener was, then, blended with the resin and mixed together until a homogeneous mixture was obtained. The mix ratio of the two components was 3 to 1 for the resin and the hardener, respectively (MBrace 2007). Table 3.1 shows typical material properties of the adhesive used for the present study.

Table 3.1. Mechanical properties of Steel strips and epoxy adhesive

Property	Steel strips	Epoxy Adhesive [a]
Modulus of Elasticity, E (GPa)	200	>1.5
Tensile strength, f_y (MPa)	>250	>30
Poison ratio, υ	0.30	0.40
Strain at yield, ε_{ult}	0.2%	2.5%

[a]: manufacturer (MBrace 2007)

3.4.2. Specimen Configuration

A double-lap shear specimen was used to examine the bond performance of adhesives, as shown in Fig. 3.1. The double-lab shear test assures that the bonding agent is subjected to pure shear without any bending effect that is commonly observed in a single-lap shear test (Custodio et al. 2009). A total of 100 specimens were fabricated. Prior to applying the adhesive, the surface of the steel strips was prepared with a mechanical grinder and cleaned with acetone. The surface with and without the preparation is shown in Fig. 3.2(a). The mixed epoxy adhesive was applied on the surface of the steel strips using a

spatula. The assembled double-lap shear specimen was then gently pressed, as shown in Fig. 3.2(b). The specimens were cured for a minimum of 7 days in room temperature.

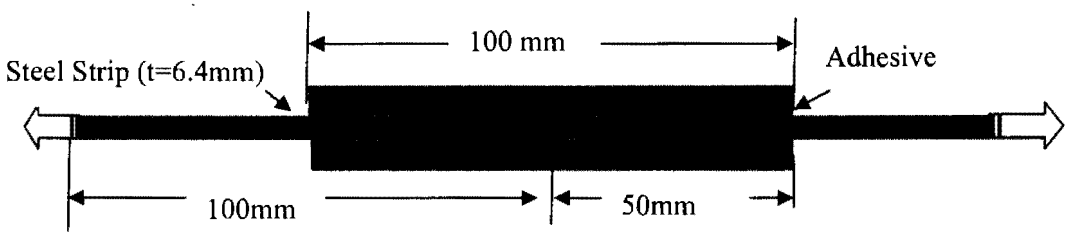

Figure 3.1. Double-lab shear test specimen

3.4.3. Environmental Effects

A total of 100 epoxy coupons were fabricated. Tables 3.2-3.7 summarize the environmental simulation studied here, including the constant cold temperatures (0°C, -10 °C, -20 °C and -30 °C), wet-dry, freezing-submersing-drying and freeze-thaw cycles. Five epoxy coupons tested at room temperature as control (shown in Table 3.2) and 95 coupons were sub-categorized into Task I and Task II and exposed to different environmental conditions. The environmental simulations for Task I and Task II were different in terms of duration and freezing temperatures.

Tables 3.3 and 3.4 summarize the environmental conditions studied here, including the wet-dry and freeze-thaw cycles. The identification code of test specimens shows the test environments (*WD* = wet-dry and *FT* = freeze-thaw), the number of repetition, and the number of environmental cycles. For example, FT3-25 indicates the third specimen tested in 25 cycles of freeze-thaw. For the wet-dry cycles, the specimens were submerged in a water bath for 8 hours (Fig. 3.3a) and dried for 16 hours in a room temperature (1 cycle). The freeze-thaw cycles included a similar condition, namely, 8 hours of freezing at -20°C (Fig. 3.3b) and 16 hours of thawing at a room temperature (1 cycle). The specimens were

tested at a typical interval of 10, 25, 50, and 100 cycles, as shown in Tables 3.3 and 3.4. The temperature was almost constant at -20 °C and the temperature was measured by a thermometer. The temperature variation of the freezer is shown in Fig. 3.3(c). Tables 3.5-3.7 summarize the environmental conditions studied here for Task II, including the wet-dry and freeze-wet-dry cycles and constant freezing. The identification code of the test specimens shows the test environments (*WD* = wet-dry and *FWD* = freeze-wet-dry), the number of repetition, and the number of environmental cycles. For example, FWD3-150 indicates the third specimen tested in 150 cycles of freeze-wet-dry.

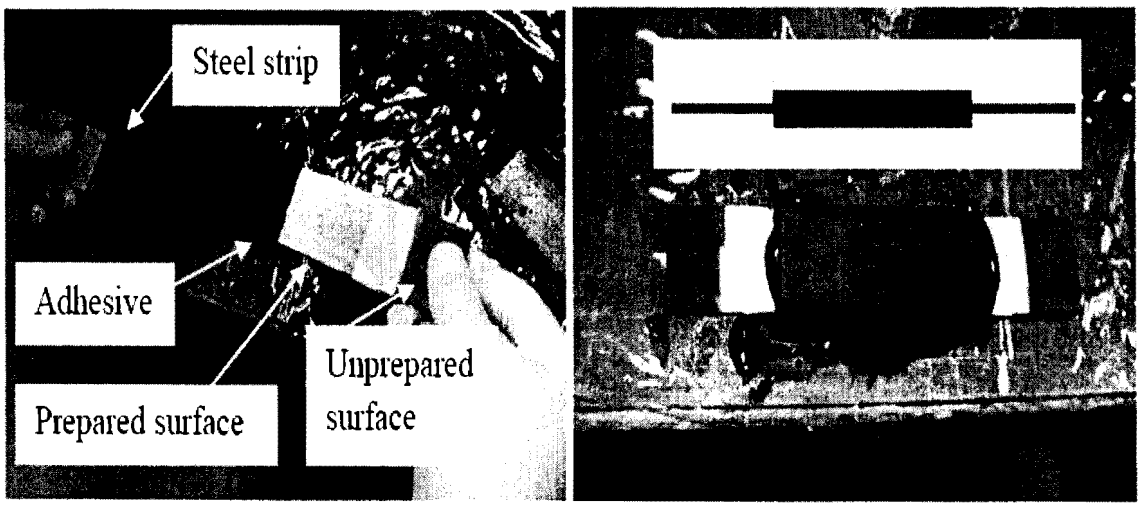

(a) (b)

Figure 3.2. Test specimens: (a) Bonding steel strips; (b) Assembled specimen

For the wet-dry cycles, the specimens were submerged in a water bath for 16 hours and dried for 8 hours in a room temperature (1 cycle). The freeze-wet-dry cycles included a 16 hours of freezing at -30°C, 4 hours of submersing in water bath and 4 hours of drying at room temperature (1 cycle) shown in Fig. 3.3(d). The specimens were tested at a typical interval of 25, 50, 100, and 150 cycles, as shown in Tables 3.5 and 3.6.

The freezer (Fig. 3.4a) used for this research was equipped a digital temperature adjustment function. Temperature was almost constant at -30 °C and the temperature was recorded daily. The temperature variation of the freezer is shown in Fig. 3.4(b). Twenty epoxy coupons were simulated in different constant cold temperatures such as 0°C, -10 °C, -20 °C and -30 °C for 2000 hours. A minimum of 5 epoxy coupons were tested per category as shown in Tables 3.5-3.7.

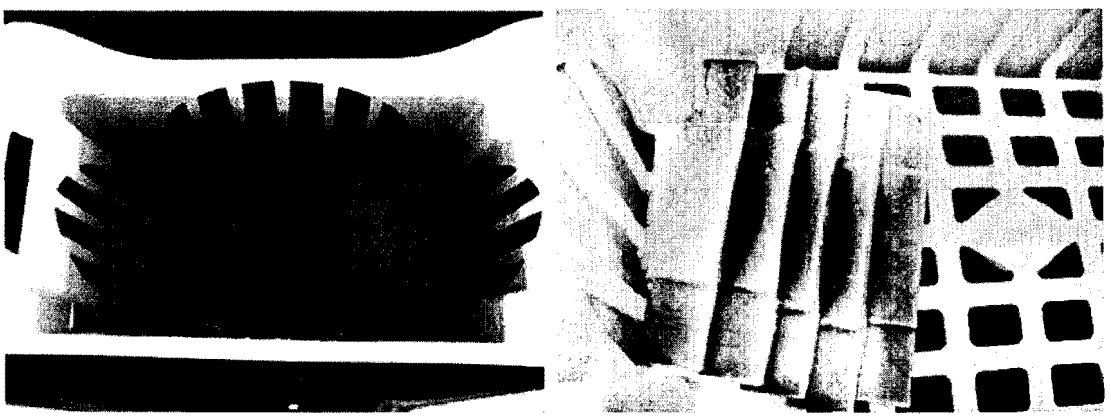

(a) (b)

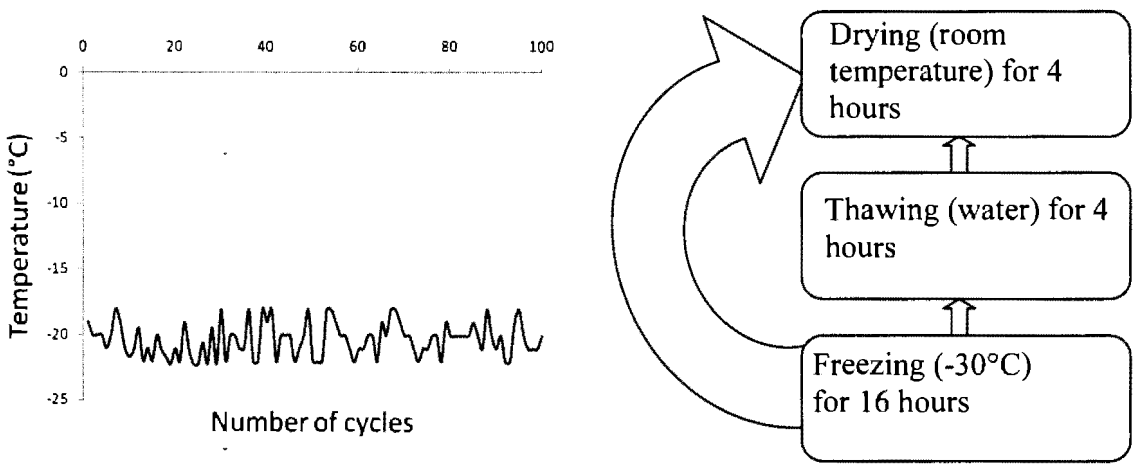

(c) (d)

Figure 3.3. Environmental cycling: (a) water bath; (b) freezing; (c) temperature variation in the environmental chamber for Task I; (d) environmental cycling for Task II

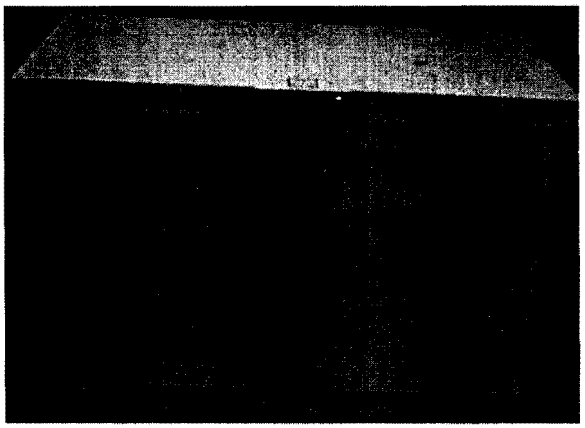

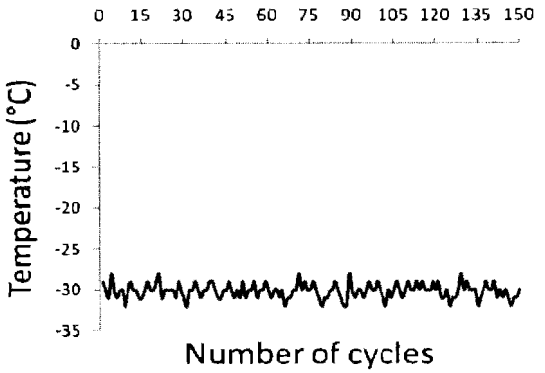

(a) (b)

Figure 3.4. Freezing: (a) environmental chamber; (b) temperature variation in the environmental chamber for Task II

3.4.4. Test Equipment and Loading Information

An MTS 810 servo-hydraulic testing machine was used with a capacity of 1000 kN and a maximum displacement of 500 mm. A tension load was monotonically applied with a rate of 0.5 mm/min until complete failure of the specimen occurred. The clamping area was 38 mm x 50 mm, as shown in Fig. 3.5.

Figure 3.5. A specimen clamped in the testing machine before test starts

3.5. EXPERIMENTAL RESULTS

3.5.1. Load-carrying Capacity (Task I)

Table 3.2 summarizes test results of the epoxy coupons for Task I. The average ultimate load of the control coupons was 15.7 kN [3.5 kips], while the specimens subjected to the environmental effects showed increased load-carrying capacity. The load-carrying capacity of the specimen were increased by 10.2%, 8.3%, and 36.3% in the ultimate capacity in comparison to the control specimens, on average, for the specimens exposed to 10, 25 and 50 wet-dry cycles, respectively, as shown in Fig. 3.6(a),(b) and Table 3.3. The load carrying capacity of the wet-dry cycled specimens, however, reduced when the number of wet-dry cycles increased from 50 to 100, but still 31.8% higher compared to control specimens. These observations indicate that the epoxy adhesive experienced additional curing possibly due to the presence of moisture during the wet-dry simulation up to 50 cycles and then the moisture effect degraded the strength of the adhesive. The specimens subjected to freeze-thaw cycles exhibited different responses. The load carrying capacity was consistently enhanced up to 50 cycles, as shown in Fig. 3.6(a),(b) and Table 3.4. The load-carrying capacity of the specimen were increased by 3.2%, 22.9%, 33.8%, and 17.2% in the ultimate capacity in comparison to the control specimen, on average, for the specimens exposed to 10, 25, 50 and 100 wet-dry cycles respectively, as shown in Fig. 3.6(c),(d) and Table 3.2. This observation may indicate that the strength improvement induced by the moisture curing during the freeze-thaw cycles takes longer when compared to the case of wet-dry, possibly due to the amount of available moisture ingress. Fig. 3.6(a) and (c) showed a comparison of load-carrying capacity of wet-dry and freeze-thaw cycled specimens.

Table 3.2. Test results of control specimens

ID	Environmental effect	Failure load (kN)			Shear stress (MPa)			Slope (N/mm^3)		
		P_u	Ave	S	τ_u	Ave	S	slope	Ave	S
R1	No	14.7	15.7	3.5	3.9	4.1	0.9	58.2	60.9	2.7
R2	No	12.0			3.2			59.0		
R3	No	17.8			4.7			63.4		
R4	No	13.5			3.5			63.1		
R5	No	20.7			5.4			--		

Ave = average; *S* = standard deviation; P_u = ultimate load; τ_u = maximum average shear stress; *Slope* = slope from average shear stress vs displacement diagram

Table 3.3. Test results of wet-dry effects (Task I)

ID	No. of cycling	Failure load (kN)			Shear stress (MPa)			*Slope* (N/mm^3)		
		P_u	Ave	S	τ_u	Ave	S	*slope*	Ave	S
WD1-10	10	12.9	17.3	4.9	3.4	4.5	1.3	63.7	62.7	1.4
WD2-10	10	19.2			5.1			61.7		
WD3-10	10	11.2			2.9			---		
WD4-10	10	22.2			5.8			---		
WD5-10	10	20.9			5.5			---		
WD1-25	25	14.5	17.0	5.4	3.8	4.5	1.4	59.6	60.1	0.8
WD2-25	25	17.4			4.6			60.6		
WD3-25	25	9.8			2.6			---		
WD4-25	25	24.4			6.4			---		
WD5-25	25	19.1			5.0			---		
WD1-50	50	26.6	21.4	8.3	7.0	5.6	2.2	61.2	60.9	4.3
WD2-50	50	33.9			8.9			60.9		
WD3-50	50	20.4			5.4			68.4		
WD4-50	50	22.0			6.5			65.9		
WD5-50	50	24.8			5.8			---		
WD6-50	50	11.4			3.0			---		
WD7-50	50	10.4			2.7			---		
WD1-100	100	21.8	20.7	3.8	5.7	5.4	1.0	50.4	49.2	1.1
WD2-100	100	23.7			6.2			49.0		
WD3-100	100	16.4			4.3			48.2		

Ave = average; *S* = standard deviation; P_u = ultimate load; τ_u = maximum average shear stress; *Slope* = slope from average shear stress vs displacement diagram

The load-carrying capacity increased up to 50 cycles in both cases; however it reduced when the environmental cycling incases from 50 to 100. Average shear stress in both cases showed the same trends as failure loads (Fig.3.7).

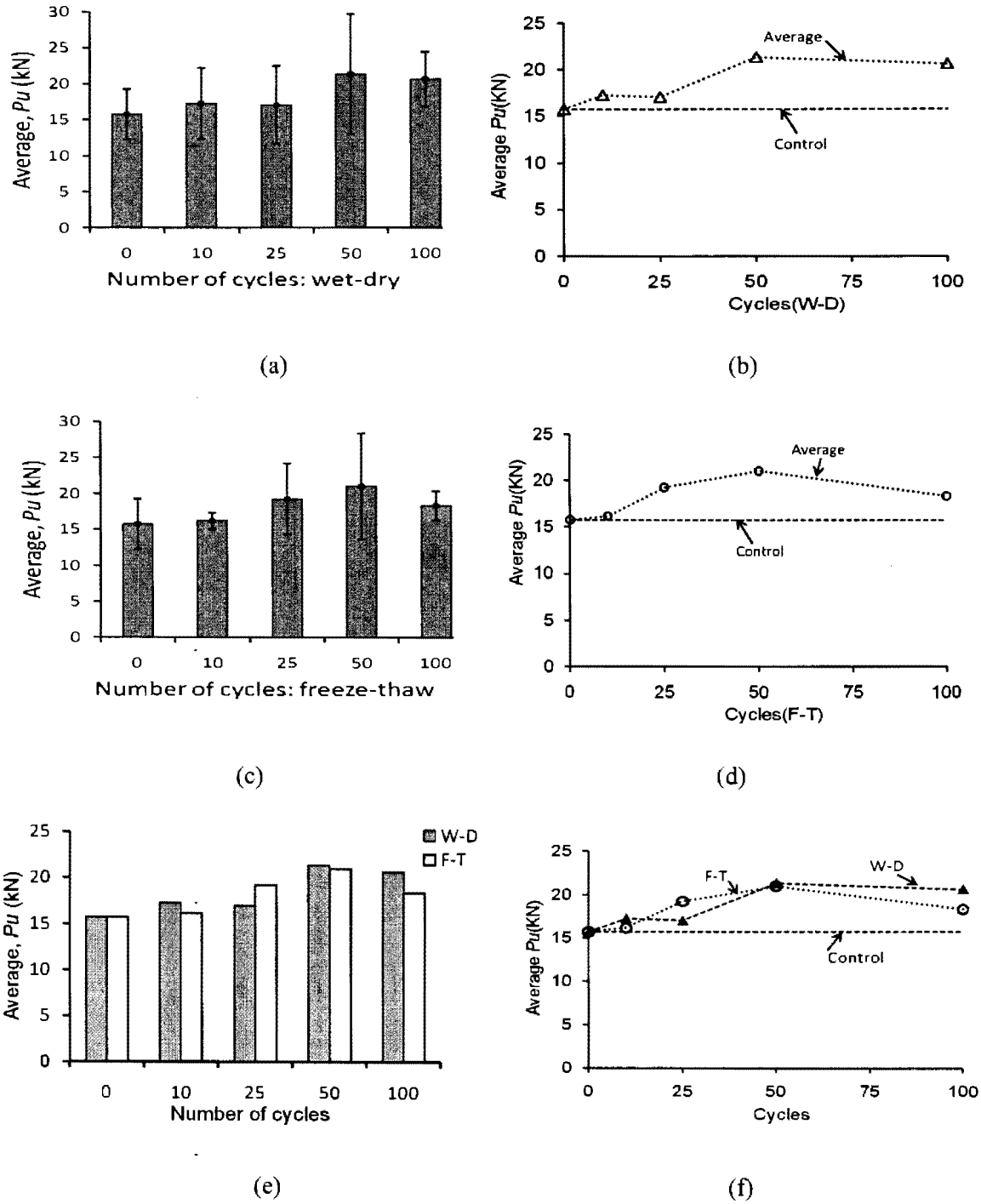

Figure 3.6. Load carrying capacity (Task I): (a) effect of wet-dry cycles; (b) failure Load(W-D); (c) effect of freeze-thaw; (d) failure Load(F-T); (e) failure load comparison; (f) comparisons of the effect of wet-dry and freeze-thaw cycles

A constant stiffness with some variations was observed after the environmental effects up to 50 cycles (Fig. 3.8) and then started to decrease with increasing wet-dry and freeze-thaw cycling. Another observation may indicate that the stiffness was reduced in a little bit higher rate in case of wet-dry than that of freeze-thaw effects (Fig. 3.8f).

The average stiffness tended to decrease within the range studied in the present experimental program, as shown in Fig. 3.8. This observation suggests that water ingression was more detrimental than simple freezing and thawing.

Table 3.4. Test results of freeze-thaw effects (Task I)

ID	No. of cycling	Failure load (kN)			Shear stress (MPa)			*Slope* (N/mm^3)		
		P_u	Ave	S	τ_u	Ave	S	*slope*	Ave	S
FT1-10	10	19.0			5.0			62.6		
FT2-10	10	17.0			4.5			62.4		
FT3-10	10	17.7	16.2	3.5	4.7	4.3	0.8	---	62.5	0.1
FT4-10	10	16.3			4.3			---		
FT5-10	10	10.9			2.9			---		
FT1-25	25	17.4			4.6			62.1		
FT2-25	25	14.5			3.8			59.8		
FT3-25	25	27.6	19.3	1.1	7.3	5.1	1.3	---	60.9	1.7
FT4-25	25	17.8			4.7			---		
FT5-25	25	19.0			5.0			---		
FT1-50	50	31.8			8.4			65.8		
FT2-50	50	28.0			7.4			60.8		
FT3-50	50	21.3	21.0	7.4	5.6	5.5	2.5	68.1	64.9	3.8
FT4-50	50	15.1			4.0			---		
FT5-50	50	8.8			2.3			---		
FT1-100	100	17.3			4.6			50.5		
FT2-100	100	20.7	18.4	2.0	5.4	4.8	0.5	51.9	51.9	1.5
FT3-100	100	17.0			4.5			53.4		

Ave = average; *S* = standard deviation; P_u = ultimate load; τ_u = maximum average shear stress; *Slope* = slope from average shear stress vs displacement diagram

3.5.2. Load-carrying Capacity (Task II)

Tables 3.5-3.7 summarize test results of the epoxy coupons for Task II. The average ultimate load of the control specimens was 15.7 kN [3.53kips], while the specimens

subjected to the environmental effects (wet-dry and freeze-wet-dry cycling) showed slight increasing in the load-carrying capacity initially. The load-carrying capacity of the specimen were increased by 5.1% and 22.3% in the ultimate capacity in comparison to the control specimens, on average, for the specimens exposed to 25 and 50 wet-dry cycles respectively, as shown in Fig. 3.8(a),(b) and Table 3.5. The load carrying capacity of the wet-dry cycled specimen was, however, reduced when the number of wet-dry cycles increased from 50 to 150, but still 11.5% and 10.8% higher in the ultimate capacity in comparison to the control specimens, on average, for the specimens exposed to 100 and

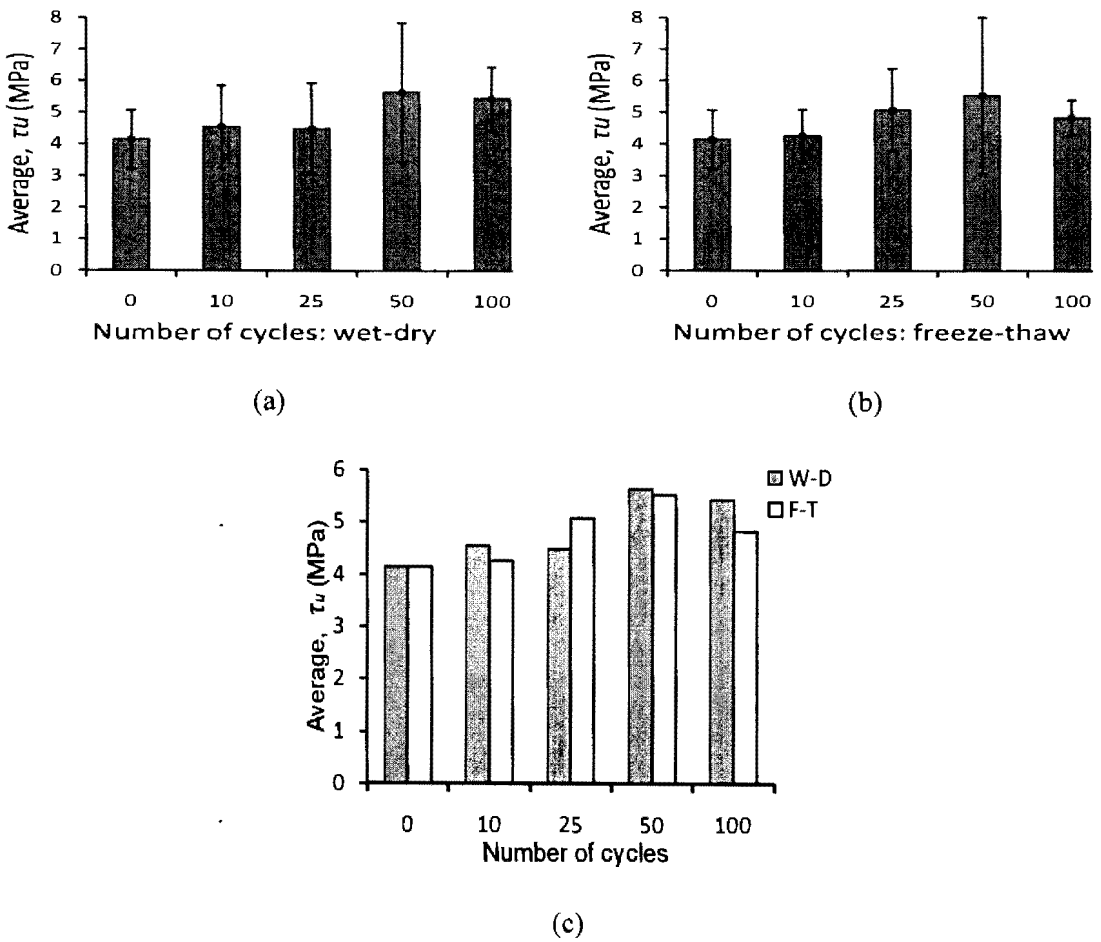

Figure 3.7. Average shear stress (Task I): (a) effect of wet-dry cycles; (b) effect of freeze-thaw cycles; (c) comparisons the effects of freeze-wet-dry and wet-dry cycles

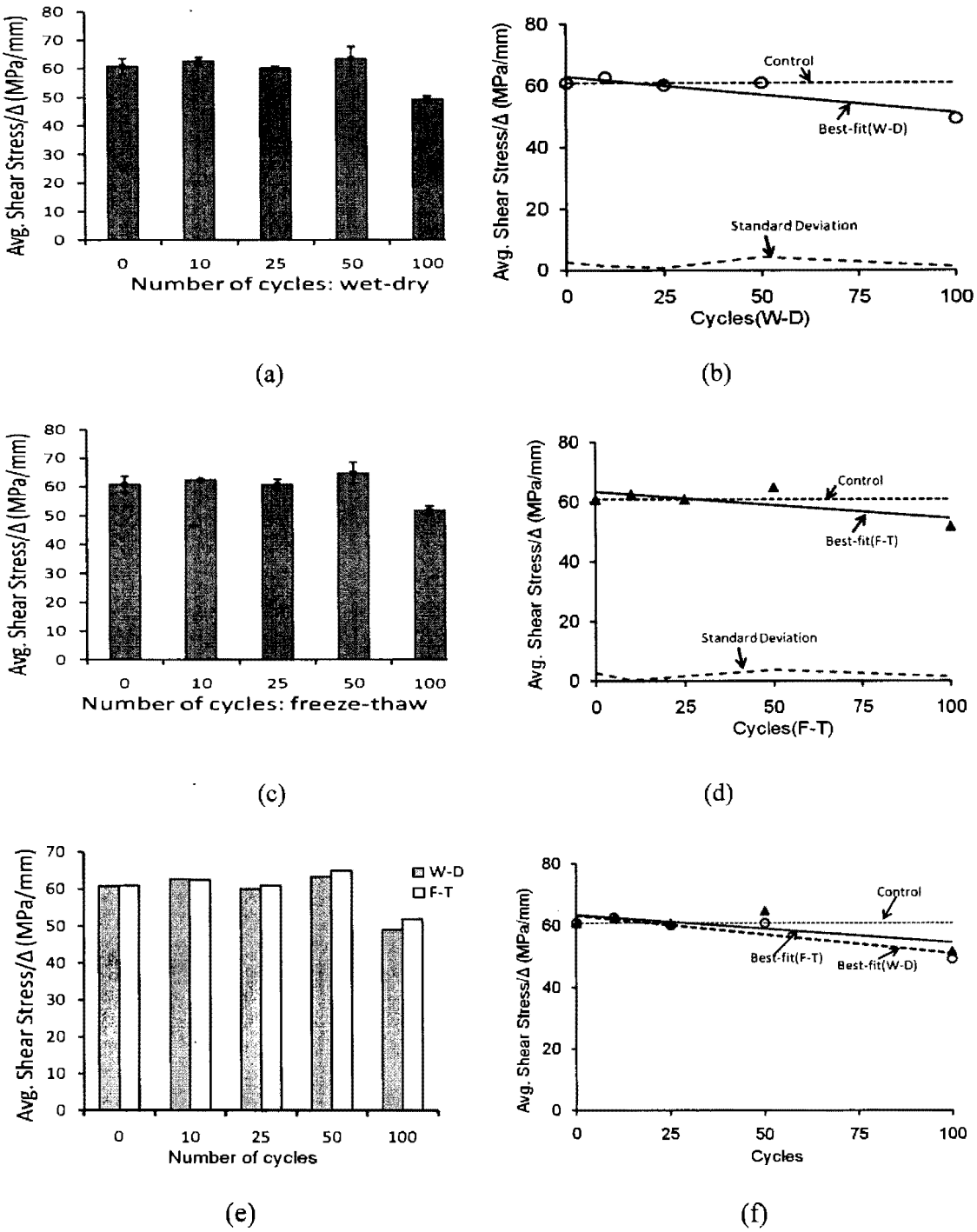

Figure 3.8. Average stiffness (Task I): (a) effect of wet-dry cycles; (b) best-fit (W-D); (c) effect of freeze-thaw cycles; (d) best-fit (F-T); (e) comparisons of the effect of wet-dry and freeze-thaw cycles; (f) stiffness comparison

150 wet-dry cycles respectively, as shown in Fig. 3.9(a), (b) and Table 3.5. These observations indicate that the epoxy adhesive experienced additional curing possibly due to the presence of moisture during the wet-dry simulation up to 50 cycles and then the moisture ingression degraded the strength of the adhesive. The specimens subjected to freeze-wet-dry cycles exhibited almost same trend responses. The load carrying capacity was consistently enhanced up to 50 cycles, as shown in Fig. 3.9(c), (d) and Table 3.6. The load-carrying capacity of the specimen were increased by 4.5%, and 15.9% in the ultimate capacity in comparison to the control specimens, on average, for the specimens exposed to 25 and 50 freeze-wet-dry cycles respectively, as shown in Fig. 3.9(c), (d) and Table 3.6.

The load carrying capacity of the freeze-wet-dry cycled specimens was, however, reduced when the number of freeze-wet-dry cycles increased from 50 to 150, but still 3.2% and 8.3% higher in the ultimate capacity in comparison to the control specimens, on average, for the specimens exposed to 100 and 150 freeze-wet-dry cycles respectively, as shown in Fig. 3.9(c), (d) and Table 3.6. 3.9(a) and (c) showed a comparison of load-carrying capacity of wet-dry and freeze-wet-dry cycled specimens. The load-carrying capacity increased up to 50 cycles in both cases, however, it was reduced when the environmental cycling incases from 50 to 150. Average shear stress in both cases showed almost the same trends as failure loads (Fig.3.10).

This observation may indicate that the effect of freezing-wet-dry was more detrimental than the simply wet-dry effects in respect to ultimate load carrying capacity. A slight increasing trend in stiffness was observed up to 50 environmental cycles and then tended to decrease with increasing environmental effects.

The average stiffness tended to be decrease within the range studied in the present experimental program, as shown in Fig. 3.11. Another observation may indicate that the stiffness reduced in little bit higher rate in case of wet-dry than that of freeze-wet-dry effects.

Table 3.5. Test results of wet-dry effects (Task II)

ID	No. of cycling	Failure load (kN)			Shear stress (MPa)			*Slope* (N/mm^3)		
		P_u	Ave	S	τ_u	Ave	S	*slope*	Ave	S
WD1-25	25	9.1	16.5	3.1	2.4	4.4	0.8	58.8	60.2	1.9
WD2-25	25	19.1			5.0			63.4		
WD3-25	25	14.0			3.7			59.9		
WD4-25	25	13.8			3.6			59.7		
WD5-25	25	19.2			5.1			59.0		
WD1-50	50	21.6	19.2	1.7	5.7	5.1	0.4	70.0	67.1	2.6
WD2-50	50	17.8			4.7			64.9		
WD3-50	50	18.3			4.8			66.4		
WD4-50	50	19.2			5.0			64.4		
WD1-100	100	21.0	17.5	2.2	5.5	4.6	0.9	45.3	42.9	5.7
WD2-100	100	14.6			3.9			35.1		
WD3-100	100	18.3			4.8			48.4		
WD4-100	100	13.3			3.5			50.9		
WD5-100	100	16.2			4.3			47.9		
WD6-100	100	21.3			5.6			49.5		
WD1-150	150	12.2	17.4	3.8	3.2	4.6	1.0	43.1	38.6	9.1
WD2-150	150	19.2			5.1			39.2		
WD3-150	150	21.0			5.5			25.7		
WD4-150	150	17.2			4.5			46.5		

Ave = average; *S* = standard deviation; P_u = ultimate load; τ_u = maximum average shear stress; *Slope* = slope from average shear stress vs displacement diagram

3.5.3. Cold Temperature Effects

Table 3.7 and Fig. 3.12 show comparisons of load-carrying capacity, average shear stress and stiffness variations at room and different low temperatures such as 0°C, -10 °C, -20 °C and -30 °C. It can be seen that in all cases specimens constantly freezing at different low temperatures had higher ultimate failure loads, average shear stress and stiffness than

that of the room temperature specimens. This suggests that there was no detrimental effect from the constantly low temperature exposure.

Table 3.6. Test results of freeze-wet-dry effects (Task II)

ID	Number of cycling	Failure load (kN)			Shear stress (MPa)			*Slope* (N/mm^3)		
		P_u	Ave	S	τ_u	Ave	S	*slope*	Ave	S
FWD1-25	25	12.7	16.4	3.0	3.3	4.3	0.8	64.3	62.4	1.8
FWD2-25	25	17.6			4.6			61.8		
FWD3-25	25	17.0			4.5			62.6		
FWD4-25	25	20.5			5.4			62.7		
FWD5-25	25	14.3			3.8			60.8		
FWD1-50	50	14.3	18.2	3.9	3.8	4.8	1.0	67.8	68.4	1.1
FWD2-50	50	19.9			5.2			70.2		
FWD3-50	50	13.1			3.4			68.6		
FWD4-50	50	21.7			5.7			68.2		
FWD5-50	50	17.4			4.6			68.5		
FWD6-50	50	22.6			6.0			67.0		
FWD1-100	100	14.7	16.2	3.3	3.9	4.3	0.9	52.3	46.4	4.0
FWD2-100	100	13.7			3.6			40.0		
FWD3-100	100	15.2			4.0			45.3		
FWD4-100	100	23.6			6.2			47.0		
FWD5-100	100	16.4			4.3			48.2		
FWD6-100	100	15.0			4.0			45.6		
FWD7-100	100	15.2			4.0			---		
FWD1-150	150	24.3	17.0	1.7	6.4	4.5	1.3	49.3	47.8	2.6
FWD2-150	150	13.2			3.5			44.8		
FWD3-150	150	16.5			4.3			46.7		
FWD4-150	150	14.2			3.7			50.5		

Ave = average; *S* = standard deviation; P_u = ultimate load; τ_u = maximum average shear stress; *Slope* = slope from average shear stress vs displacement diagram

3.5.4. Failure Mode

Fig. 3.13 shows typical failure modes of test specimens. All of the specimens exhibited shear failure, as schematically shown in Fig. 3.13(a). Two types of failure modes were observed: i) *cohesion failure* where the failure was within the adhesive layer and ii) *debonding failure* where the failure was along the interface between the adhesive and steel

strip. The cohesion failure was a primary determinant for the control specimens, whereas

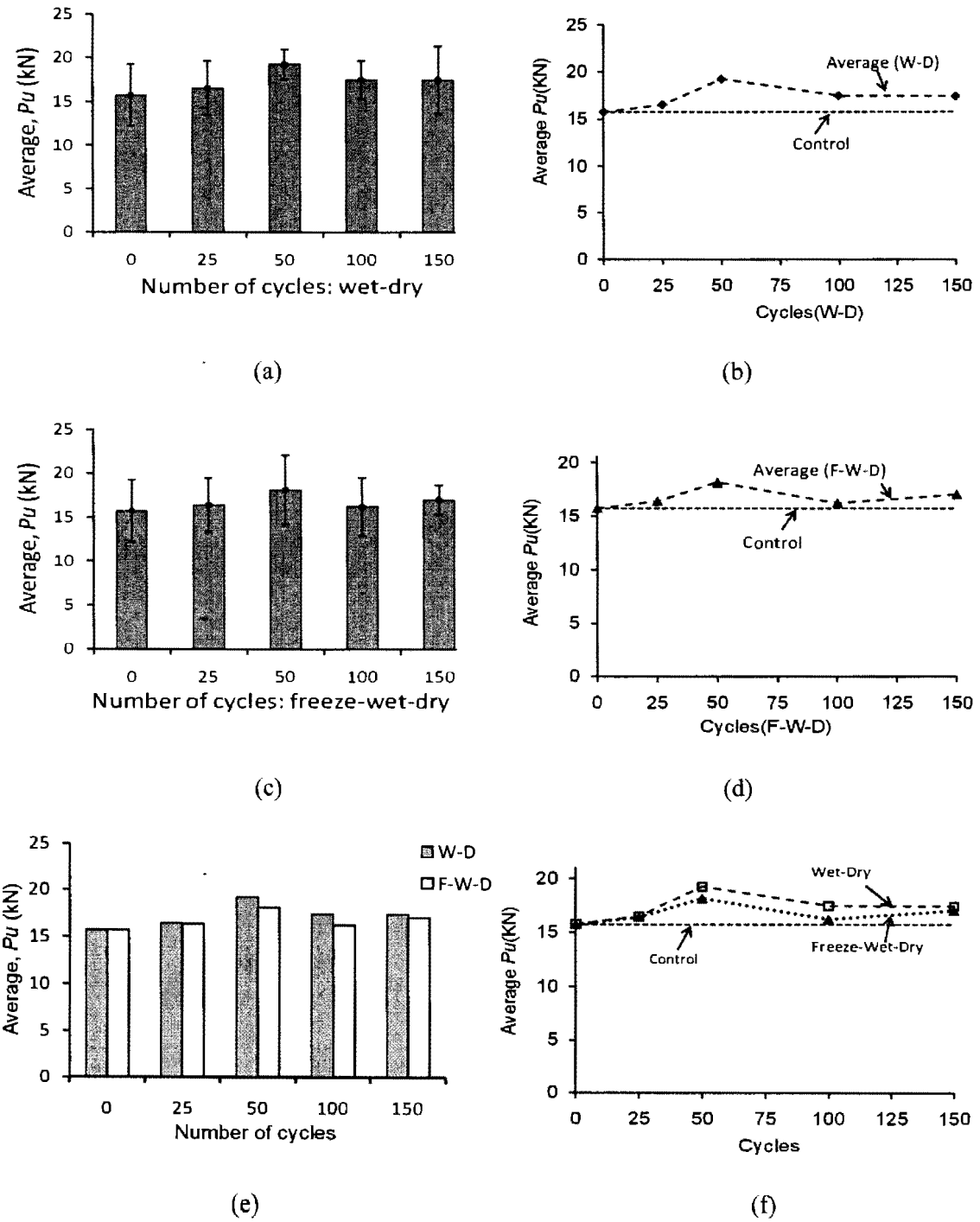

Figure 3.9. Load-carrying capacity (Task II): (a) effect of wet-dry cycles; (b) effect of freeze-wet-dry; (c) failure Load(W-D); (d) failure Load(F-W-D); (e) failure load comparisons; (f) comparisons of the effect of wet-dry and freeze-wet-dry cycles

the debonding was dominant for the environmentally-cycled specimens, as shown in Fig. 3.13. This observation indicates that the bond strength of the control specimens was greater than the material strength (i.e., cohesive strength between constitutive molecules of the adhesive); on the other hand, the material strength was greater than the bond strength of the specimens subjected to the environments (possibly due to the additional curing of the adhesive under the presence of moisture).

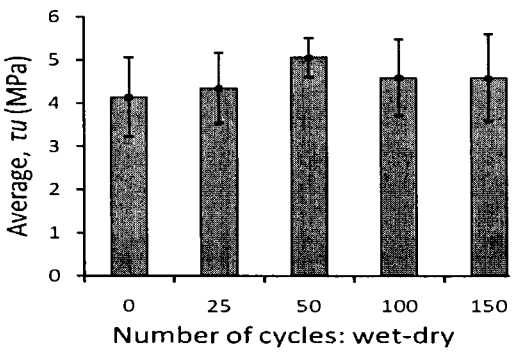

(a)

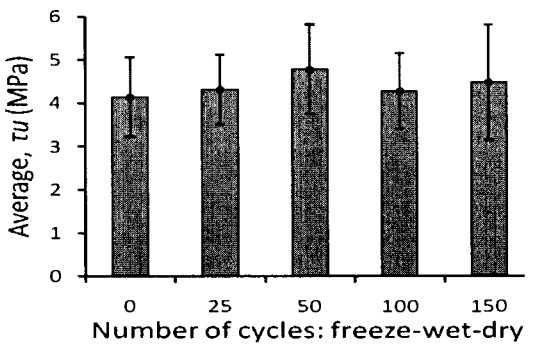

(b)

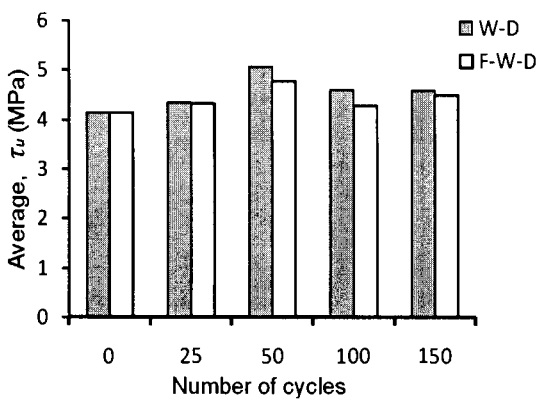

(c)

Figure 3.10. Average shear stress: (a) effect of wet-dry cycles; (b) effect of freeze-wet-dry cycles; (c) comparisons the effects of freeze-wet-dry and wet-dry cycles

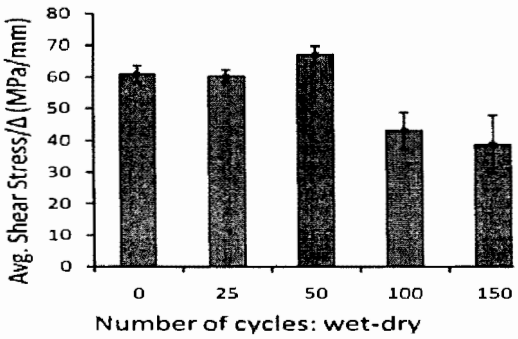

(a)

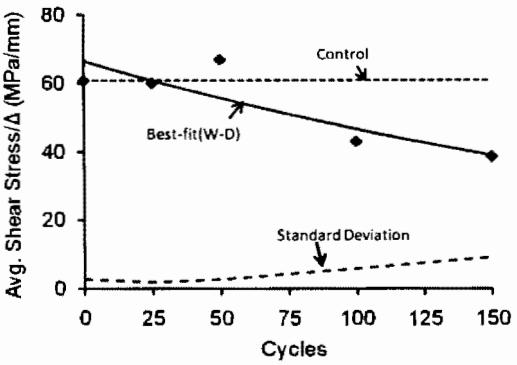

(b)

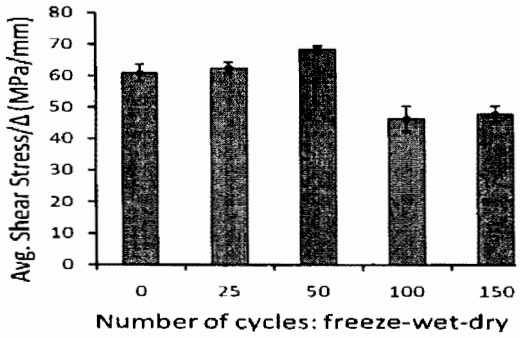

(c)

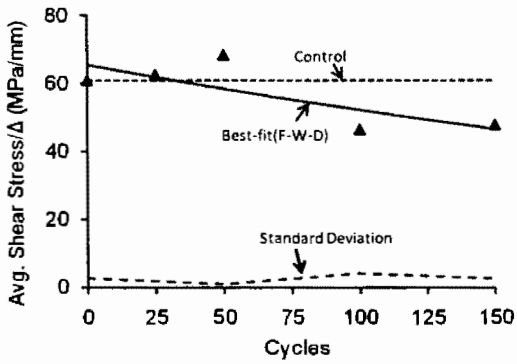

(d)

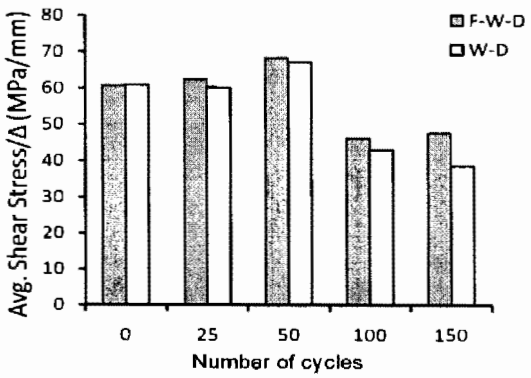

(e)

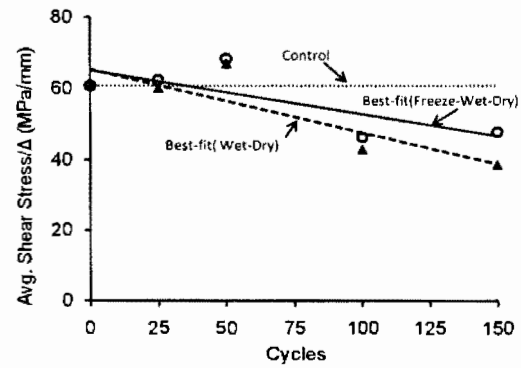

(f)

Figure 3.11. Average stiffness (Task II): (a) effect of wet-dry cycles; (b) effect of freeze-wet-dry; (c) effect of wet-dry cycles; (d) effect of freeze-wet-dry; (e) comparison the effects of wet-dry and freeze-wet-dry cycles; (d) effects of wet-dry/freeze-wet-dry cycles

Table 3.7. Test results of constant freezing for 2000 hours (Task II)

ID	Temperature (°C)	Failure load (kN)			Shear stress (MPa)			*Slope* (N/mm^3)		
		P_u	Ave	S	τ_u	Ave	S	*slope*	Ave	S
CT-0-1	0	17.4	18.2	1.1	4.6	4.8	0.3	65.9	66.3	0.5
CT-0-2	0	18.2			4.8			66.2		
CT-0-3	0	17.4			4.6			66.2		
CT-0-4	0	19.7			5.2			67.1		
CT-10-1	-10	19.8	15.5	3.5	5.2	4.1	0.9	67.0	65.7	1.2
CT-10-2	-10	17.7			4.7			65.3		
CT-10-3	-10	10.6			2.8			64.0		
CT-10-4	-10	14.4			3.8			66.3		
CT-10-5	-10	15.0			3.9			66.1		
CT-20-1	-20	18.3	20.0	2.8	4.8	5.3	0.7	61.6	64.8	2.2
CT-20-2	-20	24.8			6.5			64.5		
CT-20-3	-20	17.9			4.7			67.6		
CT-20-4	-20	19.5			5.1			65.5		
CT-20-5	-20	19.4			5.1			64.9		
CT-30-1	-30	17.8	16.9	1.1	4.7	4.4	0.3	66.0	64.9	1.6
CT-30-2	-30	16.6			4.4			66.2		
CT-30-3	-30	16.6			4.4			62.3		
CT-30-4	-30	15.4			4.0			64.4		
CT-30-5	-30	17.9			4.7			65.6		

Ave = average; *S* = standard deviation; P_u = ultimate load; τ_u = maximum average shear stress; *Slope* = slope from average shear stress vs displacement diagram

3.6. ANALYTICAL MODEL

The equations derived by Yuan et al. (2004) for externally bonded FRPs with concrete as shown in Fig. 3.14 are used for analytically determine the bond strength of epoxy coupons. They described the full-range load displacement curve (Fig. 3.15) in different conditions.

The experimental results obtained from the laboratory testing clearly showed first two states. The equations for first two states (*Elastic stage & Elastic-softening stage),* provided by Yuan et al. (2004) for describing the full range load displacement are used for comparison with experimental plots. The equations for *Elastic stage & Elastic-softening*

stage are discussed below.

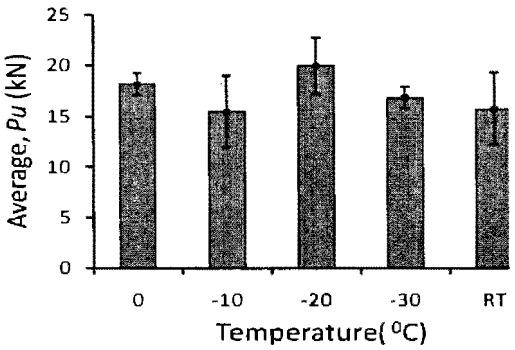

(a)

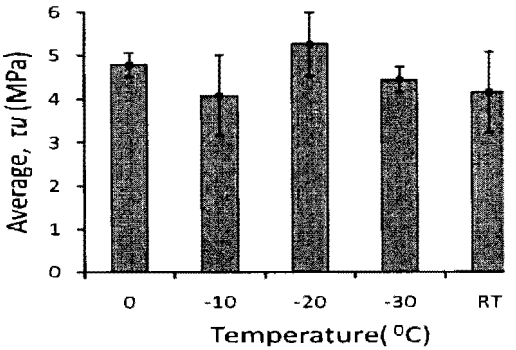

(b)

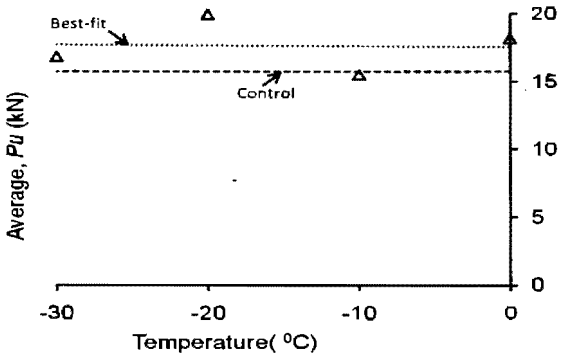

(c)

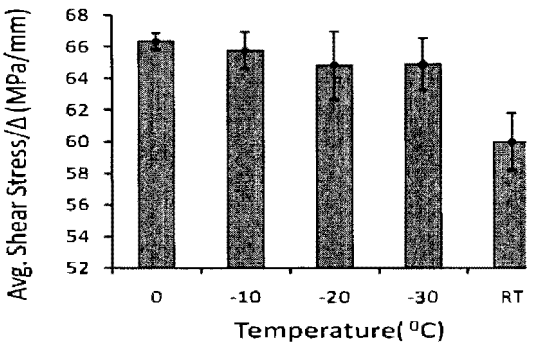

(d)

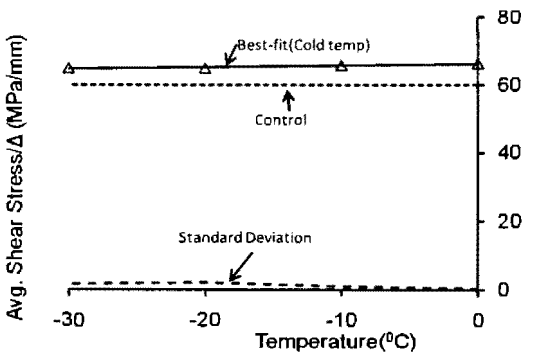

(e)

Figure 3.12. Summary of test results of 2000 hours constant freezing at different low temperatures: (a) average failure load variation with temperature; (b) average stifneess variation; (c) failure load; (d) stiffness variations; (e) effects of cold temperature

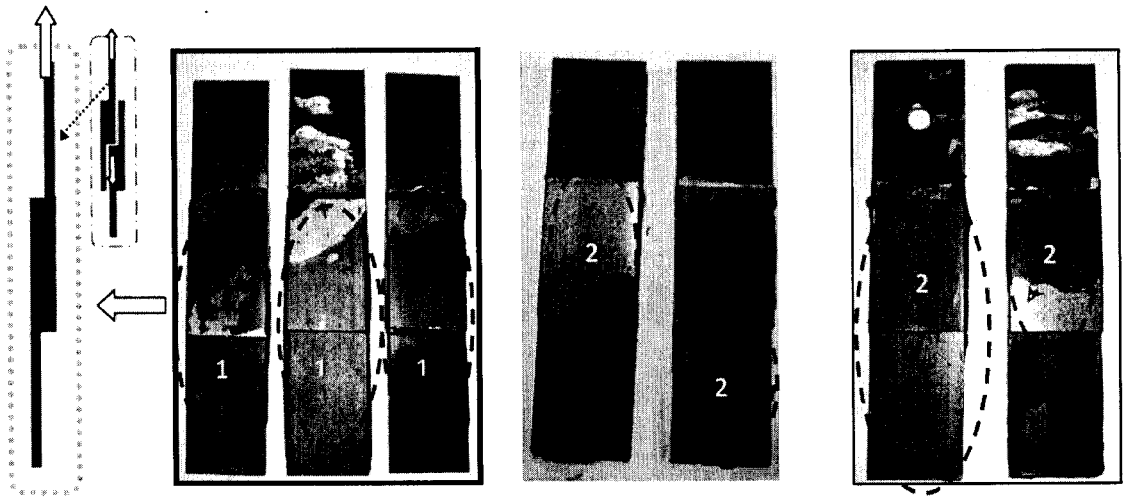

Figure 3.13. Failure mode of test specimens: (a) schematic view of the failed specimen; (b)control; (c) wet-dry; (d) freeze-thaw ([1]: cohesion failure and [2]: debonding failure)

The analysis for the double-strap joint, which is symmetric with respect to both X and Z axis is shown in Fig. 3.16. The width and thickness of the main plate (steel strips) are denoted by b_p (38 mm) and t_p (6.4 mm) respectively, those of the cover plate by b_c (= b_p) and t_c (3.2 mm) respectively, and the bonded length of the plate (i.e. bond length) is denoted by L. The bond length is 50 mm. The Young's modulus of steel strips, E is 200 GP.

Initially, the load is very small, so there should be no crack initiated along the bond line, so the entire bonding surface is in elastic stress state. To describe the elastic state (segment O to A) the following equations may be used (Yuan et al.2004):

$$P = \frac{\tau_f b_p}{\lambda_1}\frac{\Delta}{\delta_1}\tanh(\lambda_1 L) \quad \text{and where } \lambda_1^2 = \lambda^2\frac{2G_f}{\delta_1\tau_f} = \frac{\tau_f}{\delta_1}\left(\frac{1}{E_p t_p} + \frac{b_p}{b_c E_c t_c}\right) \tag{1}$$

where τ_f= Local bond strength, G_f= Interfacial fracture energy, P = Load, and Δ = Axial

displacement. All other parameters are defined in detail in the following pages. Once the shear stress exceeds the elastic limit at the end (x = L) of the joint, the elastic softening stage starts. The segment A to B (elastic softening state) is described by the following equations (Yuan et al. 2004):

$$\delta = (\delta_f - \delta_1)\left\{\frac{\lambda_2}{\lambda_1}\tanh[\lambda_1(L-a)\times\sin[\lambda_2(x-L+a)]-\cos[\lambda_2(x-L+a)]+\frac{\delta_f}{\delta_f-\delta_1}\right\} \quad (2)$$

$$P = \frac{\lambda}{\lambda_2}\left\{\frac{\lambda_2}{\lambda_1}\tanh[\lambda_1(L-a)]\times\cos(\lambda_2 a)+\sin(\lambda_2 a)\right\} \quad (3)$$

$$\Delta = \frac{(\delta_f-\delta_1)}{\delta_f}\left\{\frac{\lambda_2}{\lambda_1}\tanh[\lambda_1(L-a)\times\sin(\lambda_2 a)-\cos(\lambda_2 a)+\frac{\delta_f}{\delta_f-\delta_1}\right\} \quad (4)$$

$$\lambda_2^2 = \lambda^2\frac{2G_f}{(\delta_f-\delta_1)\tau_f} = \frac{\tau_f}{\delta_f-\delta_1}\left(\frac{1}{E_p t_p}+\frac{b_p}{b_c E_c t_c}\right) \quad (5)$$

$$P_u = \frac{\tau_f b_p}{\lambda_2}\frac{\delta_f}{\delta_f-\delta_1}\sin(\lambda_2 a) \quad (6)$$

The parameter, a, may be solved by numerical iteration based on the following equation (Yuan et al. 2004):

$$\tanh[\lambda_1(L-a)] = \frac{\lambda_2}{\lambda_1}\tan(\lambda_2 a) \quad (7)$$

In Fig. 3.16, the co-ordinates of A (Δ_1, P_1) and B (Δ_2, P_2) are elastic limit and elastic softening limit, respectively. The following equations are used to determine the interfacial parameters (Yuan et al. 2004):

$$\delta_f = u_2 \;;\; \delta_1 = u_1\;\tau_f = \frac{P_2^2}{E_p t_p b_p^2 u_2} \;;\; \delta_1 = \frac{P_1^2}{E_p t_p b_p^2 \tau_f} \;;\; G_f = \frac{1}{2}\tau_f\delta_f$$

From the experimental results the following interfacial parameters were obtained as: Displacement at failure, $\delta_f = 0.202$ mm, Average shear stress, $\tau_f = 3.6$ MPa, Interfacial fracture energy, $G_f = \frac{1}{2}\tau_f \delta_f = 0.36 N/mm$, and Elongation at elastic limit

$$\delta_1 = \frac{P_1^2}{E_p t_p b_p^2 \tau_f} = 0.043$$

The experimental load-displacement curve of the three representative epoxy coupons are compared with the analytical solution in Fig. 3.17. The predicted response agreed well with the test data with an error of 4.8% in the ultimate load, on average, compared to the experimental specimen.

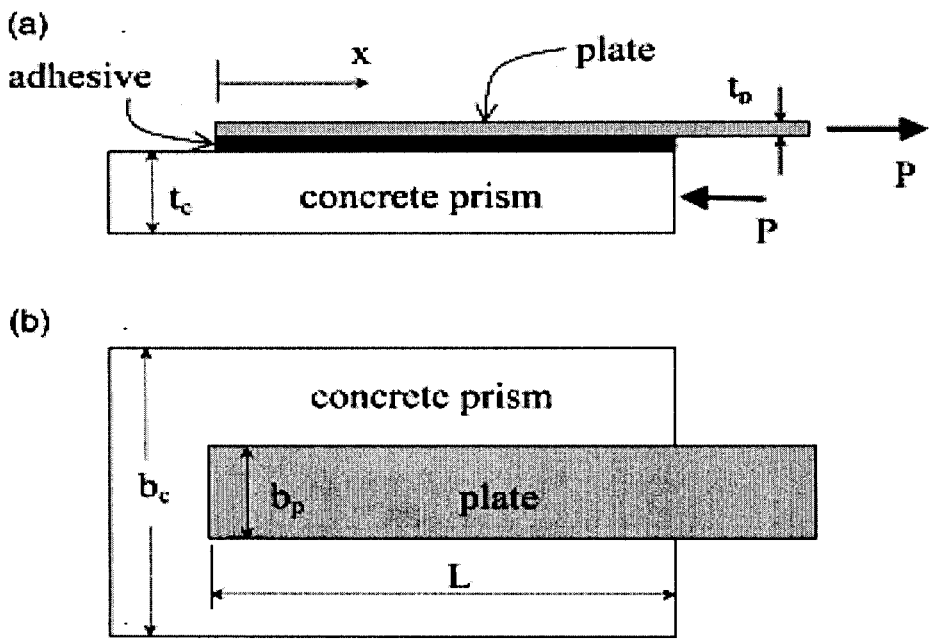

Figure 3.14. Pull–push shear test of a single-lap plate-to-concrete bonded joint: (a) elevation; (b) plan (Yuan et al. 2004)

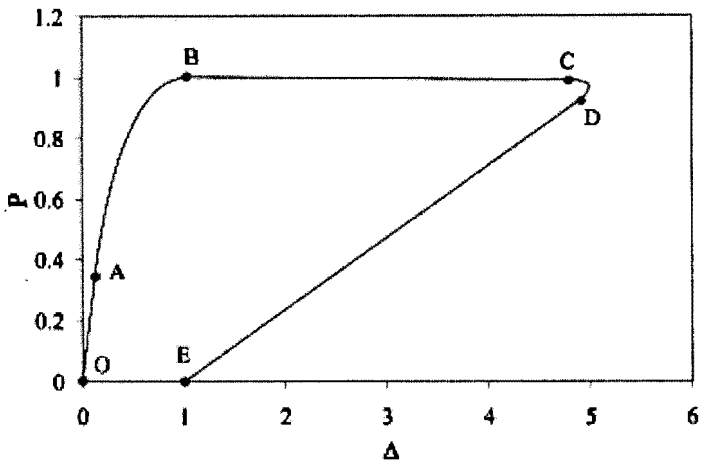

Figure 3.15. Different state of load displacement curve (Yuan et al. 2004)

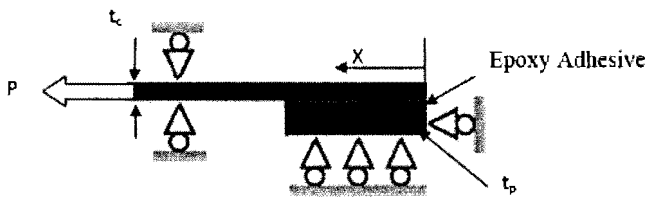

Figure 3.16. Quarter of Double strap joint, boundary conditions and loads

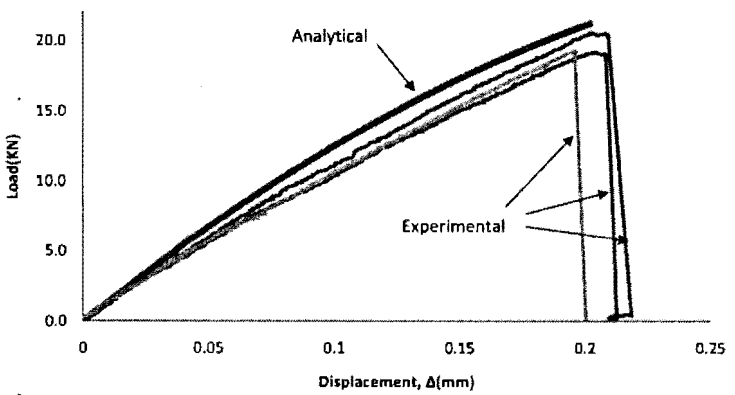

Figure 3.17. Load-displacement response of double strap joints

3.7. MATERIALS PROPERTIES OF CFRP COMPOSITE

3.7.1. Carbon Fiber Reinforced Polymer Sheet

Carbon fiber reinforced polymer sheets used for this research work was MBrace CF 130. CFRP sheets were chosen because of their superior mechanical properties and durability to other types of FRP sheets such as GFRP sheets. CFRP sheets may be used for strengthening concrete and masonry structures by bonding onto the tensile soffit of a member to improve the flexural and shear behaviour. The thickness of the CFRP sheets as specified by the manufacturer was 0.165 mm. The sheets were supplied in a roll form as shown in Fig. 3.18. The mechanical properties of the CFRP sheets are shown in Table 3.8.

3.7.2. Coupon Preparation

The CFRP coupons were tested to obtain actual mechanical properties under harsh environmental conditions after at certain time intervals. Eighteen test specimens (Fig. 3.19) of around 15 mm wide and 200 mm long were prepared and cured for seven days.

Figure 3.18. CFRP sheets uses in the research project

3.7.3. Environmental Effects

Table 3.9 summarizes the environmental conditions studied here, including freeze-wet-dry cycles and constant freezing at -30 °C for 2,400 hours. Same environmental simulation was imposed in this case as was imposed for epoxy coupons of Task II, for example, freeze-wet-dry cycles included a 16 hours of freezing at -30°C, 4 hours of thawing in water bath and 4 hours of drying at room temperature(1 cycle). The specimens were tested at a typical interval of 25, 50, 75 and100 cycles, as shown in Table 3.9. A minimum of 3 CFRP coupons were tested per category based on 3039/D 3039M-00 (ASTM 2005).

Table 3.8. Mechanical properties of CFRP sheet as given by the manufacturer*

Tensile strength, f_f	3800 MPa
Modulus of Elasticity, E	227 GPa
Thickness, t	0.165 mm
Ultimate strain, ε_{frp}	0.0167 mm/mm

manufacturer (MBrace 2007)

Figure 3.19. Some prepared CFRP coupons before testing

3.7.4. Testing and Instrumentation

Testing was performed using an ESTON Machine at a loading rate of 2 mm/min as shown in Fig. 3.20 and load applied up to failure at a loading rate of 2 mm/min. Specimens were placed in the grips of the ESTON and tensioned until failure occurred. An extensometer was used to measure the elongation of the coupons.

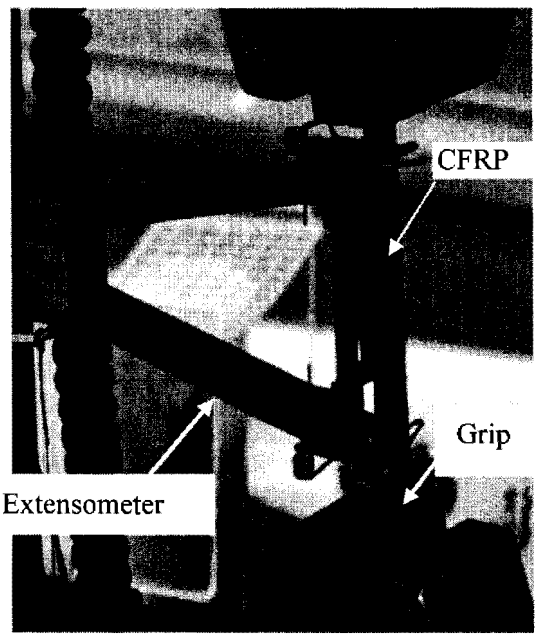

Figure 3.20. Typical CFRP coupons tested in uniaxial tension after exposure to harsh environment

3.7.5. Test Results

The results of eighteen uniaxial tensile coupons of CF-130 CFRP sheets are summarized in Table 3.9. All coupons displayed linear stress strain behavior until failure occurred. Some of the coupons (Coupon1, Coupon5, Coupon10 and Coupon12) showed significantly different stress-strain behaviour than all other tests, this was most likely due to premature failure of the CFRP coupons. The obtained tensile strength, rupture strain and the elastic modulus are shown in Table 3.9. The measure stress-strain responses compared

with that of the manufacturer are shown in Fig. 3.21 and the typical failure mode of the CFRP coupons are shown in Fig. 3.22.

Discounting the erroneous coupon's results, the average tensile strength of the CFRP sheet was found to be 3589 ± 106 MPa, while the average modulus of elasticity and average ultimate strains were found to be 231 GPa and 0.0152 mm/mm respectively for the control specimens. The ultimate tensile strength (f_{ult}) was calculated from the ultimate load divided by the manufacturers specified cross sectional area of 15 mm width and 0.0165 mm thick cross section. The modulus of elasticity (E_f) was calculated between 0 and 3,000 micro-strain according to ASTM D 3039/D 3039M-00 (ASTM 2005).

The following equation was used for the computation of elasticity modulus of FRP, E_f:

$$E_f = \frac{\Delta\sigma}{\Delta\varepsilon} = \frac{\sigma_{3000} - \sigma_0}{\varepsilon_{3000} - \varepsilon_0} \tag{8}$$

where E_f = modulus of elasticity of CFRP specimens; σ_{3000} = stress in the CFRP coupons corresponding to 3,000 micro strain (ε_{3000}) elongation and σ_0, ε_0 were the initial stress and strain, respectively, both were assumed to be zero.

The ultimate strain was calculated, rather than measured from the extensometer, because at higher strain levels localized fiber breakage close to the extensometer caused errors in the strain data. The ultimate strain in the CFRP (ε_{fult}) was calculated based the following equation:

$$\varepsilon_{fult} = \frac{f_{ult}}{E_f} \tag{9}$$

where f_{ult} = ultimate tensile strength and E_f = modulus of elasticity. Table 3.9 summarizes test results of the CFRP coupons. The average ultimate tensile strength was 3589± 106

MPa, while the average modulus of elasticity and average ultimate strains were recorded as 231GPa and 0.0152mm/mm, respectively, for control specimen, which agreed well with the properties provided by the manufacturer (Table 3.8), while the specimens subjected to the environmental effects (freeze-wet-dry) showed slight increasing trend in ultimate tensile stress from 25 to 75 cycles. The ultimate strength of the specimens were increased up to 14.3% and 19.1% in comparison to the control specimen, on average, for the specimens exposed to 50 and 75 freeze-wet-dry cycles, respectively, as shown in Fig. 3.23(a), and Table 3.9. These values, however, decreased when the number of freeze-wet-dry cycles increased from 75 to 100, but still higher in the ultimate capacity in comparison to the control specimen, on average, for the specimens exposed to 100 freeze-wet-dry cycles. These observations indicate that the epoxy adhesive experienced additional curing possibly due to the presence of moisture during the freeze-wet-dry simulation up to 75 cycles and then the moisture effect degraded the strength of the CFRP composites. On the other hand, a slight decrease in the elastic modulus was observed consistently with increasing environmental effects as shown in Fig. 3.23(b). Fig. 3.23 (c) and Table 3.5 show a comparison of the elastic modulus of the specimens exposed to freeze-wet-dry cycles and constant freezing at -30 °C for 2400 hours. It can be seen that specimens subjected to constant freezing had little bit higher ultimate tensile strength (3747 MPa) and elastic modulus (233 GPa) than room temperature specimens as shown in Table 3.5 and Fig. 3.23(c).

Table 3.9. Test Result for mechanical properties of CFRP coupon

No. of Cycles	ID	Ultimate Strength (MPa)			Elastic Modulus, E_f(GPa)			Ultimate Strain (mm/mm)		
		f_{ult} [a]	Ave	SD	E_f	Ave	SD	ε^*_{ult}	Ave	SD
0 (Ctrl)	1	1528	3589	106	108	231	--	0.0141	0.0152	--
	2	3664			362			0.0101		
	3	3514			231			0.0152		
25	4	3574	3574	--	218	219	2	0.0164	0.0109	0.0078
	5	1175			221			0.0053		
	6	2815			172			0.0164		
50	7	4270	4101	236	222	214	7	0.0193	0.0192	0.0008
	8	3831			209			0.0183		
	9	4203			211			0.0199		
75	10	1147	4275	--	200	214	20	0.0058	0.0123	0.0092
	11	4275			228			0.0188		
	12	1112			290			0.0038		
100	13	4018	4013	7	176	201	9	0.0229	0.0149	0.0063
	14	4007			207			0.0194		
	15	2027			195			0.0104		
Constant freezing at -30 ^{0}C for 2400h	16	2925	3747	--	210	233	32	0.0139	0.0112	0.0038
	17	2182			256			0.0085		
	18	3749			317			0.0118		
Manufacturer[1]		3800±20% (3040-4560)			227±20% (182-272)			0.0167±20%		---

[a]:Strength between 3040-4560 MPa includes for Average/Standard Deviation Computations; [1]: As quoted by Watson Bowman Acme (www.wbacorp.com); *: Ultimate Strain=Ultimate Strength/Elastic Modulus; *Ave* = average; *SD* = standard deviation

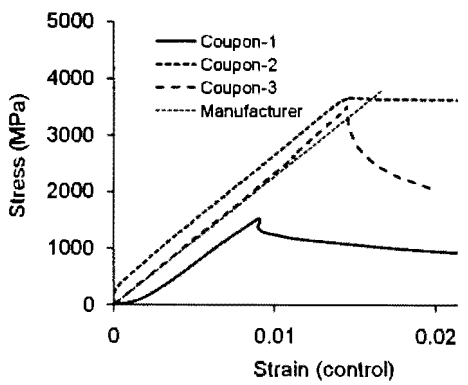

Figure 3.21. Stress-strain response of control specimens

Figure 3.22. Failure of CFRP coupons in tension

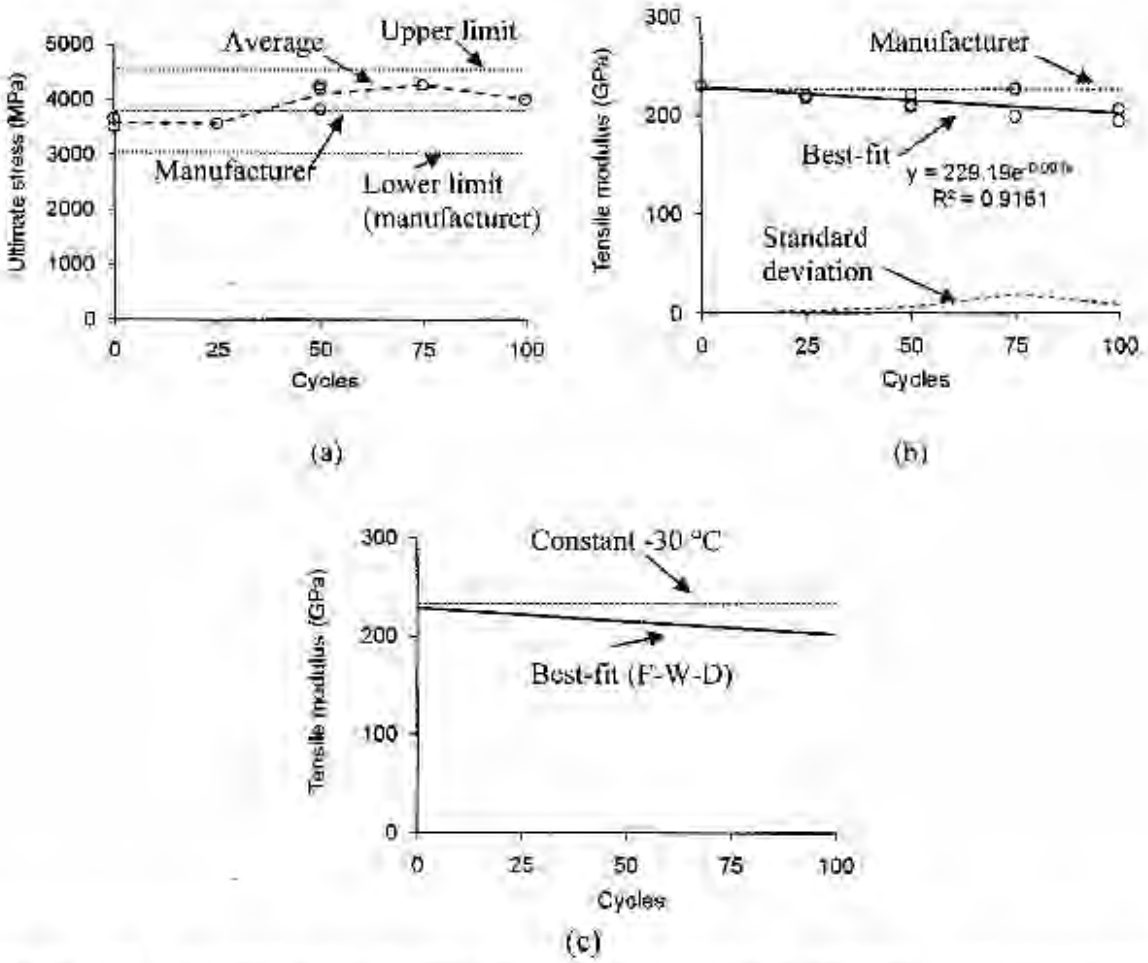

Figure 3.23. Test results: (a) ultimate tensile stress; (b) elastic modulus; (c) elastic modulus comparison

3.8. DISCUSSION AND CONCLUSION

This chapter has presented the constitutive material characteristics of epoxy adhesives and CFRP sheets that may be used in infrastructure repair subjected to wet-dry and freeze thaw environments. A total of 100 double-lap shear specimens were monotonically tested. The test results included bond characteristics of the test specimens, depending upon the environmental cycles and corresponding failure modes. The presence of moisture improved the bond strength of adhesives, in particular notable for the first 50 cycles of wet-dry and freeze-wet-dry. When the number of wet-dry/freeze-wet-dry cycles increased from 50 to 150, the bond capacity of the specimens tended to decrease. On the other hand, specimens exposed to constant cold temperatures showed very little or no variation in ultimate load carrying capacity as well as stiffness properties. In case of CFRP composite, ultimate tensile strength increased with increasing environmental effects which was particularly notable for the first 75 cycles, however strength tended to decrease after 75 cycles. On the contrary, the elastic modulus showed a consistently decreasing tends, however constant freezing didn't affects the material properties of CFRP coupons up to 2400 hours freezing at -30 ^{0}C.

3.9. REFERENCES

1. Al-Harthi, M., Kahraman, R., Yilbas, B., Sunar, M., and Aleem, A.B.J. "Influence of water immersion on the single-lap shear strength of aluminum joints bonded with aluminum powder- filled epoxy adhesive," *Journal of Adhesion Science and Technology*, V. 18, NO. 15-16, 2004, pp. 1699-1710.

2. Apicella A, Nicolais L, Astarita G, and Drioli E. "Effect of thermal history on water sorption, elastic properties and the glass transition of epoxy resins," *Polymer*, V. 20, No. 9, 1979, pp. 1143-1148.

3. Ashcroft, I.A., Abdel Wahab, M.M., Crocombe, A.D., Hughes, D.J., and Shaw, S.J. "The effect of environment on the fatigue of bonded composite joints. Part I: testing and fractography", *Composites:* Part A, 32(1), 2001, 45–58.

4. ASTM Standard D 3039/D 3039M. "*Standard Test Method for Tensile Properties of Polymer Matrix Composite Materials*", Annual Book of ASTM Standards, American Society of Testing Materials, West Conshohocken, 2005.

5. Bakis, C.E., Bank, L.C., Brown, V.L., Cosenza, E., Davalos, J.F., Lesko, J.J., Machida, A.,Rizkalla, S.H., and Triantafillou, T.C. "Fiber-reinforced polymer composites for construction: State-of-the-art review," *Journal of Composites for Construction*, ASCE, V. 6, No. 2, 2002, pp. 73-87.

6. Bao, L.R., Yee, A.F., and Lee, C.Y.C. "Moisture absorption and hygrothermal aging in a bismaleimide resin," *Polymer*, V. 42, No. 17, 2001, pp. 7327-7333.

7. Bowditch, M.R. "The durability of adhesive joints in the presence of water," *International Journal of Adhesive and Adhesion*, V. 16, No. 2, 1996, pp. 73-79.

8. Crasto, A.S. and Kim, R.Y. "Environmental durability of a composite-to-composite adhesive bond in infrastructure applications," *28th International SAMPE Technical Conference*, 1996, pp. 837- 849.

9. Comrie R, Affrossman S, Hayward D, Pethrick RA, Zhou X, Thompson GE. "Study of ageing of adhesive bonds with various surface treatments: Part VI. Dicyandiamide-cured epoxy joints aged at 70°C in a water bath," *Journal of Adhesion Science and Technology*, V.20, No. 16, 2006, pp. 1847-1872.

10. Custodio, J., Broughton, J., and Cruz, H. "A review of factors influencing the durability of structural bonded timber joints," *International Journal of Adhesive and Adhesion*, V. 29, No. 2, 2009, pp. 173-185.

11. Green, M.F. "FRP repair of concrete structures: performance in cold regions," *International Journal of Materials and Product Technology*, V. 28, No. 1/2, 2007, pp. 160-177.

12. Hand H.M., Arah C.O., McNamara D.K., and Mecklenburg M.F. "Effects of environmental exposure on adhesively bonded joints," *International Journal of Adhesive and Adhesion*, V. 11, No. 1, 1991, pp. 15-23.

13. Kim, Y.J., Green, M.F., Fallis, G.J., Wight, G.R., and Eden, R. "Damaged Bridge Girder Strengthening: Field Application of Prestressed Fiber-Reinforced Polymer Sheets," *Concrete International*, ACI, V. 28, No. 11, 2006, pp. 47-52.

14. Kim, Y.J. and Yoon, D.K. "Identifying critical sources of bridge deterioration in cold regions through the constructed bridges in North Dakota," *Journal of Bridge Engineering*, ASCE, 2010, in-press

15. Kim, Y.J. and Heffernan, P.J. "Fatigue behavior of externally strengthened concrete beams with fiber-reinforced polymers: State of the art," *Journal of Composites for Construction*, ASCE, V. 12, No. 3, 2008, pp. 246-256.

16. Loh, W.K., Crocombe, A.D., Wahab, M.A., Watts, F.J., and Ashcroft, I.A. "The effect of moisture on the failure locus and fracture energy of an epoxy-steel interface," *Journal of Adhesion Science and Technology*, V. 16, No. 11, 2002, pp. 1407-1429.

17. MBrace. "MBrace saturant datasheet," Degussa, 2007, available online at http://www.basf-cc.ae/en/products/

18. Minford J.D. "Handbook of aluminum bonding technology and data," New York: Marcel Dekker Inc., 1993

19. Teng, J.G, Chen, J.F., Smith, S.T., and Lam, L. "Behavior and strength of FRP strengthened RC structures: a state-of-the-art review," *Structures and Buildings*, ICE, V. 156, No. 1, 2003, pp. 51-62.

20. Yuan , H., Teng, J. G., Seracino, R., Wu, Z. S., and Yao, J. "Full-range behavior of FRP-to-concrete bonded joints", *Engineering Structures*, Volume 26, Issue 5, April 2004, 553-565

Houchin Bindery

Pages 63-104 were never provided by printer.

PLEASE REBIND – We have provided missing pages.

Thank you
NDSU LIBRARIES

CHAPTER 4. AXIAL CONCRETE MEMBER

4.1. SYNOPSIS

This chapter presents the results of an experimental study on the durability of 15 CFRP confined and 16 unconfined air entrained concrete cylinders (75mm x 150 mm) when simultaneously exposed to harsh environmental conditions and live load effects. The simulated environments consist of 100 cycles of freezing-submerging-drying at a freezing temperature of -30 °C. The instantaneous live load effects are 20%, 40% and 60% of the compressive strength of the control cylinders. The experimental program reports that the environmental effects are critical on the durability of concrete members and the presence of live load effects accelerates the deterioration of the unconfined concrete. Confined cylinders showed improved durability performance after the extreme exposure to aggressive environment when compared to the confined cylinders. Internal damage due to the load cycling affects the axial stiffness and crack propagation of the conditioned cylinders. The ultimate load-carrying capacity of the confined cylinders is almost constant, whereas a trend of decreased stiffness with increasing live load effects is observed.

4.2. INTRODUCTION

Strengthening of concrete columns with CFRP composites, fibers applied to the circumferential direction of the column, is one of the promising techniques to increase the load-carrying capacity. CFRP wrapping may prevent premature cracking or spalling of reinforced concrete members induced by the corrosion of steel. Strengthened concrete member's condition may be exposed to harsh environmental conditions during service life. Green et al. (2006) studied the effect of freeze-thaw (-40°C) combined with sustained loads

on the behavior of concrete cylinders confined with CFRP sheets and showed that the strength reduction was 2% due to freeze-thaw combined with sustained load effects, whereas that was recorded 5% in absence of sustained load.

Mechanical properties of FRP composites may be directly affected due to long term exposure at various low temperatures or freeze-thaw cycling and thus affects the FRP confinement efficiency. For example, Karbhari (2002) studied the effects of long term cold temperature (-18 °C) on FRP confined cylinders and reported a more brittle failure modes and reduced strength of FRP composites due to freeze-thaw cycling at low temperature in a soaked condition. CFRP-wrapped cylinders exposed to 300 freeze-thaw cycles experienced approximately 20 % reduction in compressive strength (Karbhari 2002); while a decrease 19% in the strength was observed in a salt solution (Toutanji and Balaguru 1998). Soudki and Green (1996) tested CFRP-wrapped concrete cylinders exposed to 200 cycles of freezing (16 hrs) at -18°C and thawing (8 hrs) at 20°C. They found that CFRP wrapped concrete cylinders experienced 15% reduction in strength. Toutanji and Balaguru (1998) examined the behavior of FRP (CFRP and GFRP)-wrapped concrete cylinders subjected to 300 freeze-thaw cycles. They found some deterioration due to freeze-thaw cycles. However, CFRP showed better performance than GFRP. Teng et al. (2003) compared the field application of FRP-wrapped columns to laboratory tests in freeze-thaw conditions. FRP-wrapped columns showed relatively better performance in field condition than the specimens simulated in laboratory.

Although extensive research efforts have been made to understand the long term durability of FRP composites under different aggressive environmental conditions, insufficient knowledge still exists on the long-term performance of FRP-strengthened axial

concrete members when subjected to freeze-wet-dry as well as live load effects simultaneously that represents a service state. This chapter presents an experimental program to evaluate the durability performance of concrete members when simultaneously exposed to freeze-thaw and live load effects. Test results include the axial response of the concrete, strength variation, and failure modes.

4.3. RESEARCH SIGNIFICANCE

Long term durability of CFRP-wrapped axial concrete members under harsh environmental conditions is the critical issue for wide acceptance to the infrastructure community for repair of old structures. Although significant amounts of research works reported in literature on the behavior of CFRP-wrapped axial concrete members under freeze-thaw effects combined with sustained loads; very limited information is available as to combined environmental and live load effects. The majority of existing experimental investigations had been conducted with uncracked concrete members prior to applying CFRP sheets, which might not adequately represent the performance of deteriorated concrete members strengthened with CFRP sheets. The long-term durability of CFRP composites under freeze-thaw condition followed by physical loading, such as highway bridges in cold regions under heavy trucks, may be an important consideration needed for their successful field implementation. Frost damage induced by moisture ingress into a concrete member can change the permeability characteristics of the concrete so that micro- and macro-cracks may develop during the service life of the member. The research explains the combined load effects (environmental and physical load) on the axial behavior FRP-strengthened of concrete members.

4.4. BACKGROUND

The following briefly summarizes a research project to identify the critical sources of bridge deterioration in cold regions through the constructed bridges in North Dakota that is one of the coldest states in the US. Further details are available in Kim and Yoon (2010).

4.4.1. Bridges in North Dakota

A comprehensive bridge inspection was conducted by the North Dakota Department of Transportation between 2006 and 2007. A total of 5,289 constructed bridges and 2,801 deck slabs were examined. The bridges with structurally deficient and functionally obsolete categories were 13.9% and 5.3%, respectively. The bridges maintained by the county governments showed higher structurally deficient ratings when compared to those maintained by the state agencies or city governments. The bridges located in the interstate highways were adequately maintained even though the level of deterioration of the deck slabs was substantial. The bridges in major cities with large population exhibited noticeable problems in the functionally obsolete category in comparison to those in small cities. Overall, the bridges were well maintained and the level of deterioration was lower than that of the national average.

4.4.2. Critical Sources of Bridge Deterioration

A statistical analysis combined with geographic information system (GIS) was conducted to identify the critical sources of bridge deterioration, based on the inspection data in 2006 and 2007. Fig. 4.1(a) plots a typical GIS map to visually assess the condition of existing bridges in North Dakota, including three categories such as structurally deficient, functionally obsolete, and non-deficient. The sources of bridge deterioration were determined by an ordinary least-square multiple regression analysis. The parameters

studied included the number of spans, year-built, material types, structural systems, precipitation, temperature, bridge geometry, replacement length, land use, population, and traffic volumes. A Pearson correlation analysis was also conducted to examine the mutual relationship between test parameters. Fig. 4.1(b) summarizes the standardized coefficient (β) of selected parameters with a confidence level of 95%. The coefficient shows a relationship between the structurally deficient rating and the parameters. Many of the structurally deficient bridges were replaced (β = 0.45). The ageing of the bridges (year-built) was the most critical factor (β = 0.14) followed by other parameters. The contribution of the traffic volume (average daily truck traffic) was significant (β = 0.06). It was, therefore, concluded that the ageing and live load effects were the critical factors for bridge deterioration in cold regions such as North Dakota.

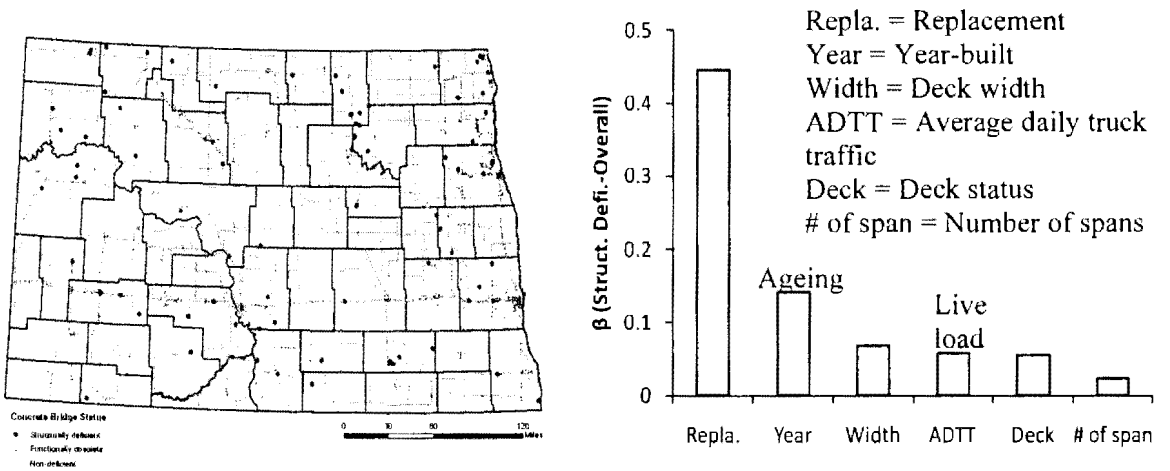

(a) (b)

Figure 4.1. Critical sources of bridge deterioration in North Dakota (Kim and Yoon 2010): (a) bridge status; (b) relationship between structurally deficient bridges and contributing factors

4.5. EXPERIMENTAL PROGRAM

An experimental program was conducted to examine the contribution of the critical factors identified in previous research (described above) to bridge deterioration. Harsh environmental conditions were simulated to represent the effects of ageing and various levels of instantaneous loads were reproduced for daily traffic effects.

4.5.I. Materials

The specified concrete strength was 20 MPa, while the tested strength at 28 days was 22.4 MPa on average. The maximum aggregate size was 9.5 mm with a water-cement ratio of 0.45. A 5.5% air-entrained concrete was used to better resist harsh environmental conditions. The effect of air-entrainment in concrete is significant; for example, a concrete specimen without air-entrainment may be disintegrated in cold climate environments (Kong et al. 2005).

4.5.2. Casting of Concrete Cylinders

Reusable cylinder molds (75 mm diameter, 150 mm height and 6.2 mm wall thickness) were used to caste the concrete cylinders. Lubricant was applied to the inner surface of the plastic molds to ensure a smooth surface and to easily remove the cylinders from the molds. All 31 concrete cylinders (diameter: 75 mm and height: 150 mm) were caste from a single batch of concrete mix. Crushed stone for coarse aggregate and river sand for fine aggregate and Type-I Portland cement was used to produce the concrete. The concrete was carefully placed in the plastic molds. During the pouring of concrete in the molds, roding (ASTM guide line followed: compact in three layers; each layer 25 times roding with a rod diameter of 12.5 mm) instead of vibrator was used to compact the concrete and avoid any honeycombing. Once the concrete cylinders casting completed,

they were covered with plastic sheets to minimize the moisture losses. The cylinders were moistened each day. After 5 days, all cylinders were removed from the plastic molds by using air compressor in order to avoid chipping of the concrete and allowed the specimens to moist cure for 28 days at room temperature. Four control cylinders were tested after 28 days to obtain the strength of control cylinders (f_c').

4.5.3. CFRP Sheet Application

Before wrapping CFRP sheets on the cylinders, a preload up to 45 percent of the ultimate load of the control was monotonically applied to induce micro-cracks which could existing structures subjected to service loads. These micro-cracks could accelerate moisture ingress into the concrete cylinders when environmental cycles were applied. Before wrapping the CFRP sheets to the concrete cylinders, concrete surface was thoroughly cleaned by using medium coarse sand papers, as shown in Fig. 4.2, to ensure proper bonding of CFRP sheets through the epoxy layer.

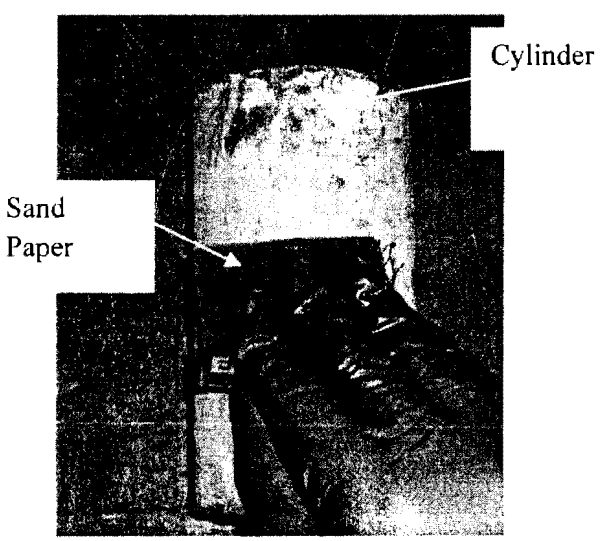

Figure 4.2. Surface cleaning

This is recommended by the FRP manufacturer for the purpose to enhance bond between the epoxy matrix and the concrete surface. Dusting from surface grinding was removed using high speed water flow to achieve dust free and clean surface and then allowed drying at room temperature for a day. In case of field applications, sand blasting instead of sand paper may be used before CFRP sheets application for strengthening concrete structures to ensure proper bonding between CFRP sheets and concrete through epoxy adhesive.

Next, 150 mm width and 250 mm length (perimeter of cylinder 235 mm +15 mm overlap in joint) rectangular pieces of CFRP sheets shown in Fig. 4.3(a) were cut from a 500 mm wide CFRP roll for the concrete cylinders using scissors. Mechanical properties of CFRP sheets and the epoxy adhesive are given in Table 3.4. Two parts (Part A and Part B) epoxy adhesives as described in Chapter 3 were prepared in accordance with the manufacturer's instructions. The adhesive was applied to the CFRP sheets to make it saturate and then the preloaded plane concrete cylinders were put on the CFRP sheets and rolling the cylinders, as shown in Fig. 4.3(b). Total 15 cylinders were wrapped with one layer of CFRP sheet with a 15 mm overlapping at the joint. The main fibers were in transverse direction, as shown in Fig. 4.3(c). A completely wrapped cylinder is shown in Fig. 4.3(d). The remaining 12 cylinders were left unconfined to measure the concrete strength after the completion of the environmental cycling associated with instantaneous load effects. Once wrapping was complete, both ends of all the cylinders were sealed with epoxy as shown in Fig. 4.4 to prevent the water absorption through the ends. The wrapped cylinders were put 10 days in room temperature for additional curing. After 10 days, these epoxy sealed ends were carefully grounded by using sand papers to achieve a smooth

surface perpendicular to the main axis of the cylinder. Then three confined control cylinders were tested at 10 days to obtain the confined concrete strength (f'_{cc}).

(a)

(b)

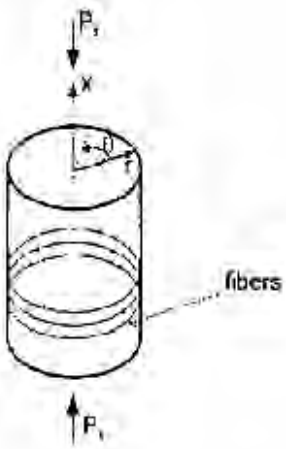

(c)

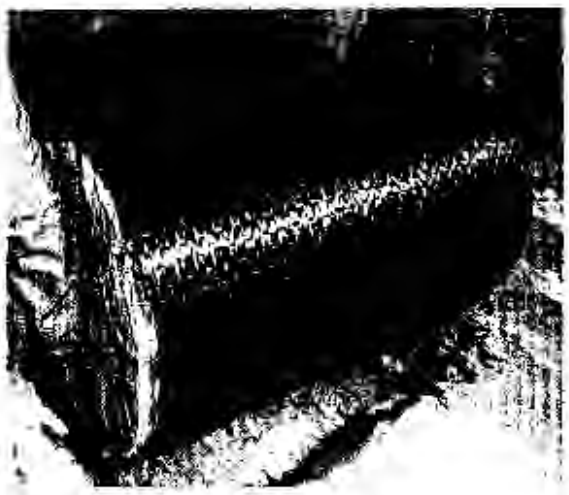

(d)

Figure 4.3. Wrapping of cylinder with CFRP sheets: (a) CFRP sheet; (b) apply epoxy to CFRP sheet and cylinder rolling on it; (c) fiber direction; (d) complete confined cylinders

Figure 4.4. Sealing both ends of cylinders with epoxy adhesive

4.5.4. Environmental Cycling and Live Load Effects

A total of 31 concrete cylinders (75 mm diameter x 150 mm long) were cast in the laboratory, as shown in Tables 4.1 and 4.2. Four cylinders were tested at room temperature and 12 plane and 12 confined cylinders were exposed to environmental conditions. Fig. 4.5 summarizes the environmental simulation.

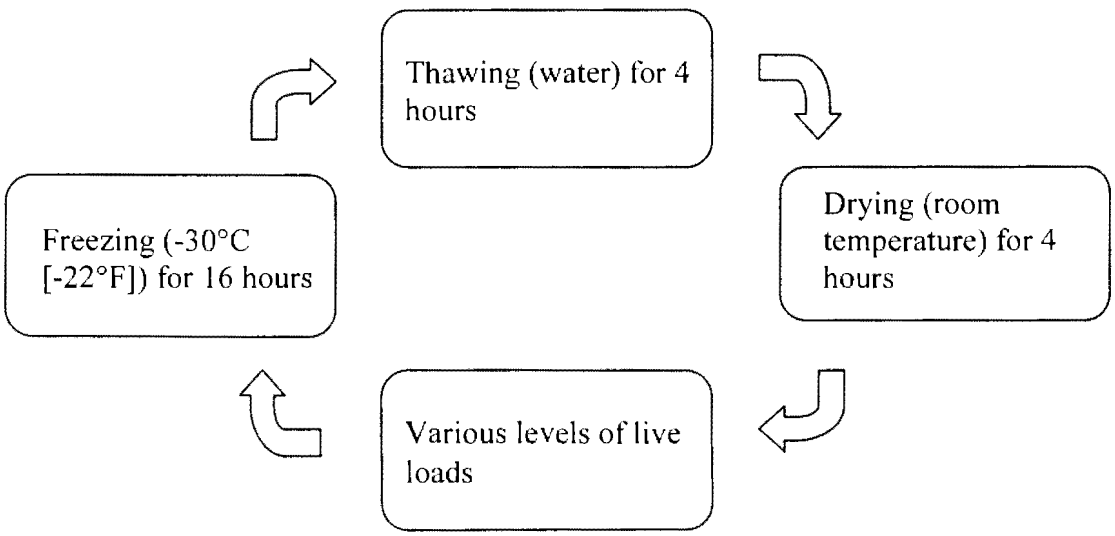

Figure 4.5. Sequences of environmental cycling

One cycle of the load effects included 16 hours of freezing at -30°C, 4 hours of thawing in water, 4 hours of drying at room temperature, and various levels of instantaneous loads, as shown in Fig. 4.6. The simulated live load effects were 0% (Env+0%), 20% (Env+20%), 40% (Env+40%), and 60% (Env+60%) of the concrete strength at 28 days (f'_c) for

(a)

(b)

(c)

(d)

Figure 4.6. Environmental sequence: (a) freezing; (b) submerging; (c) drying; (d) live load per cycles

unconfined concrete cylinders and the strength of confined concrete cylinders (f'_{cc}) at 10 days after wrapping for confined cylinders, respectively. The "Env" term denotes the environmental effect: freezing-submerging-drying. A minimum of 3 cylinders were tested per category, as shown in Tables 4.1 and 4.2. The environmental chamber used for this research was equipped with an accurate digital temperature adjustment function and electronic display. The daily measured temperature is shown in Fig. 4.7.

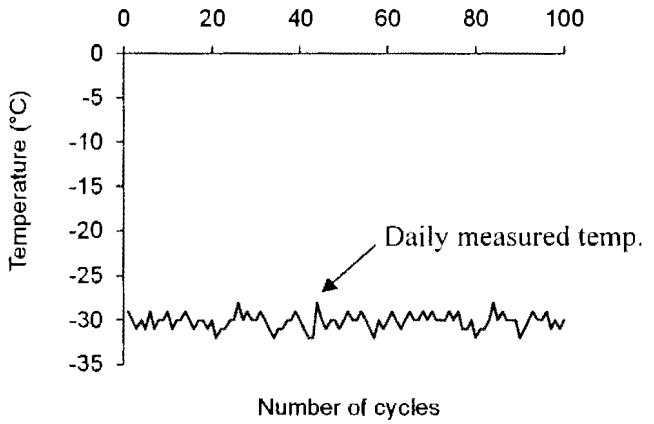

Figure 4.7. Temperature variation in the environmental chamber

4.5.5. Crack Width Measurement

Crack measuring microscope shown in Fig. 4.8(a) specially designed simple instrument was used to measure the crack width in concrete cylinders manually. The microscope operates via manually adjustable light source. Before measuring the crack width, few cracks were selected and marked as shown in Fig. 4.8(b) to measure the crack width in different time intervals. Crack microscope itself has no defined scale, so after getting the reading from the crack microscope shown in Fig. 4.8(c), then it was calibrated with a standard scale on that specific focus and recorded the reading in mm unit. Crack width was measure for the specimens subjected to different environmental conditions and

live load effects at a typical interval of 30, 60, 80 and 100 cycles. No visual crack was observed for the confined cylinders.

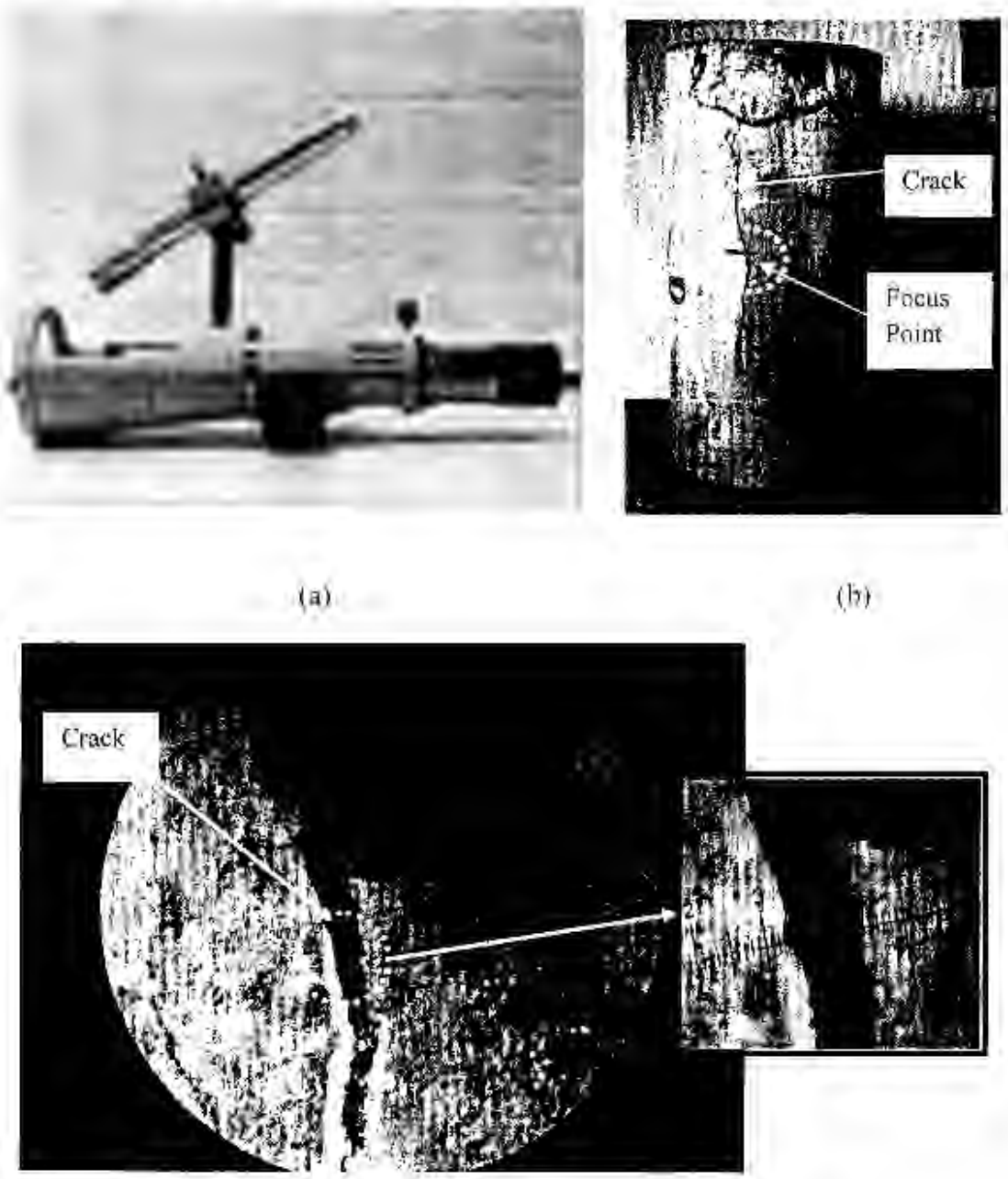

(a) (b)

(c)

Figure 4.8. Crack width measurement during the load cycle: (a) crack measuring microscope; (b) cracked cylinder; (c) typical crack width measured with crack microscope

4.5.6. Instrumentation and Testing

A SATEC hydraulic testing machine was used to load the cylinders (Fig. 4.9a). The machine had a compression capacity of 1,250 kN with a maximum travel distance of 50 mm. The loading rate was 1 kN/sec. No instrumentations were given for the cylinders during the environmental cycling. Upon the completion of 100 cycles of the environmental and live load effects, two strain gages, one in axial and the other in hoop directions were bonded at mid-height of the cylinders as shown in Fig. 4.9(b). KYOWA® KFG-5-120-C1-11 (5 mm in gage length and 120Ω gage resistance) general-purpose unidirectional foil strain gages (Fig. 4.9d) were used to record strains in the CFRP sheets. CC-33A of gage cement was used for bonding the strain gages on the specified location of the specimen. All strain gages were mounted according to manufacturer's instructions. One linear potentiometer was used to measure the axial response of the cylinders. Novotech link TR100 Linear potentiometer (LP) shown in Figs. 4.9(a) and 4.9(c) was used to continuous record vertical displacements during cylinder testing. The potentiometer meter was placed on the extended plate that was placed under the cylinder as shown in Fig. 4.9(a). The linear potentiometer was calibrated prior to testing the cylinders. All cylinders were monotonically loaded until a complete failure occurred. All data were recorded by a data acquisition system.

4.6. EXPERIMENTAL RESULTS

4.6.1. Load-carrying Capacity

Tables 4.1 and 4.2 summarize test results of the unconfined and confined cylinders, respectively. The average strength of the control cylinders was 22.9 MPa and 79.1 MPa for

the unconfined, and the confined specimens, respectively. The cylinders subjected to environmental and live load effects, however, showed noticeable decreases in the load-carrying capacity in case of the unconfined cylinders. The unconfined cylinders exposed to the environment (Env-0%) exhibited a decrease of 10.0% in the ultimate capacity in comparison to the control cylinders, on average, while that value was 0.8% for the confined cylinders. When the live load effects increased, the load-carrying capacity was reduced by

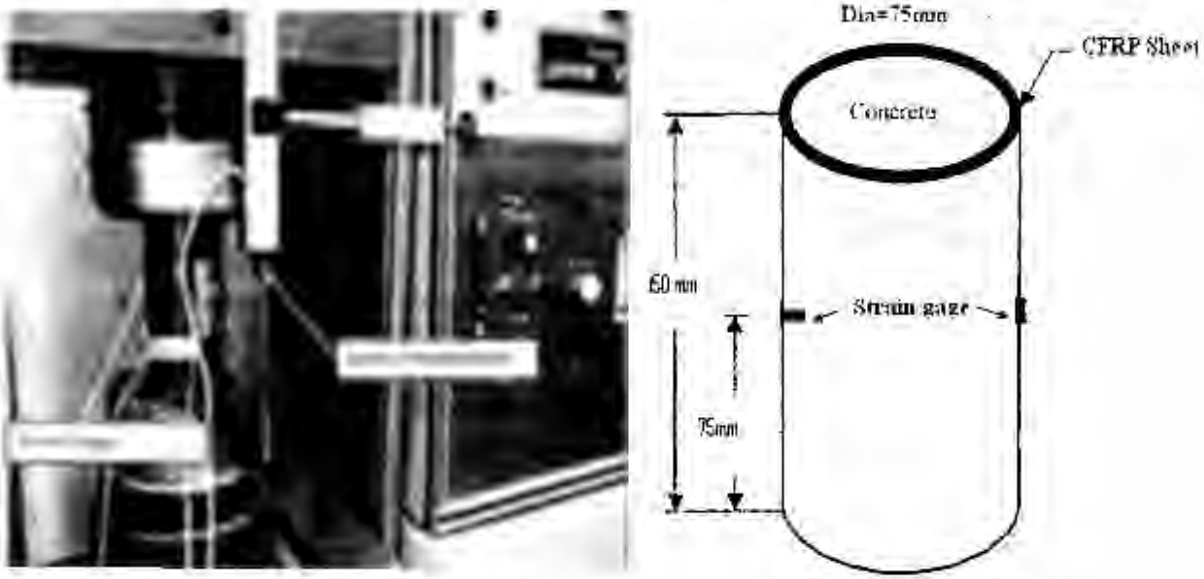

Figure 4.9. Instrumentations: (a) testing; (b) strain gage locations; (c) Novotechlink TR100 linear potentiometer; (d) foil strain gage

15.7%, 34.1%, and 41.9% for the unconfined cylinders subjected to 20% (Env+20%), 40% (Env+40%), and 60% (Env+60%) of the concrete strength at 28 days ($f_c^{'}$), respectively, while that value was 0.4% and 3.7% for confined cylinders subjected to 20% (Env+20% $f_{cc}^{'}$), and 40% (Env+40% $f_{cc}^{'}$), respectively. On the other hand, a 7.6% higher load recorded for 60% (Env+60% $f_{cc}^{'}$) confined cylinders, on average. It should be noted that two unconfined cylinders in the Env+60% category failed prior to the target cycle of 100, namely, Cylinders L and O failed at 54 and 80 cycles, respectively. This premature failure may be attributed to the excessive live load effect (60% of $f_c^{'}$) that was associated with the harsh environmental conditions. Fig. 4.10(a) compares the strength variation of the unconfined cylinders with respect to the level of live load effects. The average strength-decrease rate tended to be linear within the range studied in the present experimental program, while the average strength of the confined cylinders didn't changed significantly except some scattering of the test results as shown in Fig. 4.10(b).

4.6.2. Stress-strain Response

Figs. 4.11 and 4.12 show the stress-strain response of selected unconfined and confined cylinders, respectively, when loaded to failure. The axial strain of the control cylinder (Cylinder A) was linear up to approximately 55% of the ultimate stress (i.e., 15 MPa), while confined control cylinder (Cylinder 2) behaved linear up to approximately 40% of the ultimate stress (i.e., 30 MPa) and a reduced modulus (stiffness) was recorded in both cases as the cylinders approached the failure. This observation is due to the damage propagation inside the cylinder when the applied stress level increased. The contribution of the environmental and live load effects to the change of the modulus was not significant up

to 20% live load effects (Env+20%), as shown in Figs. 4.11(a) and 4.12(a).The confined cylinders, however, showed decreasing trends in elastic modulus with increasing the live load effects as shown in Fig. 4.12(a). The unconfined cylinder subjected to Env+40% (Cylinder K), however, exhibited a noticeable decrease in the modulus. The low modulus was related to the failure characteristics of the cylinders subjected to the simulated load effects (to be discussed). An improved modulus was observed for the unconfined cylinder with Env+60% (Cylinder N), as shown in Fig. 4.11(a). The increased modulus of Cylinder N is inconclusive and more testing may be recommended to confirm the stiff response. It should be noted that only one unconfined cylinder was instrumented for the Env+60% category because of the premature failure of the two cylinders (Table 4.1) and hence the

Table 4.1. Results of unconfined concrete cylinders

Group	ID	Environmental effect[1]	Live load[2]	Ultimate capacity, f'_c(MPa)		
				Individual	*Ave*	*S*
Control	Cylinder A	No	0%	27.1	22.9	3.6
	Cylinder B	No	0%	24.6		
	Cylinder C	No	0%	19.0		
	Cylinder D	No	0%	21.0		
Env+0%	Cylinder E	Yes	0%	19.2	20.6	2.3
	Cylinder F	Yes	0%	23.2		
	Cylinder G	Yes	0%	19.4		
Env+20%	Cylinder H	Yes	20%	15.6	19.3	3.9
	Cylinder I	Yes	20%	23.3		
	Cylinder J	Yes	20%	19.0		
Env+40%	Cylinder K	Yes	40%	17.8	15.1	2.5
	Cylinder L	Yes	40%	14.5		
	Cylinder M	Yes	40%	13.0		
Env+60%	Cylinder N	Yes	60%	19.0	13.3	5.0
	Cylinder O	Yes	60%	10.1[a]		
	Cylinder P	Yes	60%	10.6[b]		

Ave = average; *S* = standard deviation [1]: freeze (16 hrs at-30 °C) -wet (4 hrs under water)-dry (4hrs at room temperature) [2]: percentage of f'_c [a]: failed at 54 cycles [b]: failed at 80 cycles

observation on the stress-strain response of Env+60% could be limited. The modulus based on the hoop strain response of the cylinders subjected to the load effects was lower than that of the corresponding control cylinder, as shown in Figs. 4.11(b) and 4.12(b), except for the cylinder with Env+60% (Cylinder N) that could be related to the stiff behavior in the axial strain response (Fig. 4.10a). The reduced modulus of the conditioned cylinders may indicate the growth of internal damage during the load cycling. In addition to the internal damage during the environmental cycling and live load effects, confined cylinders may also be faced damage in the matrix due to live loads effects and hence water ingression could influence the interface between CFRP and concrete, resulting in more damages with increasing live loads.

Table 4.2. Results of confined concrete cylinders

Group	ID	Environmental effect[1]	Live load[2]	Ultimate capacity, f'_{cc} (MPa)		
				Individual	Ave	S
Control	Cylinder 1	No	0%	82.9	79.1	3.3
	Cylinder 2	No	0%	77.2		
	Cylinder 3	No	0%	77.1		
Env+0%	Cylinder 4	Yes	0%	84.6	78.5	5.4
	Cylinder 5	Yes	0%	74.3		
	Cylinder 6	Yes	0%	76.5		
Env+20%	Cylinder 7	Yes	20%	77.6	78.8	8.2
	Cylinder 8	Yes	20%	71.3		
	Cylinder 9	Yes	20%	87.5		
Env+40%	Cylinder 10	Yes	40%	83.1	76.2	6.0
	Cylinder 11	Yes	40%	71.9		
	Cylinder 12	Yes	40%	73.7		
Env+60%	Cylinder 13	Yes	60%	87.7	85.1	2.5
	Cylinder 14	Yes	60%	84.9		
	Cylinder 15	Yes	60%	82.7		

Ave = average; *S* = standard deviation [1]: freeze (16 hrs at-30 °C) -wet (4 hrs under water)-dry (4hrs at room temperature) [2]: percentage of f'_{cc}

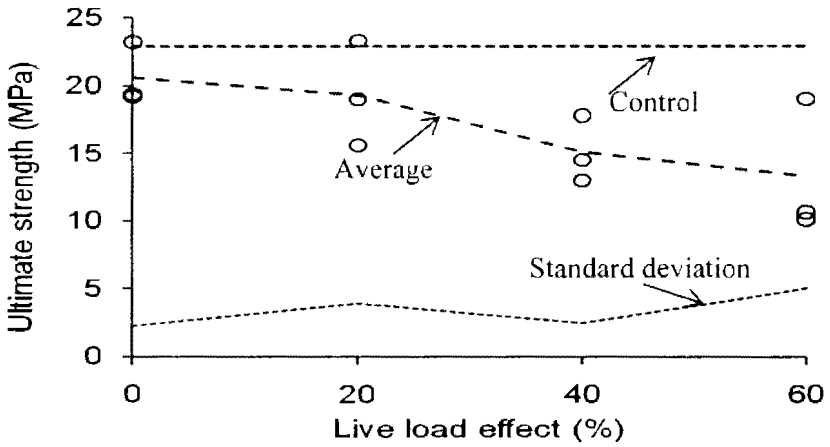

(a)

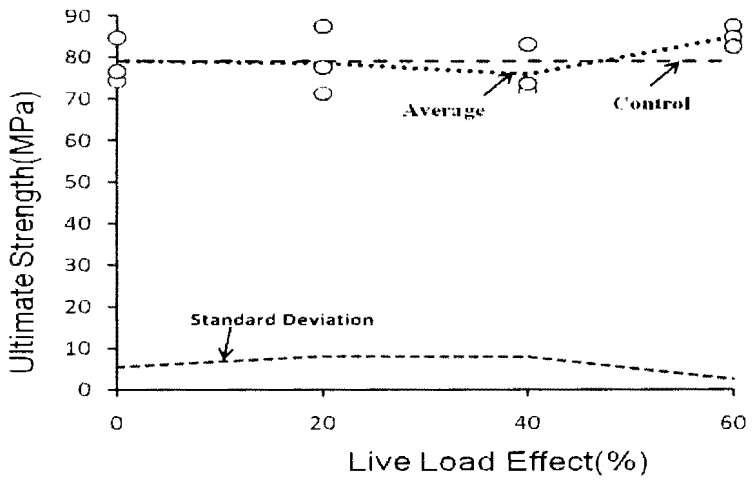

(b)

Figure 4.10. Relationship between the ultimate strength of cylinders and live load effect: (a) unconfined cylinders; (b) confined cylinders

4.6.3. Relationship between Hoop and Axial Strains

Figs. 4.13 and 4.14 show the relationship between the axial and hoop strains of the unconfined and confined cylinders, respectively. The hoop strain of the control unconfined cylinder (Cylinder A) varied linearly up to 65% of the maximum hoop strain when the axial strain increased in compression, while confined cylinders showed linear behavior up to approximately 40%. A Poisson's ratio of 0.24 and 0.32 was obtained from the unconfined (Cylinder A) and confined control cylinder (Cylinder 2), respectively.

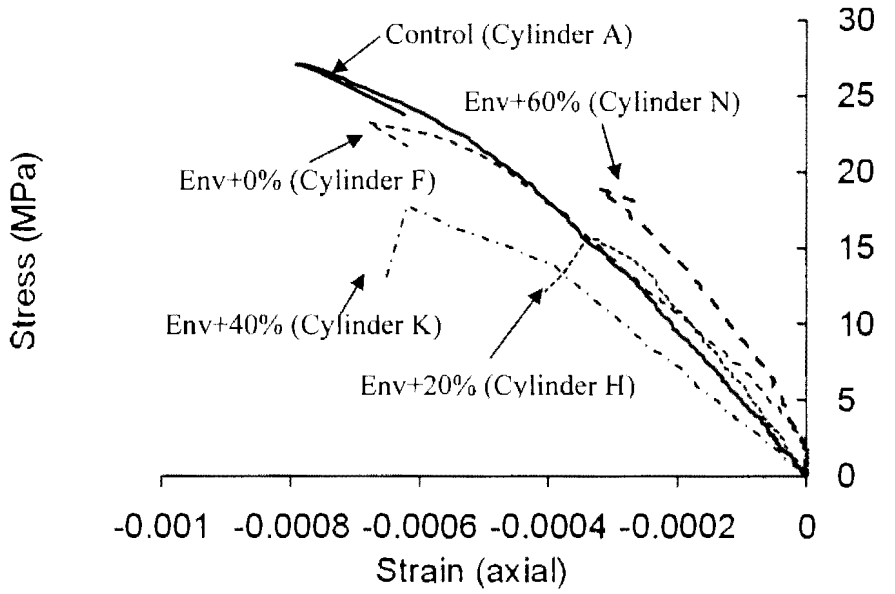

(a)

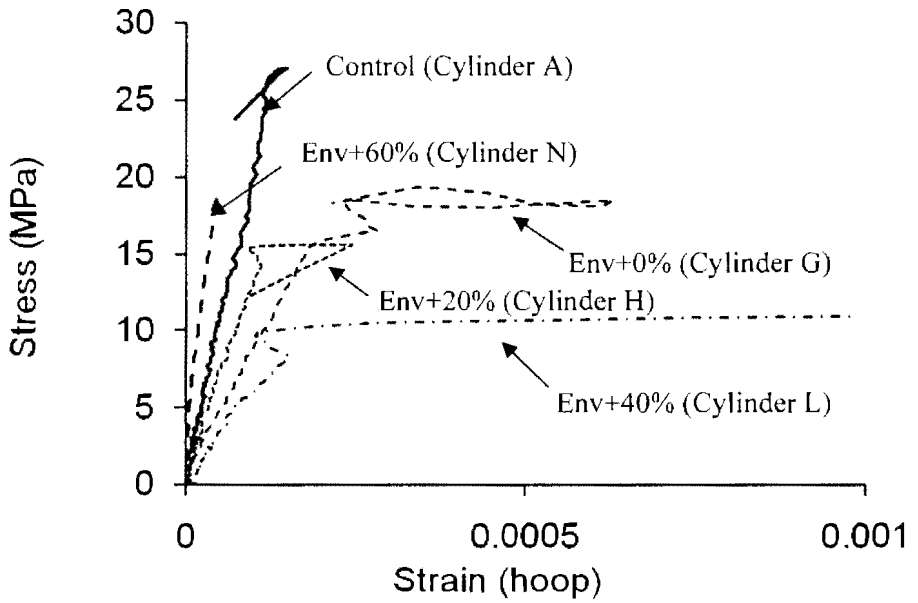

(b)

Figure 4.11. Stress-strain responses of unconfined cylinders: (a) axial direction; (b) hoop direction

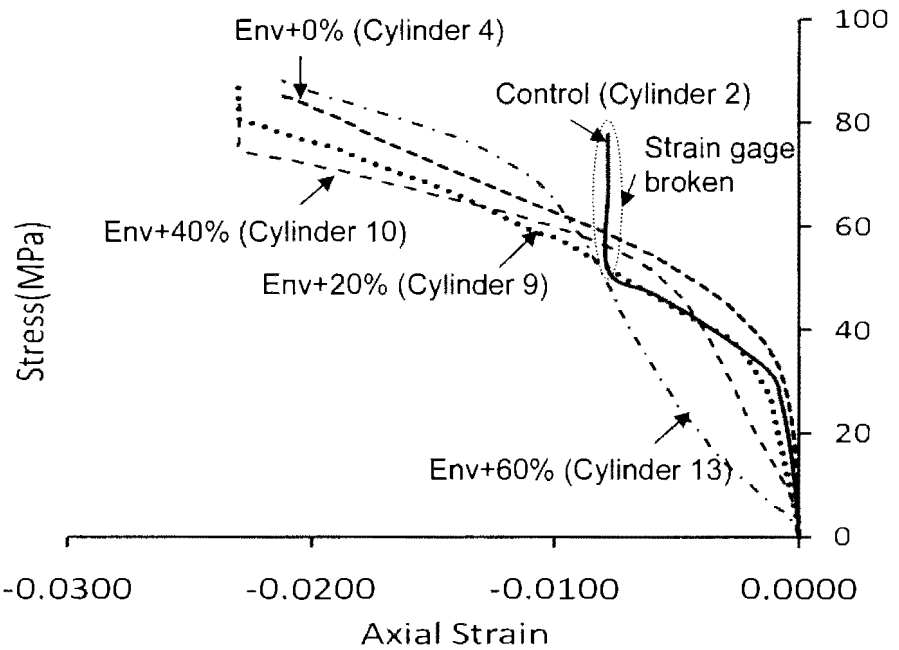

(a)

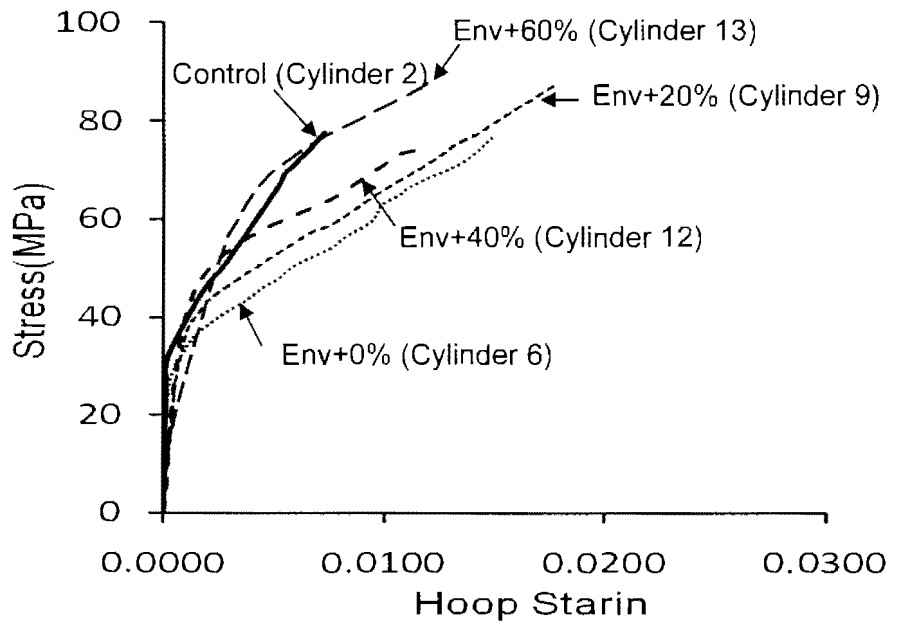

(b)

Figure 4.12. Stress-strain responses of confined cylinders: (a) axial direction; (b) hoop direction

The modulus of the strain response of the unconfined cylinders became stiff beyond the linear limit. This observation may indicate that macro-cracks developed inside the concrete (i.e., the concrete is not an elastic body anymore) so that the applied energy tended to be consumed by the large cracks, rather than an increase in hoop strains (the circumferential strain gage could be located near the cracks). The confined cylinders became stiffer when the load increases. This observation indicates that although confined cylinders internally damage more but due to confinement action the concrete materials could be compacted more with increasing live load effects and showed a stiffer behavior and finally failure occurred in an explosive manner. The cylinders exposed to the Env+0% (Cylinder G) and Env+20% (Cylinder H) showed a reduced stiffness when compared to the control cylinder, as shown in Fig. 12(a) and (b). Similar trend was observed for confined cylinders with Env+0% (Cylinder 6), and Env+20% (Cylinder 9), as shown in Fig. 4.14(a) and (b). A Poisson's ratio of 0.42 and 0.37 was measured in the linear range of Cylinders G and H, respectively, while that of Cylinder 6 (Env+0%) and Cylinder 9 (Env+20%) was 0.46 and 0.44, respectively. The increase in the Poisson's ratio of the cylinders in comparison to the ratio of the control cylinder implies that the conditioned concrete tended to be soft (i.e., a large increase in hoop strains under a unit axial strain) and included micro-damage inside the concrete constituents. The response of Cylinder 12 (Env+40%) was almost similar to that of the control cylinder up to linear range, as shown in Fig. 4.14(c). The Poisson ratio was 0.36, while that value of the control cylinder (Cylinder 2) was 0.32. The cylinder with Env+60% (Cylinder 13) shown in Fig. 4.14(d) showed a very stiff response in hoop strains (Poisson's ratio 0.27) that implies more compacted mass due to heavy loads. On the other hand, the unconfined cylinder with Env+40% (Cylinder K)

showed a very stiff response of the hoop strains, as shown in Fig.4.13(c). The insignificant development of the hoop strains indicates that the axial load applied to the cylinder was not associated with the change of circumferential dimensions. This observation may be attributed to the fact that Cylinder K (Env+40%) was severely damaged during the load cycling and hence some cracks

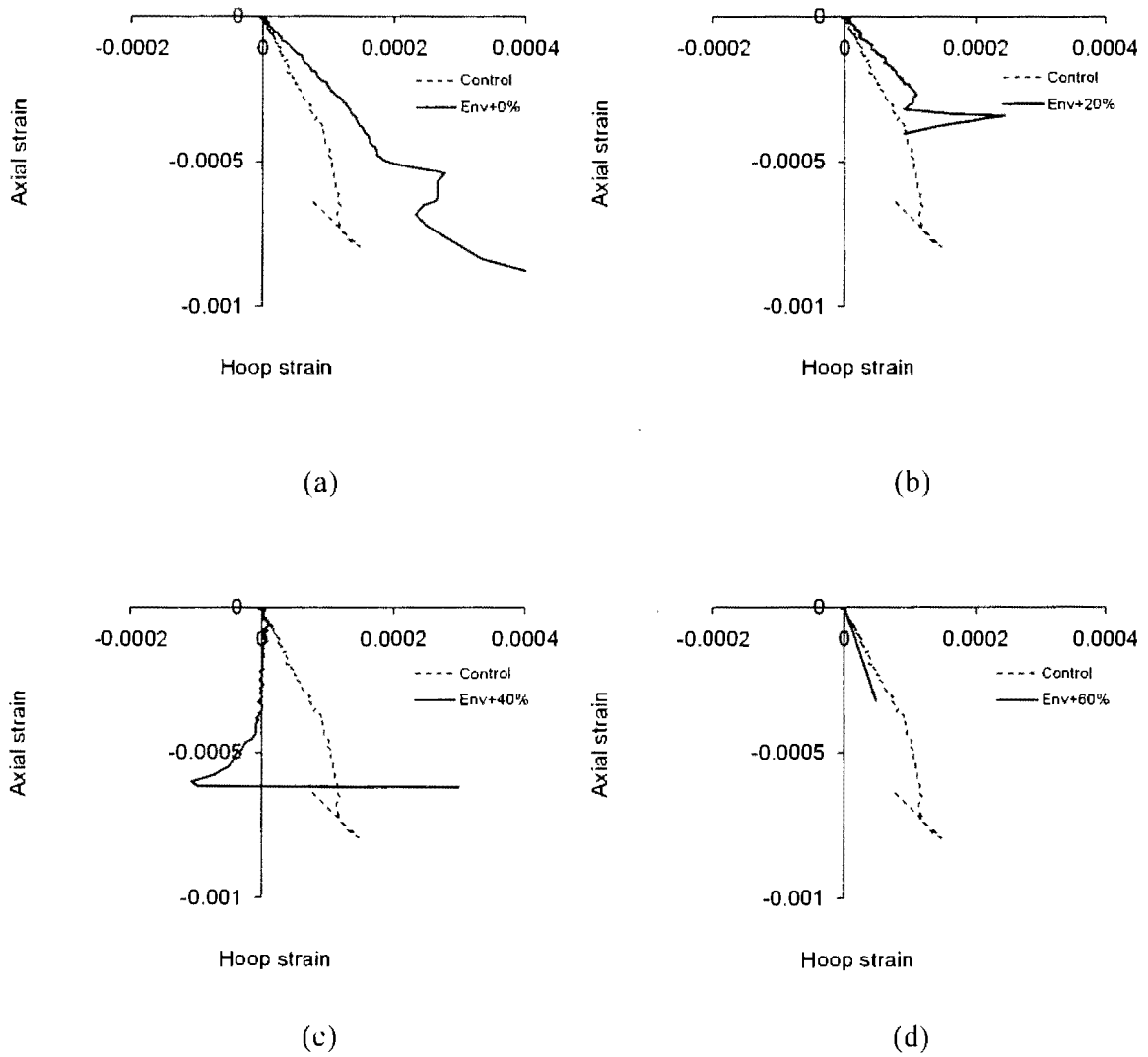

Figure 4.13. Relationship between axial and hoop strains of unconfined cylinders: (a) Env+0% (Cylinder G); (b) Env+20% (Cylinder H); (c) Env+40% (Cylinder K); (d) Env+60% (Cylinder N)

developed near the strain gage, which could influence the strain readings when the cylinder was loaded to failure. The response of Cylinder N (Env+60%) was similar to that of the control cylinder, as shown in Fig. 4.12(d). As mentioned in the previous section, the stiff response of the cylinder subjected to the environmental and load effects (Env+60%) may need an additional investigation with more test results.

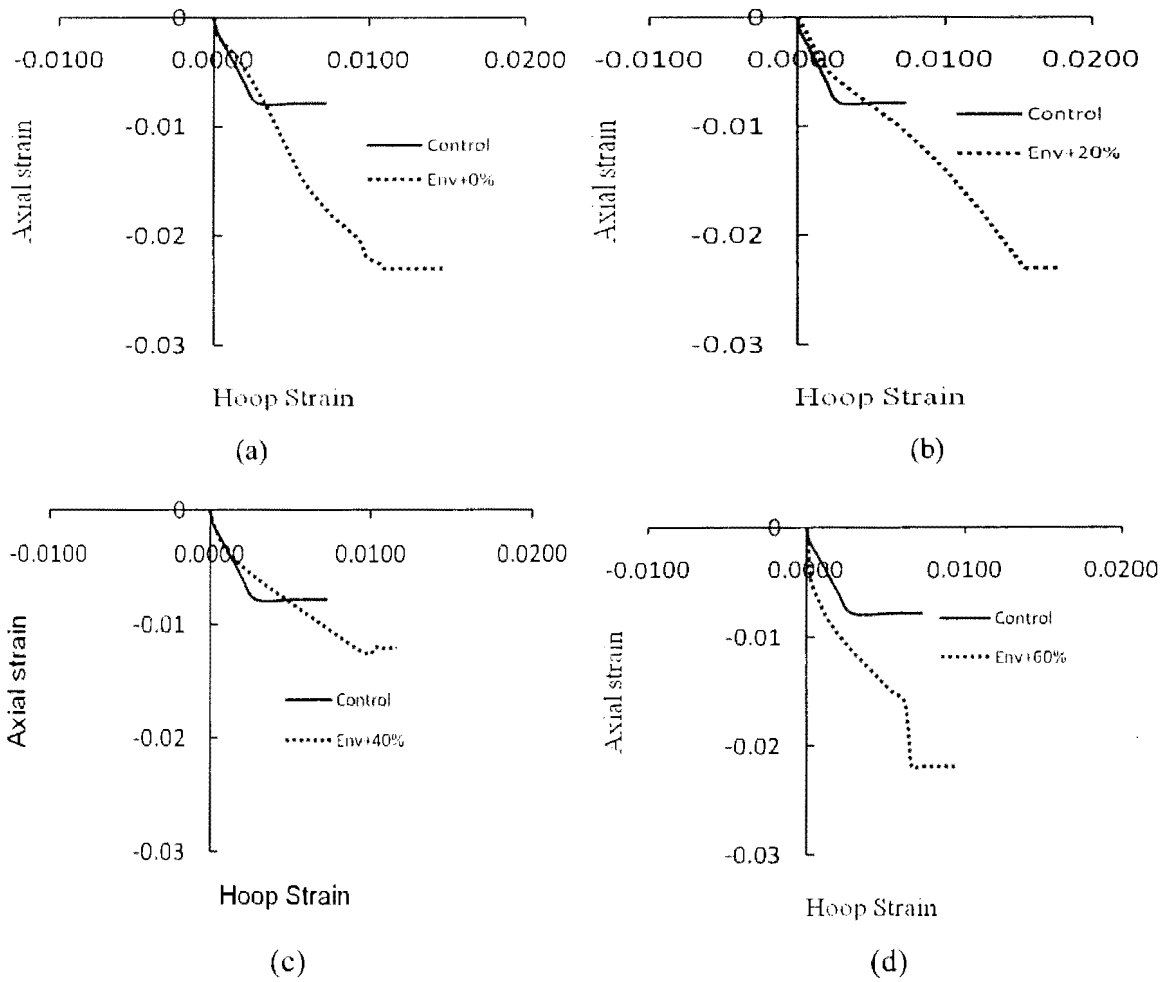

Figure 4.14. Relationship between axial and hoop strains of confined cylinders: (a) Env+0% (Cylinder 6); (b) Env+20% (Cylinder 9); (c) Env+40% (Cylinder 12); (d) Env+60% (Cylinder 15)

4.6.4. Volumetric Strains

The change of volumetric strains of test cylinders is shown in Figs. 4.15 and 4.16. The volumetric strain of a cylinder, ε_{vol}, is defined as (Fenner 1999)

$$\varepsilon_{vol} = 2\varepsilon_{\theta} + \varepsilon_{z} \tag{1}$$

where ε_{θ} is the hoop strain and ε_{z} is the axial strain. All of the cylinders exhibited negative volumetric strains that denoted a reduction in volume of the concrete. Such volumetric changes continued until the axial stress reached the critical state, namely, a sudden increase

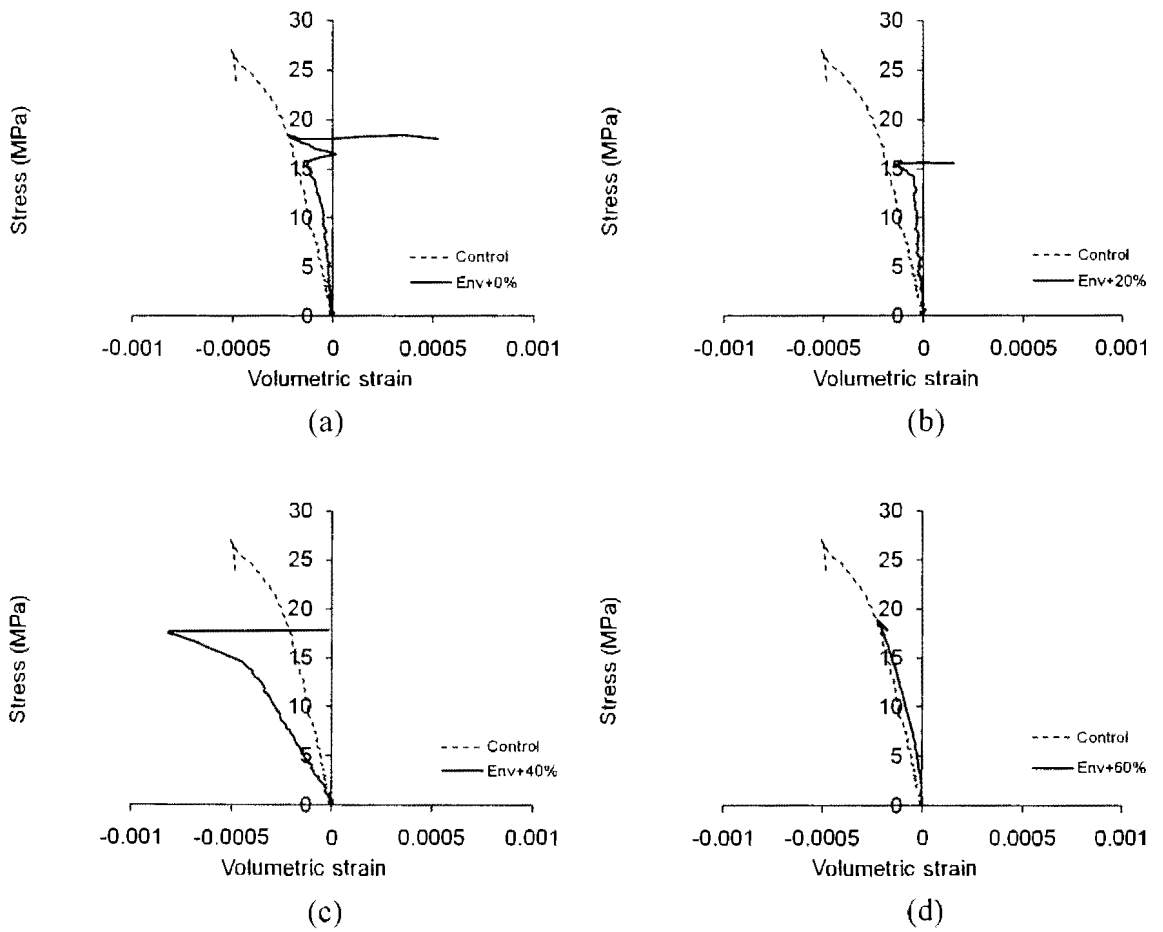

Figure 4.15. Variation of volumetric strain of unconfined cylinders: (a) Env+0% (Cylinder G); (b) Env+20% (Cylinder H); (c) Env+40% (Cylinder K); (d) Env+60% (Cylinder N)

in the volumetric strains (dilatation of the cylinders at failure). The unconfined cylinders exposed to the environmental and live load effects showed stiff responses when compared to the control cylinder, except for the cylinder with Env+40% (Fig. 4.15c). The low stiffness of the cylinder with Env+40% (Fig. 4.15c) may be due to the significant damage of the concrete during the load cycling (to be discussed). The confined cylinders exposed to the environmental and live load (40% and 60%) effects showed soft responses when compared to the confined control cylinder, while the cylinders with Env+0% (Cylinder 6) and Env+20 % (Cylinder 9) showed similar responses in comparison to the control cylinder (Fig. 4.16a and b). The low stiffness of the cylinder with Env+40% and Env+60% live load effects (Fig. 4.16c and d) may be due to the significant internal damage of the concrete during the load cycling and looseness of the confining systems.

4.6.5. Crack Pattern during Load Cycling

Fig. 4.17 shows the crack patterns of the cylinders during the load cycling. No visible cracks were observed for the confined cylinders and the unconfined cylinder subjected to the environmental load without live load effects (Env+0%, Cylinder G), as shown in Fig. 4.17(a). The cylinder with Env+20% (Cylinder I) showed some tiny cracks and spalling of the concrete near the bottom at 58 cycles (Fig. 4.17b). This observation indicates that the presence of live loads influenced the durability performance of concrete members. Time-dependent progression in cracking of the cylinders exposed to a load level of Env+40% and Env+60% is shown in Figs. 4.17(c), (d), and 4.18. Cylinder M with Env+40% exhibited noticeable cracks near the top and bottom at 29 cycles and some diagonal cracks formed at 56 cycles, as shown in Fig. 4.18(c). The developed cracks in Cylinder M became wide when the load effect increased up to 89 cycles. The deterioration

level of Cylinder P (Env+60%) seemed to be analogous to that of Cylinder M (Env+40%), as shown in Fig. 4.18(c) and (d); however, Cylinder O failed at 80 cycles. Figs. 4.18 and 4.19 summarize the crack growth during the environmental cycling. Cracks initiated faster in the cylinders with Env+60% (Cylinders P and O as shown in Fig. 4.18a and b, respectively) and Env+40% (Cylinders M as shown in Fig. 4.18d) than the cylinders Env+20% cycles. Crack were observed after few cycles in the cylinders exposed to a load level of Env+60% (Cylinder P as shown in Fig. 18a) and Env+40% (Cylinder M as shown

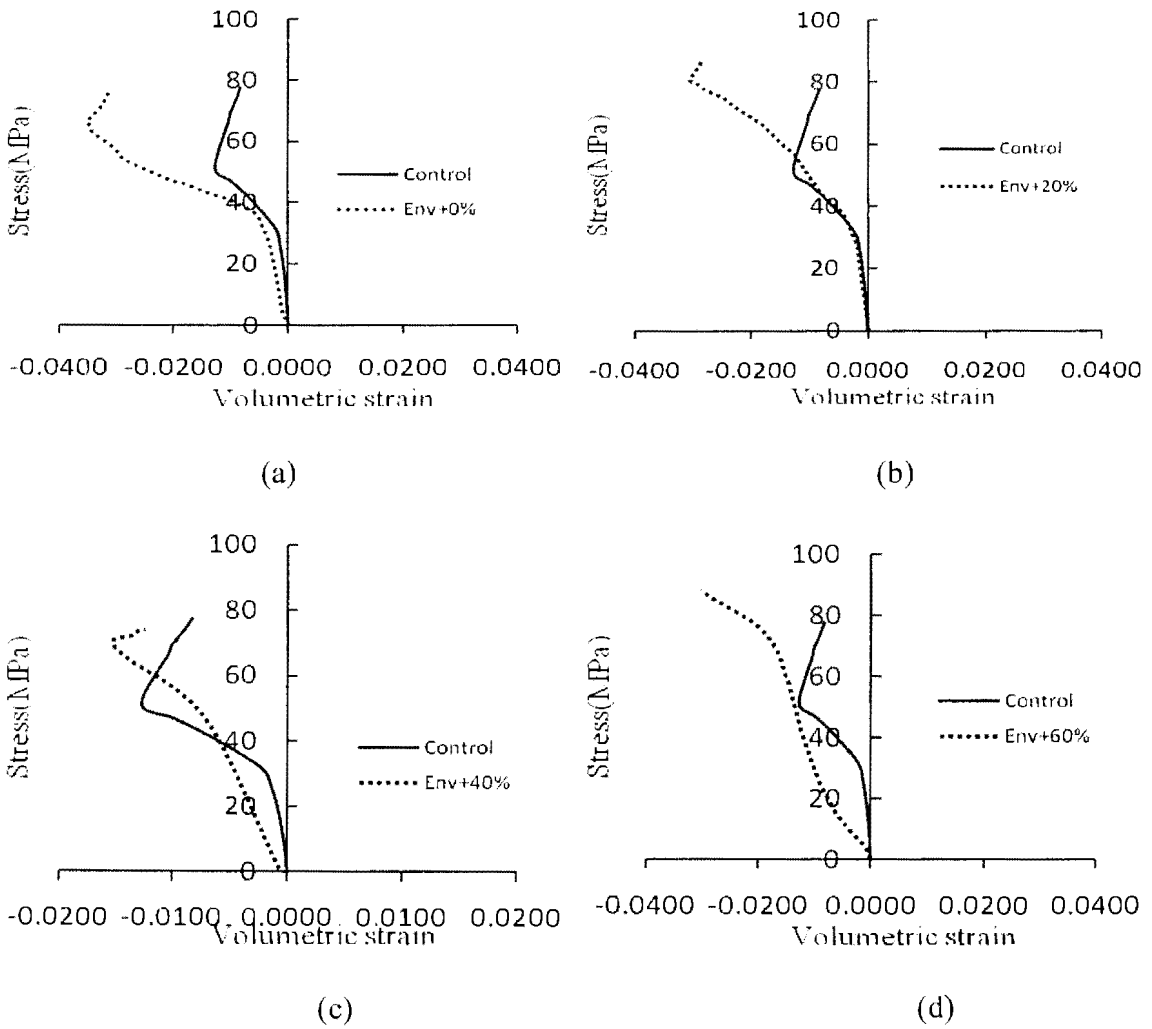

Figure 4.16. Variation of volumetric strain of confined cylinders: (a) Env+0% (Cylinder 6); (b) Env+20% (Cylinder 9); (c) Env+40% (Cylinder 12); (d) Env+60% (Cylinder 13)

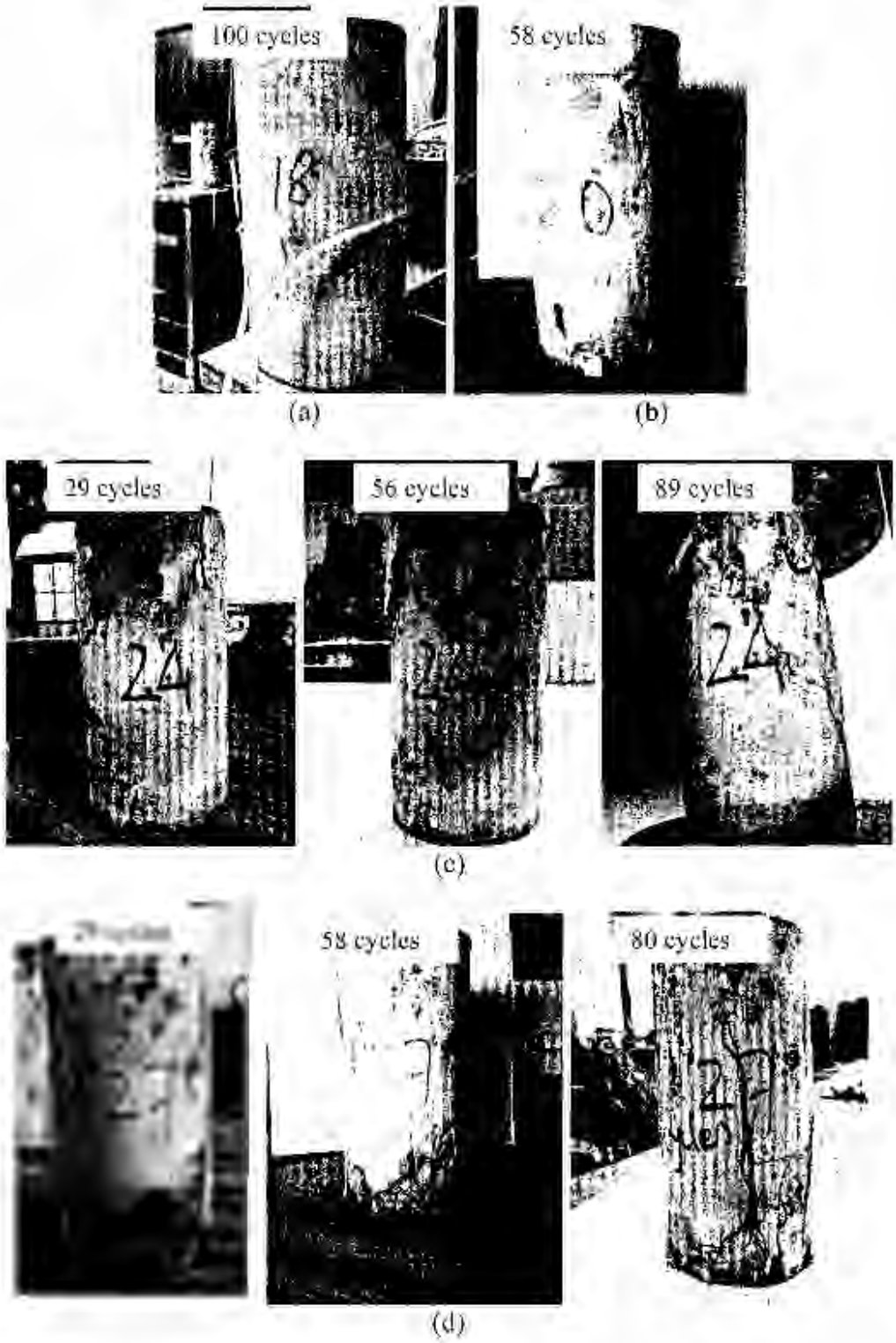

Figure 4.17. Crack patterns during the load cycle: (a) Env + 0% (Cylinder G); (b) Env + 20% (Cylinder I); (c) Env – 40% (Cylinder M); (d) Env + 60% (Cylinder P)

in Fig. 18d).Whereas, cracking initiated after approximately 25 cycles for the cylinders with Env+20% (Cylinders J shown in Fig.4.19), with some exceptions, that implies the deterioration or damage rate increases with increasing the live load effects.

4.6.6. Failure Modes

The failure mode of the individual cylinders is shown in Figs. 4.20, 4.21 and 4.22. For the unconfined cylinders, the control cylinders showed a moderate level of damage at failure with a couple of large cracks (Fig. 4.20a), whereas the cylinders exposed to the environment exhibited severe diagonal cracks (Fig. 4.20b). Cylinder H with Env+20% showed some tiny cracks near the top of the cylinder, which could be related to the live load effects. The damage level of the cylinders with Env+40% was substantial, as shown in Fig. 4.21(b). All of the cylinders showed significant spalling and splitting of the concrete. This noticeable failure mode can explain the reduced modulus (or stiffness) of the cylinders in the Env+40% category shown in Figs. 4.11 and 4.15(c). The cylinders with Env+60% (Fig. 4.21c) showed somewhat wider cracks when compared to the cylinders with Env+20% (Fig. 4.21a), whereas the level of damage seemed to be less than that of the cylinders with Env+40% (Fig. 4.21b). However, the confined cylinders had a brittle failure mode and the failure was governed by tensile fracture of the CFRP sheets in the transverse direction. Once the stress level induced by the confinement pressure in the transverse direction namely fibers direction exceeded the fiber's ultimate tensile strength, a loud popping sounds was heard which provided the warning of the failure initiation and fibers suddenly ruptured and catastrophic failure occurred as shown in Fig. 4.21.The most observed failure mode was broken or rupture of the fibers near mid-height of the cylinders.

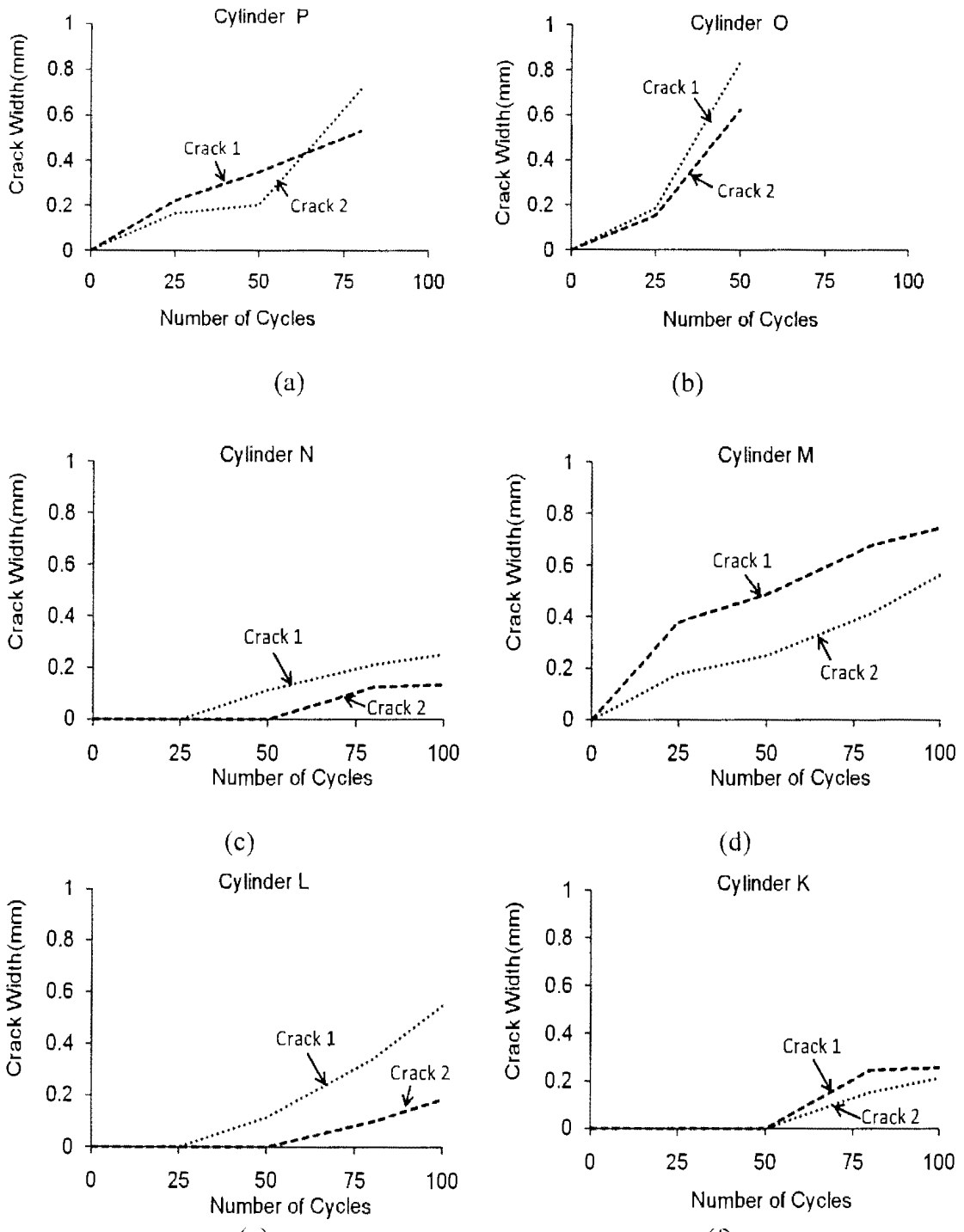

Figure 4.18. Crack width variations with the load cycle: (a) Env + 60% (Cylinder P); (b) Env + 60% (Cylinder O); (c) Env + 60% (Cylinder N); (d) Env + 40% (Cylinder L) ; (d) Env + 40% (Cylinder K)

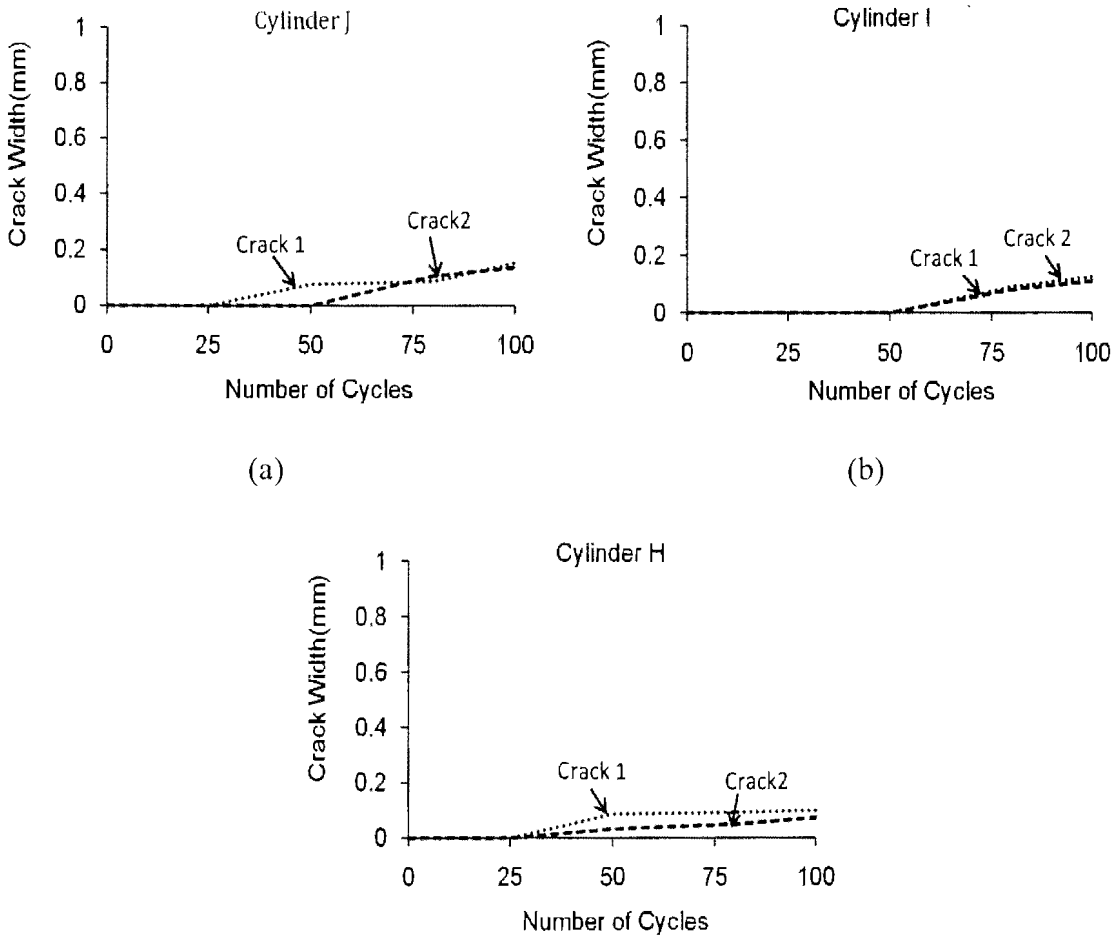

Figure 4.19. Crack width variations with the load cycle: (a) Env + 20% (Cylinder J); (b) Env + 20% (Cylinder I); (c) Env + 20% (Cylinder H)

4.7. ANALYTICAL MODELS

The following section gives an overview of some available theoretical models for FRP-strengthened axial members. Three modes will be summarized and brief comparisons will be provided, including the ACI440 (2002) model, ISIS Canada (2001) model and Karbhari and Gao (1997) model.

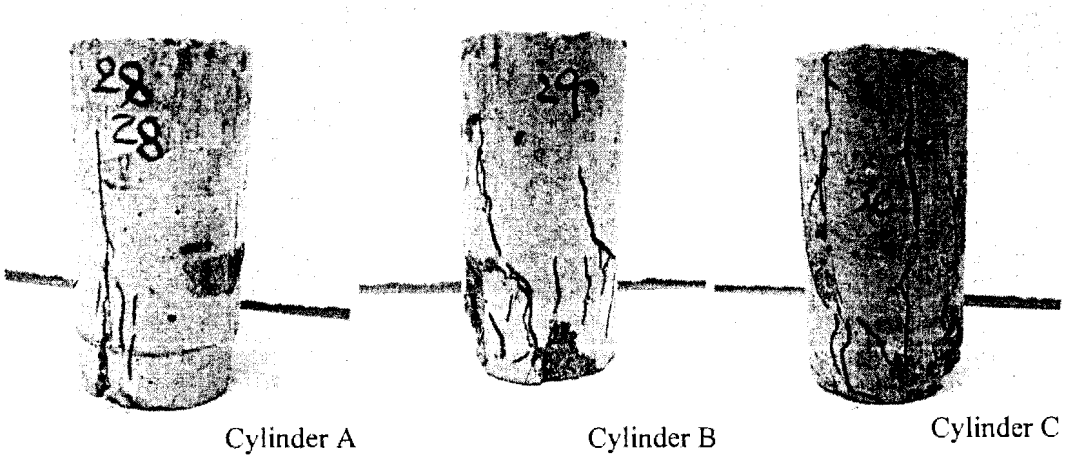

(a)

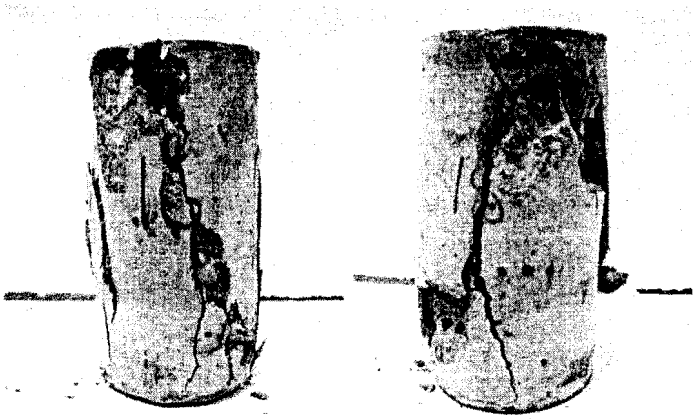

(b)

Figure 4.20. Failed test specimens: (a) Control; (b) Environmental effect + 0% live load

4.7.1. Models by ACI440 (2001) and ISIS Canada (2001)

The following models developed by ISIS Canada (ISIS 2001) and ACI Committee 440 (ACI 2002) were used to predict the ultimate strength ($f_{cc}^{'}$) of CFRP-confined concrete cylinders.

4.7.1.1. Model by ACI 440 (2001)

$$f_{cc}^{'} = f_{c}^{'}[2.25\{1+7.9\frac{f_l}{f_c^{'}}\}0.5 - 2\frac{f_l}{f_c^{'}} - 1.25] \quad (1)$$

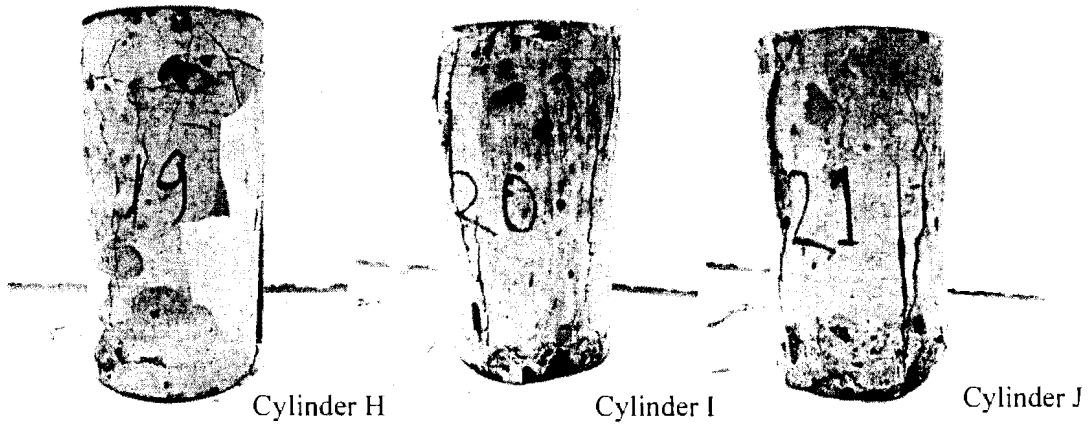

(a)

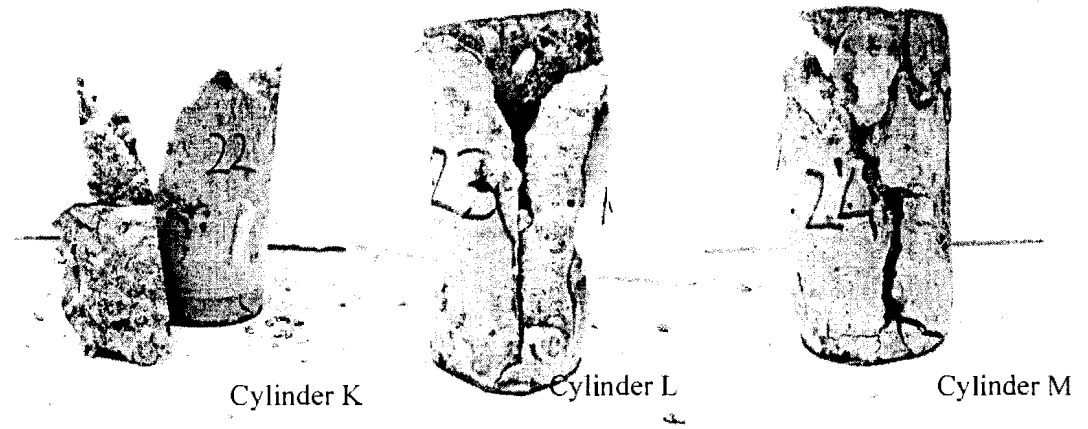

(b)

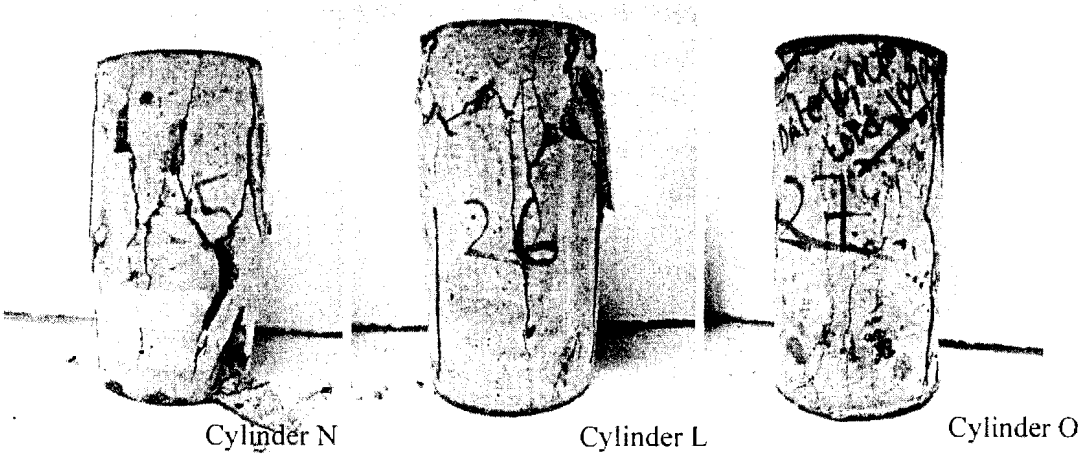

(c)

Figure 4.21. Failed test specimens: (a) Environmental effect + 20% live load; (b) Environmental effect + 40% live load; (c) Environmental effect + 60% live load

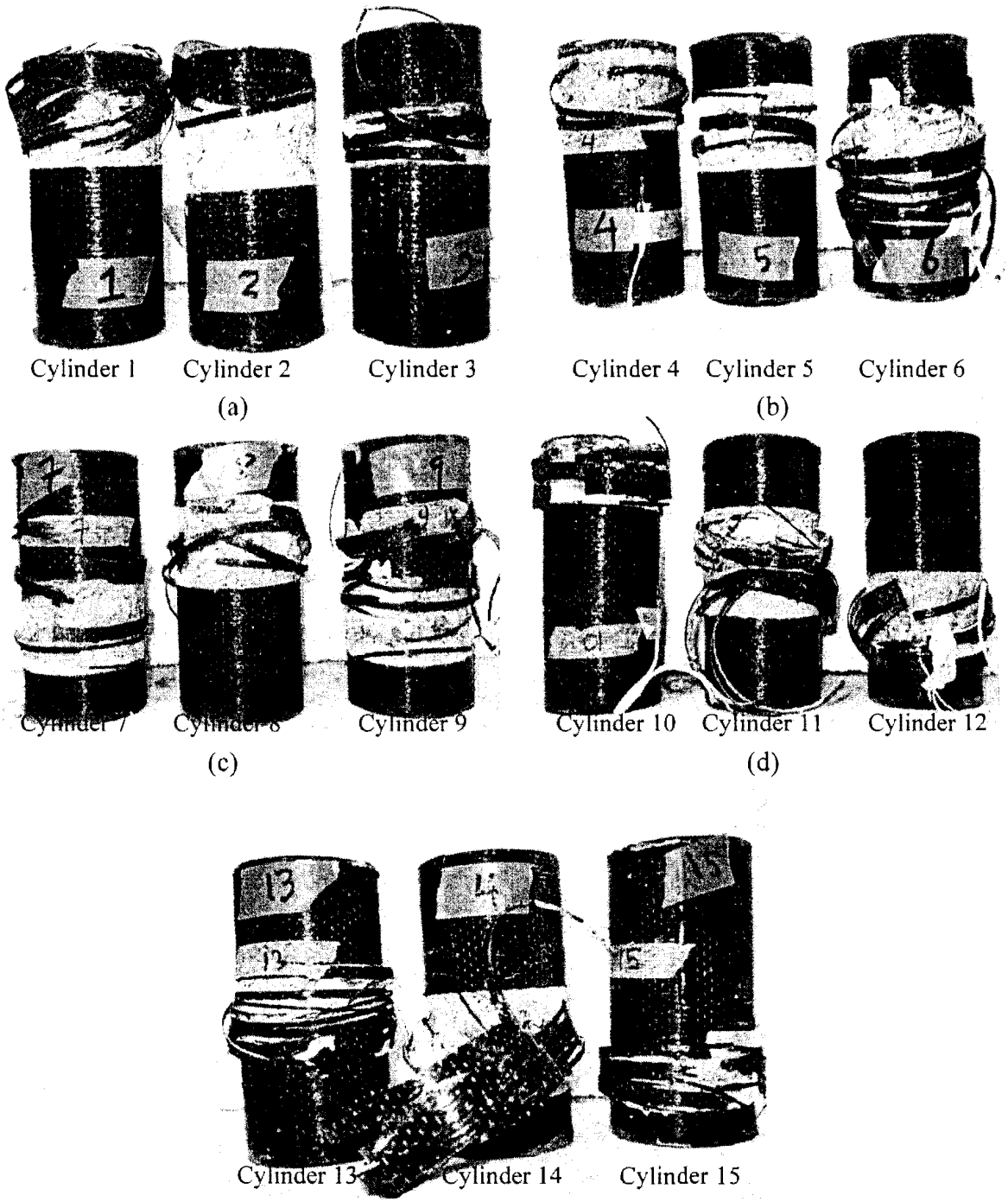

Figure 4.22. Failed test specimens: (a) Control; (b) Environmental effect + 0% live load; (c) Environmental effect + 20% live load; (d) Environmental effect + 40% live load; (e) Environmental effect + 60% live load

where $f_{cc}^{'}$ = confining strength of concrete; f_l = lateral stress produced by confinement;

$f_c^{'}$ = strength of unconfined concrete

$$f_l = \frac{K_a \rho_f f_{fe}}{2} = \frac{K_a \rho_f \varepsilon_{fe} E_f}{2} \tag{2}$$

where k_a = efficiency factor of FRP, (based on shape of section); ρ_f = reinforcement ratio;

ε_{fe} = effective strain of FRP; E_f = tensile elastic modulus of FRP

$$\rho_f = \frac{4nt_f}{h} \tag{3}$$

where n = no of plies; t_f = nominal thickness of one ply

$$\varepsilon_{fu} = C_E \varepsilon^*_{fu} \tag{4}$$

where ε_{fu} = ultimate rupture strain of FRP; C_E = environmental reduction factor;

ε^*_{fu} = ultimate rupture strain of FRP by manufacture

$$f_{fu} = C_E f^*_{fu} \tag{5}$$

where f_{fu} = design ultimate tensile strength of FRP; f^*_{fu} = tensile strength of FRP by manufacture;

$$E_f = f_{fu} / \varepsilon_{fu} \tag{6}$$

where E_f = tensile elastic modulus of FRP; f_{fu} = design ultimate tensile strength of FRP;

ε_{fu} = ultimate rupture strain of FRP

4.7.1.2. Model by ISIS Canada (2001)

$$f_{cc}^{'} = f_c^{'}(1 + \alpha_{pc}\, \varpi_w) \tag{7}$$

where $f_{cc}^{'}$ = confining strength of concrete; $f_c^{'}$ = strength of unconfined concrete; α_{pc} = performance coefficient of circular column; ϖ_w = volumetric ratio of FRP strength to concrete strength

$$\varpi = 2 f_{lfrp} / \Phi_c f_c^{'} \quad (8)$$

where f_{lfrp}= confining pressure due to FRP reinforcement; Φ_c = resistance factor of concrete; $f_c^{'}$ = strength of unconfined concrete

$$f_{lfrp} = 2N_b \ \Phi_{frp} f_{frpu} t_{frp} / h_c \quad (9)$$

where N_b = number of layers; Φ_{frp} = resistance factor of FRP; f_{frpu} = tensile strength of FRP; t_{frp} = thickness of FRP; h_c = diameter of circular column.

4.7.2. Model by Karbhari and Gao (1997)

$$f_{cc}^{'} = f_{c0}^{'} + 2.1 f_{c0}^{'} \left(\frac{2\sigma_{11} * t}{d f_{c0}^{'}} \right)^{0.87} \quad (10)$$

where $f_{cc}^{'}$ = maximum strength of confined concrete; $f_{c0}^{'}$ = unconfined concrete strength;

σ_{11} = tensile strength of the fiber reinforced polymer composite in polymer direction;

t = thickness of the composite jacket; and d = diameter of the concrete core.

4.7.3. Comparisons

The ultimate confined concrete strength ($f_{cc}^{'}$) was computed according to the models provided by the ACI Committee 440 (ACI 2002), ISIS Canada (2001) and Karbhari and Gao (1997) and compared to them to the present results. Detail of the test results are given in Tables 4.3-4.8. Based on the percentage errors, all the three models conservatively predicted the ultimate compressive strength of the CFRP-wrapped cylinders. In these predictions, the maximum compressive strength of the confined cylinders was computed based on the average unconfined concrete compressive strength $f_c^{'}$ at 28 days. The ACI model (2002) was based on the maximum rupture strain reported by the manufacturer while the ISIS Canada (2001) and Karbhari and Gao (1997) models did not depend on the

strain. ISIS (2001) and Karbhari and Gao (1997) models depend on the ultimate tensile strength of the FRP provided by the manufacturer. A minimum confinement ratio f_e/f_c' of 0.08 was used in the ACI model (2002). Therefore, changing the environmental reduction factor from 0.85 for exterior exposure to 1.0 did not affect the prediction for the ultimate strength. Similarly, the prediction using the ISIS Canada (2001) model was governed by the minimum confinement pressure $f_{eFRP} \geq 4MPa$. Therefore, changing the material resistance factor for the CFRP from 0.75 to 1.0 would not affect the prediction.

Tables 4.3-4.8 show the results of the three analytical models compared against the experimental values for the control and environmentally conditioned cylinders. Tables 4.5, 4.6 and 4.8 give the percentage differences between the experimental results and those obtained by the three models. The ACI 440 (2002) model gave a slightly better prediction than both ISIS (2001) and Karbhari and Gao (1997) models. For control cylinders, the differences between the experimental results and the models were: ACI 440 (2002) 11.9 %, ISIS Canada (2001) 31.0 % and Karbhari and Gao (1997) 27.1 %. For environmental conditioned cylinders the difference between experimental and the models were: ACI 440 (2002) 17.1 %, ISIS Canada (2001) 26.9 % and Karbhari and Gao (1997) 23.0 %. In both of the ISIS (2001) and Karbhari and Gao (1997) models, they consider the ultimate tensile strength of FRP, whereas ACI 440 (2002) considers the ultimate rupture strain. In all cases, the confinement models more conservatively estimated the strength of the CFRP-confined cylinders. Bisby et al. (2005) recently reported the same thing, they compared the ISIS and ACI confinement models against a much wider database of experimental results and found that the ISIS model was generally conservative than the ACI 440 model. As can be

observed from these comparisons, the ACI 440 model, in general, shows good agreement with the experimental results, else though it is conservative.

Table 4.3. Numerical results obtained using ISIS Canada (2001) Model

Test Cond.	Parameters								Results			Exp.
	α_{pc}	N_b	Φ_{frp}	t_{frp} m	D_g mm	f_{frpu} MPa	Φ_c	f'_c MPa	f_{lfrp} MPa	ω_w	f'_{cc} MPa	f'_{cc} MPa
Control	1	1	1.0	0.1	75	3589	1.0	22.9	15.8	1.38	54.5	79.1
100cyc	1	1	1.0	0.1	75	4013	1.0	22.9	17.7	1.54	58.2	79.6
Manf[1]	1	1	1.0	0.1	75	3800	1.0	22.9	16.5	1.46	56.3	---

[1]: manufacturer (MBrace 2007)

Table 4.4. Numerical results obtained using ACI 440 (2001) confinement model

Test Cond.	Parameters								Results		Exp.
	f'_c MPa	K_a	n	t_f mm	h mm	C_E	ε^*_{fu}	E_f GPa	f_l MPa	f'_{cc} MPa	f'_{cc} MPa
Control	22.9	1	1	0.165	75	1.0	0.0152	231	15.21	69.7	79.1
100 cyc	22.9	1	1	0.165	75	.85	0.0149	201	12.97	66.0	79.6
Manf[1]	22.9	1	1	0.165	75	1.0	0.0167	227	16.42	71.5	-

[1]: manufacturer (MBrace 2007)

Table 4.5. Comparison of confinement models (Control)

	Strength(MPa)	% Difference to experimental*
Experimental	79.1	
ISIS	54.5	31.0%
ACI 440	69.7	11.9%

*: Percentage difference is determined by (experimental - analytical)/experimental x 100

Table 4.6. Comparison of confinement models (100 Cycles)

	Strength(MPa)	% Difference to experimental*
Experimental	79.6	
ISIS	58.2	26.9%
ACI 440	66.0	17.1%

*: Percentage difference is determined by (experimental - analytical)/experimental x 100

Table 4.7. Numerical results obtained using Karbhari and Gao (1997) model

Test condition	Parameters				Results	Exp.
	f'_{c0} (MPa)	t_f (mm)	d (mm)	σ_{11} (MPa)	f'_{cc} (MPa)	f'_{cc} (MPa)
Control	22.9	0.165	75	3589	57.7	79.1
100cyc	22.9	0.165	75	4013	61.3	79.6
Manufacturer[1]	22.9	0.165	75	3800	59.5	---

[1]: manufacturer (MBrace 2007)

Table 4.8. Comparison of confined concrete strength

Exposure condition	Compressive strength (MPa)		Percentage difference [a]
	Experimental	Analytical	
Control	79.1	57.7	27.1%
100 cycles	79.6	61.3	23.0%

[a]: Percentage difference is determined by (experimental - analytical)/experimental X 100

4.8. SUMMARY AND CONCLUSION

This chapter has presented an experimental program to examine the effects of harsh environments and live loads on the durability of CFRP strengthened axial concrete members. A total of 16 unconfined and 15 confined cylinders were tested under the freezing-submerging-drying conditions plus different levels of live load effects up to 100 cycles. The investigation focused on the load-carrying capacity, strain responses, crack patterns during the load cycling, and failure mode. The unconfined cylinders exposed to the environmental condition showed an average decrease of 10% in the load-carrying capacity, while the cylinders subjected to a combination of the environment and the live load effects exhibited a decrease up to 41.9% when compared to the control specimens. However, the load carrying capacity of the CFRP-wrapped cylinders exposed to the harsh environmental

and live load effects was not changed significantly. The modulus in the stress-strain response of the conditioned cylinders decreased due to the growth of internal damage during the load cycling. Cracks of the unconfined cylinders developed and the crack opening increased when the load cycle increased. Such behavior influenced the axial stiffness of the conditioned cylinders. However, no visual cracks were observed for the confined cylinders. All of the test cylinders demonstrated volumetric contraction until failure occurred. A sudden increase of the volume was, however, observed at failure. The confined cylinders showed a brittle and explosive failure mode.

4.9. REFERENCES

1. Abdel-Fattah, H., and Ahmad, S. H. "Behavior of Hoop-Confined High-Strength Concrete under Axial and Shear Loads", *ACI Structural Journal*, Vol. 86, No 6, 1989, pp. 652- 659.

2. Akkaya, Y., Voigt, T., Subramaniam, K.V., and Shah, S.P. "Nondestructive measurement of concrete strength gain by an ultrasonic wave reflection method", *Materials and Structures*, 36, 2003, 507-514.

3. ASCE. "Report card for America's infrastructure", *American Society of Civil Engineers*, Reston, VA, 2005, available online at http://www.asce.org.

4. Basheer, L., Kropp, J., and Cleland, D. "Assessment of the durability of concrete from its permeation properties: a review", *Construction and Building materials*, 15, 2001, 993-103.

5. Bisby, L.A., Dent, A.J.S., and Green, M.F. "A Comparison of Models for FRP Confined Concrete," *ACI Structural Journal*, Vol. 102, No. 1, 2005, pp. 62-72.

6. Cai, H. and Liu, X. "Freeze-thaw durability of concrete: ice formation process in pores", *Cement and Concrete Research*, 28(9), 1998, 1281-1287.

7. Enright, M.P. and Frangopol, D.M. "Survey and Evaluation of Damaged Concrete Bridges", *Journal of Bridge Engineering*, ASCE, 5(1), 2000, 31-38.

8. Fenner, R.T. "Mechanics of solids", CRC Press, Boca Raton, FL, 1999.

9. ISIS. "Strengthening Reinforced Concrete Structures with Externally-Bonded Fiber Reinforced Polymers", Design Manual No. 4, The Canadian Network of Centers of Excellence on Intelligent Sensing for Innovative Structures, ISIS Canada Corporation, Manitoba, Canada, 2001.

10. Green, M.F., Bisby, L.A., Fam, A. and Kodur, K.R. "FRP confined columns: Behaviour under extreme conditions", *Cement & Concrete Composites* 28, 2006, 928-937,

11. Karbhari, V.M. "Response of fiber reinforced polymer confined concrete exposed to freeze and freeze-thaw regimes", *ASCE J Compos Construction* 6(1), 2002, pp. 35–40.

12. MBrace. "MBrace saturant datasheet", Degussa, 2007, available online at http://www.basf-cc.ae/en/products/

13. Lau K.T., Zhou, L. M., Tse, P.C., and Yuan L.B. "Applications of Composites, Optical Fibre Sensors and Smart Composites for Concrete Rehabilitation: An Overview", *Applied Composite Materials* 9: 2002, pp. 221-247.

14. Kong, A., Fam, A., and Green, M.F. "Freeze-thaw behavior of FRP-confined concrete under sustained load," *ACI Special Publication on Fiber Reinforced Polymer Reinforcement for Concrete Structures* (SP-230), 2005, pp. 705-722.

15. Kim, Y.J., Green, M.F., and Fallis, G.J. "Repair of bridge girder damaged by impact loads with prestressed CFRP sheets", *Journal of Bridge Engineering*, ASCE, 13(1), 2008 15-23.

16. Kim, Y.J. and Yoon, D.K. "Identifying critical sources of bridge deterioration in cold regions through the constructed bridges in North Dakota, Journal of Bridge Engineering", *American Society of Civil Engineering* (ASCE), 2010 (in-press, submission number-BEENG-130)

17. Mu, R., Miao, C., Luo, X., and Sun, W. "Interaction between loading, freeze-thaw cycles, and chloride salt attack of concrete with and without steel fiber reinforcement", *Cement and Concrete Research*, 32, 2002, 1061-1066.

18. Prado, P.J., Balcom, B.J., Beyea, S.D., Bremner, T.W., Armstrong, R.L., and Grattan-Bellew, P.E. "Concrete freeze-thaw as studied by magnetic resonance imaging", *Cement and Concrete Research*, 28(2), 1997, 261-270.

19. Shahrooz, B.M., Saraf. V., Godbole, B., and Miller, R.A. "Response of Slab Bridges Before, During, and After Repair", *Journal of Bridge Engineering*, ASCE, 7(5), 2002, 267-275.

20. Silva, C.A.R., Reis, R.J.P., Lameiras, F.S., and Vasconcelos, W.L. "Carbonation-related microstructural changes in long-term durability concrete", *Material Research*, 5(3), 2002, 287-293.

21. Soudki KA, Green MF. "Performance of CFRP retrofitted concrete columns at low temperatures", In: *Proceedings of the advanced composite materials in bridges and structures (ACMBS) conference*, Montreal, Quebec, 1996, p. 427–42.

22. Teng, M. H., Sotelino, E.D., and Chen,W. F. "Performance evaluation of reinforced concrete bridge columns wrapped with fiber reinforced polymers", *ASCE J Compos Construction* 7, (2), 2003, pp. 83–92.

23. Toutanji, H. and Balaguru, P. Durability characteristics of concrete columns wrapped with FRP tow sheets, *ASCE J Mater Civil Eng* 10 (1), 1998, pp. 52–57.

rror: **Unable to store job at printer**
eason: **Disk is not present or is full.**

olution: **Add disk (RAM or EIO hard disk) or delete files.**

CHAPTER 5. CONCRETE BLOCKS

5.1. SYNOPSIS

This chapter presents an experimental program to examine the bond performance of CFR-concrete interface subjected to harsh environmental conditions. The simulated environments consist of 150 cycles of freeze-wet-dry and wet-dry and constant cold temperatures (0°C, -10°C, -20°C, and -30°C) for 2,000 hours. A total fifty three single lap concrete prisms strengthened with CFRP sheets are tested to examine the bond response and corresponding failure modes. The experimental program reports that the cold regions environments are critical on the durability of CFRP-concrete. The results indicate that the bond strength are reduced by 17.1 %, 1.2%, and 16.5 % at 150 cycles of freeze-wet-dry, wet-dry and constant freezing at -30°C for 2,000 hours, respectively.

5.2. INTRODUCTION

Very limited literature is currently available on the effect of cold regions environments on the bond performance between FRP and concrete substrate. Most of these research found in available literature was related to the durability aspects. Sen et al. (1999) conducted an experimental study to investigate the durability performance of epoxy-bonded CFRP-to-concrete interface under marine environmental conditions. In this study, the specimens were simulated for two years under four different environmental conditions such as i) combined wet-dry cycles and hot-cold cycles in 5% salt-water; ii) wet-dry cycles in 15% salt water; iii) outdoor conditions; and iv) room temperature. The bond strength between the concrete and CFRP sheet was degraded least amount under outdoor exposure and greatest bond degradation was recorded under the wet-dry cycles which suggested that

moisture inclusion into epoxy could be detrimental to CFRP-concrete interface. This was attributed to the degradation of the epoxy, which led to weakening of bond between the concrete and CFRP sheet. FRP strengthened beams subjected to wet-dry cycling showed reduction in load carrying capacity when compared to the control specimens (Toutanji and Gomez 1997).

The effectiveness of CFRP strengthening strongly depends on the bond strength of CFRP-to-concrete interface. Green (2000) investigated the effects of freeze-thaw effects on the durability of bond between FRP plate to concrete. The specimens were exposed up to 300 freeze–thaw cycles consisting of 16 hours of freezing and 8 hours of thawing in a water bath. The results indicated that the bond strength between CFRP strips and concrete did not significantly decrease up to 300 freeze–thaw cycles. However, Ren et al. (2003) showed that freeze-thaw cycles decreased the bond strength and thus reduced the effectiveness of FRP repair.

Grace (2004) cited that long-term exposure of FRP-strengthened reinforced concrete beams to humidity may cause a significant decrease in their load carrying capacity due to decrease the bonding strength, and even short-term exposure to humidity could significantly degrade the strengthening system. The degradation of the strength of adhesively bonded joints through the effects of moisture is one of the major concerns affecting their wide implementation in structural applications. Moisture influenced the behavior of adhesives by plasticization and swelling which decreased joint strength (Toutanji and Gomez 1997). In addition, water can disrupt interfacial bond non-reversible damage, as predicted by the theories of adhesion, or cause failure by corrosion of the underlying metal substrate. Apicella et al. (1979) proposed that micro cavities could form

in adhesives by moisture ingression which caused irreversible damage. Hand et al. (1991) also demonstrated that micro cavities were the major contributing factor to reducing the bond strength of CFRP-concrete and induce permanent damaging to the epoxy system.

Although intensive research has been reported on the debonding mechanism of CFRP sheets from the concrete substrate, there is still a dearth of understanding on the bond behavior of CFRPs subject to cold regions environmental conditions. The research investigates the effects of freeze-wet-dry, wet-dry, and different low temperatures (0°C, -10°C, -20°C and -30°C). The residual load-carrying capacity and interfacial fracture energy of the test specimens are evaluated.

5.3. RESEARCH OBJECTIVE

The CFRP sheets may be bonded on the tensile soffit of a deteriorated concrete structure using a bonding agent to enhance load-carrying capacity. The success in such strengthening or retrofitting technologies for concrete structures strongly depends on bond between CFRP sheets and concrete substrate. In this method, possible failure may occur due to debonding of CFRP sheets. Premature debonding of the bonded CFRP sheets may cause a significant loss of the strengthening effect. The first objective of this experimental study is to investigate the effects of harsh environmental conditions. Various low temperatures up to -30°C, freeze-wet-dry, and wet-dry effects were applied to CFRP strengthened concrete. The residual load-carrying capacity, interfacial fracture energy and strain response along the bonding line on the CFRP was evaluated. The second objective is to compare the experimental results with predictive models proposed by Wu et al. (2009).

5.4. EXPERIMENTAL PROGRAM

An experimental program was setup to examine the bond characteristics of CFRP–to–concrete subjected to different low temperatures (0 °C, -10 °C, -20 °C and -30 °C), wet-dry, and freeze-wet-dry effects. Test parameters were temperature, and the number of freeze-wet-dry and wet-dry cycles. The specimens were tested at a typical interval of 25, 50, 100, and 150 cycles.

5.4.1. Materials

5.4.1.1. Carbon Fiber Reinforced Polymer (CFRP) Sheets

The CFRP sheet used for this research work was MBrace CF 130. CFRP sheets were chosen because of their superior mechanical properties and durability under aggressive environmental conditions (Green 2000). The thickness and modulus of elasticity of the CFRP sheets as specified by the manufacturer was 0.165 mm and 227 GPa, respectively. The mechanical properties of the CFRP sheets are shown in Table 5.1.

5.4.1.2. Epoxy Adhesive

The epoxy adhesive used was a two-part epoxy, including saturant resin (Part A) and hardener (Part B). The saturant resin was premixed for 3 minutes. The hardener was, then, blended with the resin and mixed together until a homogeneous mixture was obtained. The mix ratio of the two components was 3 to 1 for the resin and the hardener, respectively (MBrace 2007). Table 5.2 shows typical material properties of the adhesive used for the present study.

5.4.2. Formwork

The formwork was constructed with 10 mm thick plywood, using small nails for connections to secure the walls dividing the concrete blocks.

The form as shown in Fig. 5.1(a) was used for providing room for sixty concrete blocks to be poured at a time. Plastic papers were used on the bottom of the form to obtain a smooth surface.

Table 5.1. Mechanical properties of CFRP sheet as given by the manufacturer*

Tensile strength, f_y	3800 MPa
Modulus of Elasticity, E	227 GPa
Thickness, t	0.165 mm
Ultimate strain, ε_{frp}	0.0167 mm/mm

*: manufacturer (MBrace 2007)

Table 5.2. Material properties of epoxy adhesive

Property	Epoxy Adhesive [a]
Modulus of Elasticity, E (GPa)	>1.5
Tensile strength, f_y (MPa)	>30
Poison ratio, υ	0.40
Strain at yield, ε_{ult}	2.5%

[a]: manufacturer (MBrace 2007)

5.4.3. Casting of Concrete Blocks

A total fifty three concrete blocks (length: 150 mm, width: 100 mm and height: 50 mm) were cast from a single batch of concrete mix (Fig. 5.1b). Crushed aggregate with a maximum size 9.5 mm, river sand for fine aggregate, and Type-I Portland Cement were used to produce the concrete. Normal strength concrete with a compressive strength 20 MPa was designed for the concrete blocks to simulate deteriorated concrete structures. The mix design included a 5.5% air-entertainer and w/c ratio of 0.45. Concrete mix included 513 kg/m^3 of cement, 845 kg/m^3 of sand and 930 kg/m^3 of coarse aggregate. The concrete was carefully placed in the forms to preclude aggregate segregation. The concrete was evenly distributed to avoid uneven pressure on either side of the dividing walls. A vibrator was used to compact the concrete. Once the form was filled with concrete, a hand trowel

was used to smooth the top surface of the concrete block, as shown in Fig. 5.1(b). Along with the concrete blocks, two standard concrete cylinders (diameter: 150 mm and height: 300 mm) were also cast to obtain the 28 days' compressive strength (f_c'). Once the concrete pouring was completed, the concrete specimens were covered with plastic papers to minimize moisture losses. Concrete blocks and cylinders were stripped from the form by carefully removing the dividing walls to avoid chipping of the concrete.

Some of the finished concrete blocks are shown in Fig. 5.2(a). The specimens were moist cured for 28 days at room temperature. After 28 days, 2 standard cylinders were tested and an average concrete strength of 22.9 MPa was obtained.

(a) (b)

Figure 5.1. Casting of Concrete: (a) plywood formwork; (b) smooth of surface after trowelling

5.4.4. CFRP Sheet Application

Before bonding the CFRP sheets to the concrete blocks, the surface of the concrete was thoroughly cleaned to remove surface cement paste and minor exposure of aggregates

to ensure adequate bonding of the CFRP sheets to the concrete. For cleaning the surface, medium coarse sand paper was used. Dusts from the surface then was removed by using high speed water flow, as shown in Fig. 5.2(b), to achieve a dust-free and clean surface. The specimens were dried at room temperature for one day prior to CFRP-bonding. The bonded dimensions were 100 mm length and 75 mm width, and the free length was 150 mm, as illustrated in Fig. 5.3(a).

The distance from the end of the block to the CFRP sheet was 35 mm, and 15 mm clear distance (i.e., unbounded length) was given at the loaded end. Tape was used along the marking line of the bond area to fix the specified bonding area between the concrete and CFRP sheet, as shown in Fig. 5.3(b). Then, 75 mm width and 250 mm length rectangular CFRP sheets were cut from a 500 mm wide CFRP roll by using scissors. Surface preparation for the CFRP sheet was performed in accordance with the manufacturer's guidelines and recommendations. The surface of CFRP sheets was wiped by clean cloth to remove all the dust and broken pieces of carbon fibers.

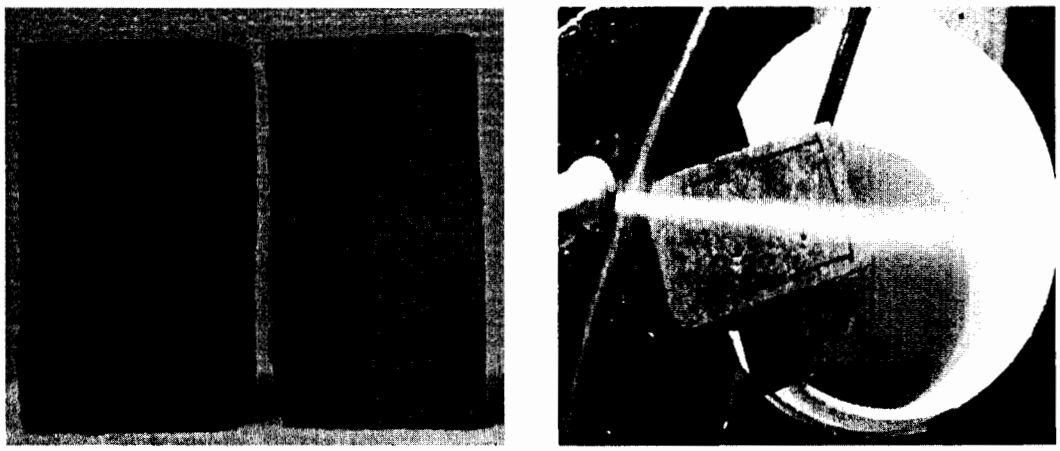

(a) (b)

Figure 5.2. Surface preparation: (a) concrete blocks after removal from formwork; (b) high speed water flow for cleaning the surface

Two-part epoxy resins with a mix ratio (Part A: Part B= 3:1 by weight) as recommended by the manufacturer were used for bonding the CFRP sheets to concrete substrate. The specified guide lines regarding the mix ratio of components, application, and time provided by the manufacturer was also followed. The adhesive was applied in a thin layer with a spatula to the marked area, as shown in Fig. 5.3(b), immediately after mixing. The adhesive was also applied to the surface of the CFRP sheets to make it saturated (Fig. 5.3c) to reduce the risk of forming voids when the sheets were applied to the concrete blocks. The epoxy saturated CFRP sheet was then centred along the longitudinal axis of the concrete block and a 12.5 mm shoulder was left on both sides to minimize the edge effects. The saturated CFRP sheet was positioned to the concrete surface without applying pressure until checking its correct place. Pressure was applied started from the end of the concrete block to the far ends using a spatula to ensure intimate contact with the concrete, and not allowing the formation of voids as shown in Fig. 5.3(d). Once bonding the CFRP sheets to concrete blocks was completed, the specimens were kept at room temperature for a minimum of 10 days for curing.

5.4.5. Environmental Effects

Seven specimens were stored at room temperature to serve as control and the rest of the specimens were exposed to different environmental conditions. Tables 5.4-5.6 summarize the environmental conditions for the CFRP strengthened concrete blocks, including the wet-dry and freeze-wet-dry cycles and constant freezing at different low temperatures. The identification code of the test specimens showed the test environments (*WD* = wet-dry and *FWD* = freeze-wet-dry), the number of repetition, and the number of environmental cycles, whereas the identification code (*CT* = constant temperature) for

specimens exposed to constant freezing was little bit different. For example, FWD2-100 indicates the second specimen tested in 100 cycles of freeze-wet-dry, whereas CT-30-3 indicates the third specimen exposed to -30 °C for 2,000 hours. For the wet-dry cycles, the specimens were submerged under water in a water bath for 16 hours and dried for 8 hours in room temperature (1 cycle).

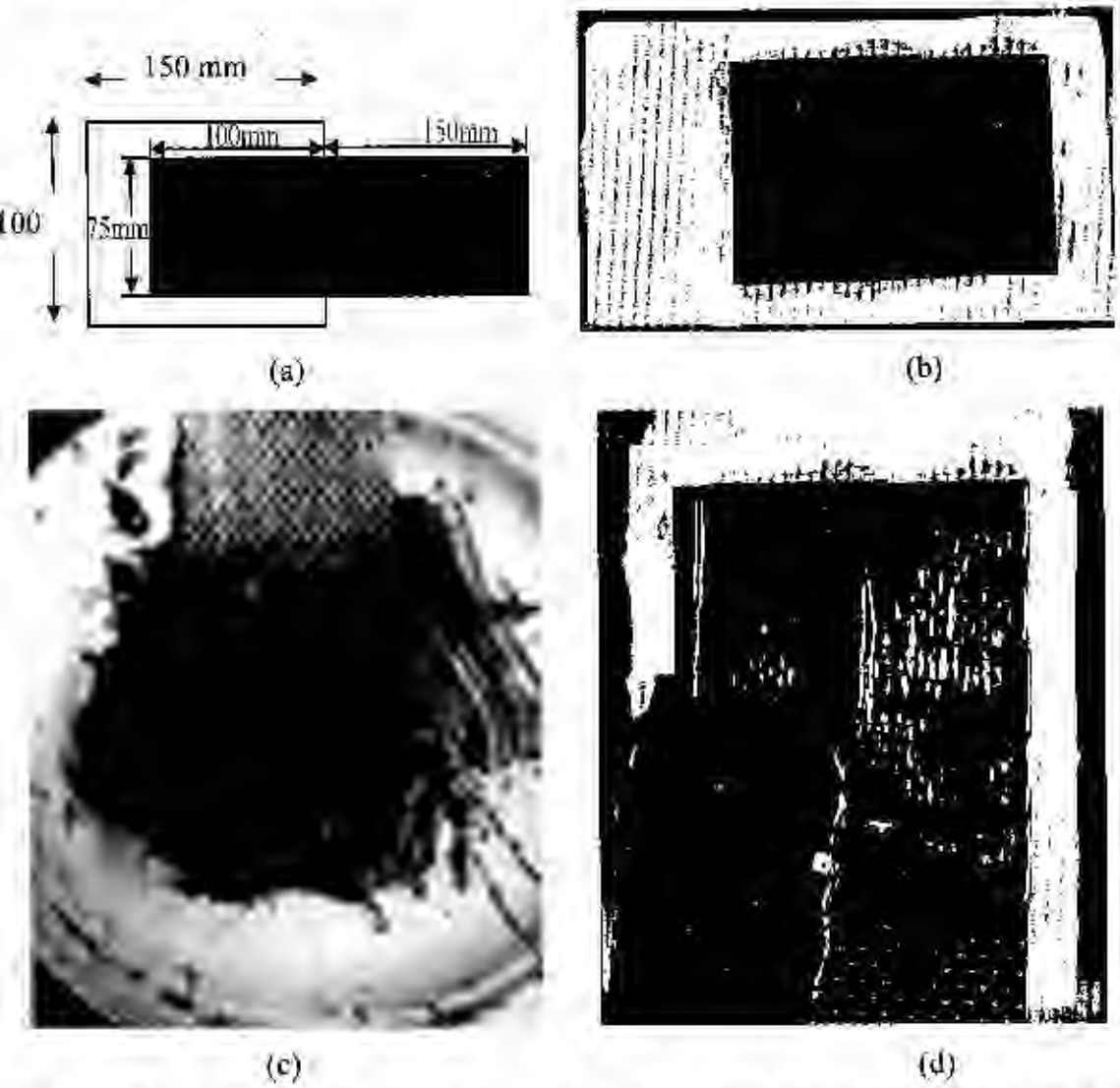

Figure 5.3. CFRP application; (a) location of CFRP sheets; (b) epoxy applied to the concrete surface; (c) epoxy saturated CFRP sheet; (d) CFRP sheet bonding with concrete block

The freeze-wet-dry cycles included 16 hours of freezing at -30°C (Fig. 5.4a), 4 hours of submersing in a water bath (Fig. 5.4b) and 4 hours of drying at room temperature (1 cycle), as shown in Fig. 5.4(c). The environmentally conditioned specimens were tested at a typical interval of 25, 50, 100, and 150 cycles, as shown in Tables 5.4 and 5.5. The freezer (Fig. 5.4d) used for this research was equipped with a digital temperature adjustment function. The temperature was set at -30 °C and the temperature was recorded daily. The daily temperature variation of the freezer is shown in Fig. 5.5. Twenty epoxy coupons were simulated in different constant cold temperatures such as 0°C, -10 °C, -20 °C and -30 °C for 2,000 hours. A minimum of 3 specimens were tested per category as shown in Tables 5.3-5.6.

5.4.6. Instrumentation and Testing

No instrumentations were given for the concrete blocks during the environmental cycling. The instrumentation used for the concrete blocks during testing is illustrated in Fig. 5.6. Upon the completion of the environmental cycling, four strain gages were bonded along the center line of the specimens (Fig. 5.6). Strain gages (G1, G2, G3 and G4) were bonded on the CFRP sheet at a distance of 0, 20, 40, and 70 mm, respectively, from the loaded end as illustrated in Fig. 5.6. Theses strain gages were used to measure the strain responses on the CFRP sheet.

An MTS 810 servo-hydraulic testing machine with a capacity of 1,000 kN and a maximum displacement of 500 mm was used for testing the specimens. The tests were conducted under displacement control, and a tension load was monotonically applied at a rate of 2.5 mm/min until complete debonding occurred. A special gripping system as shown in Fig. 5.7(a) was used to hold the specimen during testing. The test setup is shown

in Fig. 5.7(b). The clamping area was 38 mm x 50 mm, as shown in Fig. 5.7(b). Strain gage readings were recorded by a data acquisition system.

(a)

(b)

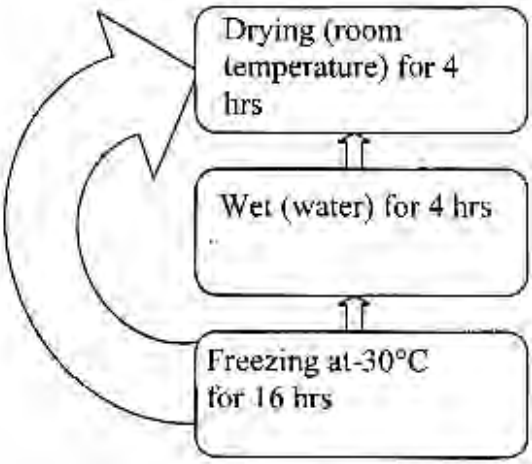

(c)

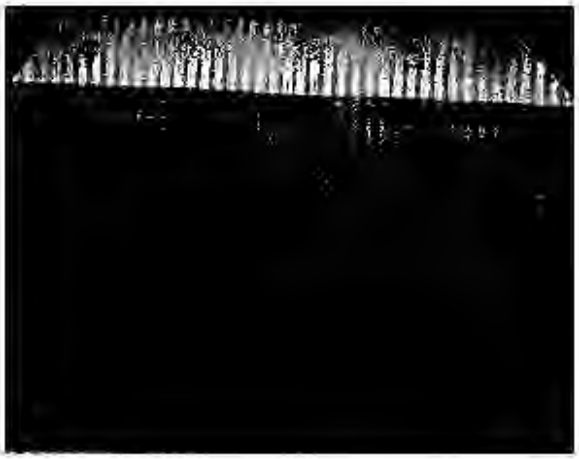

(d)

Figure 5.4. Environmental cycling: (a) freezing; (b) specimen submerse in water bath; (c) environmental cycling; (d) environmental chamber

5.4.7. Laser Scanning

Laser scanning (Fig. 5.8) was performed to examine the interfacial behavior of the

debonded CFRP sheets. All the debonded CFRP surfaces were scanned by using a laser scanner and the Surfer 8.0 software was used to post process the scanned surfaces. Surfer is a contouring and 3D surface mapping program that quickly and easily converts scanned data into 3D surface, 3D wireframe, vector, image, shaded relief, and post maps. Virtually all aspects of the contour maps can be customized to produce publishable images. Surfer contour maps provide users with full control over all the map parameters.

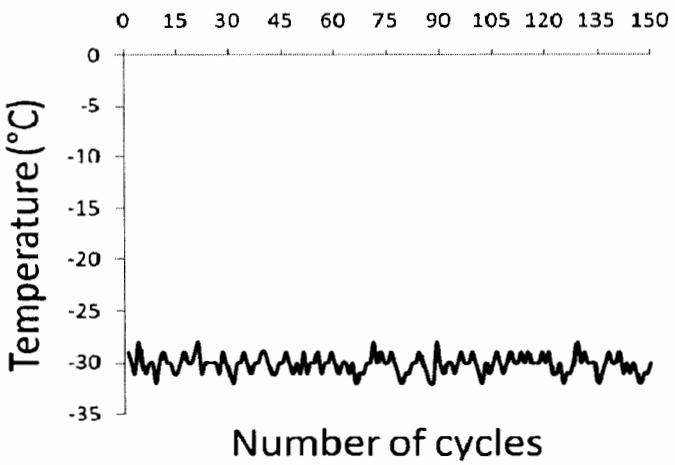

Figure 5.5. Temperature variation in the environmental chamber

5.5. EXPERIMENTAL RESULTS

5.5.1. Load-carrying Capacity and Interfacial Fracture Energy

Tables 5.3-5.6 show the test results of the CFRP strengthened concrete blocks. The average ultimate load of the control specimens was 17.0 kN, while the specimens subjected

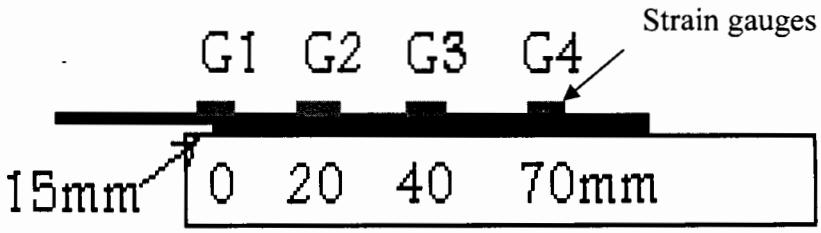

Figure 5.6. Strain gage locations along CFRP sheet

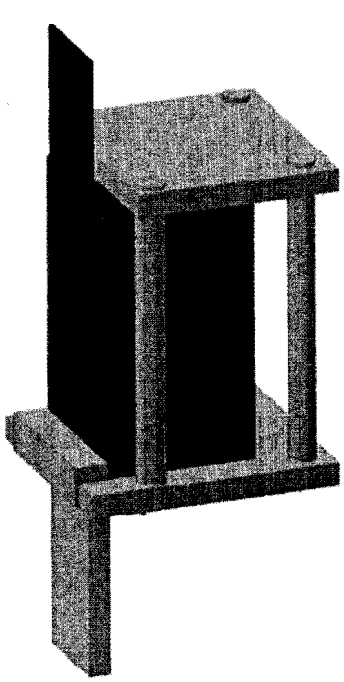

(a) (b)

Figure 5.7. Single lap test: (a) illustration of gripping frame; (b) tension test

to the environmental effects (wet-dry and freeze-wet-dry cycling) showed slight decreasing in the load-carrying capacity initially, for example 16.1 and 16.6 kN after 25 cycles of wet-dry and freeze-wet-dry, respectively. The load-carrying capacity of the specimens exposed to 25 and 50 wet-dry cycles decreased up to 5.3% and 25.9% in the ultimate capacity in comparison to that of the control specimens, on average, respectively, as shown in Fig. 5.9(a), (b) and Table 5.4. The load carrying capacity of the wet-dry cycled specimens, however, showed an increasing trend when the number of wet-dry cycles increased from 50 to 100, however still 1.2% lower in the ultimate capacity in comparison to the control specimens, on average, for the specimens exposed to 100 and 150 wet-dry cycles, as shown

in Fig. 5.9(a) and Table 5.4. These observations indicate that the water ingression could influence the bond strength of the CFRP to concrete interface. Existing research has shown that the bond strength is directly proportional to the square root of both FRP stiffness, $E_p t_p$ (E_p= modulus of elasticity of CFRP, t_p= thickness of CFRP sheet) and interfacial fracture energy, G_F (Wu et al. 2009). Interfacial fracture energy is also related to the compressive strength of concrete, f_c' (Wu et al. 2009).

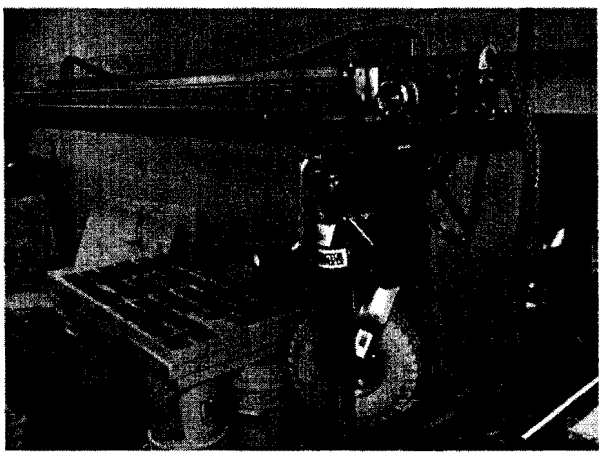

Figure 5.8. Laser scanning of the failed CFRP sheets

Fig. 5.9(c), (d) and Table 5.4 show that the fracture energy was also reduced up to 50 cycles which was also related to the bond strength. Interfacial debonding, in most of the cases, dominates the failure of the specimens. The moisture ingression degraded the strength of the adhesive. The concrete and adhesive experienced additional curing possibly due to the presence of moisture during the wet-dry cycles. The specimens subjected to freeze-wet-dry cycles exhibited consistently decreased load carrying capacity and interfacial fracture energy, as shown in Fig. 5.10 and Table 5.5. The load-carrying capacity of the specimens exposed to 25, 50, 100 and 150 freeze-wet-dry cycles were reduced by 2.4%, 8.8%, 14.7% and 17.1% in comparison to the control specimens, on average,

respectively, as shown in Fig. 5.10(a), (b) and Table 5.5. The interfacial fracture energy of the freeze-wet-dry cycled specimens was, however, reduced in a little bit higher rate than that of the load carrying capacity when the number of freeze-wet-dry cycles increased.

Table 5.3. Test results of control specimens

ID	Environmental effect	Failure load (kN)			Shear stress (MPa)			Interfacial fracture energy (N/mm)		
		P_u	Ave	S	τ_u	Ave	S	G_F	Ave	S
R1	No	17.3	17.0	2.1	2.3	2.3	0.3	4.0	3.9	0.5
R2	No	15.2			2.0			3.1		
R3	No	17.6			2.3			4.3		
R4	No	13.5			1.8			3.6		
R5	No	20.0			2.7			4.1		
R6	No	18.0			2.4			4.7		
R7	No	17.3			2.3			3.7		

Ave = average; *S* = standard deviation; P_u = ultimate load; τ_u = maximum average shear stress; G_F = interfacial fracture energy

Table 5.4. Test results of wet-dry effects

ID	Number of cycling	Failure load (kN)			Shear stress (MPa)			Interfacial fracture energy (N/mm)		
		P_u	Ave	S	τ_u	Ave	S	G_F	Ave	S
WD1-25	25	15.9	16.1	2.3	2.1	2.2	0.3	3.5	3.7	0.8
WD2-25	25	14.7			2.0			2.7		
WD3-25	25	19.2			2.6			4.5		
WD4-25	25	14.5			1.9			3.9		
WD1-50	50	6.3	12.6	1.2	0.8	1.7	0.1	1.4	2.6	0.9
WD2-50	50	13.9			1.9			3.0		
WD3-50	50	14.1			1.9			2.4		
WD4-50	50	16.1			2.1			3.5		
WD1-100	100	13.0	16.8	3.5	1.7	2.2	0.5	2.0	3.9	1.7
WD2-100	100	17.3			2.3			5.2		
WD3-100	100	20.0			2.7			4.5		
WD1-150	150	17.2	16.8	1.1	2.3	2.2	0.1	3.1	3.4	0.6
WD2-150	150	15.6			2.1			2.9		
WD3-150	150	17.6			2.3			4.1		

Ave = average; *S* = standard deviation; P_u = ultimate load; τ_u = maximum average shear stress; G_F = interfacial fracture energy

The interfacial fracture energy of the specimens was reduced by 2.6%, 10.3%, 23.0% and 28.2% in comparison to the control specimens, on average, for the specimens exposed to 25, 50, 100 and 150 freeze-wet-dry cycles, respectively, as shown in Fig. 5.10(c), (d) and Table 5.5. Fig. 5.11(a) and (b) showed a comparison of load-carrying capacity and interfacial fracture energy of wet-dry and freeze-wet-dry cycled specimens. The load-carrying capacity and interfacial fracture energy of the specimens exposed to freeze-wet-dry cycles decreased up to 100 cycles by 14.7% and 23%, respectively; however, those were reduced by 2.4% and 5.2% more when the environmental cycling incases from 100 to 150 (Fig. 5.11).

Table 5.5. Test results of freezing-wet-dry effects

ID	Number of cycling	Failure load (kN)			Shear stress (MPa)			Interfacial fracture energy (N/mm)		
		P_u	Ave	S	τ_u	Ave	S	G_F	Ave	S
FWD1-25	25	19.2	16.6	2.9	2.6	2.2	0.4	4.4	3.8	0.9
FWD2-25	25	17.2			2.3			4.6		
FWD3-25	25	17.4			2.3			3.6		
FWD4-25	25	12.5			1.7			2.7		
FWD1-50	50	13.5	15.5	1.5	1.8	2.1	0.2	2.5	3.5	1.0
FWD2-50	50	17.0			2.3			4.9		
FWD3-50	50	16.2			2.2			3.4		
FWD4-50	50	15.1			2.0			3.1		
FWD1-100	100	16.7	14.5	5.2	2.2	1.9	0.7	3.0	3.0	1.2
FWD2-100	100	7.0			0.9			1.4		
FWD3-100	100	18.9			2.5			4.2		
FWD4-100	100	15.2			2.0			3.5		
FWD1-150	150	10.7	14.1	2.6	1.4	1.9	0.4	2.1	2.8	0.5
FWD2-150	150	16.4			2.2			3.2		
FWD3-150	150	15.7			2.1			3.3		
FWD4-150	150	13.5			1.8			2.7		

Ave = average; *S* = standard deviation; P_u = ultimate load; τ_u = maximum average shear stress; G_F = interfacial fracture energy

This observation may indicate that the detrimental effects of freeze-wet-dry was more crucial up to 100 cycles and afterwards the bond properties was not significantly affected by the freeze-wet-dry cycles. On the other hand, the specimens exposed to wet-dry effects showed a decreasing trend in both interfacial fracture energy and load-carrying capacity initially, whereas after 50 cycles the bond strength was regained and remained almost constant up to 150 cycles.

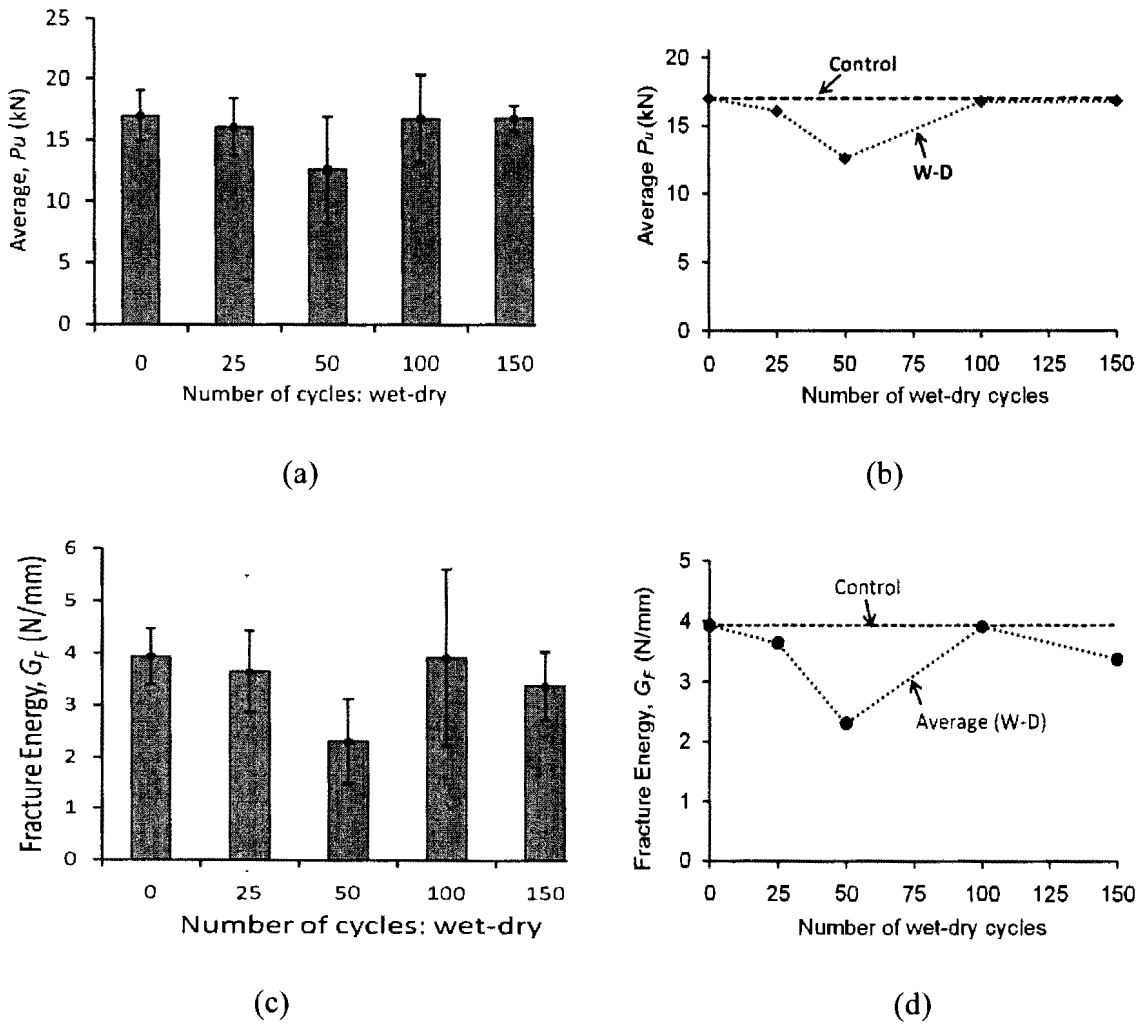

Figure 5.9. Effect of wet-dry cycles: (a) average ultimate strength with standard deviation; (b) average ultimate strength; (c) interfacial fracture energy with standard deviation; (d) interfacial fracture energy

This observation suggests that wet-dry effects also may decrease the load-carrying capacity of the concrete specimens strengthened with CFRP; however, the duration of exposure to wet-dry cycles had no significant effect after 100 cycles. Average shear stress in both cases showed similar trends to the failure loads as shown in Fig.5.12.

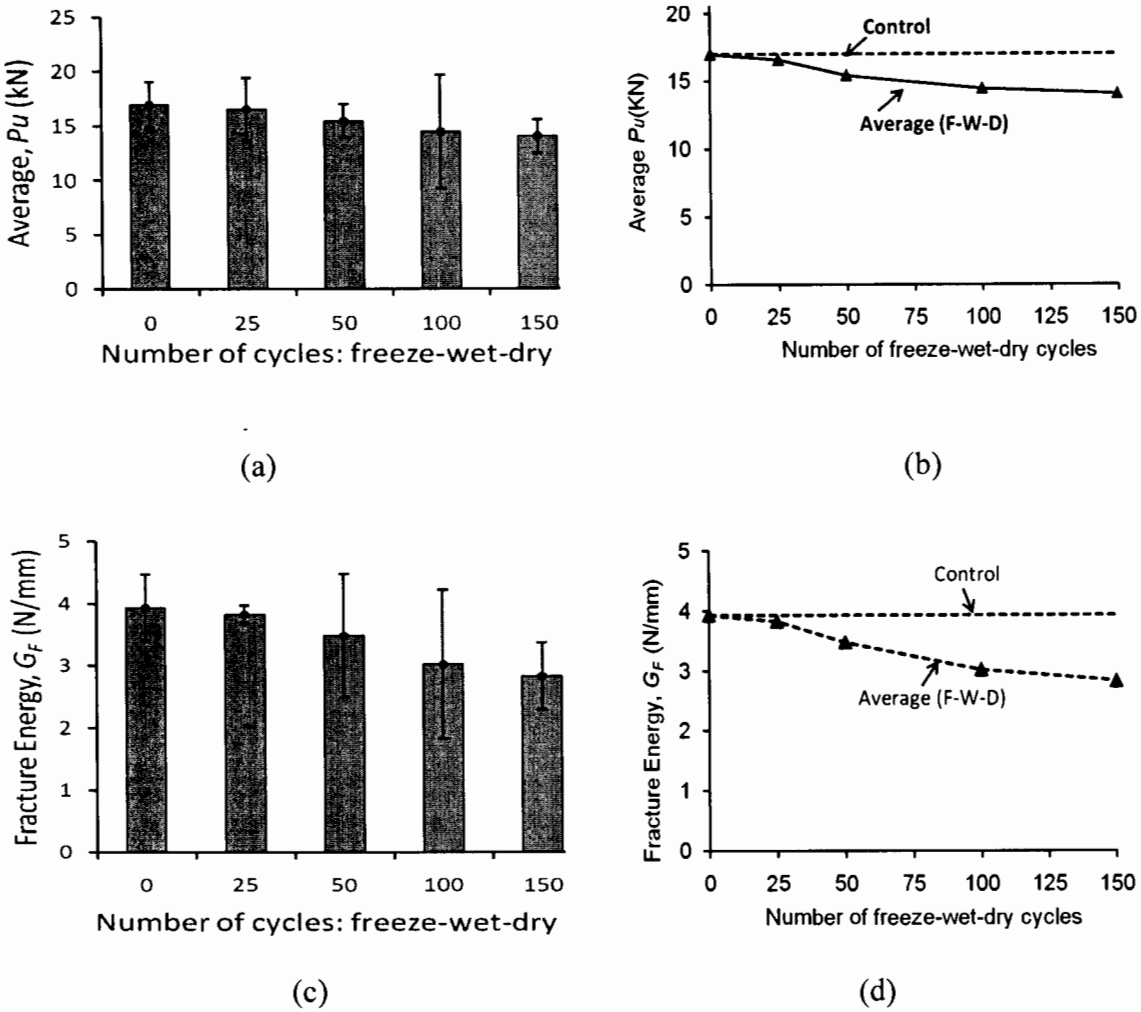

Figure 5.10. Effect of freeze-wet-dry cycles: (a) average ultimate strength with standard deviation; (b) average ultimate strength; (c) interfacial fracture energy with standard deviation; (d) interfacial fracture energy

5.5.2. Cold Temperature Effects

Table 5.6 and Fig. 5.13 show comparisons of load carrying capacity and interfacial fracture energy at room and different low temperatures, namely 0°C, -10 °C, -20 °C and -30 °C. The load-carrying capacity decreased by 8.8%, 12.9% and 16.5% in comparison to the control specimens, on average, for the specimens exposed to constant 0°C, -10 °C and -30 °C, respectively, for 2,000 hours (Fig. 5.13a and Table 5.6). Whereas the specimens exposed to -20 °C for 2,000 showed a 6.5% increase in load carrying capacity. The specimens exposed to constant low temperatures showed a decreasing trend in average load-carrying capacity with increasing the negative temperatures with some exceptions. The interfacial fracture energy of the specimen was increased by 7.7% and 5.1% in comparison to the control specimens, on average, for the specimens exposed to constant 0 °C and -10 °C, respectively. However, the interfacial fracture energy consistently decreased with increasing the negative temperature. The interfacial fracture energy of the specimen was reduced by 5.1% and 25.6% in comparison to the control specimens, on average, for

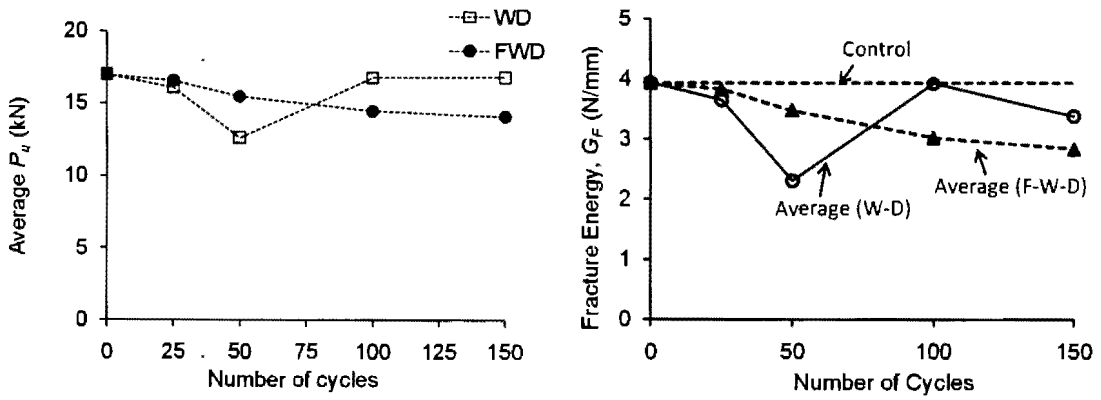

Figure 5.11. Effects of freeze-wet-dry and wet-dry cycles: (a) average ultimate load; (b) average fracture energy

the specimens exposed to constant -20 °C and -30 °C, respectively (Fig. 5.13b, c and Table 5.6). This observation may indicate that the detrimental effects of constant low temperature increases with decreasing the temperature. The most possible reason is the mismatch of the coefficient of thermal expansion (CTE) of concrete, CFRP sheet, and epoxy adhesive. Due to the differences of CTEs, peeling force may be developed along the interface. This peeling force increases with decreasing the temperature and thus reduces the bond strength.

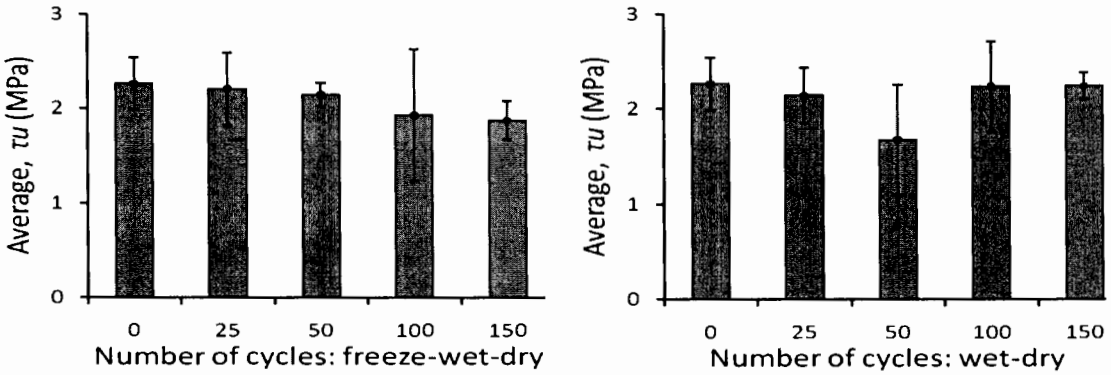

(a) (b)

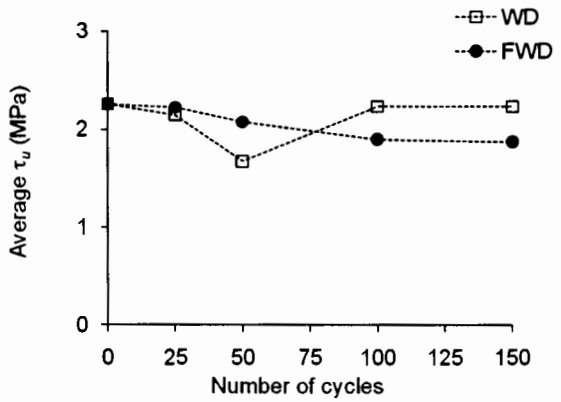

(c)

Figure 5.12. Average shear stress: (a) freezing (-30°C: 16 hours)-wet (4 hours)-dry (8 hours); (b) wet (16 hours)-dry (8 hours); (c) comparison between freeze-wet-dry and wet-dry cycles

5.5.3. Strain Distribution

Figs. 5.14-5.17 show the strain response at different locations G1, G2, G3 and G4 along the bonded CFRP length. The local strain response can be divided into two stages. In the first one, no debonding occurs and the response is primarily linear, as shown in Figs. 5.14-5.17. The second stage is characterized by the beginning of debonding. This is particularly noticeable at the location of G1 (loaded end). Ultimate experimental strain values included some scatter, as shown in Figs. 5.14-5.17; this is due in part to the failure mechanism of specimens, for example, premature debonding occurred in FWD2-100. Once the peak load is reached, the failure occurs in a brittle and unstable manner. During this process, some strain gages failed by debonding, giving inaccurate readings.

Table 5.6. Test results of constant freezing effects for 2,000 hours

ID	Temperature	Failure load (kN)			Shear stress (MPa)			Interfacial fracture energy (N/mm)		
		P_u	Ave	S	τ_u	Ave	S	G_F	Ave	S
CT0-1	0°C	16.2	15.5	3.4	2.2	2.1	0.5	5.3	4.2	1.0
CT0-2	0°C	17.1			2.3			3.9		
CT0-3	0°C	18.1			2.4			4.5		
CT0-4	0°C	10.5			1.4			3.0		
CT-10-1	-10°C	14.1	14.8	1.5	1.9	2.0	0.2	3.2	4.1	0.8
CT-10-2	-10°C	15.5			2.1			4.9		
CT-10-3	-10°C	13.0			1.7			3.6		
CT-10-4	-10°C	16.4			2.2			4.7		
CT-20-1	-20°C	18.0	18.1	0.9	2.4	2.4	0.1	3.4	3.7	0.4
CT-20-2	-20°C	19.1			2.5			3.8		
CT-20-3	-20°C	18.2			2.4			4.2		
CT-20-4	-20°C	17.0			2.3			3.3		
CT-30-1	-30°C	13.6	14.2	1.5	1.8	1.9	0.2	2.1	2.9	0.6
CT-30-2	-30°C	12.3			1.6			2.8		
CT-30-3	-30°C	15.0			2.0			3.3		
CT-30-4	-30°C	15.8			2.1			3.5		

Ave = average; *S* = standard deviation; P_u = ultimate load; τ_u = maximum average shear stress; G_F = interfacial fracture energy

The strain distribution at low load levels is highly nonlinear (Figs. 5.14-5.17). Fig. 5.14 and 5.15 illustrate the strain vs. strain gage (G) location diagram for the specimens R5 and different constant low temperatures, respectively. Both of the graphs show a trend in which the strain value in each of the strain gage increases when the load increases. Figs. 5.14 and 5.15 illustrate significant differences between the strain values of G1 and G2. In Fig. 5.14, for ultimate load, G1 exhibited approximately 2,800 micro-strains and G2 showed

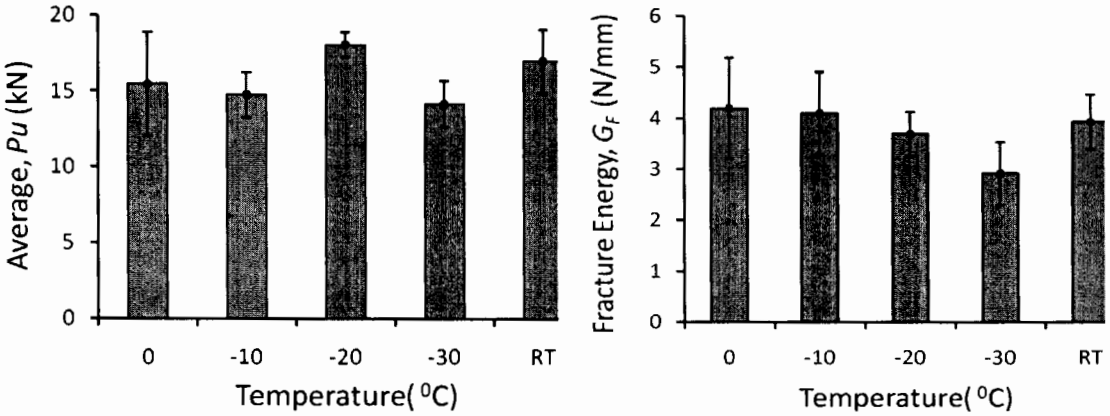

(a) (b)

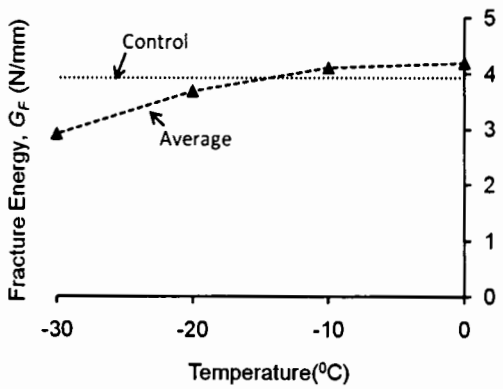

(c)

[Room temp = 25°C]

Figure 5.13. Effect of constant freezing of 2000 hours: (a) average load-carrying capacity; (b) interfacial fracture energy with standard deviation; (c) interfacial fracture energy

approximately 2,000 micro-strains. G4 exhibited strain values that were less than 200 micro-strains. The strain reading of G1 was 1,900 micro-strains, 900 micro-strains, 5,200 micro-strains and 1,200 micro-strains for the specimens CT-0-1, CT-10-2, CT-20-1 and CT-30-4, respectively. All low temperature specimens, except for CT-20-1, in Fig. 5.15 exhibited lower strain values than that shown in Fig. 5.14. This observation may indicate that the debonding of the CFRP sheets initiated much faster than that of the control specimens.

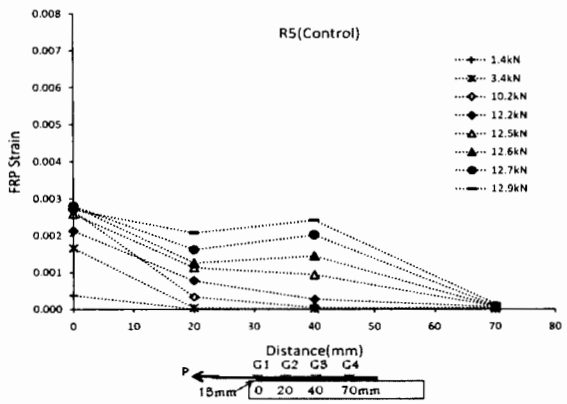

Figure 5.14. Stain distribution along CFRP-concrete of control specimen (R5)

Figs. 5.16 and 5.17 show the strains distributions along the CFRP sheets of the specimens subjected to freeze-wet-dry and wet-dry effects, respectively. These strains were found from strain gages bonded on the surface of the CFRP sheets. When the applied load P was smaller than about 80% of the ultimate load P_u, the CFRP strain was insignificant beyond a small distance of about 40% of the bond length from the loaded end (Figs. 5.16 and 5.17), indicating that almost all the applied load was resisted within this small area. For Specimen FWD4-25, the increase in CFRP strains was gradual until P reached to $0.89P_u$ (P_u = 12.5 kN) (Fig. 5.16a). Debonding at the loaded end could be occurred and led to an obvious change of the strain distribution along the CFRP sheets, resulting in the

propagation of debonding. The specimen failed soon thereafter. The strain in the debonded part of the CFRP sheet was almost constant at P = 11.4 kN (P/P_u = 0.91). For Specimen FWD2-50 debonding initiated at P =14.7 kN, whereas the failure occurred at a load P_u of 17.0 kN (P/P_u = 0.86). The propagation of debonding was more clearly represented by the strain distribution, as shown in Fig. 5.16(b).

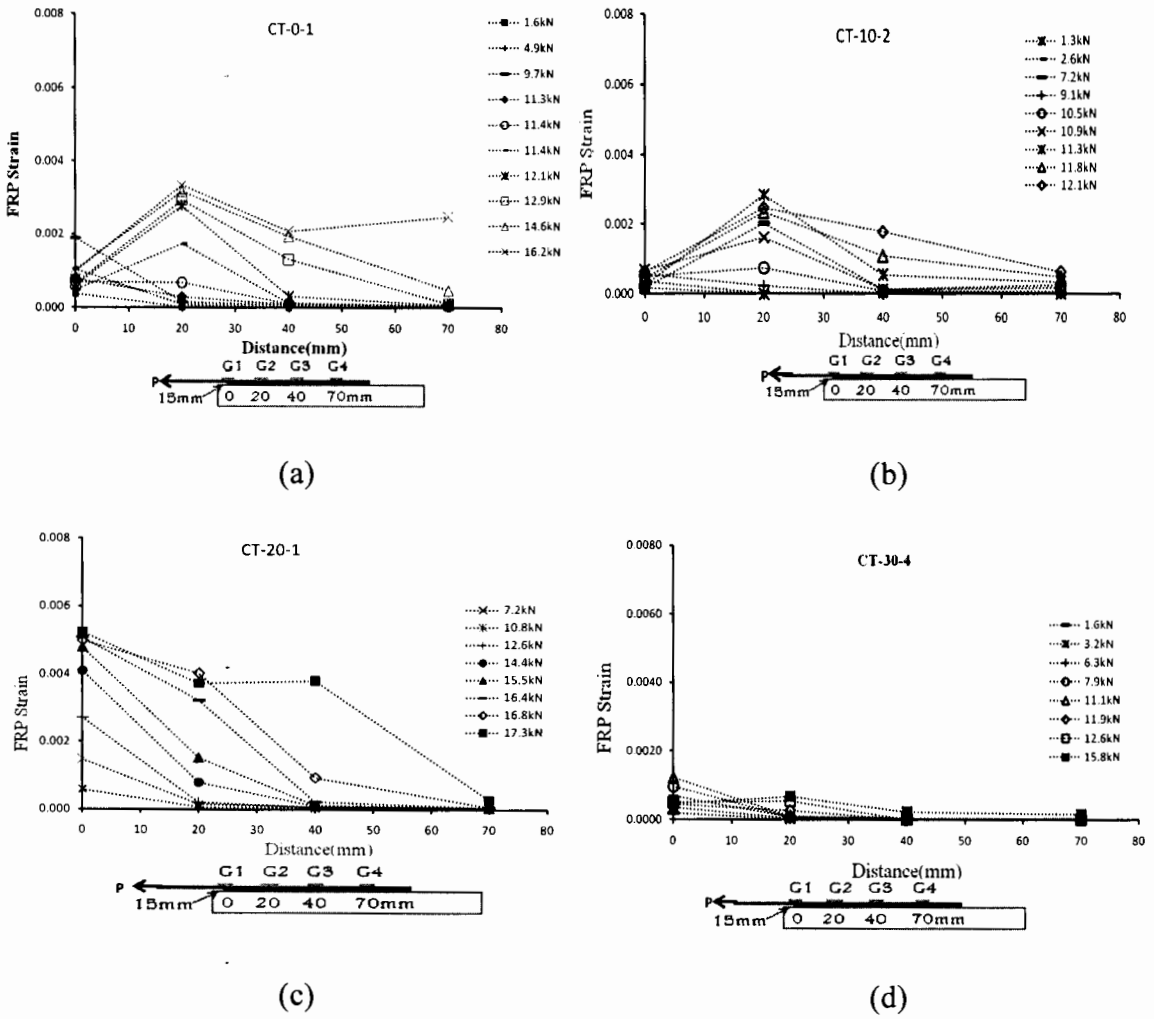

Figure 5.15. Stain distribution along CFRP-Concrete joint of constant freezing for 2000 hours: (a) freeze at 0 ^{0}C (CT-0-1); (b) freeze at -10 ^{0}C (CT-10-2); (c) freeze at -20 ^{0}C (CT-20-1); (d) freeze at -30 ^{0}C (CT-30-4)

For Specimens FWD2-100 and FWD4-150, debonding initiated at 6.1 kN and 12.5 kN, respectively, but ultimate failure occurred at 7.0 kN ($P/P_u = 0.87$) and 13.5 kN ($P/P_u = 0.93$), respectively, as shown in Fig. 5.16(c) and (d). However, Specimens WD4-25, WD3-50, WD2-100, and WD2-150 showed debonding initiations at load 13.6 kN, 12.0 kN, 14.6 kN and 14.1 kN, respectively, and the ultimate failure load was 14.5kN ($P/P_u = 0.94$), 14.1 kN ($P/P_u = 0.94$), 17.3 kN ($P/P_u = 0.84$) and 15.6kN ($P/P_u = 0.90$), respectively. Careful inspection of Figs. 5.14-5.17 shows that local debonding near the loaded end occurred earlier than ultimate failure. Fig. 5.15(a) shows that there was a significant change in the local strain distribution near the loaded end ($x = 0$) when the applied load increases from $0.1P_u$ to $0.6P_u$. When P was $0.1P_u$, the strain at x = 0 was significantly larger than the measured strain of the CFRP at $x = 20$ mm. The strain decreased rapidly away from the loaded end. When the load increases to over $0.6P_u$, the deduced strain at $x = 0$ became slightly smaller than that measured at $x = 20$ mm and this pattern remains unchanged until failure. This phenomenon may be due to the local debonding that occurred before the applied load reached $0.6P_u$. This local debonding shifted the effective length of stress transfer from the CFRP to the concrete by a small distance towards the far end of the CFRP sheets. This phenomenon has also been noted by Yuan et al. (2001) and may be attributed to local stress concentrations near the loaded end. The same phenomenon is evident from the strain distributions, as shown in Fig. 5.15(a), of Specimen CT-0-1, where the local debonding occurred at a load P of less than $0.6P_u$.

5.5.4. Failure Modes

All the specimens failed due to debonding of the CFRP from concrete adjacent to the interface in which a thin layer of concrete was attached to the CFRP sheets after failure

(Fig. 5.18). It should be noted that this is not strictly 'debonding' because the failure actually occurred in concrete. Nevertheless, the term is still adopted here because it has been widely used by the research community. The typical failure surface of each group of the specimen is shown in Figs. 5.19-5.24. Fig. 5.19 shows a contour and 3D map of the debonded surface of the control specimens.

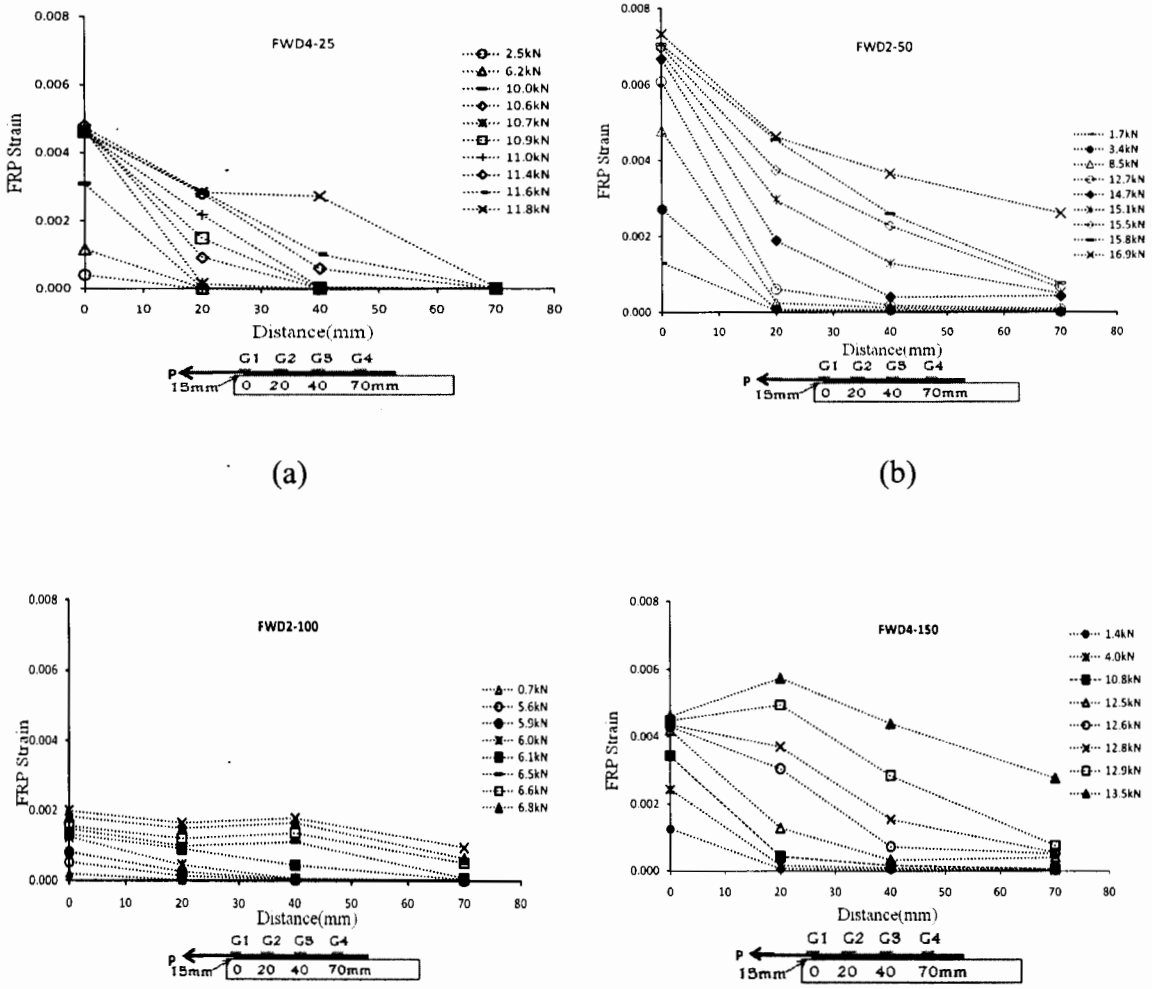

Figure 5.16. Stain distribution along CFRP-to-concrete joint under freeze-wet-dry effects: (a) 25 cycles (FWD4-25); (b) 50 cycles (FWD2-50); (c) 100 cycles (FWD2-100); (d) 150 cycles (FWD4-150)

From this figure, it can be seen that a thin concrete layer was attached near the loaded-end. From Fig. 5.20 and Fig. 5.21, the location of the concrete layer attachment was shifted from the loading end to the far end of the CFRP sheet. The concrete attachment most frequently observed at the loaded-end due to damage concentrations. This indicates that freeze-wet-dry cycling reduced the effective bonding area.

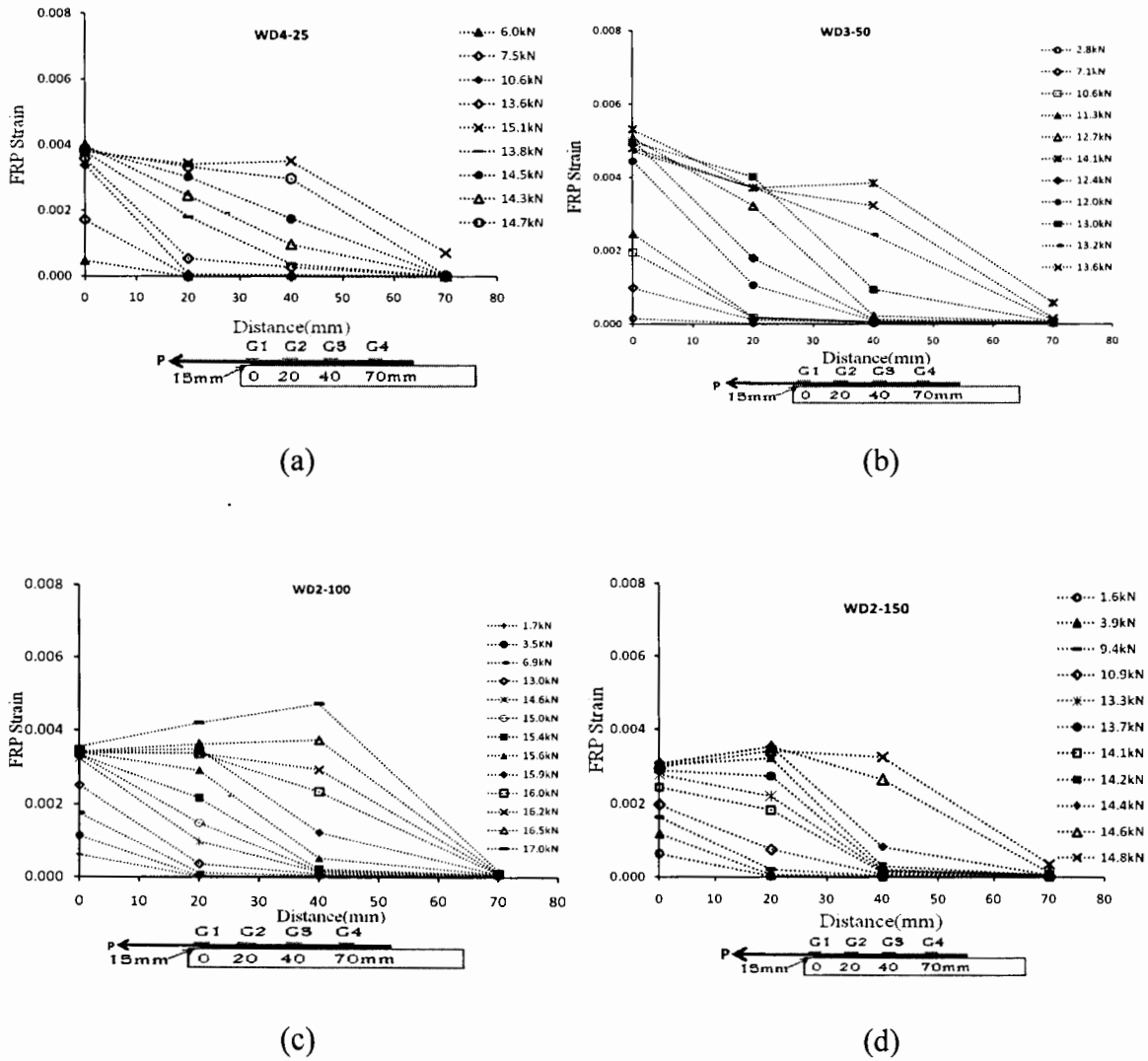

Figure 5.17. Stain distribution along CFRP-to-concrete joint under wet-dry effects: (a) 25 cycles(WD4-25); (b) 50cycles(WD3-50); (c) 100 cycles(WD2-100); (d) 150 cycles (WD2-150)

Figure 5.18. Debonded CFRP sheet (CT-30-1/4)

The most possible reason could be water ingression in the bonding line during submerging and freezing effects. The location of the concrete attachment shifted more with increasing the number of freeze-wet-dry cycles as shown in From Figs. 5.20 and 5.21. The bond area didn't change due to constant freezing at low temperature; for example, the specimens exposed to 0°C and -10 °C for 2,000 hours; however, the specimens exposed to -20 °C and-30 °C showed a reduced bonding area, as shown in Fig 5.22 and Fig. 5.23. A similar trend to the freeze-wet-dry cycles was also observed in the wet-dry cycles. With increasing the number of wet-dry cycles, the location of stress concentration shifted from the loaded-end to the far end of the CFRP sheets as shown in Figs. 5.24 and 5.25. Such a behavior suggests that moisture ingression into bonding area reduced the bonding area and hence reduced the bond strength.

5.6. ANALYTICAL MODEL

This section provides a comparison of experimental results with three parameter bond strength model proposed by Wu et al. (2009) for FRP–concrete interface. Wu et al. (2009)

showed that the bond strength varied with the width (b_p), thickness (t_p), and elastic modulus (E_p) of FRP sheets and the behavior of concrete interface.

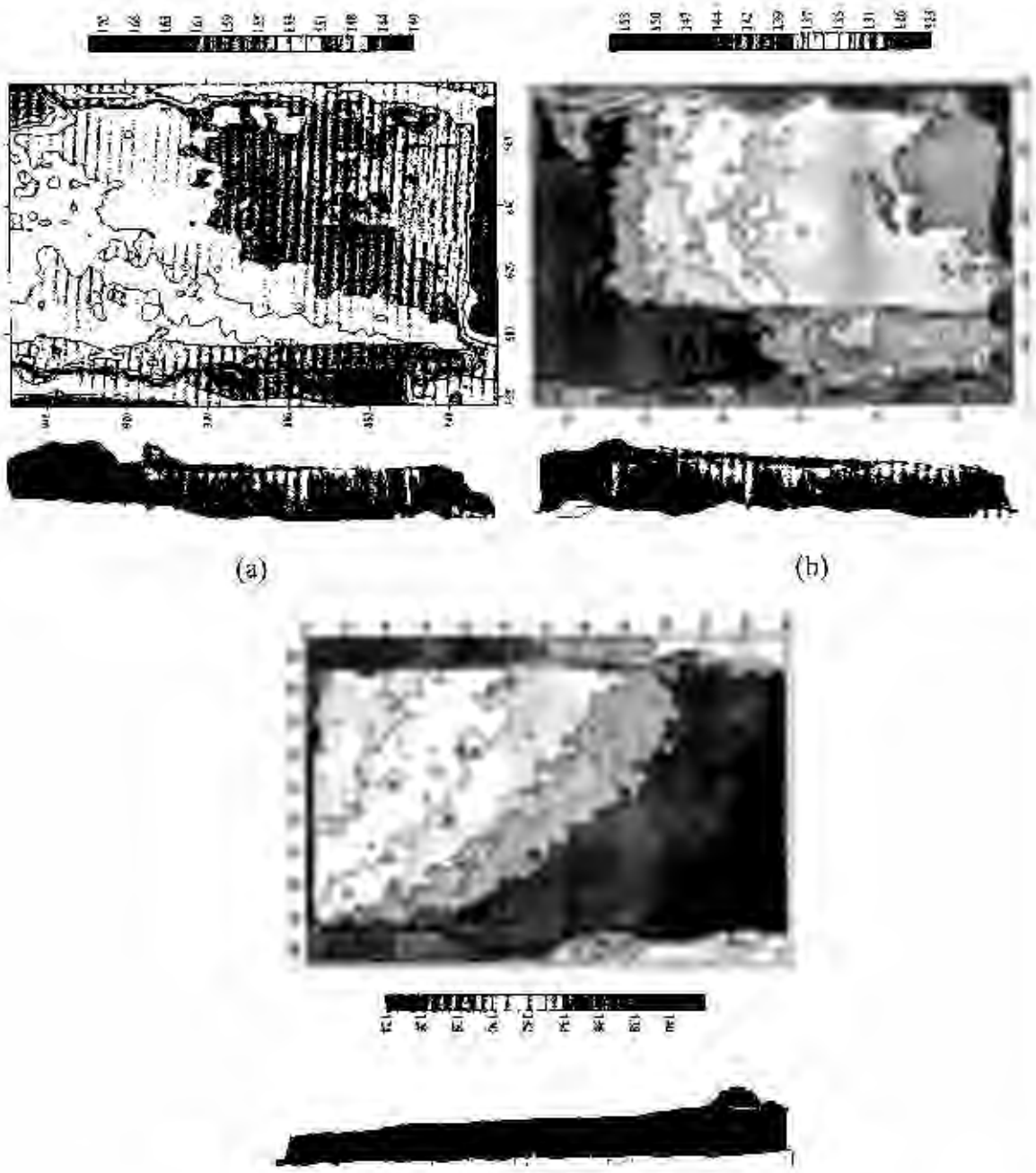

Figure 5.19. Interface of control specimen: (a) control (R6); (b) control (R7); (c) control (R2)

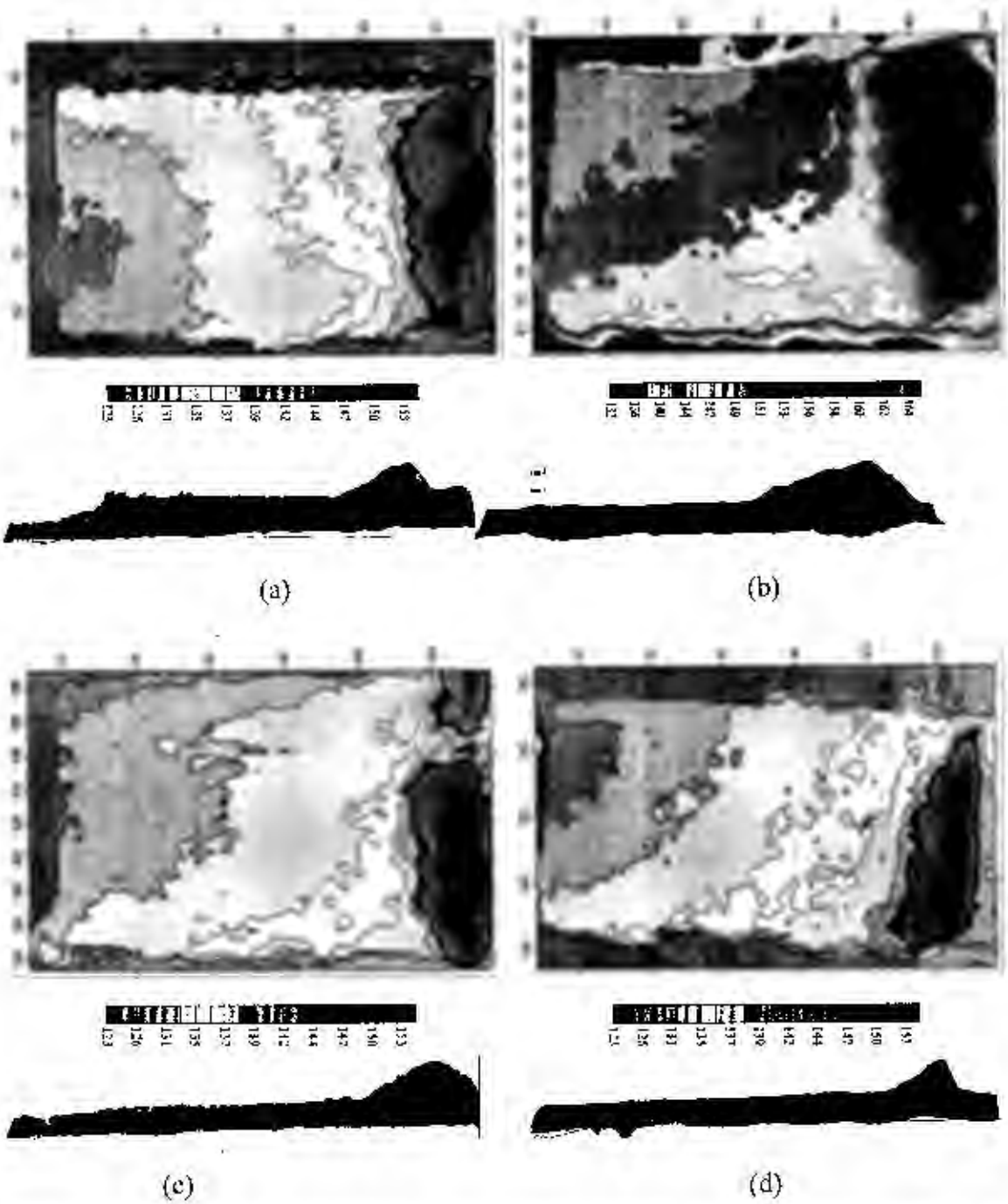

Figure 5.20. Effect of freeze-wet-dry: (a) 25 cycles (FWD1-25); (b) 25 cycles (FWD3-25); (c) 50 cycles (FWD3-50); (d) 100 cycles (FWD1-100)

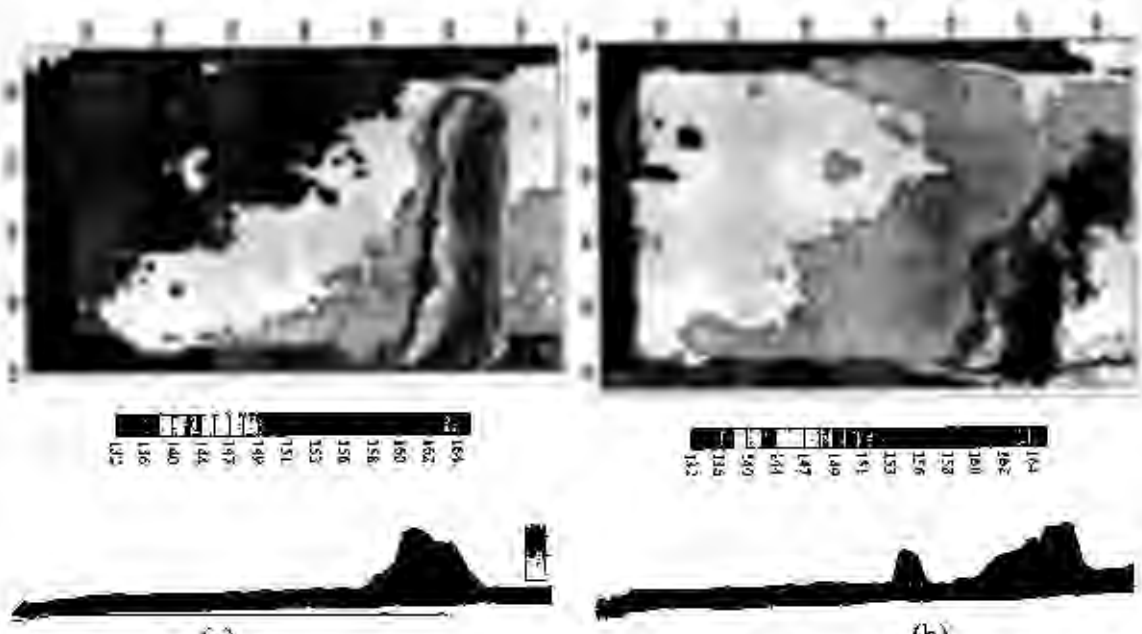

(a) (b)

Figure 5.21. Effect of wet-dry-freezing cycles: (a) 100 cycles (FWD4-100); (b) 150 cycles (FWD2-150)

The parameters considered in extent predictive models are given below (Wu et al. 2009):

Bond strength model	**Compressive strength, f_c'**	**FRP stiffness, E_{frp}**	**Effective bonding length, L_e**	**Width ratio, b_p**
Van Gemert (1980)	Yes	No	No	No
Tanaka (1996)	No	No	No	No
Maeda et al. (1997)	Yes	Yes	Yes	No
Neubauer and Rostasy (1997)	Yes	Yes	Yes	Yes
Khalifa et al. (1998)	Yes	Yes	Yes	No
Niedermeier (2000)	Yes	Yes	Yes	Yes
Sato (2000)	Yes	Yes	Yes	No
Chen and Teng (2001)	Yes	Yes	Yes	Yes
Yang (2001)	Yes	Yes	Yes	No
JCI(2003)	Yes	Yes	Yes	No
Monti et al. (2003)	Yes	Yes	Yes	Yes

The optimized form of the equation of Wu et al. (2009) model:

$$P_u = \begin{cases} 0.595 b_p k_b f_c'^{0.1} (E_p t_p)^{0.54} & \text{if } L > L_e \\ 0.595 b_p k_b f_c'^{0.1} (E_p t_p)^{0.54} \left(\frac{L}{L_e}\right)^{1.2} & \text{if } L \le L_e \end{cases} \quad (1)$$

where width influence factor, $k_b = \sqrt{\frac{2-(b_p/b_c)}{1+(b_p/b_c)}}$, and E_p, t_p, and b_p are modulus of elasticity, thickness and width of the FRP, respectively.

The effective bond length suggested by Wu et al. (2009):

$$L_e = 0.395\frac{(E_p t_p)}{f_c'^{0.09}} \quad (2)$$

where

b_c = the width of the concrete member (mm)
b_p = the width of the FRP (mm)
E_c = modulus of elasticity of concrete (MPa)
E_p = modulus of elasticity of FRP sheet (MPa)
fc' = the cylindrical compressive strength of the concrete (MPa)
L = bonded length
Le = effective bonding length
Pu = maximum transferable load (bond capacity/bond strength)
tp = thickness of FRP plate or sheet (mm)

5.7. COMPARISON

The ultimate load-carrying capacity of specimen, P_u, was predicted based on the Wu et al. (2009) model and then compared with experimental results. Based on the percentage errors, this model conservatively predicts the ultimate load-carrying capacity. In this prediction, the bond strength was computed based on the average concrete strength f_c' at 28 days (22.9 MPa). The elastic modulus of CFRP sheets exposed to freeze-wet-dry cycles was used from the Table 3.9. Tables 5.7 and 5.8, and Fig. 5.26 summarize the results for analytical model and a comparison against the experimental values. Table 5.8 gives the percentage

differences between the experimental results and that obtained by the model. The differences between the experimental results and the model were 9.4%, 10.2%, 5.2% and

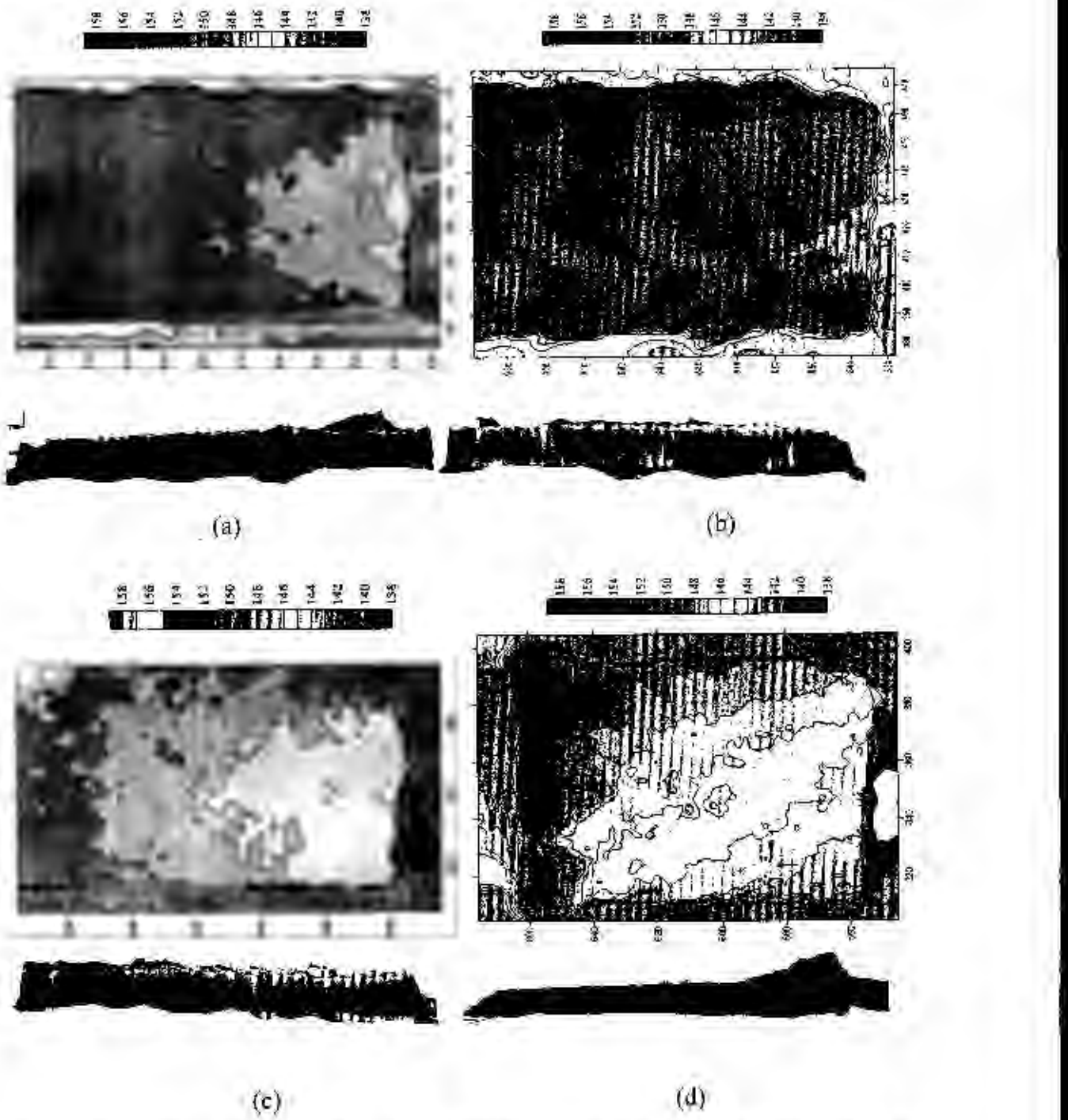

Figure 5.22. Effect of constant freezing of 2000 hours: (a) 0°C (CT-0-2); (b) 0°C (CT-0-3); (c) – 10°C (CT-10-2); (d) – 20°C (CT-20-4)

2.1% for the specimens exposed to 0, 25, 50 and 100 freeze-wet-dry cycles, respectively. The proposed empirical model based on three parameters was found to be in good agreement with the test results, even though it was slight conservative.

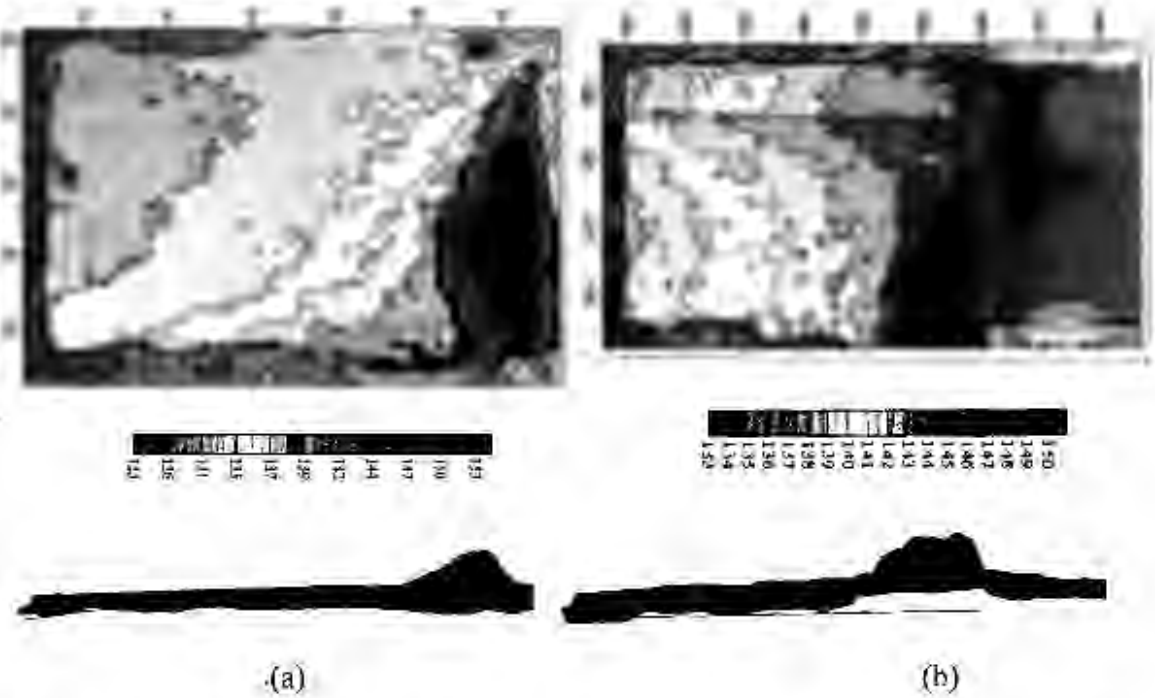

(a) (b)

Figure 5.23. Effect of constant freezing of 2000 hours: (a) at -20 °C (Specimen CT-20-1); (b) at -30°C (Specimen CT-30-4)

5.8. DISCUSSION AND CONCLUSION

This chapter has presented the bond properties of CFRP-concrete interface under typical cold regions environments. A total fifty three test specimens were monotonically loaded until failure occurred. The test results included load carrying capacity, interfacial fracture energy depending upon the environmental cycles, and corresponding failure modes. The presence of moisture decreased the bond strength and interfacial fracture energy between CFRP sheet and concrete, in particular noticeable for the first 50 cycles of wet-dry and freeze-wet-dry. When the number of wet-dry cycles increased from 50 to 100, the bond

capacity and interfacial fracture energy of the specimens tended to increase; however, after 100 wet-dry cycles the ultimate failure load was almost constant up to 150 cycles.

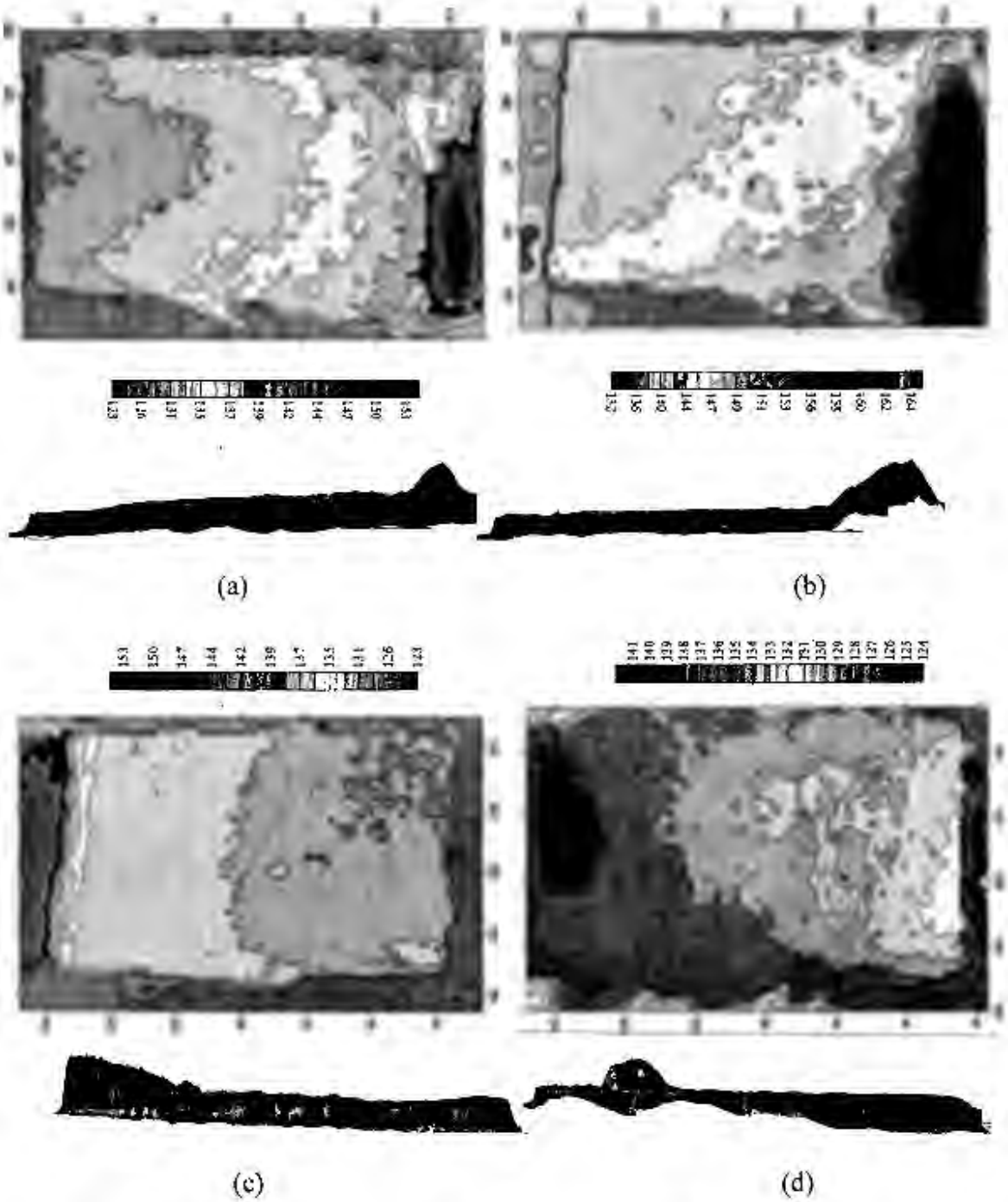

Figure 5.24. Effect of wet-dry cycles: (a) 25 cycles (WD2-25); (b) 25 cycles (WD3-25); (c) 50 cycles (WD2-50); (d) 50 cycles (WD4-50)

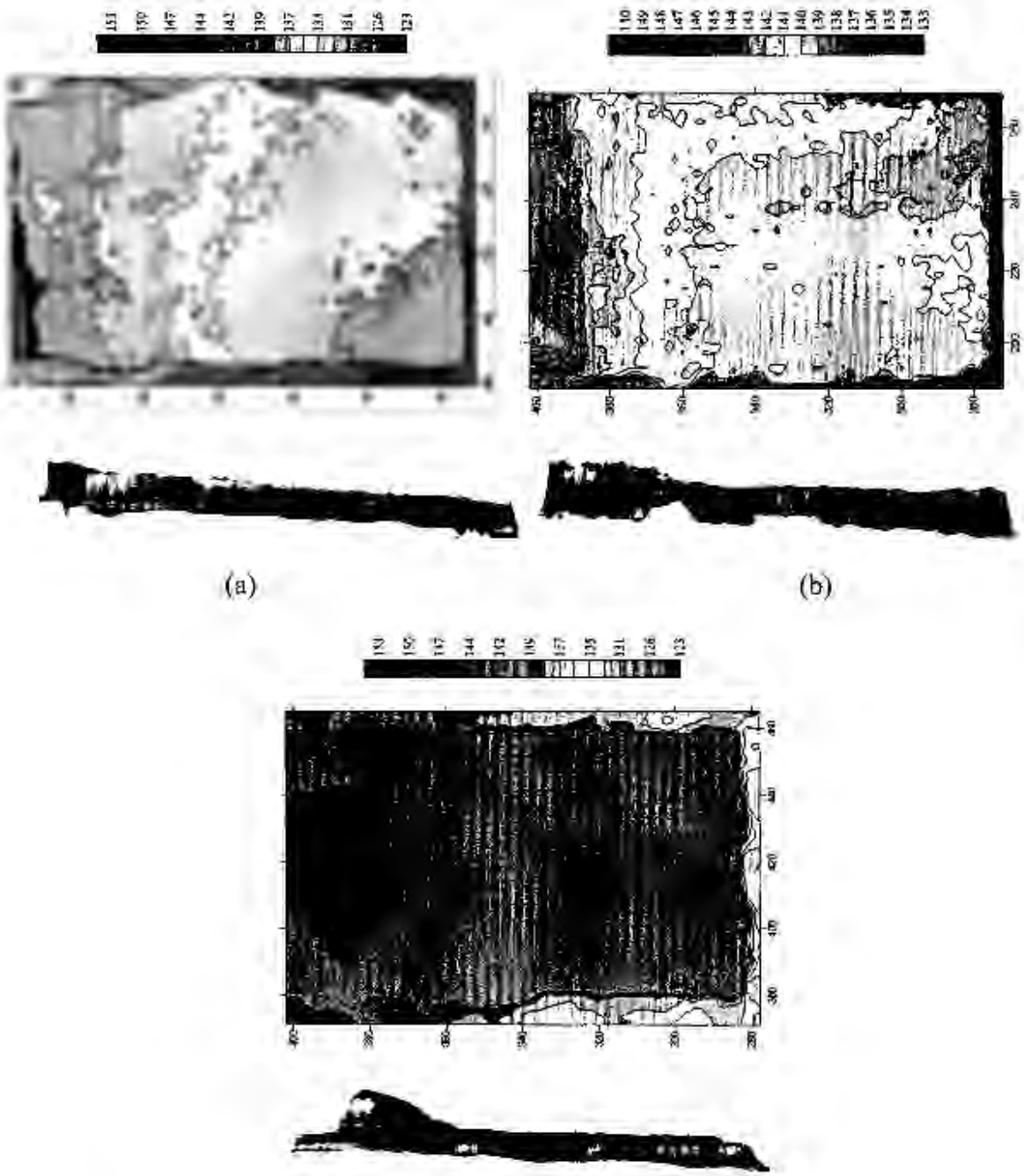

Figure 5.25. Effect of wet-dry: (a) 100 cycles (WD1-100); (b) 150 cycles (WD1-150); (c) 150 cycles (WD4-150)

Table 5.7. Numerical results obtained using Wu et al. (2008) Model

F-W-D	Parameters					Results		Exp.
	b_p(mm)	b_c(mm)	E_p(MPa)	t_p(mm)	f'_c	k_b	P_u(kN)	P_u(kN)
0	75	100	231000	0.165	22.9	0.85	15.4	17.0
25	75	100	219000	0.165	22.9	0.85	14.9	16.6
50	75	100	214000	0.165	22.9	0.85	14.7	15.5
100	75	100	201000	0.165	22.9	0.85	14.2	14.5

F-W-D= freeze (16hours at -30 °C)-wet (4hours)-dry (4 hours at room temperature);
E_p= Elastic modulus (Table 3.9)

Table 5.8. Comparison of confined concrete response

Exposure condition	No. of Cycles	Bond strength, P_u (kN)		Percentage difference*
		Experimental	Analytical	
Control	0	17.0	15.4	-9.4%
F-W-D	25	16.6	14.9	-10.2%
F-W-D	50	15.5	14.7	-5.2%
F-W-D	100	14.5	14.2	-2.1%

*: Percentage difference is determined as (analytical-experimental)/experimental X 100
F-W-D: freeze (16hours at -30 °C)-wet (4hours)-dry (4 hours at room temperature)

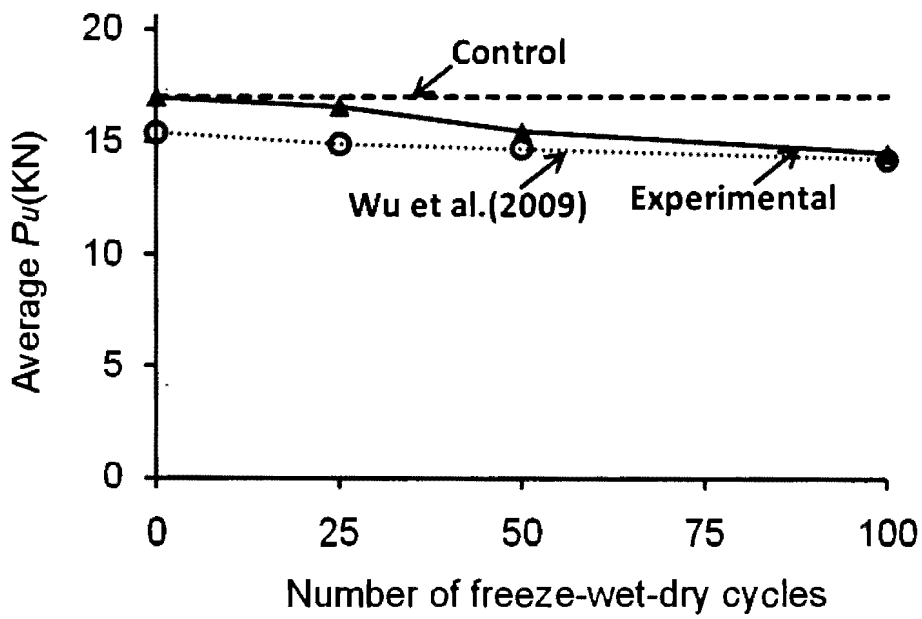

Figure 5.26. Comparison of experimental result with analytical model

The specimens exposed to freeze-wet-dry cycles showed a consistently decreasing trend up to 100 cycles and then showed insignificant change in the capacity. On the other hand, specimens exposed to constant cold temperatures showed a decreasing trend in ultimate load carrying capacity as well as interfacial fracture energy with lowering the temperature.

5.9. REFERENCES

1. Apicella, A., Nicolais, L., Astarita, G., and Drioli, E. "Effect of thermal history on water sorption, elastic properties and the glass transition of epoxy resins," *Polymer*, V 20, 1979, pp. 1143–1148.

2. Ekenel, M., and Myers, J. J. "Effect of environmental conditioning & sustained Loading on the fatigue performance of RC beams strengthened with bonded CFRP fabrics," *Submitted to ACI Materials Journal*, September 2004.

3. Grace, N. F. "Concrete repair with CFRP," *Concrete International*, V. 26, No. 5, May 2004, pp. 45-52.

4. Green, M.F. "FRP repair of concrete structures: performance in cold regions," *Int. J. Materials and Product Technology*, Vol. 28, No. 1/2, 2007, pp. 160-177.

5. Hand H.M., Arah C.O., McNamara D.K., and Mecklenburg M.F. "Effects of environmental exposure on adhesively bonded joints," *International Journal of Adhesive and Adhesion*, V. 11, No. 1, 1991, pp. 15-23.

6. Green, M. F., Bisby, L. A., Beaudoin, Y., and Labossiere, P. "Effect of freeze-thaw cycles on the bond durability between fibre reinforced polymer plate reinforcement and concrete," *Canadian Journal of Civil Engineering*, V. 27, No. 5, October 2000, pp. 949-959.

7. MBrace. "MBrace saturant datasheet," Degussa, 2007; Available online at http://www.basf-cc.ae/en/products/

8. Nakaba, K.; Kanakubo, T.; Furuta, T. and Yoshizawa, H. "Bond Behavior Between Fiber-reinforced Polymer Laminates and Concrete", *ACI Structural Journal*, 98(3): 359–367, 2001

9. Ren, H., Hu, A., and Zhao, G. "Freeze-Thaw Resistance Behavior of Bonded Joints between FRP and Concrete,' *Journal of Dalian University of Technology*, V. 43, No. 4, July 2003, pp. 495-499.

10. Sato, Y., Asano, Y. and Ueda, T. "Fundamental Study on Bond Mechanism of Carbon Fiber Sheet", *Journal of Material*, Concrete Structures and Pavements, JSCE, 47(648):2000, pp. 71–87.

11. Sen, R., Shahawy, M., Mullins, G., Spain, J. "Durability of Carbon Fiber-Reinforced Polymer/Epoxy/Concrete Bond in Marine Environment," *ACI Structural Journal*, V. 96, No. 6, November/December 1999. pp. 906-914.

12. Toutanji, H. A., and Gomez, W. "Durability Characteristics of Concrete Beams Externally Bonded with FRP Composite Sheets," *Cement and Concrete Composites*, V. 19, 1997, pp. 351-358.

13. Wu, Z.; Islam, S.M., and Said, H. "A Three-Parameter Bond Strength Model for FRP-Concrete Interface", *Journal of Reinforced Plastics and Composites*, Vol. 28, No. 19, 2009, pp. 2309-2323.

14. Wu, Z., Yuan, H., Hiroyuki, Y. and Toshiyuki, K. "Experimental/Analytical Study on Interfacial Fracture Energy and Fracture Propagation along FRP-Concrete Interface", *ACI International* SP-201-8, 2001, pp. 133–152.

15. Yuan, H.; Wu, Z.S. and Yoshizawa, H. "Theoretical Solutions on Interfacial Stress Transfer of Externally Bonded Steel/Composite Laminates", *Journal of Structural Mechanics and Earthquake Engineering, JSCE,* 18(1): 2001, pp. 27–39.

CHAPTER 6. SUMMARY AND CONCLUSIONS

6.1. SUMMARY OF RESEARCH PROGRAM

The major expected outcomes from the workshop are the definition of the state of the art for CFRP composites exposed to aggressive environmental conditions, the integrated research plan to further the state of the art, the dissemination of this work, and the anticipated implementation of the research. These outcomes will benefit society through improved application of CFRP composites in cold regions environments, where the benefits of CFRP-strengthening over conventional techniques can be fully realized.

The research presented herein was conducted in three phases. Phase I was conducted for examine the effects of freeze-wet-dry, wet-dry cycles, and different low temperature effects on the constitutive material properties of bonding agent (i.e., epoxy) that may be used for bonding CFRP sheets with concrete. This particular study looks at 100 epoxy coupons went through an exposure program where groups were subjected up to 150 freeze-wet-dry, wet-dry cycles; 2,000 hours of constant freezing at different low temperatures, or were left as control specimens. Phase I also includes the investigation of materials properties of CFRP sheets exposed up to 100 freeze-wet-dry cycles and constant freezing at different low temperatures for 2,400 hours. Following the exposure program, the specimens were tested to failure to determine their residual strength. The effects of freeze-wet-dry, wet-dry cycling and constant freezing at low temperatures on the overall strength and failure mode of the specimen were analyzed.

Phase II was conducted to examine the durability of partially cracked axial concrete members subjected to freeze-wet-dry combined with different level of live load incentives. A total of 16 unconfined and 15 CFRP-wrapped cylinders exposed to freeze-wet-dry

conditions plus different levels of live load effects up to 100 cycles were tested. The investigation focused on the load-carrying capacity, strain responses, crack patterns during the load cycling, and failure mode.

Phase III has discussed the durability of bond between CFRP-concrete interface subjected to harsh environmental conditions. A total 53 single lap concrete prisms strengthened with CFRP sheets exposed up to 150 cycles of freeze-wet-dry, wet-dry, and constant freezing at different low temperatures (0°C, -10°C, -20°C and -30°C) for 2,000 hours were tested to examine the bond response and corresponding failure modes.

6.2. DISCUSSION AND CONCLUSION

Based on the results of the experimental program described in this thesis, the following conclusions can be made:

- The load-carrying capacity of the specimens were increased by 3.2%, 22.9%, 33.8%, and 17.2% in the ultimate capacity in comparison to the control specimens, on average, for the specimens exposed to 10, 25, 50, and 100 freeze-thaw cycles, respectively.
- The specimens exposed to 50 freeze-thaw cycles ended up having 33.8% more strength than the control specimens. This was most likely due to additional curing that took place during the freeze-thaw cycles, when the specimens were stored in environmental chamber and thawing in room temperature.
- A constant stiffness was observed up to 50 freeze-thaw cycles, and then freeze-thaw cycles showed detrimental effects in stiffness of epoxy bonded joints. The average stiffness trended to decrease within the range studied in the present experimental program.

- The load-carrying capacity of the specimens were improved by 10.2%, 8.3%, 36.3% and 31.8% in the ultimate capacity in comparison to the control specimens, on average, for the specimens exposed to 10, 25, 50 and 100 wet-dry cycles, respectively. This was most likely due to additional curing that took place during the wet cycles, when the specimens were submerged in water.
- A constant stiffness with some variations was observed for the specimens exposed to environmental effects up to 50 wet-dry cycles. Then, with creasing the number of cycles, a reduced trend in stiffness was demonstrated.
- The fact that the specimens exposed to wet-dry did not show the same strength increases as the specimens subjected to freeze-thaw conditions could mean that there is the potential for negative effects when exposed to wet-dry or freeze-thaw cycles but the detrimental effects was more crucial due to freeze-thaw effects. However, these specimens had still higher bond strength than that of the control specimens and hence, it would be reasonable to assume that the wet-dry/freeze-thaw effects could be ignored when comparing average strengths.
- Two types of failure modes were observed—cohesion failure where the failure was within the adhesive layer and debonding failure. The cohesion failure was a primary determinant for the control specimens, whereas the debonding was dominant for the environmentally-cycled specimens.
- The load-carrying capacity of the specimen were improved by 4.5%, 15.9%, 3.2% and 8.3% in the ultimate capacity in comparison to the control specimens, on average, for the specimens subjected to 25, 50, 100, and 150 freeze-wet-dry cycles, respectively. The specimens exposed to wet-dry cycles showed increased bond

strength by 5.1%, 22.3%, 11.5% and 10.8% after 25, 50, 100, and 150 wet-dry cycles, respectively.

- The presence of moisture improved the bond strength of adhesives, in particular notable for the first 50 cycles of wet-dry and freeze-wet-dry. When the number of wet-dry/freeze-wet-dry cycles increased from 50 to 150, the bond capacity of the specimens tended to decrease. The detrimental effect of freeze-wet-dry cycles was more detrimental than that of the wet-dry cycles.
- The predicted load-displacement responses by suing Yuan et al. (2004) model agreed well with the experimental plots with an error of 4.8% in the ultimate load, on average, compared to the experimental specimen.
- Specimens constantly freezing at different low temperatures demonstrated higher ultimate failure loads, average shear stress and stiffness than that of the control specimens. This suggests that there was no detrimental effect from the constantly low temperature exposure and it would be reasonable to assume that the constant low temperature effects could be ignored.
- Ultimate tensile strength increased with increasing an environmental effect which was particularly notable for the first 75 cycles; however tensile strength tended to decrease after 75 cycles. On the contrary, the elastic modulus showed a consistently decreasing tends, however, constant freezing showed statistically no significant detrimental effects on the material properties of CFRP coupons up to 2400 hours freezing at -30 ^{0}C.
- The strength of CFRP-wrapped concrete cylinders exposed to freeze-wet-dry effects is not reduced significantly.

- Live load effects had a slightly negative effect on the compressive strength of both unwrapped and wrapped cylinders when compared to room temperature.
- The unconfined cylinders exposed to the environmental condition showed an average decrease of 10% in the load-carrying capacity, while the cylinders subjected to a combination of the environment and the live load effects exhibited a decrease up to 41.9% when compared to the control specimens.
- The load carrying capacity of the CFRP-wrapped cylinders exposed to the harsh environmental and live load effects was not changed significantly. The modulus in the stress-strain response of the conditioned cylinders decreased due to the growth of internal damage during the load cycling.
- Cracks of the unconfined cylinders developed and the crack opening increased when the load cycle increased. Such behavior influenced the axial stiffness of the conditioned cylinders. However, no visual cracks were observed for the confined cylinders. All of the test cylinders demonstrated volumetric contraction until failure occurred. A sudden increase of the volume was, however, observed at failure. The confined cylinders showed a brittle and explosive failure mode.
- Freeze-thaw and low temperature exposure cause FRP wrapped cylinders to fail in a more sudden and dramatic fashion than specimens kept at room temperature.
- With a single layer of CFRP sheets wrapping, the strength of the concrete cylinders increased by up to 324 % in comparison to the unconfined control cylinders, on average, while that value obtained 311%, 243% and 274% by ACI (2002) model, ISIS Canada (2001) model and Karbhari and Gao (1997) model respectively. Axial strain of the confined cylinders was approximately 20-25 times greater.

- The predicted ultimate FRP-confined concrete compressive strength using the ACI 440 (2002); Karbhari and Gao (1997), and ISIS Canada (2001) models compared well with the experimental results.
- The presence of moisture reduced the bond strength and interfacial fracture energy between CFRP sheet and concrete, in particular noticeable for the first 50 cycles of wet-dry and freeze-wet-dry.
- When the number of wet-dry cycles increased from 50 to 100, the bond capacity and interfacial fracture energy of the specimens tended to increase; however, after 100 wet-dry cycles the ultimate failure load was almost constant up to 150 cycles. The specimens exposed to freeze-wet-dry cycles showed a consistently decreasing trend up to 100 cycles and then showed insignificant change in the capacity.
- Specimens exposed to constant cold temperatures showed a decreasing trend in ultimate load carrying capacity as well as interfacial fracture energy with lowering the temperature.
- The predicted ultimate load-carrying capacity by using Wu et al. (2009) model matched well with the experimental results, even though it was slight conservative.

6.3. RECOMMENDATIONS FOR FUTURE WORK

Given the time constraints restricting the amount of work within the scope of this experimental program, further initiatives for research were not able to be pursued. The following are recommendations for future work to be completed in this area:

- A similar program should be carried out for examine the effects of freeze-thaw, wet-dry, freeze-wet-dry combined with live load and sustained loads effects on durability of confined cylinders.

- The effect of freeze-wet-dry/ wet-dry cycling or constant freezing on the individual materials (i.e., concrete) used in the study should be examined. With this added knowledge, more extensive and accurate conclusions could be made regarding the behaviour of the concrete prisms strengthened with CFRP sheets and CFRP-wrapped concrete cylinders tested in this program, as well as the specimens tested in various other studies looking at freeze-thaw cycling.
- A testing program similar to the one herein should be carried out on full scale specimens (i.e., concrete cylinders, beams) to determine if the conclusions made from this study are influenced by scaling effects.
- A study should be conducted looking at the effects of varying sustained loads combined with live loads and the resulting influence on the initiation of CFRP rupture.
- Future testing programs examining CFRP-strengthened reinforced beams should be exposed to the same conditions for the purposes of verifying the bond strength between CFRP-concrete interfaces.
- With additional test data, theoretical models should be created that predict the deterioration of strengthened concrete members exposed to different aggressive environmental conditions.
- In order to gain knowledge on the effects of combined loading on the ductility of CFRP strengthened concrete, further analysis should be conducted using the strain data collected in this experimental program.

APPENDIX A. REPORT CARD FOR AMERICAN'S INFRASTRUCTURE

Table A.1. ASCE Report Card 2005

Subject	2001	2005	Comments
Bridges	C	C	Between 2000 and 2003, the percentage of the nation's 590,750 bridges rated structurally deficient or functionally obsolete decreased slightly from 28.5% to 27.1%. However, it will cost $9.4 billion a year for 20 years to eliminate all bridge deficiencies. Long-term underinvestment is compounded by the lack of a Federal transportation program.
Dams	D	D	Since 1998, the number of unsafe dams has risen by 33% to more than 3,500. While federally owned dams are in good condition, and there have been modest gains in repair, the number of dams identified as unsafe is increasing at a faster rate than those being repaired. $10.1 billion is needed over the next 12 years to address **all critical** non-federal dams—dams which pose a direct risk to human life should they fail.
Roads	D+	D	Poor road conditions cost U.S. motorists $54 billion a year in repairs and operating costs—$275 per motorist. Americans spend 3.5 *billion* hours a year stuck in traffic, at a cost of $63.2 billion a year to the economy. Total spending of $59.4 billion annually is well below the $94 billion needed annually to improve transportation infrastructure conditions nationally. While long-term Federal transportation programs remain unauthorized since expiring on Sept. 30, 2003, the nation continues to shortchange funding for needed transportation improvements.

America's Infrastructure G.P.A. = D

Total Investment Needs = $1.6 Trillion

(estimated 5-year need—does not include security investment needs)

A = Exceptional

B = Good

C = Mediocre

D = Poor

F = Failing

I = Incomplete

Each category was evaluated on the basis of condition and performance, capacity vs. need, and funding vs. need.

Table A.2. 2003 progress report

	2001 Grade	2003 Trends		2001 Grade	2003 Trends
Roads	D+	↓	Wastewater	D	↓
Bridges	C	↔	Dams	D	↓
Transit	C-	↓	Solid Waste	C+	↔
Aviation	D	↔	Hazardous Waste	D+	↔
Schools	D-	↔	Navigable Waterways	D+	↓
Drinking Water	D	↓	Energy	D+	↓

Bottom Line - All Categories	2001 GPA
Total Investment Needs:$1.6 Trillion	D+

(estimated 5-year need)

APPENDIX B. MATERIALS PROPERTIES OF EPOXY ADHESIVE AND CFRP SHEETS

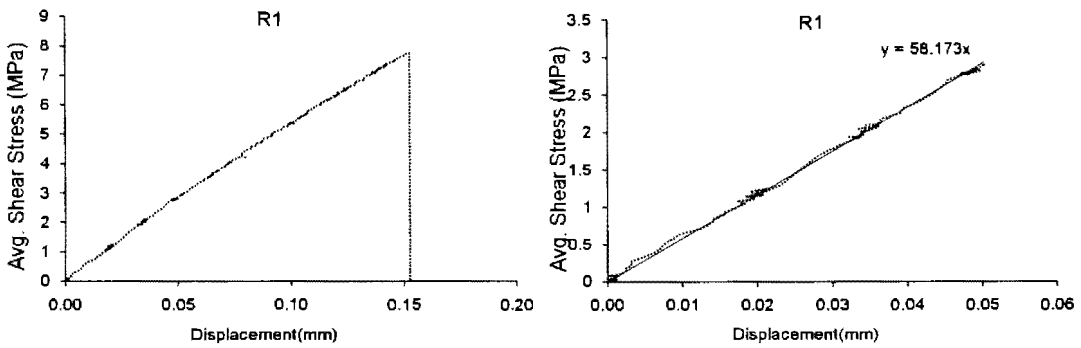

(a)

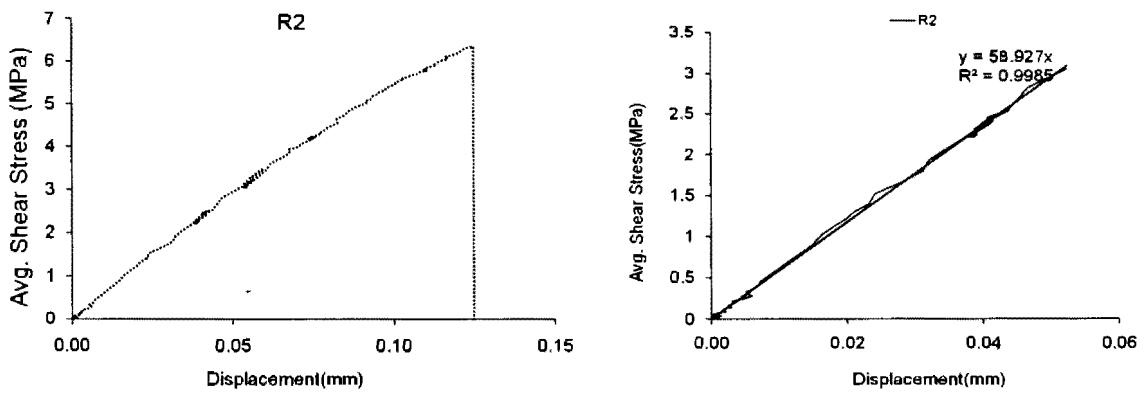

(b)

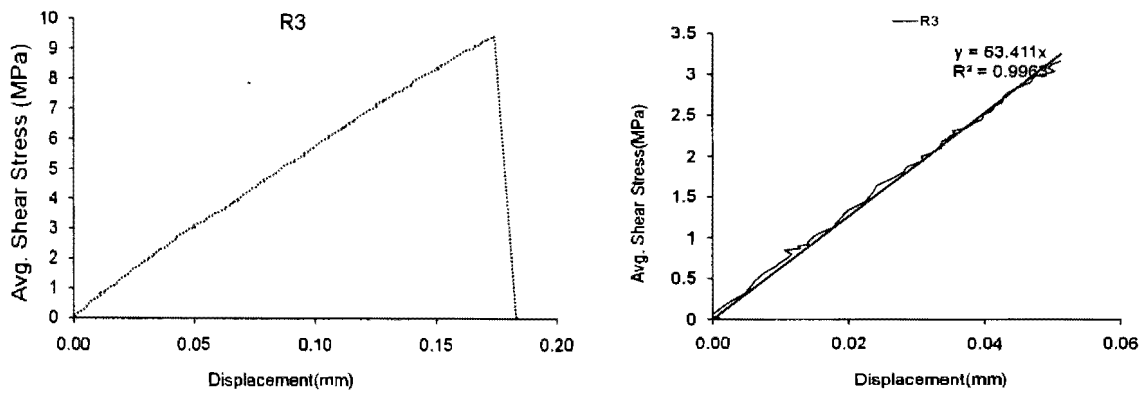

(c)

Figure B.1. Average shear stress-displacement response of specimens: (a) Control (R1); (b) Control (R2); (c) Control (R3)

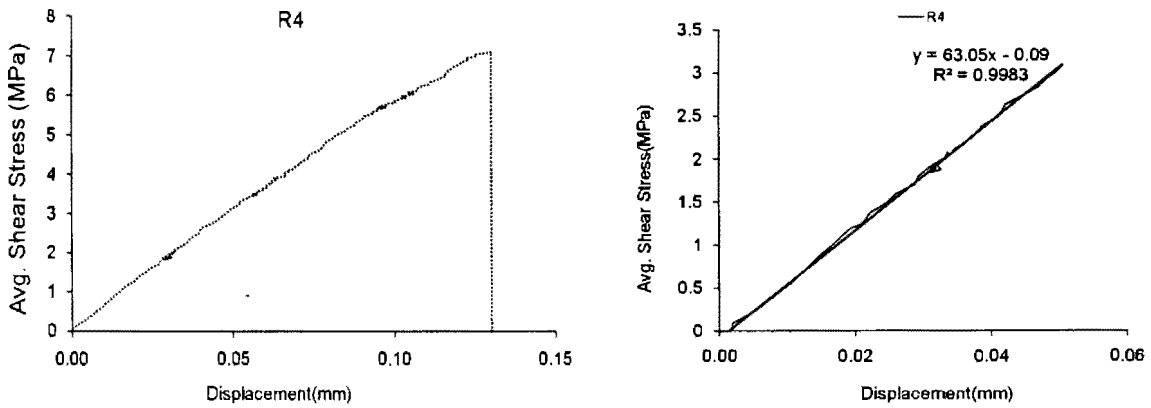

Figure B.2. Average shear stress-displacement response of Control (R4)

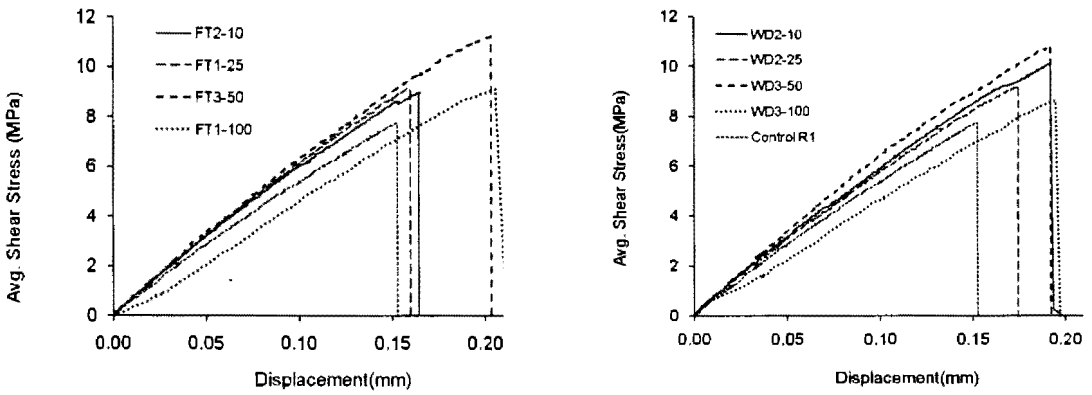

(a) (b)

Figure B.2. Average shear stress-displacement response of specimens: (a) Freeze-wet-dry condition; (b) Wet-dry condition

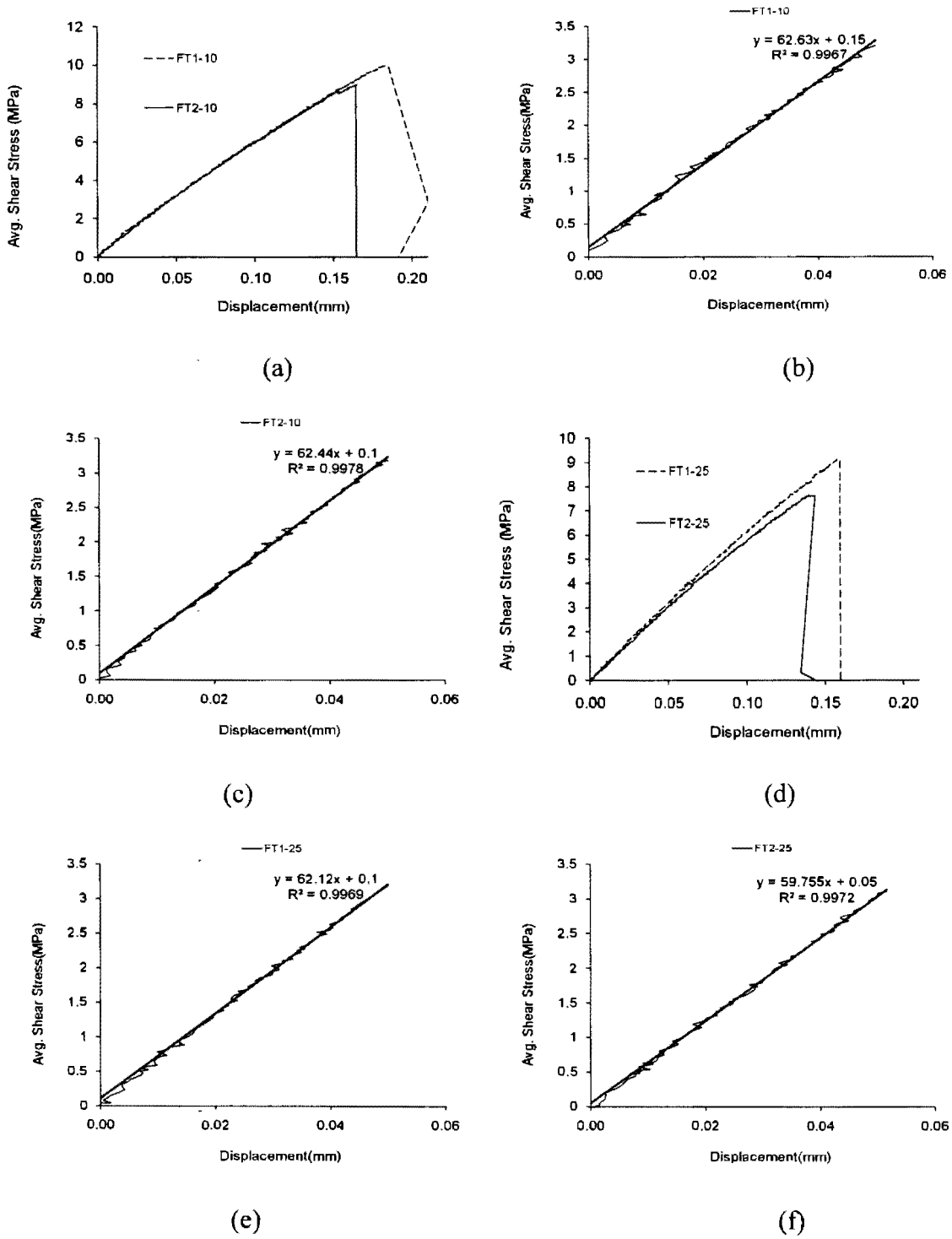

Figure B.3. Average shear stress-displacement responses under freeze-thaw effects: (a) 10 cycles (b) 10 cycles (FT1-10); (c) 10 cycles (FT2-10); (d) 25 cycles (e) 25 cycles (FT1-25); (f) 25 cycles (FT2-25)

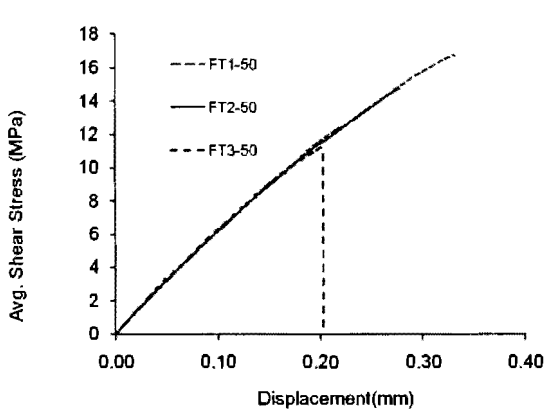

(a)

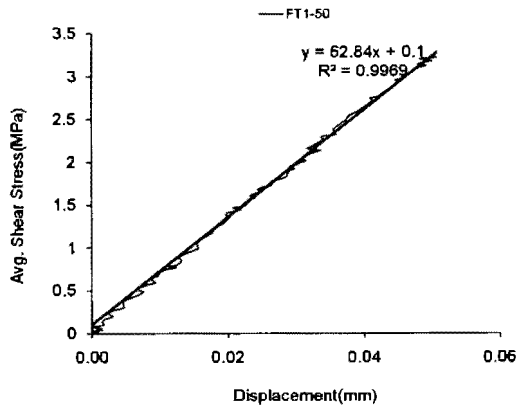

(b)

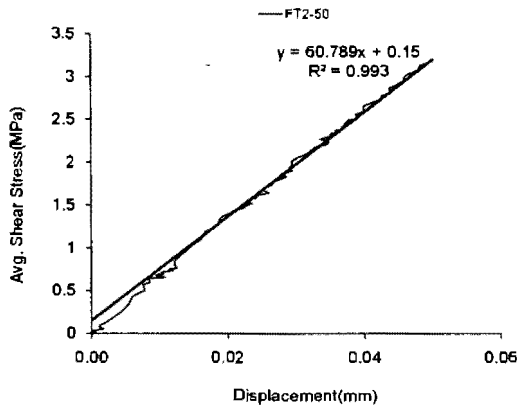

(c)

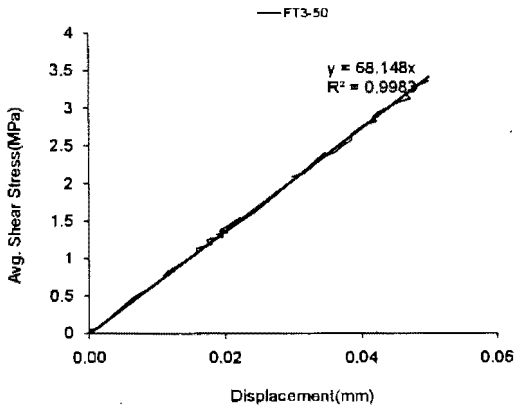

(d)

Figure B.4. Average shear stress-displacement responses under freeze-thaw effects: (a) 50 cycles (b) 50 cycles (FT1-50); (c) 50 cycles (FT2-50) ; (d) 50 cycles (FT3-50)

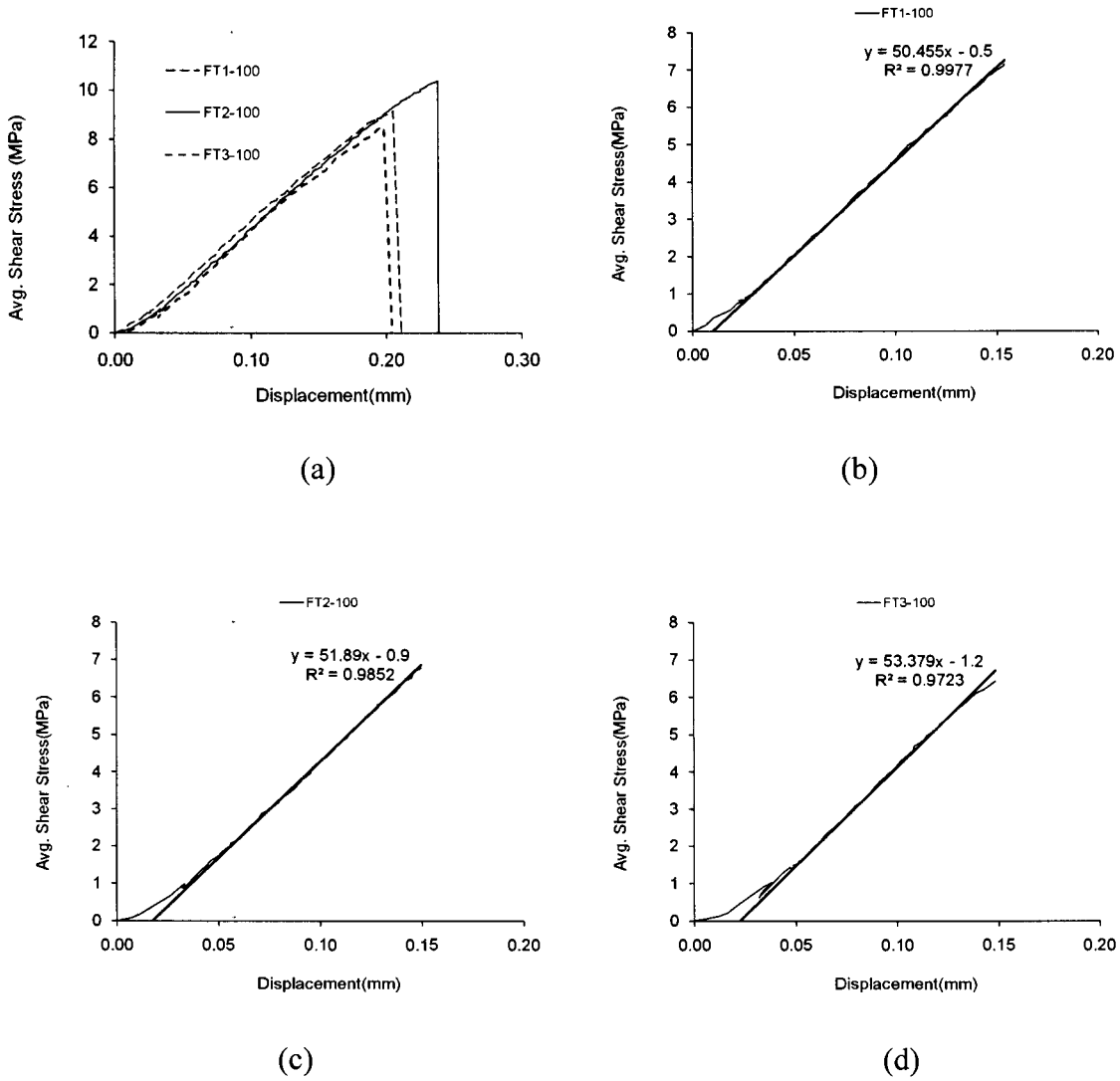

Figure B.5. Average shear stress-displacement responses under freeze-thaw effects: (a) 100 cycles (b) 100 cycles (FT1-100); (c) 100 cycles (FT2-100) ; (d) 100 cycles (FT3-100)

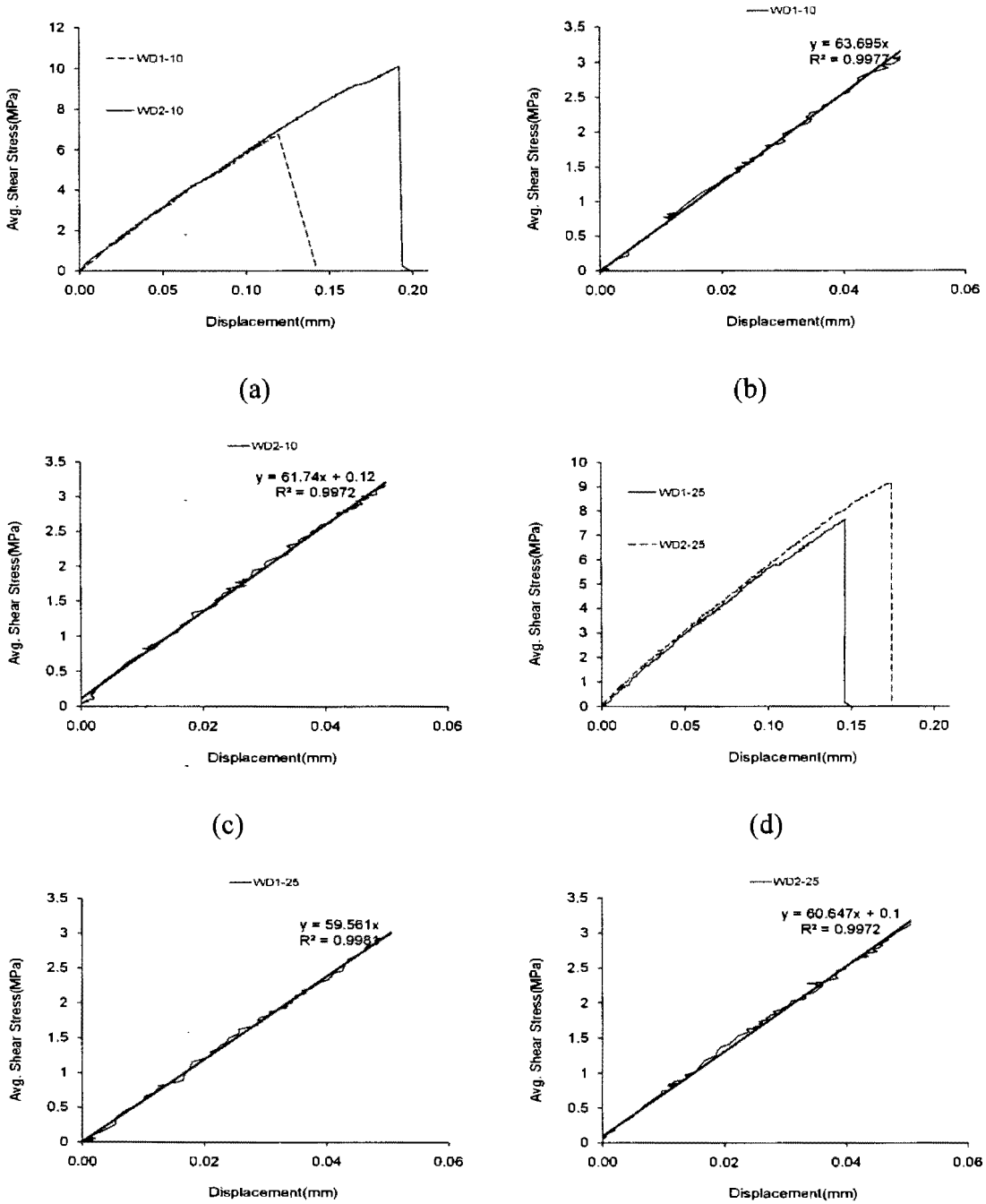

Figure B.6. Average shear stress-displacement responses under Wet-Dry effects: (a) 10 cycles (b) 10 cycles (WD1-10); (c) 10 cycles (WD2-10); (d) 25 cycles; (e) 25 cycles (WD1-25); (f) 25 cycles (WD2-25)

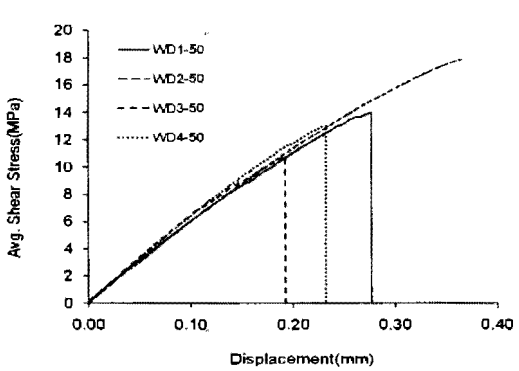

(a)

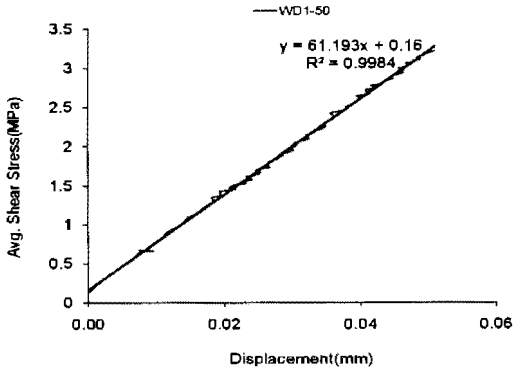

(b)

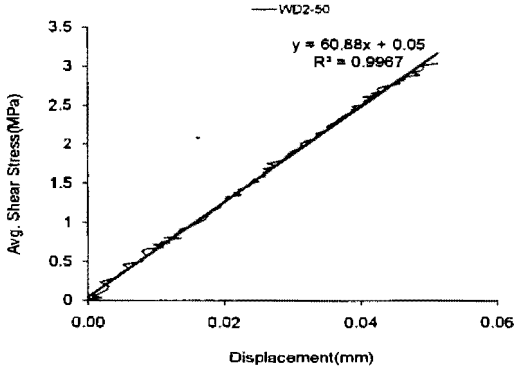

(c)

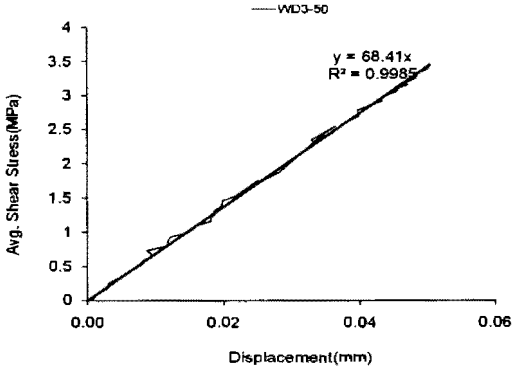

(d)

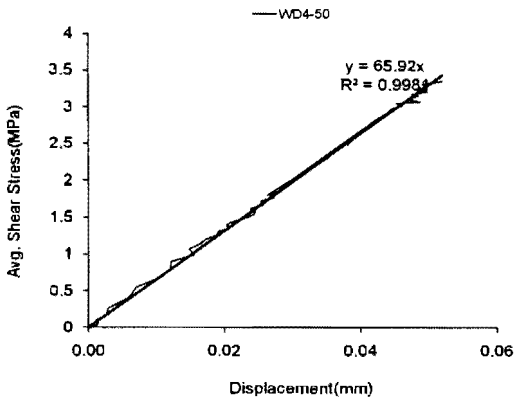

(e)

Figure B.7. Average shear stress- displacement responses under wet-dry effects: (a) 50 cycles (b) 50 cycles (WD1-50); (c) 50 cycles (WD2-50) ; (d) 50 cycles (WD3-50) ; (e) 50 cycles (WD4-50)

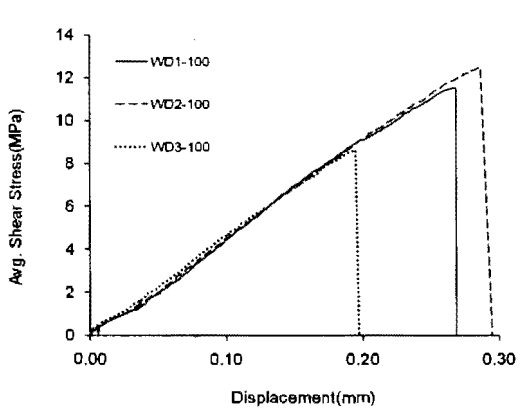

(a)

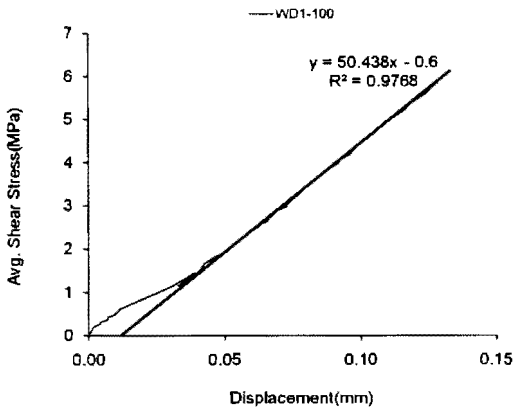

(b)

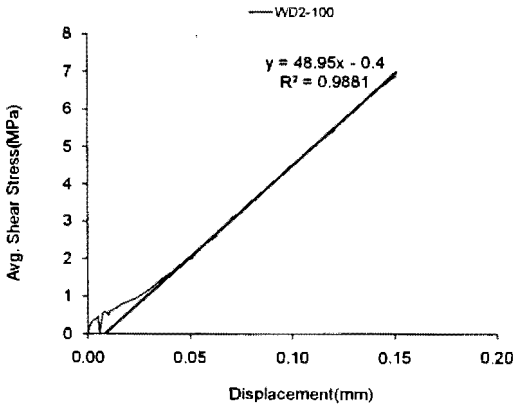

(c)

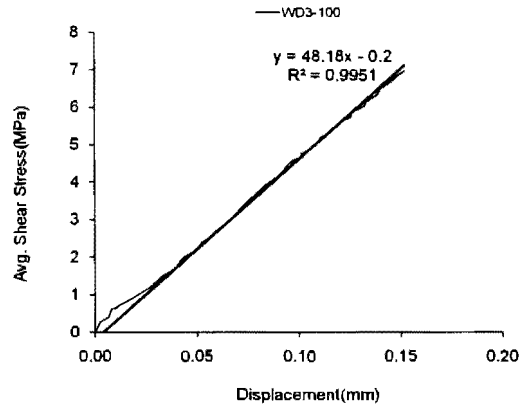

(d)

Figure B.8. Average shear stress-displacement responses under wet-dry effects: (a) 100 cycles (b) 100 cycles (WD1-100); (c) 100 cycles (WD2-100); (d) 100 cycles (WD3-100)

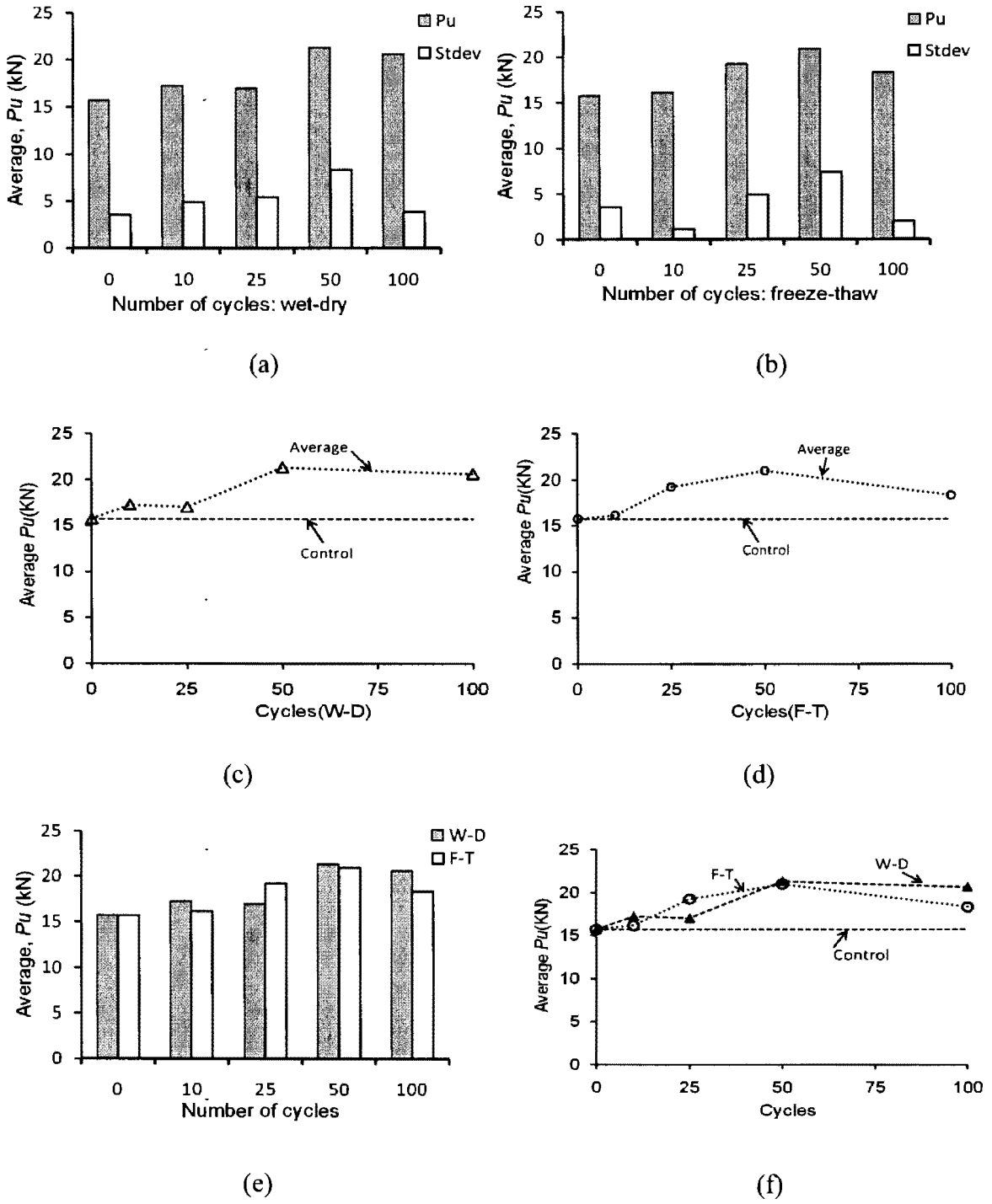

Figure B.9. Load carrying capacity (Task I): (a) effect of wet-dry cycles; (b) effect of freeze-thaw; (c) failure Load (W-D); (d) failure Load (F-T); (e) failure load comparison; (f) comparisons of the effects of wet-dry and freeze-thaw cycles

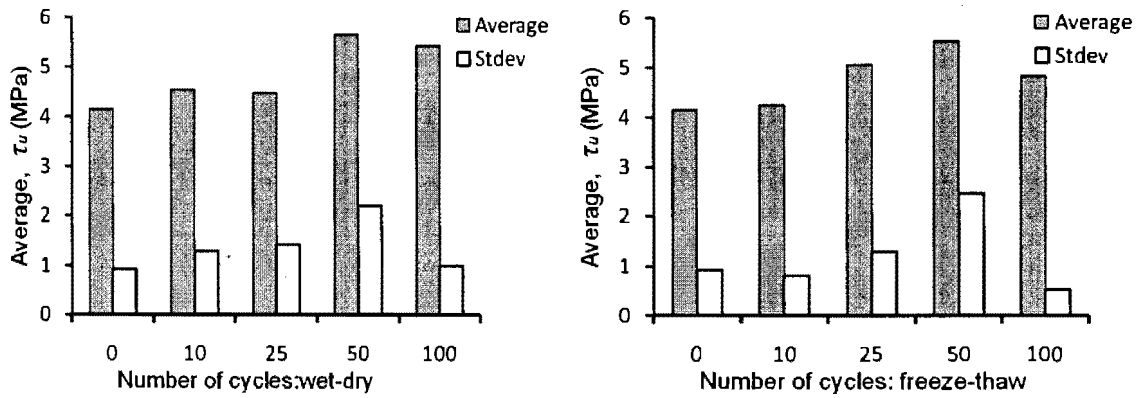

(a) (b)

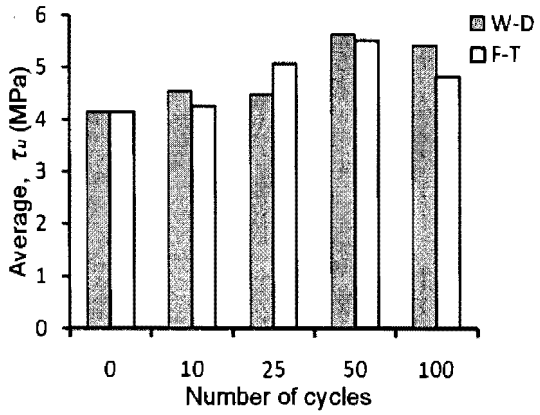

(c)

Figure B.10. Average shear stress (Task I): (a) effect of wet-dry cycles; (b) effect of freeze-thaw cycles; (c) comparisons the effects of freeze-wet-dry and wet-dry cycles

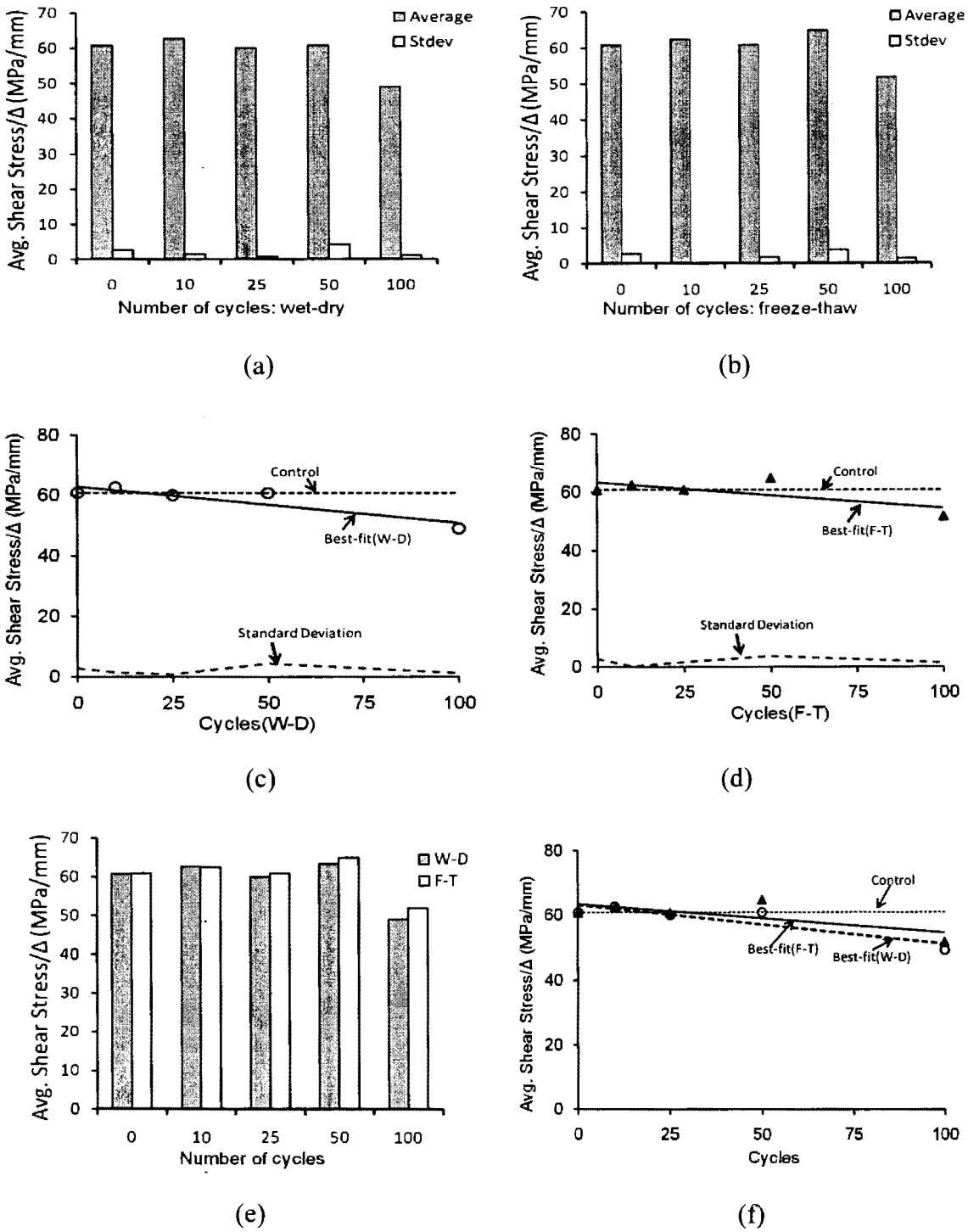

Figure B.11. Average stiffness (Task I): (a) effect of wet-dry cycles; (b) effect of freeze-thaw cycles; (c) best-fit (W-D); (d) best-fit (F-T); (e) comparisons of the effect of wet-dry and freeze-thaw cycles; (f) stiffness comparison

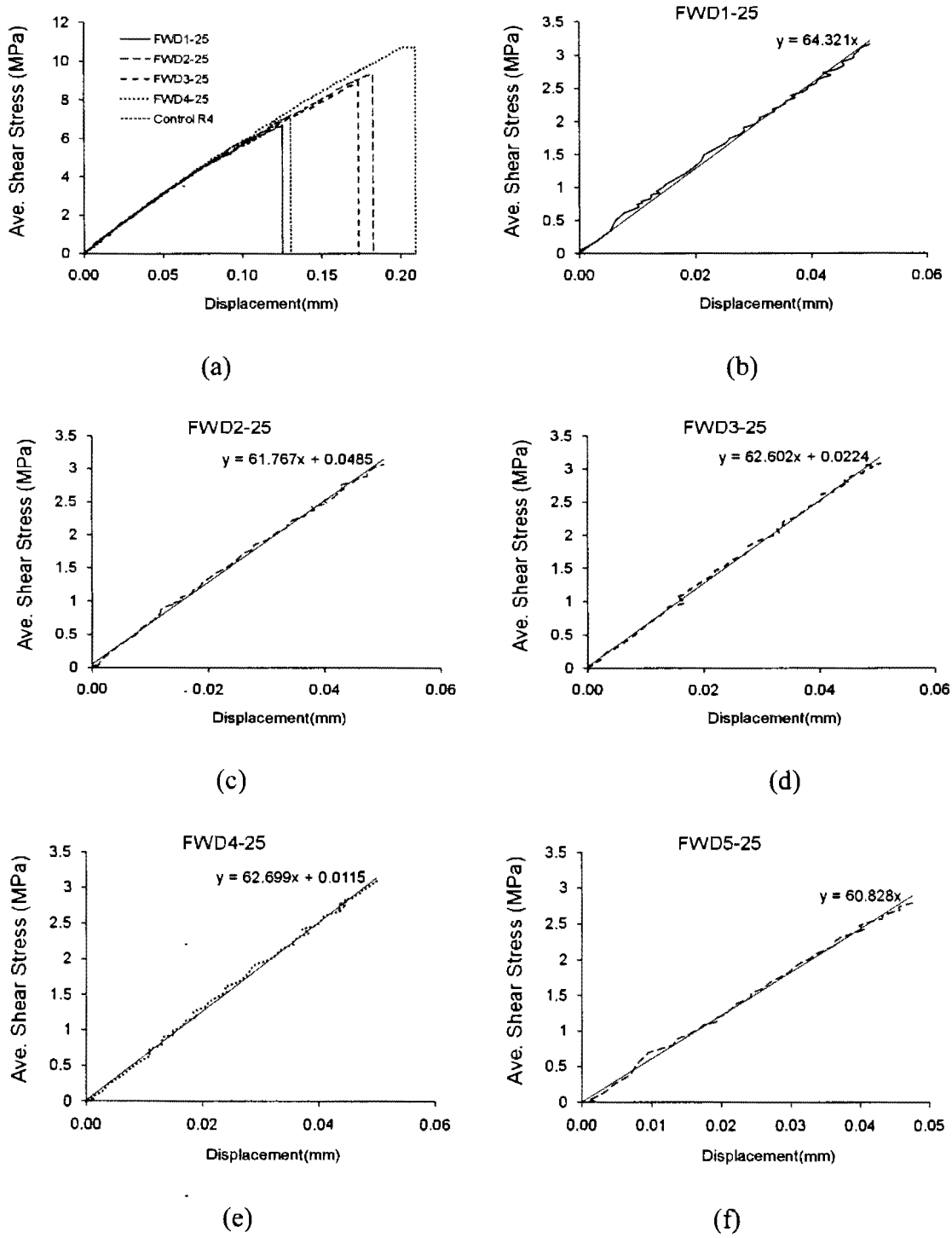

Figure B.12. Average shear stress-displacement responses under freeze-wet-dry effects: (a) 25 cycles (b) 25 cycles (FWD1-25); (c) 25 cycles (FWD2-25) ; (d) 25 cycles (FWD3-25) ; (e) 25 cycles (FWD4-25) ; (e) 25 cycles (FWD5-25)

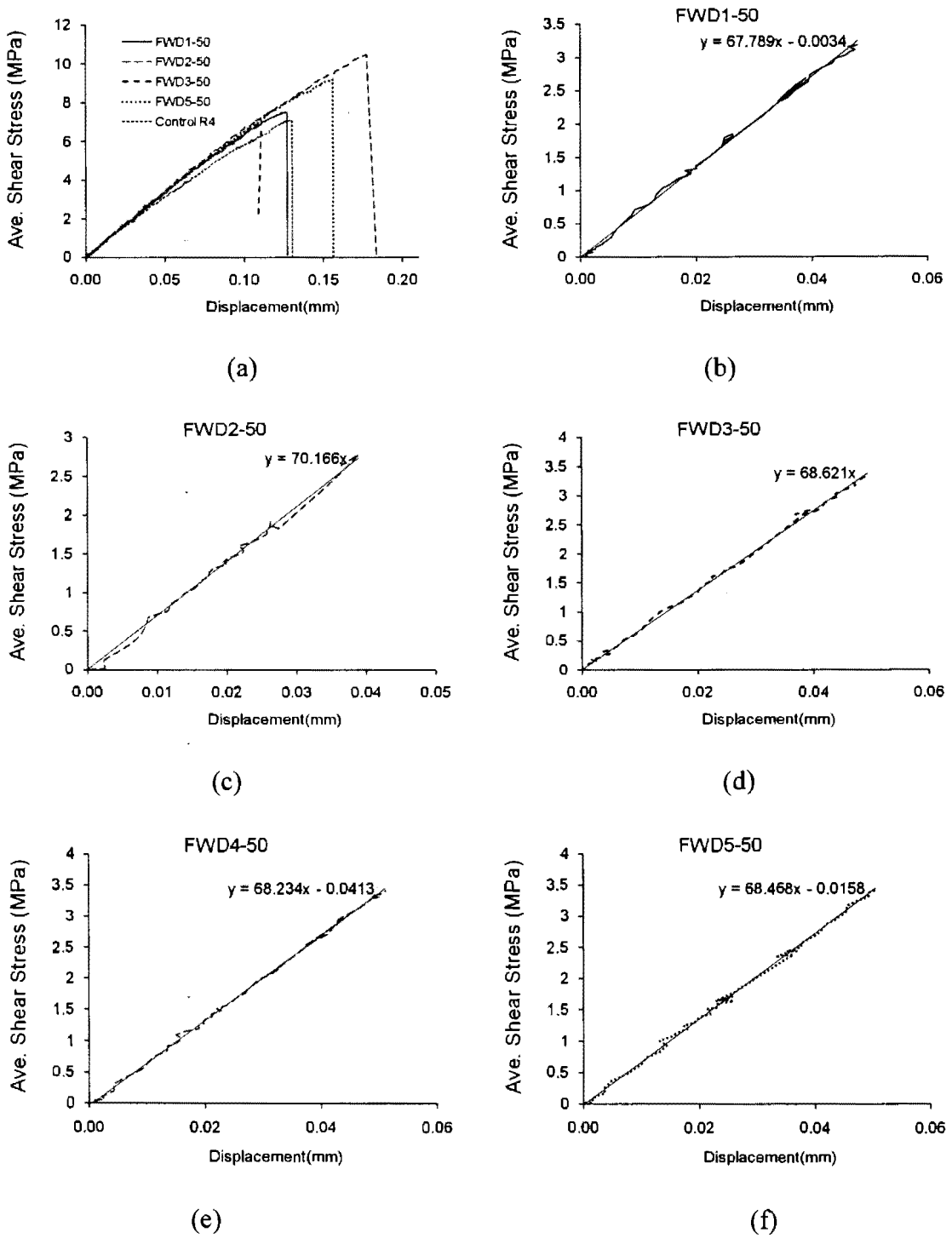

Figure B.13. Average shear stress- displacement responses under freeze-wet-dry effects: (a) 50 cycles (b) 50 cycles (FWD1-50); (c) 50 cycles (FWD2-50) ; (d) 50 cycles (FWD3-50) ; (e) 50 cycles (FWD4-50) ; (e) 25 cycles (FWD5-50)

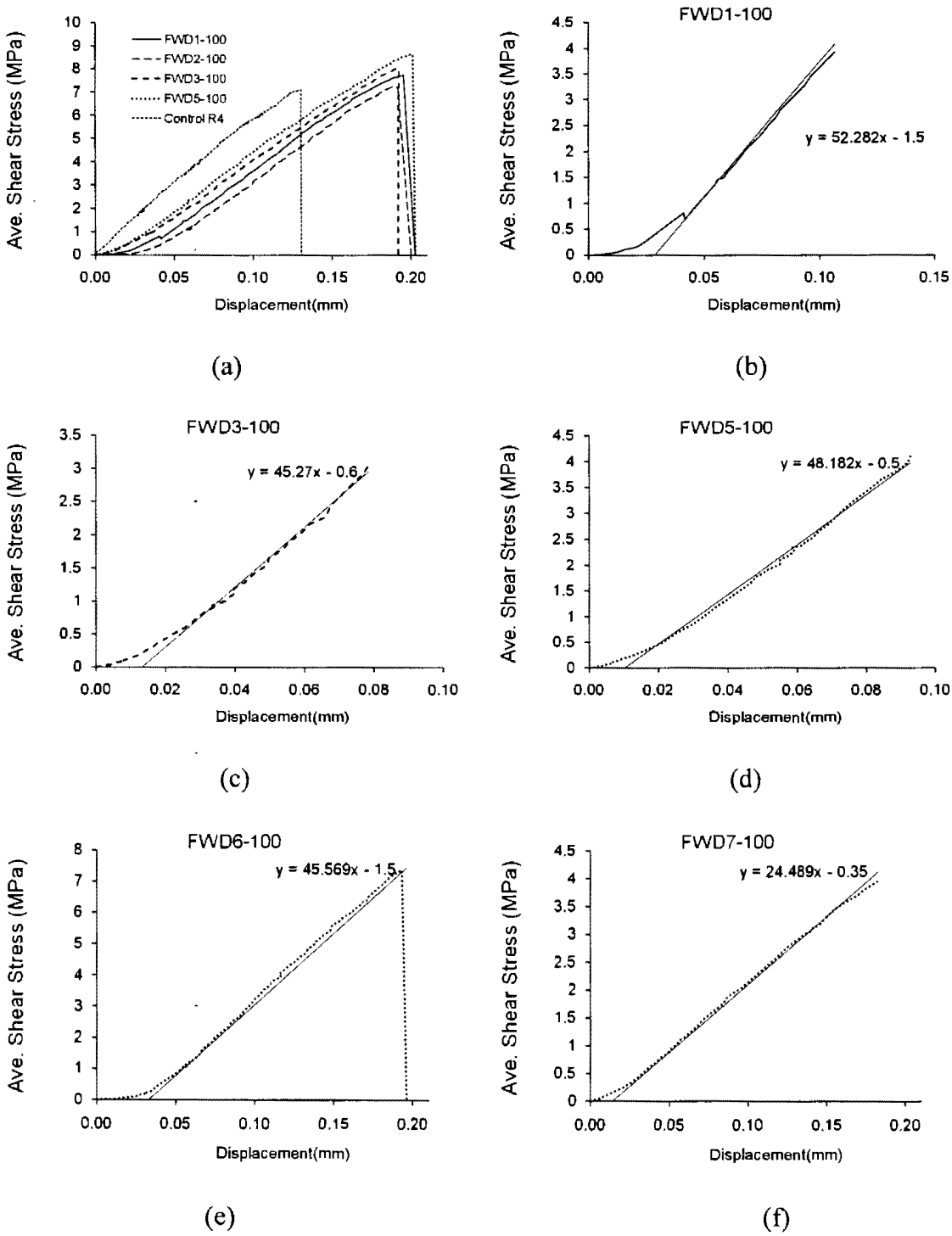

Figure B.14. Average shear stress- displacement responses under freeze-wet-dry effects: (a) At 100 cycles (b) 100 cycles (FWD1-100); (c) 100 cycles (FWD3-100) ; (d) 100 cycles (FWD5-100) ; (e) 100 cycles (FWD6-100); (f) 100 cycles (FWD7-100)

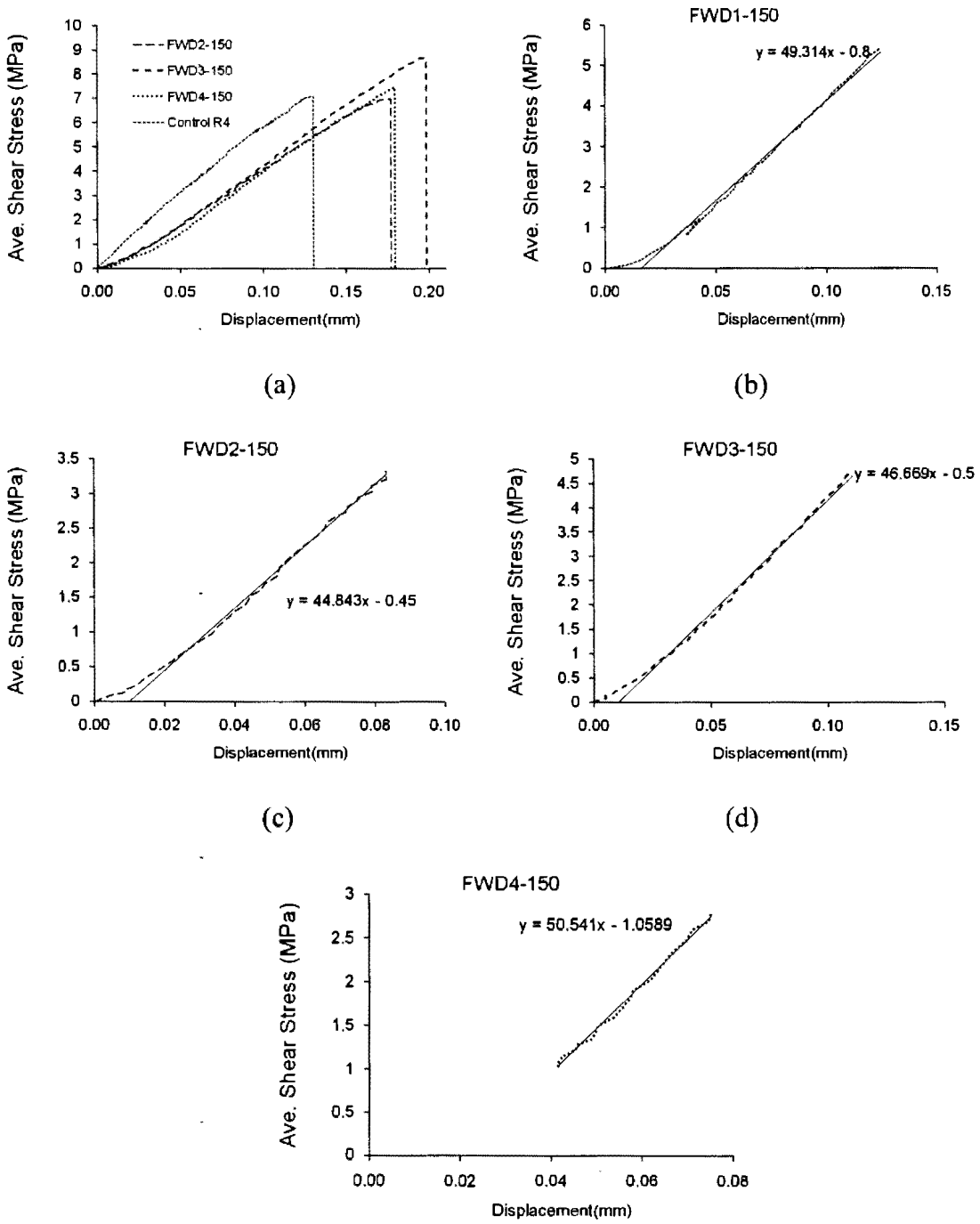

Figure B.15. Average shear stress- displacement responses under freeze-wet-dry effects: (a) 150 cycles (b) 150 cycles (FWD1-150); (c) 150 cycles (FWD2-150) ; (d) 150 cycles (FWD3-150) ; (e) 150 cycles(FWD4-150)

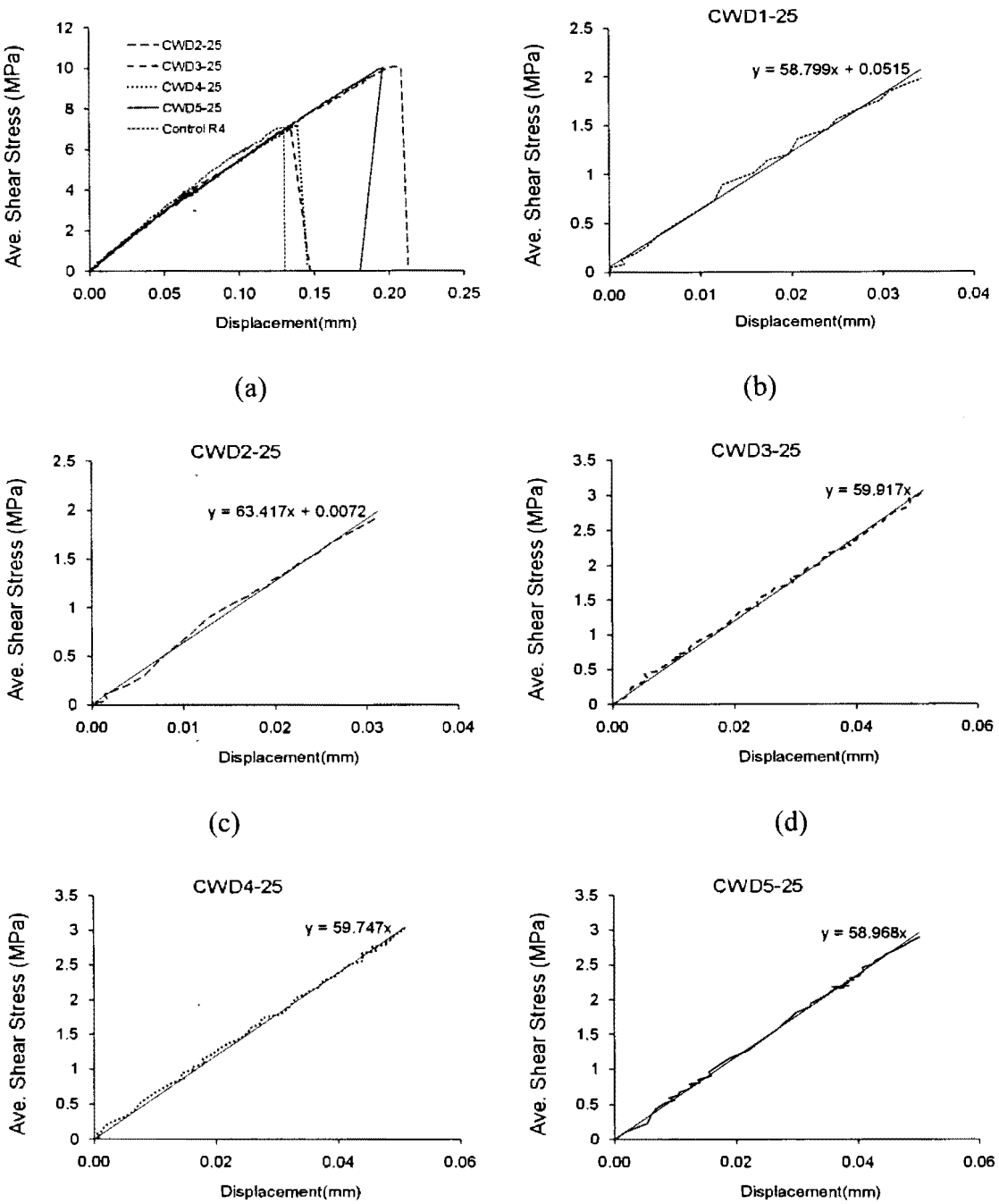

Figure B.16. Average shear stress- displacement responses under wet-dry effects: (a) 25 cycles; (b) 25 cycles (CWD1-25); (c) 25 cycles (CWD2-25); (d) 25 cycles (CWD3-25); (e) 25 cycles (CWD4-25)

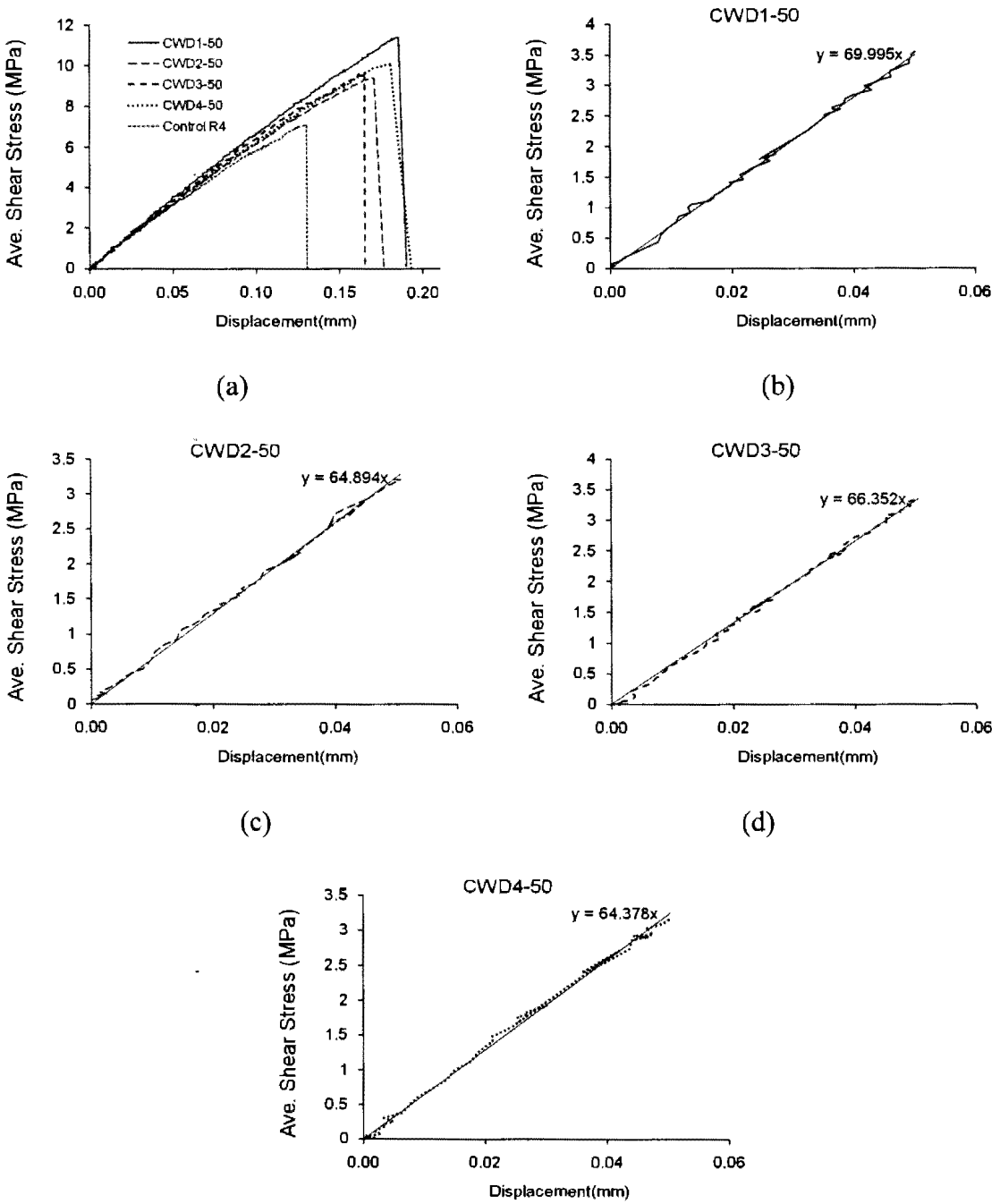

Figure B.17. Average shear stress-displacement responses under wet-dry effects: (a) 50 cycles (b) 50 cycles (CWD1-50); (c) 50 cycles (CWD2-50); (d) 50 cycles (CWD3-50); (e) 50 cycles (CWD4-50)

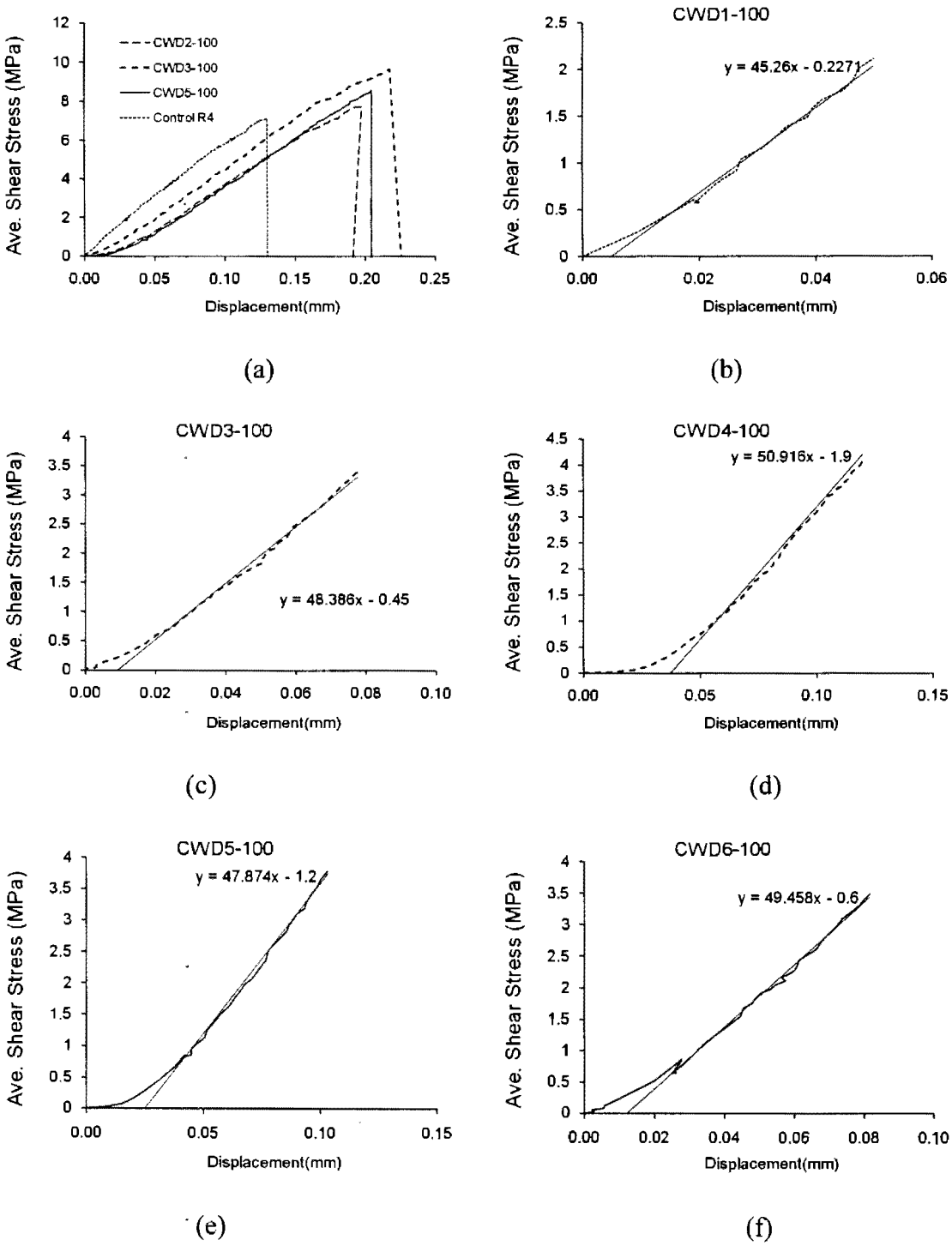

Figure B.18. Average shear stress- displacement responses under wet-dry effects: (a) 100 cycles (b) 100 cycles (CWD1-100); (c) 100 cycles (CWD3-100); (d) 100 cycles (CWD4-100); (e) 100 cycles (CWD5-100); (f) 100 cycles (CWD6-100)

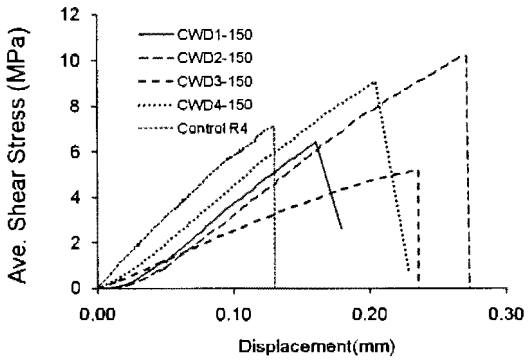

(a)

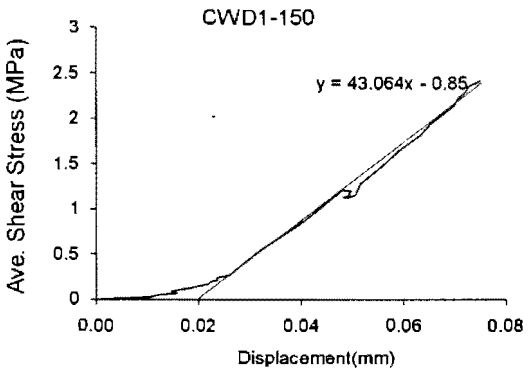

(b)

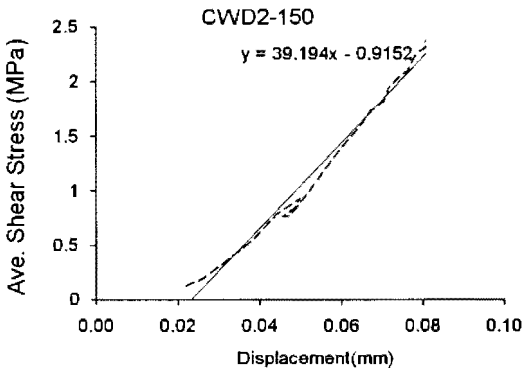

(c)

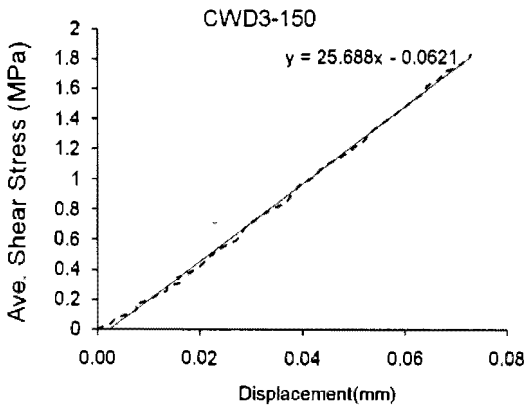

(d)

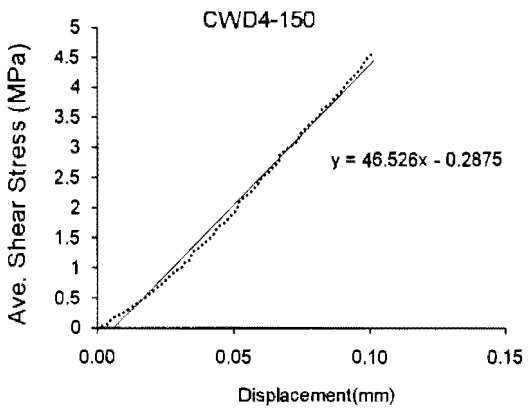

(e)

Figure B.19. Average shear stress- displacement responses under wet-dry effects: (a) 150 cycles (b) 150 cycles (CWD1-150); (c) 150 cycles (CWD2-150); (d) 150 cycles (CWD3-150); (e) 150 cycles (CWD4-150)

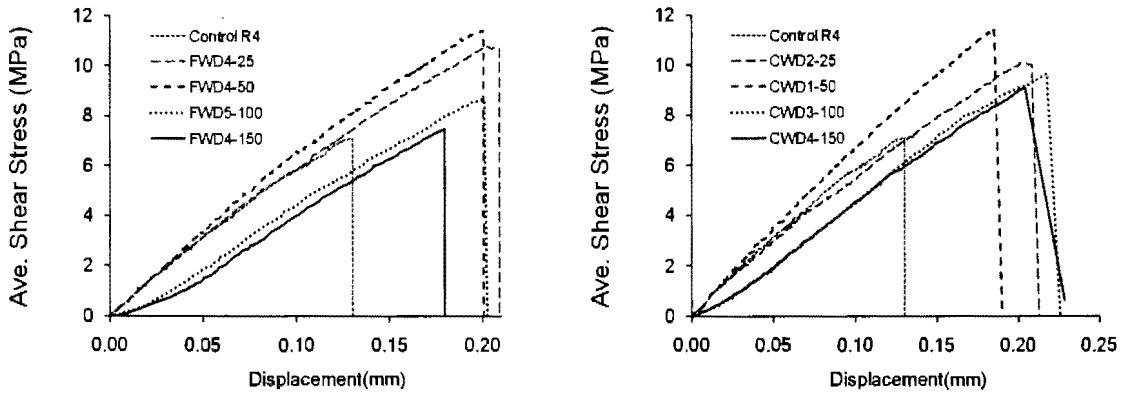

Figure B.20. Average shear stress-displacement response of specimens: (a) freeze-wet-dry condition; (b) wet-dry condition

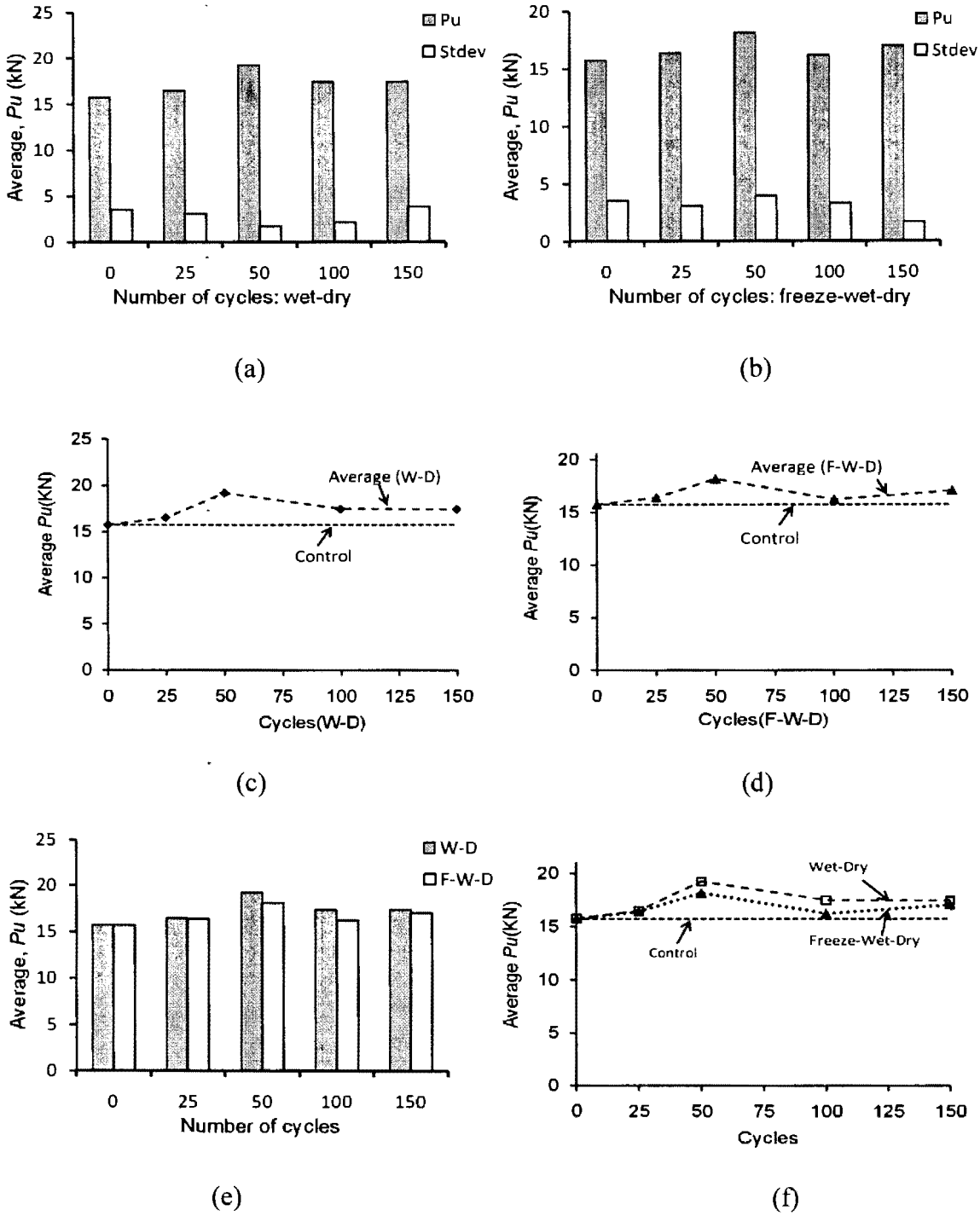

Figure B.21. Load-carrying capacity (Task II): (a) effect of wet-dry cycles; (b) effect of freeze-wet-dry; (c) failure load (W-D); (d) failure load (F-W-D); (e) failure load comparisons; (f) comparisons of the effect of wet-dry and freeze-wet-dry cycles

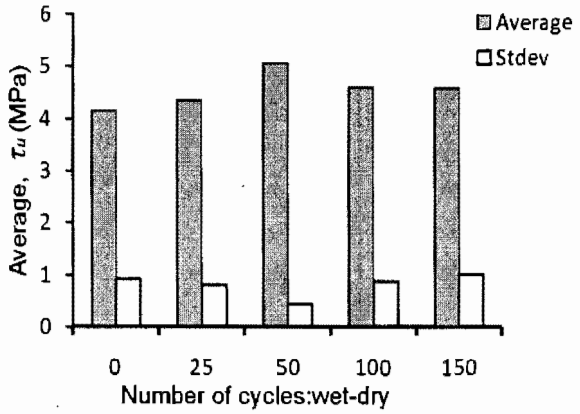

(a)

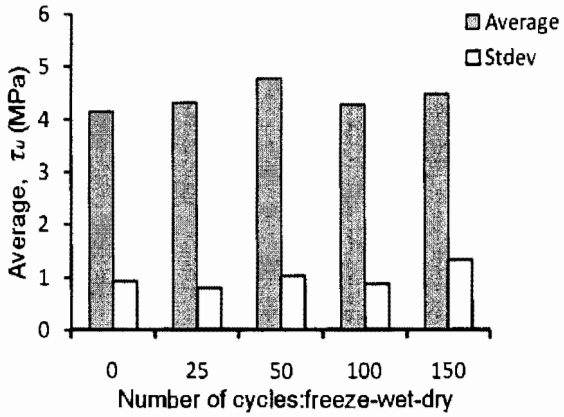

(b)

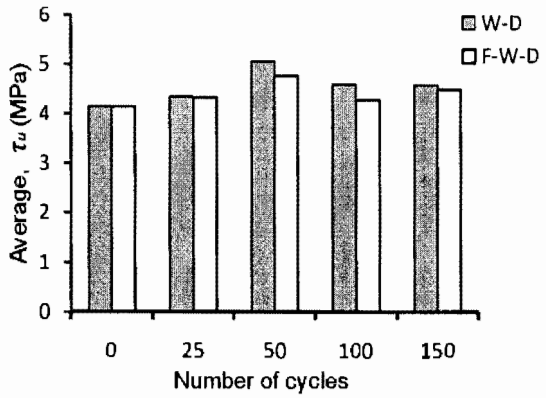

(c)

Figure B.22. Average shear stress: (a) effect of wet-dry cycles; (b) effect of freeze-wet-dry cycles; (c) comparisons the effects of freeze-wet-dry and wet-dry cycles

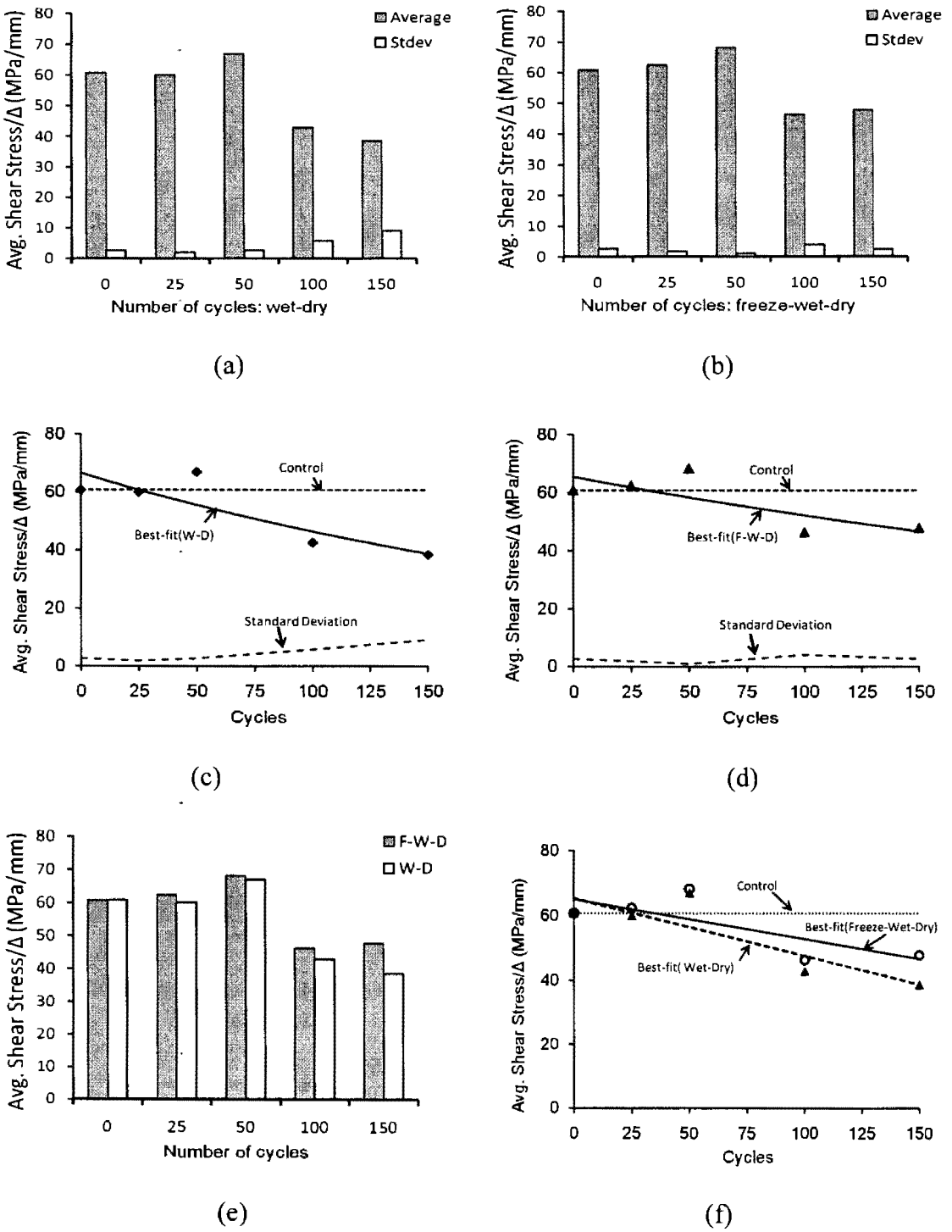

Figure B.23. Average stiffness (Task II): (a) effect of wet-dry cycles; (b) effect of freeze-wet-dry; (c) effect of wet-dry cycles; (d) effect of freeze-wet-dry; (e) comparison the effects of wet-dry and freeze-wet-dry cycles; (d) effects of wet-dry/freeze-wet-dry cycles

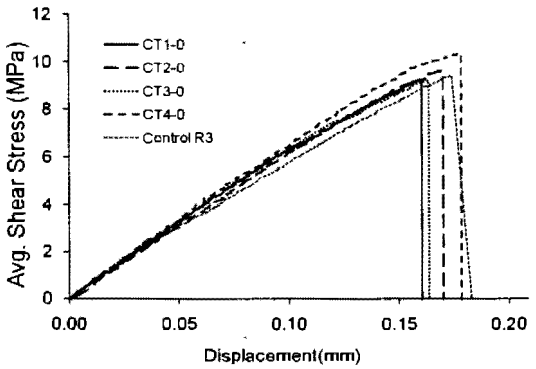

(a)

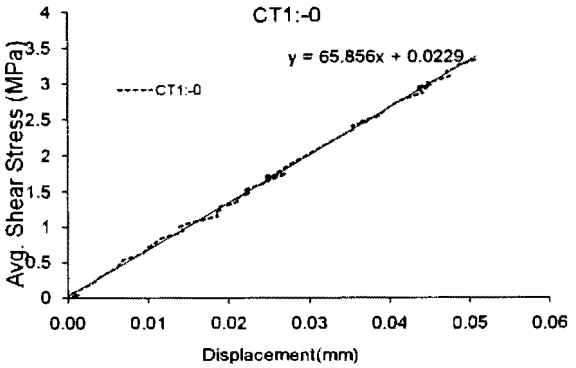

(b)

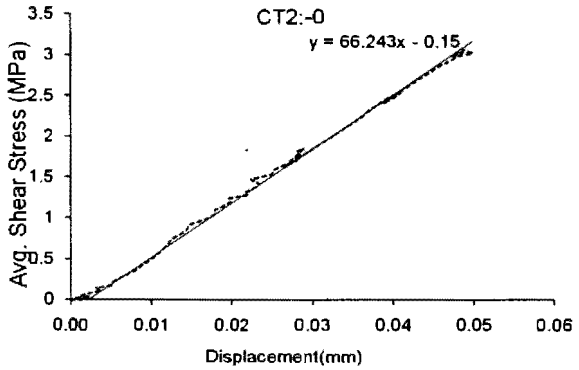

(c)

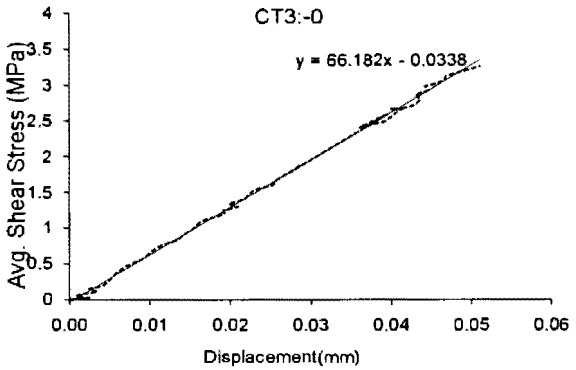

(d)

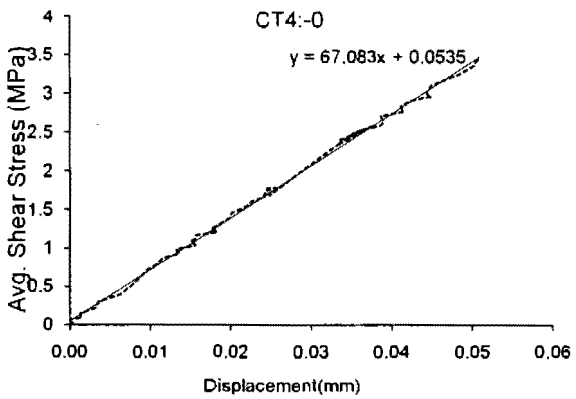

(e)

Figure B.24. Average shear stress- displacement responses of 2000 h constant freezing at -0 ^{0}C: (a) all specimens at 0 ^{0}C (b) CT1(0 ^{0}C); (c) CT2 (-0 ^{0}C); (d) CT3 (-0 ^{0}C); (e) CT4 (-0 ^{0}C)

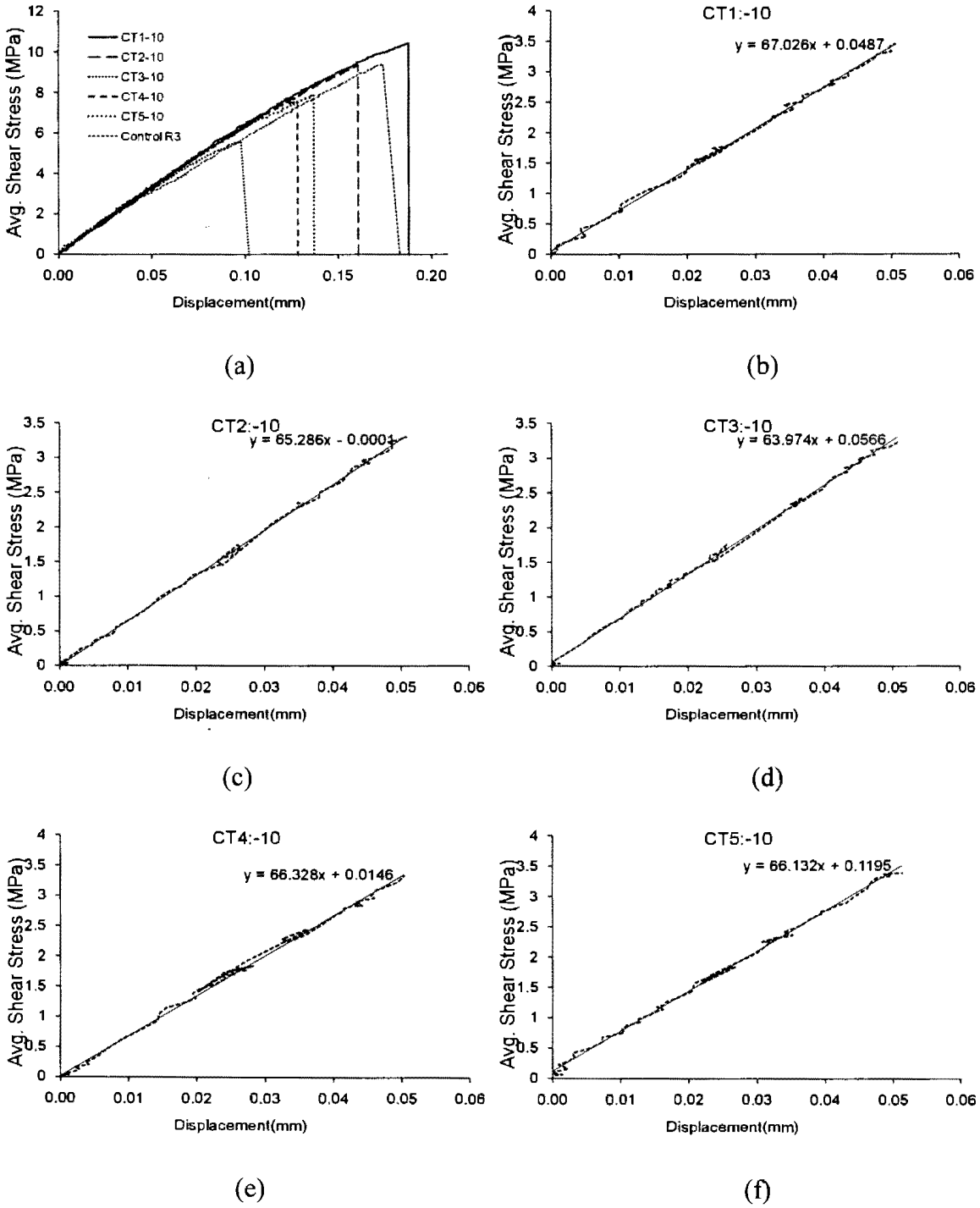

Figure B.25. Average shear stress- displacement responses of 2000 h constant freezing at -10 ^{0}C: (a) specimens at -10 ^{0}C (b) CT1(-10 ^{0}C); (c) CT2 (-10 ^{0}C); (d) CT3 (-10 ^{0}C);(e) CT4 (-10 ^{0}C) ;(f) CT5 (-10 ^{0}C)

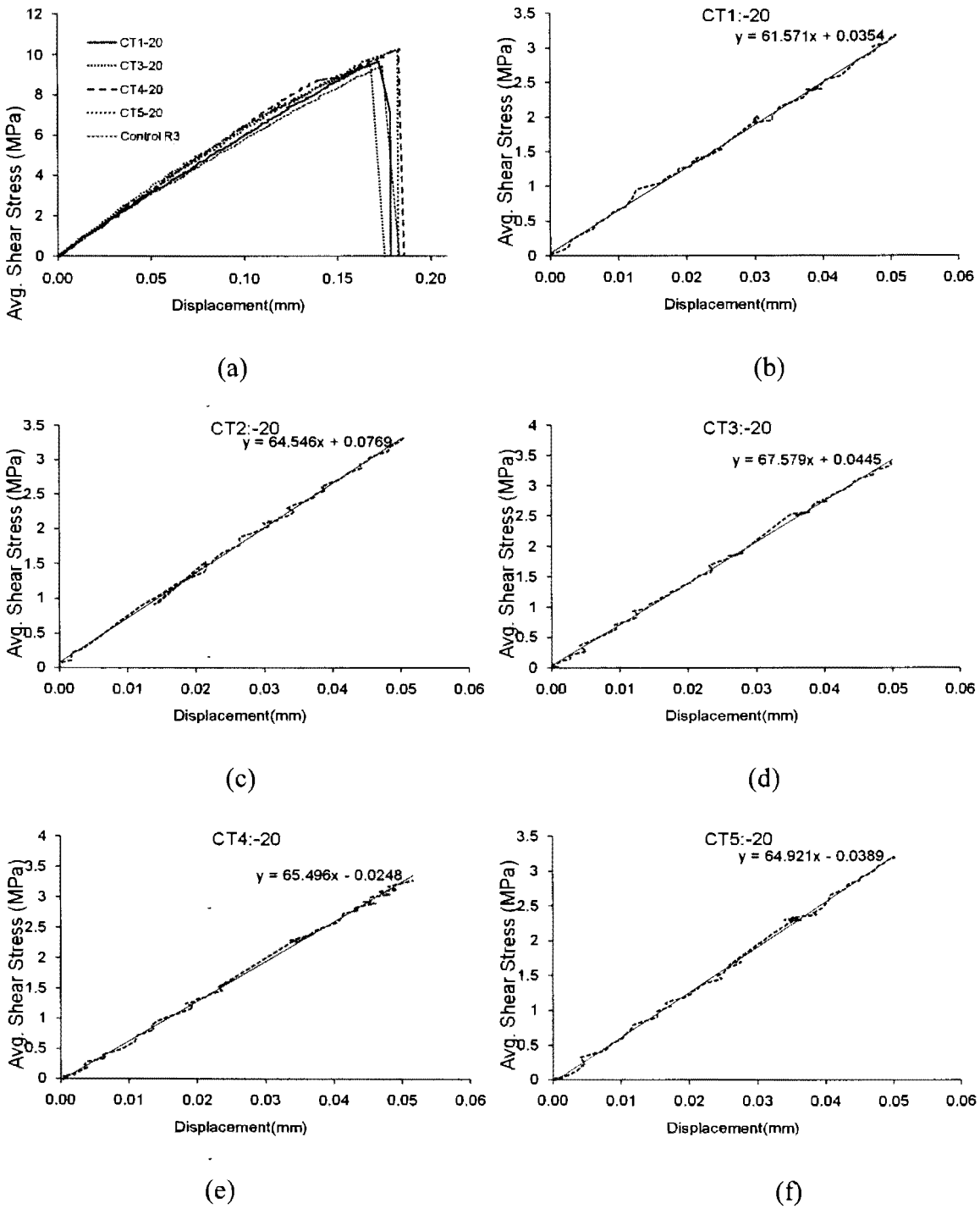

Figure B.26. Average shear stress- displacement responses after 2000 hours constant freezing at -20 ^{0}C: (a) specimens at -20 ^{0}C (b) CT1 (-20 ^{0}C); (c) CT2 (-20 ^{0}C); (d) CT3 (-20 ^{0}C); (e) CT4 (-20 ^{0}C); (f) CT5 (-20 ^{0}C)

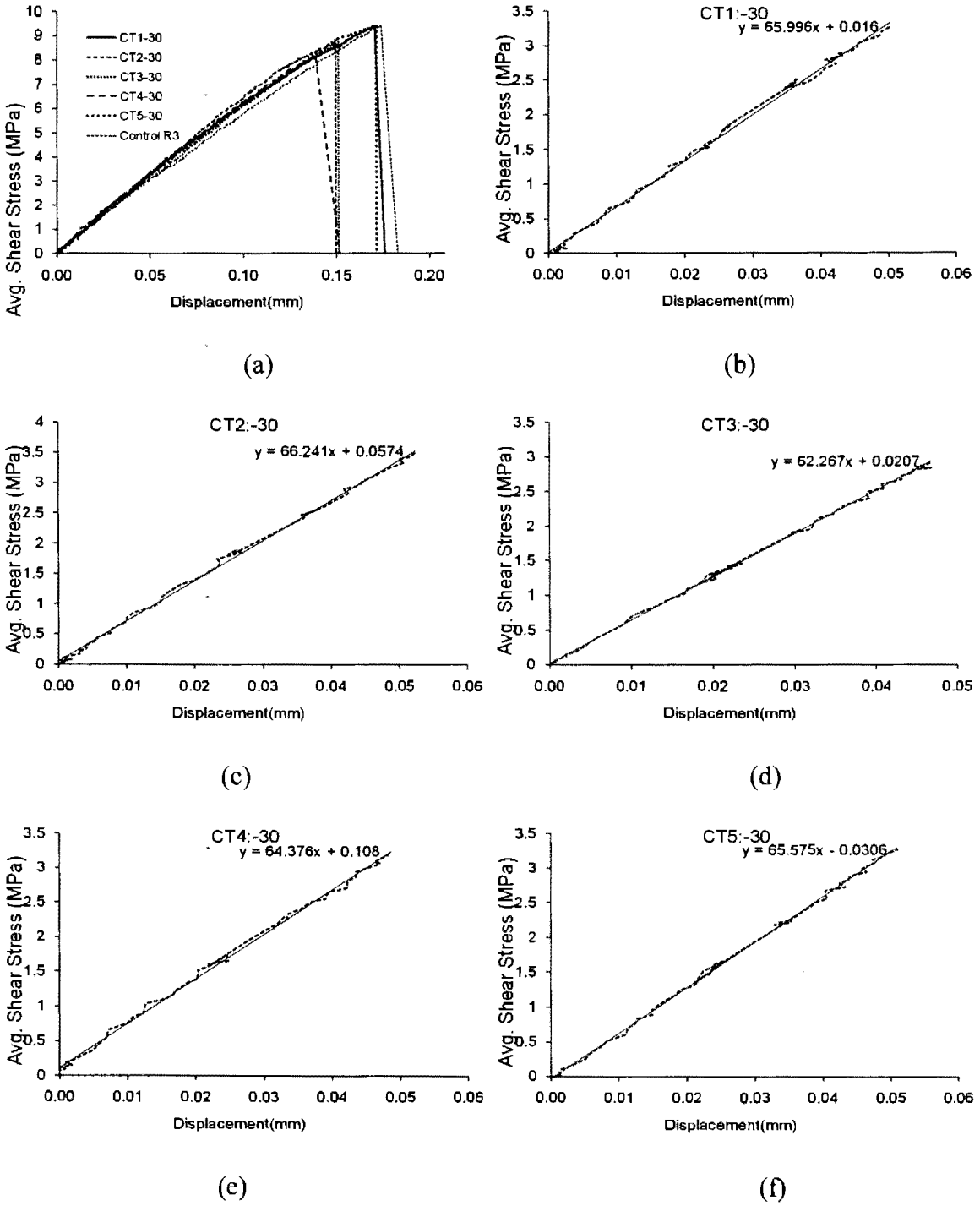

Figure B.27. Average shear stress- displacement responses after 2000 hours constant freezing at -30 ^{0}C: (a) All specimens at -30 ^{0}C (b) CT1(-30 ^{0}C); (c) CT2 (-30 ^{0}C); (d) CT3 (-30 ^{0}C); (e) CT4 (-30 ^{0}C) ; (f) CT5 (-30 ^{0}C)

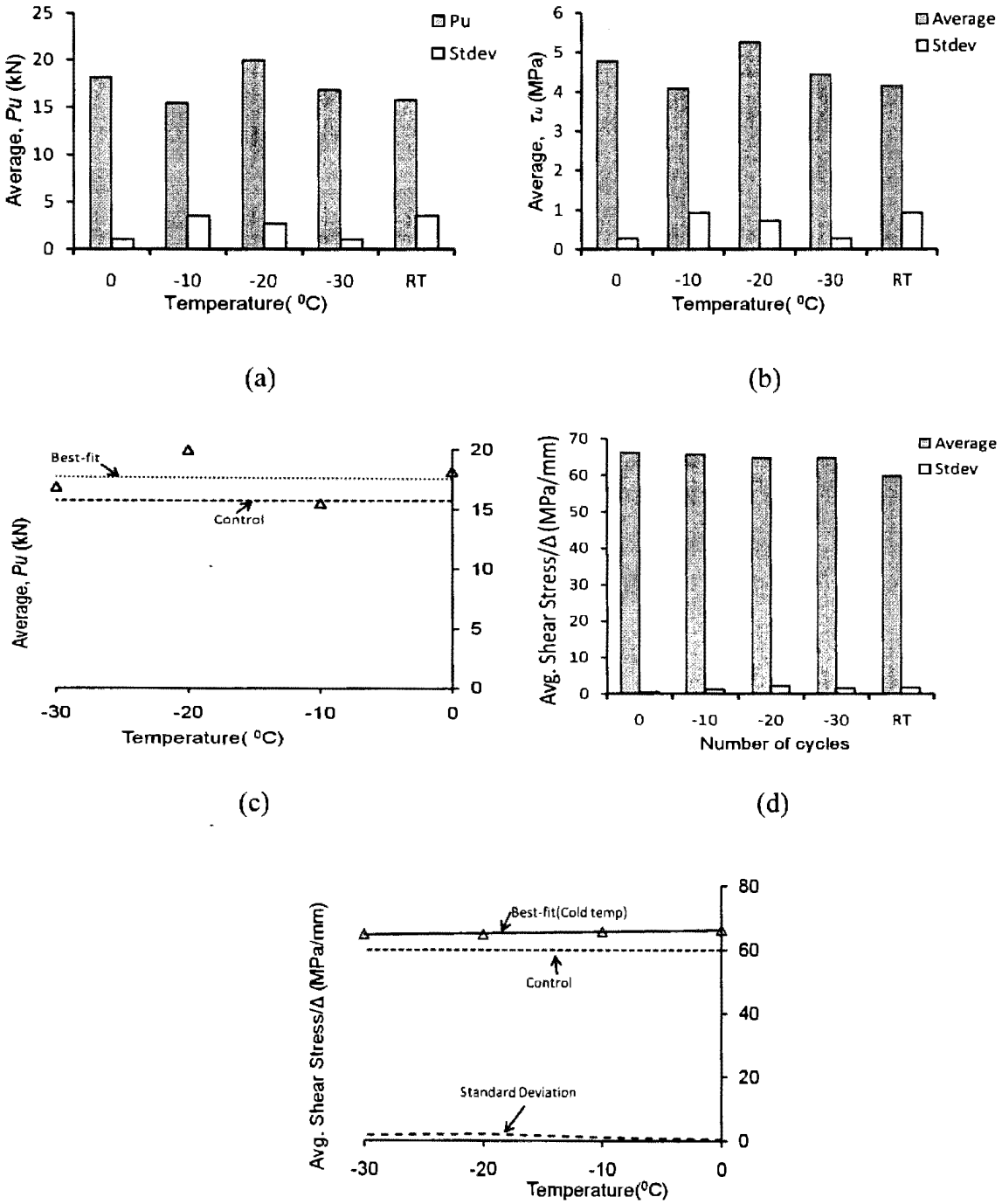

Figure B.28. Summary of test results for 2000 hours constant freezing under different low temperatures: (a) average failure load variation with temperature; (b) average stifneess variation; (c) failure load; (d) stiffness variations; (e) effects of cold temperature

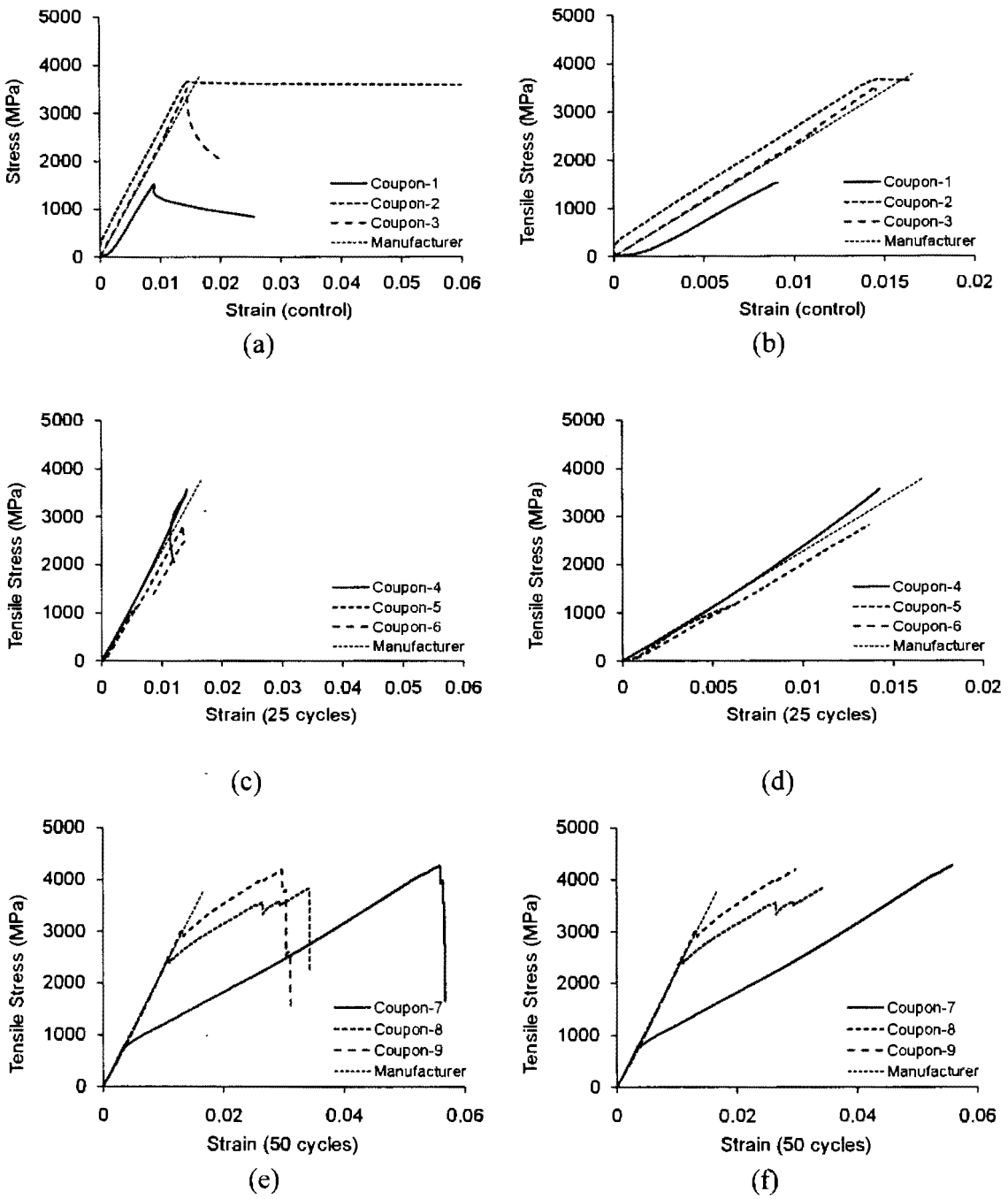

Figure B.29. Tensile stress-strain responses for CFRP coupons under freeze-wet-dry effects: (a) 0 cycles (Control); (b) 0 cycles (Control); (c) 25 cycles; (d) 25cycles; (e) 50 cycles; (f) 50 cycles

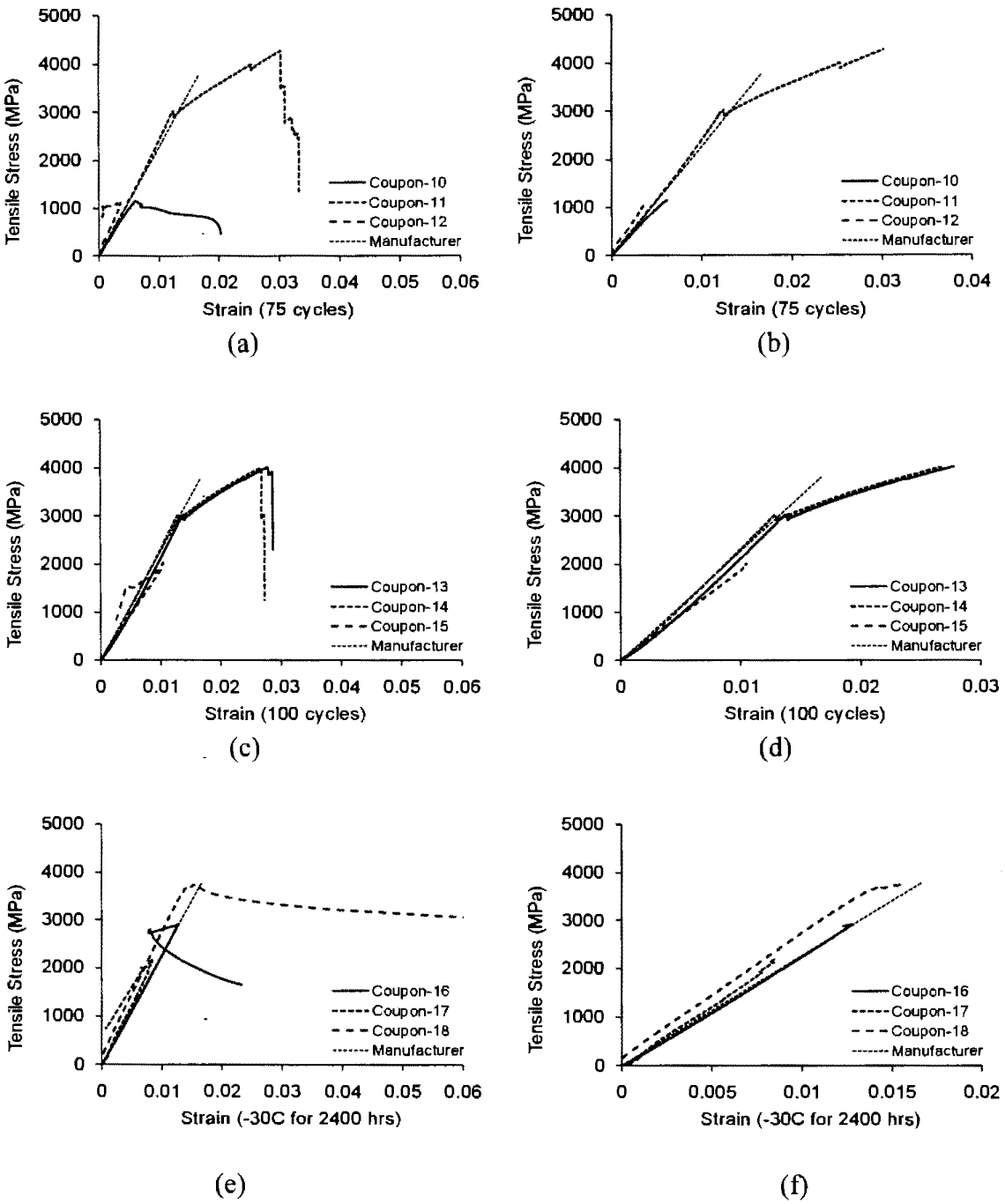

Figure B.30. Tensile stress-strain responses for CFRP coupons after environmental effects: (a) 75 cycles; (b) 75cycles; (c) 100 cycles; (d) 100 cycles; (e) constant freezing at – 30^0C for 2400 hours; (f) constant freezing at – 30^0C for 2400 hours

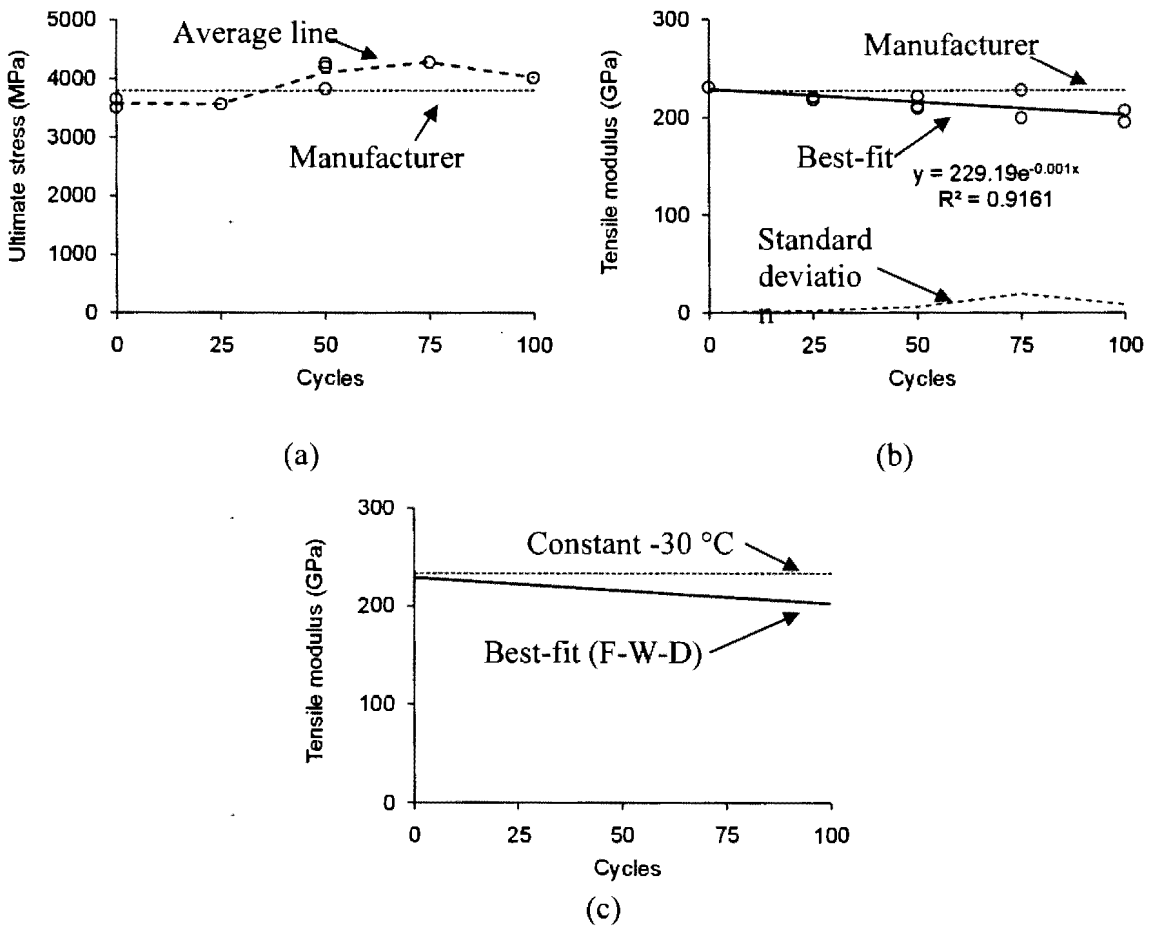

Figure B.31. Summary of test results for CFRP coupons: (a) average ultimate tensile strength variation with environmental effects; (b) effects of freeze-wet-dry cycles; (c) average stifneess variation comparisons.

APPENDIX C. STRENGTHENING OF AXIAL CONCRETE MEMBER WITH CFRP SHEETS

Table C.1. Models for compute Confined Concrete Compressive Strength

Model	Theoretical fcc'	Theoretical εcc
Fardis and Khalili	$\frac{f'_{cc}}{f'_{co}} = 1 + 4.1\left(\frac{p_u}{f'_{co}}\right)^{0.86}$ $\frac{f'_{cc}}{f'_{co}} = 1 + 3.7\left(\frac{p_u}{f'_{co}}\right)^{0.86}$	$\varepsilon_{cc} = \varepsilon_{co} + 0.0005\left(\frac{E_1}{f'_{co}}\right)$
Saadatmanesh et al.	$\frac{f'_{cc}}{f'_{co}} = 2.254\sqrt{1 + 7.94\left(\frac{p_u}{f'_{co}}\right)} - 2\left(\frac{p_u}{f'_{co}}\right) - 1.254$	$\frac{\varepsilon_{cc}}{\varepsilon_{co}} = 1 + 5\left(\frac{f'_{cc}}{f'_{co}} - 1\right)$
Samaan et al.	$\frac{f'_{cc}}{f'_{co}} = 1 + 6.0 - \left(\frac{p_u}{f'_{co}}\right)^{0.7}$	$\varepsilon_{cc} = \left(f'_{cc} - \frac{f_o}{E_2}\right)$
Toutanji	$\frac{f'_{cc}}{f'_{co}} = 1 + 3.5\left(\frac{p_u}{f'_{co}}\right)^{0.85}$	$\frac{\varepsilon_{cc}}{\varepsilon_{co}} = 1 + (310.57\varepsilon_{fu} + 1.90)\left(\left(\frac{f'_{cc}}{f'_{co}}\right) - 1\right)$
Saafi et al.	$\frac{f'_{cc}}{f'_{co}} = 1 + 2.2\left(\frac{p_u}{f'_{co}}\right)^{0.84}$	$\frac{\varepsilon_{cc}}{\varepsilon_{co}} = 1 + (537\varepsilon_{fu} + 2.6)\left(\left(\frac{f'_{cc}}{f'_{co}}\right) - 1\right)$
Spoelstra and Monti	$\frac{f'_{cc}}{f'_{co}} = 0.2 + 2.2\left(\frac{p_u}{f'_{co}}\right)^{0.5}$	$\frac{\varepsilon_{cc}}{\varepsilon_{co}} = 2 + 1.25\left(\frac{E_{co}}{f'_{co}}\right)\varepsilon_{fu}\sqrt{\frac{p_u}{f'_{co}}}$
Xiao and Wu	$\frac{f'_{cc}}{f'_{co}} = 1.1 + \left[4.1 - 0.75\left(\frac{f'^{2}_{co}}{E_1}\right)\right]\left(\frac{p_u}{f'_{co}}\right)$	$\varepsilon_{cc} = \frac{\varepsilon_{fu} - 0.0005}{7\left(f'_{co}/E_1\right)^{0.8}}$

C 1. ACI Committee 440 (2002) Model (ACI 440.2R-02)

$$f'_{cc} = f'_c + \Psi_f 3.3\kappa_a f_l \tag{C.1}$$

where f'_c = unconfined concrete compressive strength; ψ_f = additional reduction factor=0.95; K_a =efficiency factors that account for the geometry of the section=1.0 for circular cross section;

f_l = maximum confinement pressure due to FRP-jacket given by

$$f_l = \frac{2E_f n t_f \varepsilon_{fe}}{D} \tag{C.2}$$

where n=number of CFRP layers; t_f = thickness of the CFRP layer; D=diameter of the concrete cylinders; ε_{fe} = effective strain level in the FRP at failure given by

$$\varepsilon_{fe} = \kappa_\varepsilon \varepsilon_{fu} \tag{C.3}$$

where and A strain efficiency factor of K_ε of 0.55 and a minimum confinement ratio $f_e / f_c^{'}$ of 0.08 were used. E_f is the tensile modulus of elasticity of FRP given by Hooke's law

$$E_f = f_{fu} / \varepsilon_{fu} \tag{C.4}$$

where f_{fu}=design ultimate tensile strength of FRP given by

$$f_{fu} = C_e f_{fu}^{*} \tag{C.5}$$

where C_e =environmental reduction factor=0.85 for exterior exposure for FRP; f_{fu}^{*} = ultimate tensile strength of FRP as reported by manufacturer; and ε_{fu} = design rupture strain of FRP given by

$$\varepsilon_{fu} = C_e \varepsilon_{fu}^{*} \tag{C.6}$$

where ε_{fu}^{*} = ultimate rupture strain of FRP as reported by manufacturer.

C2. ISIS Canada Model (ISIS Canada 2001)

$$f_{cc}^{'} = f_c^{'}(1.0 + \alpha_{pc}\omega_w) \tag{C.7}$$

where α_{pc} = performance coefficient taken equal to 1.0; and ω_w = volumetric confinement ratio given by

$$\omega_w = \frac{\rho_{FRP}\phi_{FRP}f_{FRP_u}}{\phi_c f_c^{'}} = \frac{2f_{eFRP}}{\phi_c f_c^{'}} \tag{C.8}$$

where ρ_{FRP} = reinforcement ration of FRP taken as

$$\rho_{FRP} = \frac{4N_b t_{FRP}}{D_g} \tag{C.9}$$

f_{eFRP} is the lateral confinement pressure due to FRP-jacket given by

$$f_{eFRP} = \frac{2N_b \phi_{FRP} f_{FRP_u} t_{FRP}}{D_g} \tag{C.10}$$

The minimum confinement pressure, $f_{eFRP} \geq 4MPa$ (C.11)

The maximum confinement pressure, $f_{eFRP} \leq \frac{f_c^{'}}{2\alpha_{pc}}(\frac{1}{k_e} - \phi_c)$ (C.12)

ϕ_{FRP} = FRP material resistance factor = 0.75 for wrapped CFRP; ϕ_c = concrete material resistance factor=0.65; κ_e = strength reduction factor=0.85; N_{FRP} = number of CFRP layers; t_{FRP} = thickness of the CFRP layer; D_g=diameter of the concrete cylinders; f_{FRPu}= ultimate tensile strength of FRP as reported by manufacturer.

APPENDIX D. DURABILITY OF BOND BETWEEN CFRP AND CONCRETE

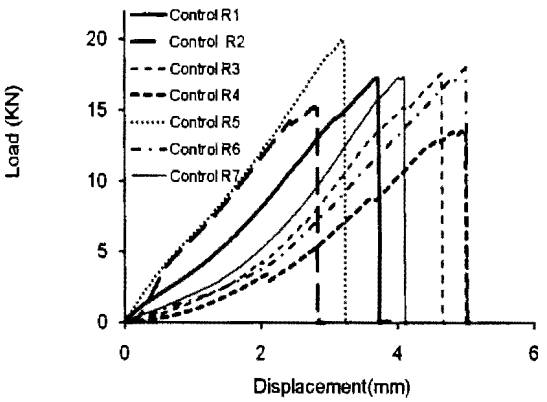

Figure D.1. Load-displacement response of control specimens

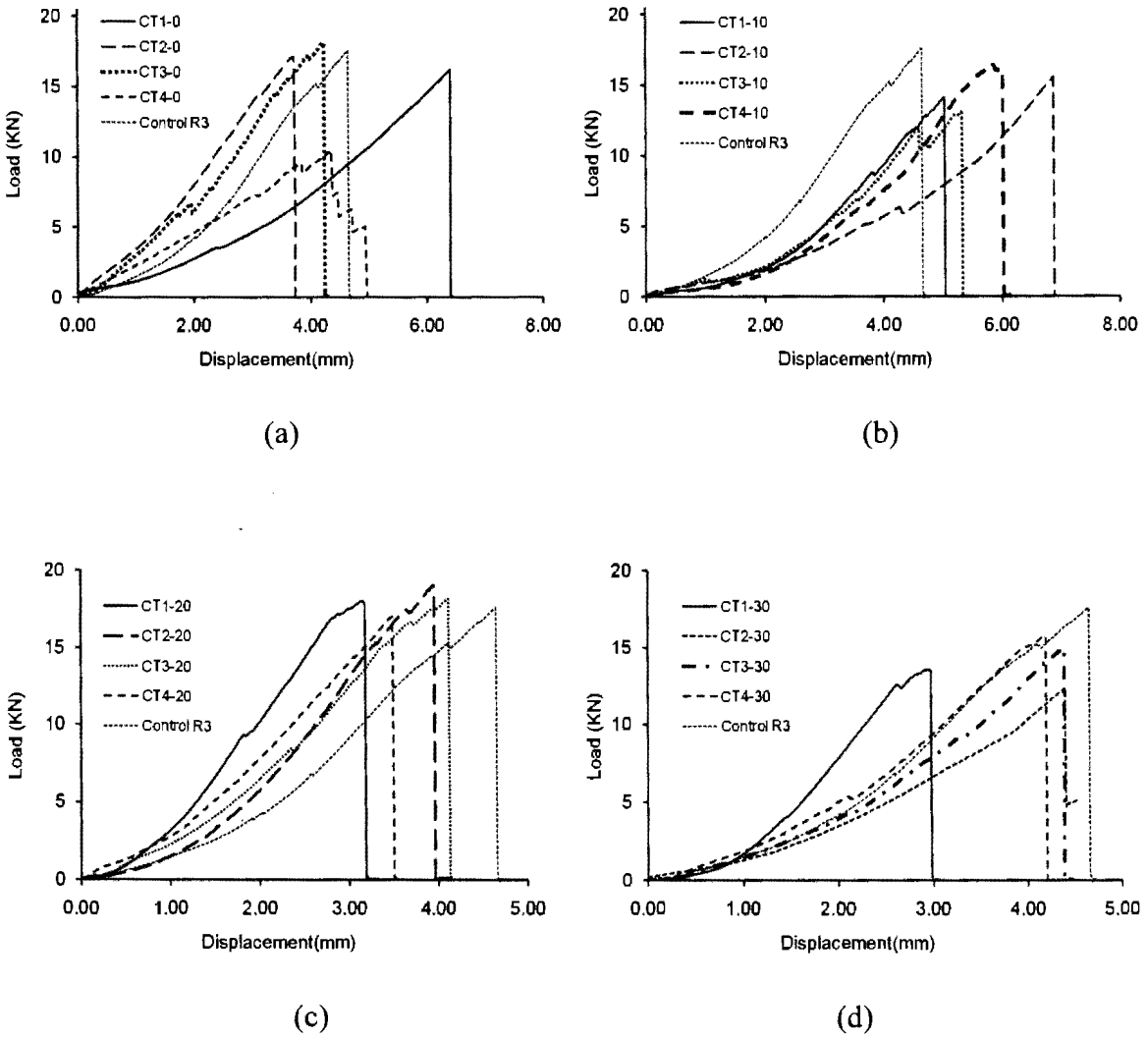

Figure D.2. Load-displacement responses under constant freezing for 2000hrs: (a) Freeze at 0 ^{0}C; (b) Freeze at -10 ^{0}C; (c) Freeze at -20 ^{0}C; (d) Freeze at -30 ^{0}C.

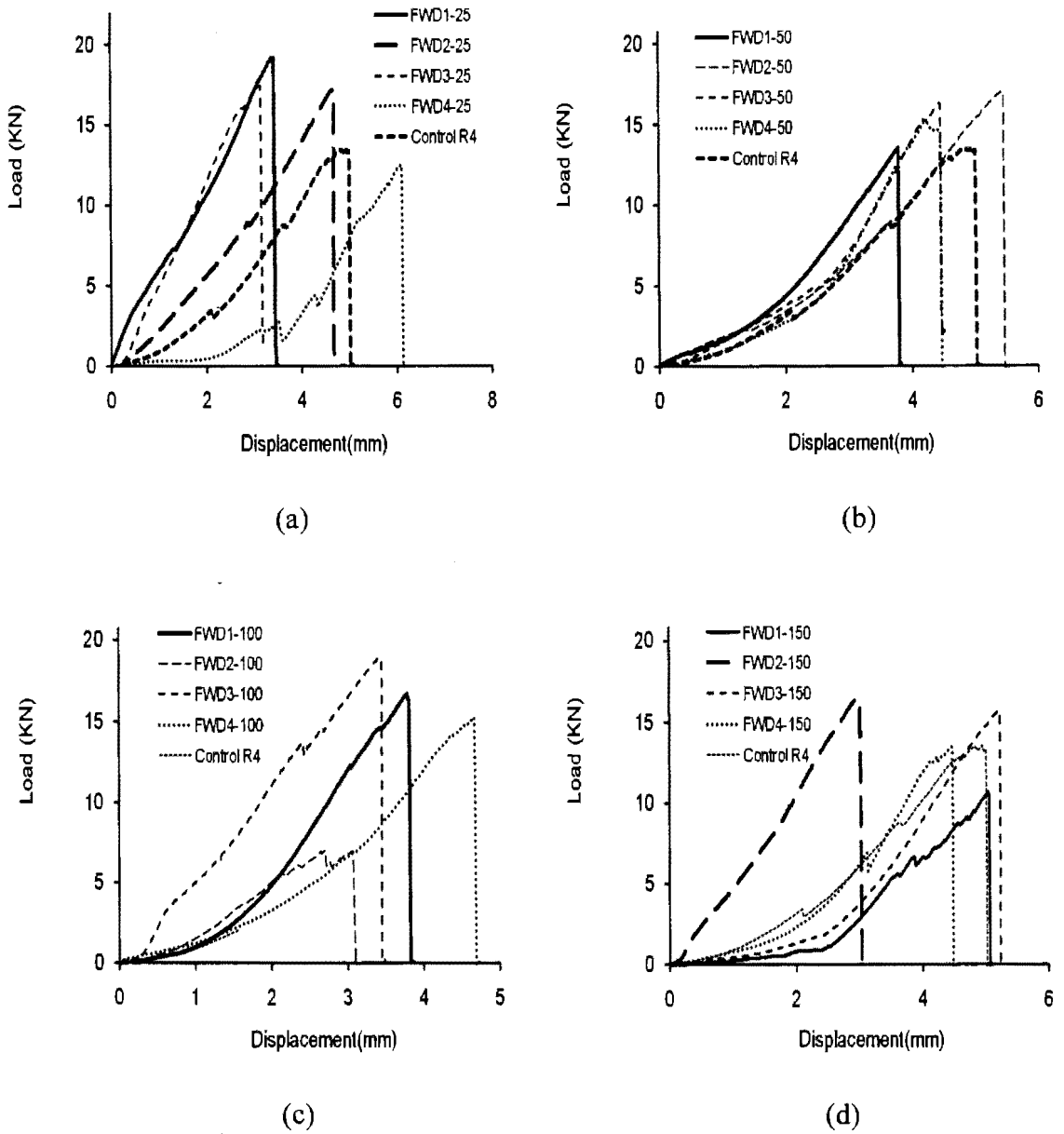

Figure D.3. Load-displacement responses under freeze-wet-dry effects: (a) 25 cycles (b) 50 cycles; (c) 100 cycles; (d) 150 cycles.

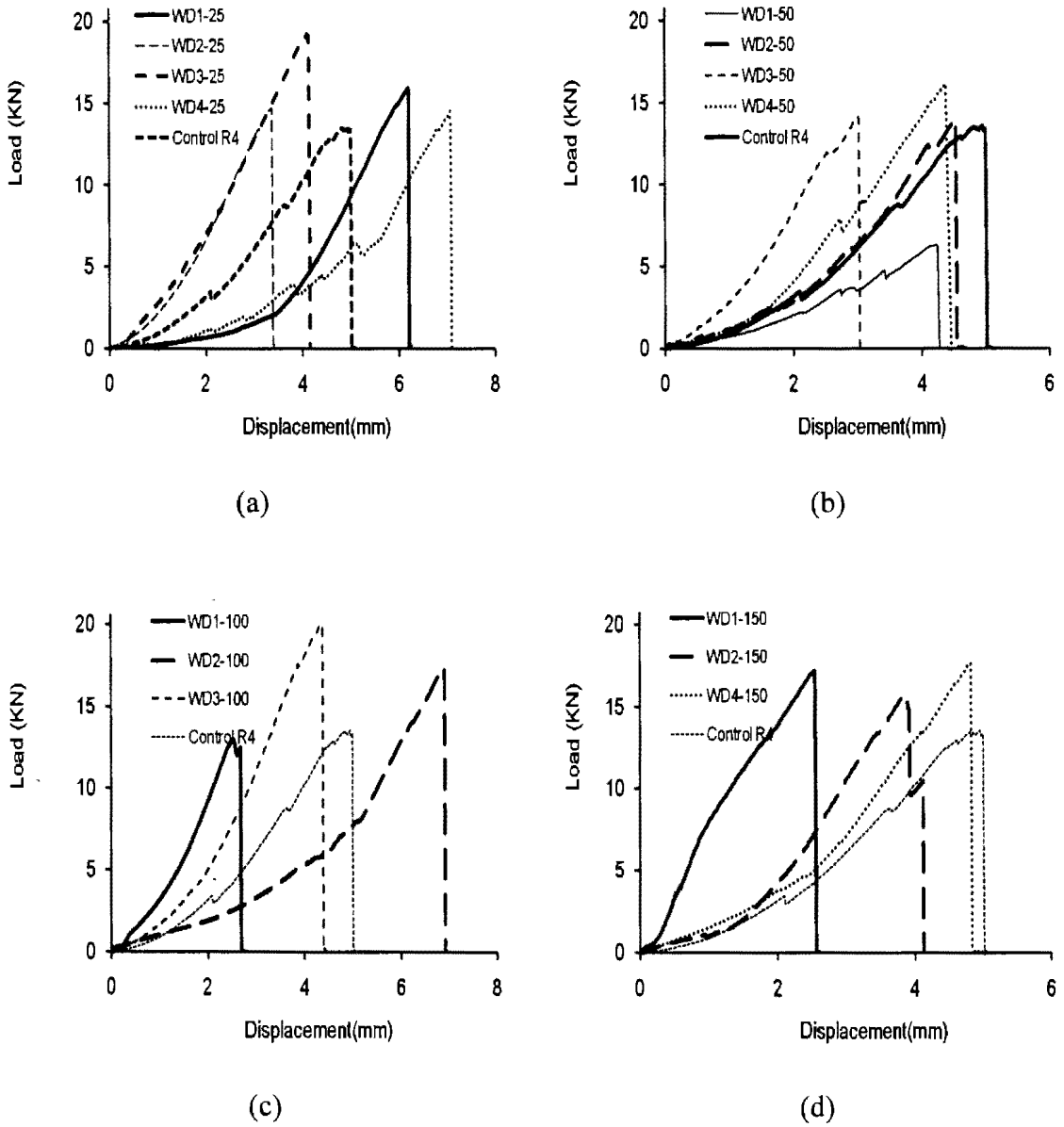

Figure D.4. Load-displacement responses under wet-dry effects: (a) 25 cycles (b) 50 cycles; (c) 100 cycles; (d) 150 cycles.